UNIVERSITY OF SOUTHAMPTON

FACULTY OF MEDICINE

Human Development and Health

Investigating the regulation of thymosin β4 by microRNAs in the developing human heart

by

Vinay Saunders

Thesis for the degree of Doctor of Philosophy

September 2014

UNIVERSITY OF SOUTHAMPTON

ABSTRACT

FACULTY OF MEDICINE

Thesis for the degree of Doctor of Philosophy

INVESTIGATING THE REGULATION OF THYMOSIN β4 BY MICRORNAS IN THE DEVELOPING HUMAN HEART

Vinay Saunders

Cardiovascular disease is the leading cause of death in the UK and there are over 25,000 new cases of heart failure in the UK each year. Studies in the field of regenerative medicine are seeking to find ways to repair the failing heart. Therapies which are being developed range from cell transplantation therapies to treatment with cardioprotective proteins. Thymosin β4 is a small, endogenous protein involved in wound healing and angiogenesis. Thymosin β4 is important in development of the murine heart and has also been noted to have cardioprotective effects in mouse models of myocardial infarction.

Currently there is little data regarding the cellular regulation of thymosin β4. miRNAs are a class of endogenous, small RNA molecules which act as post-transcriptional regulators of protein expression. It was hypothesised that thymosin β4 is present in the developing human heart and that its expression is regulated by miRNAs.

Using PCR and immunohistochemistry, thymosin β4 mRNA and protein were found to be present in human foetal hearts. Thymosin β4 protein was primarily localised to endothelial cells and was detected at higher levels in endothelial cells of the compact layer of the myocardium than the trabecular layer.

Different experimental strategies were developed in order to identify miRNAs with expression inversely correlated to that of thymosin β4. Foetal heart explants were cultured under hypoxic conditions; this was hypothesised to increase thymosin β4 expression. Western blotting was used to assess thymosin β4 protein levels, however this technique was found not to be suitable and no consistent changes in thymosin β4 expression were detected. The second experimental strategy used flow cytometry to successfully detect thymosin β4-positive and –negative CD34-expressing cells in the foetal heart. The aim of this was to separate these populations by fluorescence-activated cell sorting. Unfortunately, limited access to foetal tissue hindered this approach and an alternative experimental system was therefore needed.

The third experimental strategy involved culture of human umbilical vein endothelial cells on Matrigel basement membrane. This led to formation of tubules, a process during which thymosin β4 mRNA was reported to be up-regulated in previous studies. In the present study no changes in thymosin β4 mRNA or protein levels were detected. Expression levels of four miRNAs predicted to target thymosin β4 (miR-148b, miR-199a-3p, miR-217 and miR-495) were unchanged in tubule-forming HUVECs compared to controls.

Table of Contents

ABSTRACT ..... **i**

Table of Contents ..... **iii**

List of tables ..... **ix**

List of figures ..... **xi**

DECLARATION OF AUTHORSHIP ..... **xv**

Acknowledgements ..... **xvii**

Abbreviations ..... **xix**

Chapter 1: Introduction **1**

1.1 Coronary heart disease and heart failure 1

1.2 Regenerative medicine in the heart 3

1.2.1 Early studies into transplantation of differentiated cells 3

1.2.2 Cell therapy using non-cardiac adult stem cells 4

1.2.3 Cardiac progenitor cells 5

1.2.4 Pluripotent stem cells as a source of differentiated cardiomyocytes 9

1.2.5 Direct reprogramming into cardiomyocytes 11

1.2.6 Cell cycle re-entry of resident cardiomyocytes 11

1.2.7 Protein-based therapies 13

1.3 Thymosin β4 14

1.3.1 Discovery of thymosin β4 14

1.3.2 Distribution and mechanisms of action 15

1.3.3 Physiological and clinical roles 19

1.4 Thymosin β4 in the heart 25

1.4.1 Thymosin β4 in heart development 25

1.4.2 Activation of adult epicardial progenitor cells 26

1.4.3 Cardioprotective effects of thymosin β4 27

1.4.4 Thymosin β4 in endothelial progenitor cell therapy 29

1.5 Regulation of thymosin β4 protein expression 29
1.5.1 Post-translational regulation 30
1.5.2 Transcriptional regulation 30
1.5.3 Post-transcriptional regulation 31
1.6 microRNAs 35
1.6.1 microRNA synthesis and processing 35
1.6.2 Mechanism of action of microRNAs 37
1.6.3 Roles of microRNAs 38
1.6.4 miRNAs and thymosin β4 39
1.7 Hypothesis 40
1.8 Aims 40
Chapter 2: Methods 41
2.1 Foetal tissue and cells 41
2.1.1 Foetal tissue 41
2.1.2 HeLa cells 41
2.1.3 Human umbilical vein endothelial cells 42
2.2 RNA extraction and reverse transcription 45
2.2.1 RNA extraction using TRIzol 45
2.2.2 RNA extraction from paraformaldehyde-fixed cells 46
2.2.3 Reverse transcription of mRNA to cDNA 46
2.2.4 Reverse transcription of miRNAs to cDNA 47
2.2.5 Extraction of genomic DNA 47
2.3 PCR 49
2.3.1 Purification of PCR products 49
2.4 Quantitative PCR 50
2.4.1 TaqMan MicroRNA assays 51
2.5 Immunohistochemistry 55
2.5.1 Tissue fixation and embedding 55
2.5.2 Tissue sectioning and mounting 55

2.5.3 Immunofluorescent staining 55
2.5.4 Haematoxylin and eosin staining 56
2.5.5 Imaging 57
2.6 Protein extraction 59
2.7 SDS–PAGE and Western blotting 61
2.7.1 Laemmli SDS–PAGE 61
2.7.2 Tricine–SDS–PAGE 61
2.7.3 Western blotting 61
2.8 Hypoxia experiments 66
2.8.1 Heart tissue 66
2.8.2 HeLa cells 66
2.9 Flow cytometry 67
2.10 microRNA microarray 69
2.10.1 microRNA data mining 69
2.11 Molecular cloning 70
2.11.1 pCR2.1–TOPO vector 70
2.11.2 Transformation of competent cells 70
2.11.3 Bacterial cell culture 70
2.11.4 Extraction of plasmid DNA 71
2.11.5 Restriction digests 71
2.11.6 Ligation reactions 72
2.12 Tubule formation assays 72
Chapter 3: Results – Expression of thymosin β4 in the developing human heart 75
3.1 Introduction 75
3.2 Results 79
3.2.1 Detection of thymosin β4 mRNA in the developing human heart 79
3.2.2 Detection of TMSB4X transcripts in the developing human heart 80

3.2.3 Detection of thymosin β4 protein in the developing human heart 83
3.2.4 Localisation of thymosin β4 protein in structures of the foetal heart 86
3.2.5 Intracellular localisation of thymosin β4 within cells of the ventricle wall 90
3.2.6 Localisation of thymosin β4 protein with troponin C–positive cells within the ventricle wall 93
3.2.7 Localisation of thymosin β4 protein with CD31 and CD34–positive cells within the ventricle wall 98
3.3 Discussion 102
3.3.1 Thymosin β4 mRNA expression 102
3.3.2 Thymosin β4 protein expression 103
Chapter 4: Results – Experimental systems for the identification of thymosin β4–targeting miRNAs in the human heart 107
4.1 Introduction 107
4.2 Results 110
4.2.1 Detection of thymosin β4 protein by Western blotting 110
4.2.2 Effect of hypoxia on thymosin β4 protein 114
4.2.3 Detection of individual cell fluorescence by flow cytometry 118
4.2.4 Detection of CD31–positive cells by flow cytometry 120
4.2.5 Detection of thymosin β4–positive cells by flow cytometry 124
4.2.6 Detection of thymosin β4–positive cells within the CD31–positive population 133
4.2.7 Extraction of RNA from PFA–fixed cells 136
4.3 Discussion 138
4.3.1 Effect of hypoxia on thymosin β4 measured by Western blotting 138
4.3.2 Detection of thymosin β4–positive and negative populations of CD31–postive endothelial cells by flow cytometry 139

Chapter 5: Results – Assessment of thymosin β4 and microRNA expression in a model of endothelial cell differentiation 143

5.1 Introduction 143
5.2 Results 145
5.2.1 Identification of candidate thymosin β4–targeting miRNAs ... 145
5.2.2 Expression of candidate miRNAs in the human foetal heart .. 146
5.2.3 Creation of a pRL–TK vector containing the 3'–UTR of *TMSB4X* 151
5.2.4 HUVEC tubule formation 159
5.2.5 Thymosin β4 mRNA expression in tubule–forming HUVECs . 159
5.2.6 Thymosin β4 protein expression in tubule–forming HUVECs 165
5.2.7 Expression of candidate miRNAs in tubule–forming HUVECs 165
5.3 Discussion 169

Chapter 6: Discussion 175

6.1.1 The role of *TMSB4X-004* in miRNA–mediated regulation of thymosin β4 176
6.1.2 Candidate thymosin β4–targeting miRNAs 178
6.1.3 The extended regulatory network of thymosin β4–targeting miRNAs 181
6.1.4 Clinical potential of regulating thymosin β4–targeting miRNAs 182
6.2 Future work 186
6.2.1 Identification of thymosin β4–targeting miRNAs 186
6.2.2 Identification of miRNA networks in thymosin β4–mediated processes 186
6.2.3 Thymosin β4 expression and localisation throughout heart development 187
6.2.4 Effects of down–regulating thymosin β4–targeting miRNAs in pre–clinical models of myocardial infarction 188

Appendices **189**

Appendix 1 191
Appendix 2 193
Appendix 3 199
Appendix 4 201

References **205**

List of tables

Table 2.1 – Cardiac medium 44
Table 2.2 – HUVEC medium 44
Table 2.3 – miRNA reverse transcription reaction mixture 48
Table 2.4 – miRNA reverse transcription reaction temperature steps 48
Table 2.5 – PCR primers 52
Table 2.6 – PCR temperature steps 52
Table 2.7 – TaqMan Gene Expression Assays 53
Table 2.8 – qPCR temperature steps 53
Table 2.9 – TaqMan MicroRNA Assays 54
Table 2.10 – MicroRNA assay qPCR temperature steps 54
Table 2.11– Antibodies used in immunohistochemistry 58
Table 2.12 – RIPA buffer 60
Table 2.13 – 4X Sample Buffer A 64
Table 2.14 – Polyacrylamide gels for Laemmli SDS–PAGE 64
Table 2.15 – 4X Sample Buffer B 65
Table 2.16 – Polyacrylamide gels for tricine–SDS–PAGE 65
Table 2.17 – Antibodies used in flow cytometry 68
Table 3.1 – Pseudogenes of TMSB4X 78
Table 4.1 – RNA extraction from PFA–fixed cells 137
Table 5.1 – Candidate miRNAs present in human foetal heart 147
Table 5.2 – Candidate miRNAs present in human foetal heart and in endothelial cells 148

List of figures

Figure 1.1 Diagrammatic representation of coronary heart disease leading to heart failure....2
Figure 1.2 – Diagrammatic representation of initiation of translation 34
Figure 1.3 – Diagrammatic representation of miRNA processing and the formation of RISC 36
Figure 3.1 – Exonic structures of TMSB4X isoforms with primer binding locations 77
Figure 3.2 – Alignment of TMSB4X–002 and TMSB4XP4 sequences....78
Figure 3.3 – Detection of TMSB4X transcripts in the human foetal heart 81
Figure 3.4 – Detection of TMSB4X transcripts in the ventricles, atria and outflow tract of the foetal human heart....82
Figure 3.5 – Detection of TMSB4X transcripts with differing 3'–UTR lengths 82
Figure 3.6 – Immunolocalisation of thymosin β4 protein in the human foetal heart 84
Figure 3.7 – Immunolocalisation of thymosin β4 in the ventricle walls and interventricular septum....87
Figure 3.8 – Immunolocalisation of thymosin β4 in the atria, outflow tract and coronary vessels 88
Figure 3.9 – Intracellular localisation of thymosin β4 protein throughout a cell....91
Figure 3.10 – Intracellular localisation of thymosin β4 in relation to the nucleus....92
Figure 3.11 – Immunolocalisation of thymosin β4 and troponin C within the ventricle wall 94
Figure 3.12 – Immunolocalisation of CD31 protein within the ventricle wall 96
Figure 3.13– Immunolocalisation of CD34 protein within the ventricle wall 97
Figure 3.14 – Immunolocalisation of thymosin β4, CD31 and CD34 within the ventricle wall 99
Figure 3.15 – Localisation of thymosin β4 protein to individual cells expressing CD31 and CD34 100
Figure 4.1 – Laemmli SDS–PAGE for detection of thymosin β4 protein 112
Figure 4.2 – Tricine–SDS–PAGE for detection of thymosin β4 protein 113
Figure 4.3 –Thymosin β4 protein expression in foetal ventricle tissue cultured under hypoxic and normoxic conditions 116

Figure 4.4 – Thymosin β4 protein expression in HeLa cells cultured under hypoxic and normoxic conditions 117
Figure 4.5 – Diagrammatic representation of flow cytometry data 119
Figure 4.6 – Validation of α–CD31 antibody for flow cytometry using HUVECs 122
Figure 4.7 – Detection of CD31–positive cells in the human foetal heart 123
Figure 4.8 – Optimisation of secondary antibody for detection of thymosin β4 by flow cytometry using HUVECs 126
Figure 4.9 – Thymosin β4 staining of PFA–fixed HUVECs 128
Figure 4.10 – Thymosin β4 staining of MeAc–fixed HUVECs 129
Figure 4.11 – Detection of thymosin β4–positive cells in the human foetal heart 132
Figure 4.12 – Thymosin β4 and CD31 dual–stain of human foetal heart cells 134
Figure 4.13 – Detection of thymosin β4–positive and –negative cells within the CD31–expressing population of a human foetal heart sample 135
Figure 4.14 – Detection of cDNA derived from RNA extracted from PFA–fixed cells 137
Figure 5.1 – 15 best predicted thymosin β4–targeting miRNAs present in human foetal heart 149
Figure 5.2 – 4 best predicted thymosin β4–targeting miRNAs present in human foetal heart and endothelial cells 149
Figure 5.3 – Amplification of candidate miRNAs in human foetal heart 150
Figure 5.4 – Diagrammatic representation of the cloning strategy used 152
Figure 5.5 – Amplification of the 3'–UTR of TMSB4X 155
Figure 5.6 – Detection of pCR2.1 TOPO plasmid containing the 3'–UTR of TMSB4X in transformed colonies 156
Figure 5.7 – Digestion of pCR2.1 TOPO vector containing the 3'–UTR of TMSB4X and of pRL–TK vector containing the 3'–UTR of SMAD2 157
Figure 5.8 – Detection of pRL–TK plasmid containing the 3'–UTR of TMSB4X in transformed colonies 158
Figure 5.9 – Tubule formation of HUVECs on Matrigel 161
Figure 5.10 – Detection of TMSB4X transcripts in HUVECs cultured on Matrigel or plastic 162
Figure 5.11 – Detection of TMSB4X transcripts with differing 3'–UTR lengths in HUVECs cultured on Matrigel or plastic 163
Figure 5.12 – Relative expression of thymosin β4 mRNA in HUVECs cultured on Matrigel or plastic 164

Figure 5.13 – Detection of thymosin β4–positive cells in HUVECs cultured on Matrigel or plastic.....166
Figure 5.14 – Effect of culturing HUVECs on Matrigel on the expression of thymosin β4 protein.....167
Figure 5.15 – Relative expression of miRNAs in HUVECs cultured on Matrigel or plastic168
Figure 5.16 – Diagrammatic representation of reverse transcription using stem–loop RT primers designed for a canonical miRNA isomiR 172

DECLARATION OF AUTHORSHIP

I, Vinay Saunders, declare that this thesis and the work presented in it are my own and has been generated by me as the result of my own original research.

Investigating the regulation of thymosin β4 by microRNAs in the developing human heart.

I confirm that:

1. This work was done wholly or mainly while in candidature for a research degree at this University;
2. Where any part of this thesis has previously been submitted for a degree or any other qualification at this University or any other institution, this has been clearly stated;
3. Where I have consulted the published work of others, this is always clearly attributed;
4. Where I have quoted from the work of others, the source is always given. With the exception of such quotations, this thesis is entirely my own work;
5. I have acknowledged all main sources of help;
6. Where the thesis is based on work done by myself jointly with others, I have made clear exactly what was done by others and what I have contributed myself;
7. None of this work has been published before submission

Signed:.....

Date:.....

Acknowledgements

I'd like to acknowledge the following people who made contributions to the work presented here:

Kate Parry, Kelly Wilkinson, Anne Chad and David Wilson for the collection, dissecting and processing of human foetal tissue obtained locally and also the MRC-Wellcome Trust Human Developmental Biology Resource who also supplied human foetal tissue.

Kelly Wilkinson for extracting genomic DNA from human foetal tissue used in this study.

Cosmo Mirella Spalluto, who carried out miRNA arrays, the raw data of which I analysed in this study.

Stefanie Inglis, of the Bone and Joint Research Group, University of Southampton, who isolated HUVEC cells and kindly donated flasks of these cells for my research.

David Johnston, of the Biomedical Imaging Unit, University of Southampton, who operated the confocal microscope and provided advice and support regarding confocal experiments.

I would also like to thank Richard Jewell and Carolann McGuire, of the Clinical and Experimental Sciences Academic Unit, University of Southampton, for providing training, help and support regarding flow cytometry and the use of their FACS machines.

Further to this, I would like to thank Ita O'Kelly, Kelly Wilkinson, Melanie Lee, Alexander Mant, Rocio Martinez-Nunez, Laura Roncoroni, Sarah Williams, Jessica Sampson, Catherine Mercer and Jenny Dewing for help, advice and support in the lab over the past three years.

Thank you to the following people, and many other colleagues and friends besides, who have given me their friendship and support during my four years in Southampton:
Emma Mcmorrow, Dave Christensen, Richard McKendry, Sabrina Taylor, Gessa Sugiyarto, Charlie Cotter, Tom Jackson, Sarah Williams, Jess Rajaram, Tsiloon Li, Patrick Stumpf, Yu-Hin Man, Cameron Black, Edo Scarpa, Agnieszka Janeczek, Nunzia Sposito, Dan Page, Grace Cooper, Sophia Sander, Jenny Dewing and Jess Sampson.

Thank you to my mum and dad, who have always encouraged me to excel academically and to be the best I can be in everything I do. Without their continued support throughout my education, I would not be here now writing acknowledgements for a PhD thesis! Thank you also to my brother, Sunil, and my sister, Nayna, for always being there for me. Equally I would like to thank my closest friends, who are like my extended family; you know who you are.

Finally, I would like to thank my supervisors, Prof. David Wilson and Dr. Tilman Sanchez-Elsner for their help and guidance over the past three years and also to the Medical Research Council for funding my PhD.

I would particularly like to thank David for accepting me as his PhD student following my MRes rotation in his lab. It has been a tough three years but due to his patience, support and encouragement I made it to the finish line.

Abbreviations

Arbitrary units	a.u.
ATP-binding cassette subfamily G member 2	ABCG2
Blood vessel/epicardial substance	BVES
Cardiac progenitor cells	CPCs
c-Jun N-terminal kinase	JNK
Cycle threshold	Ct
Cytoplasmic polyadenylation-element	CPE
Cytoplasmic polyadenylation-element binding protein	CPEB
Dulbecco's Modified Eagle Medium	DMEM
Embryonic day	E
Embryonic endothelial progenitor cells	eEPCs
Embryonic stem cells	ESCs
Endothelial nitric oxide synthase	eNOS
Enzyme-linked immunosorbent assay	ELISA
Epithelial to mesenchymal transition	EMT
Eukaryotic initiation factor	eIF
Extracellular signal regulated kinase	ERK
Fas ligand	FasL
Fibroblast growth factor 2	FGF2
Foetal bovine serum	FBS
Globular actin	G-actin
Glycogen synthase kinase-3	GSK-3
Haematopoietic stem cells	HSCs
Haematoxylin and eosin	H&E
Heart- and neural crest derivatives-expressed protein 1	Hand1
Hepatocyte growth factor	HGF
High mobility group protein B1	HMGB1
Homeobox protein Meis1	Meis1
Human mutL homolog 1	hMLH1

Human umbilical vein endothelial cells	HUVECs
Hypoxia inducible factor 1α	HIF1α
Induced pluripotent stem cells	iPSCs
Insulin gene enhancer protein ISL-1	islet-1
Insulin-like growth factor-1	IGF1
Integrin-linked protein kinase	ILK
Interleukin	IL
IQ motif containing GTPase activating protein 1	IQGAP1
Lipopolysaccharide	LPS
Macrophage inflammatory protein-2	MIP-2
Matrix metalloproteinase	MMP
Mean fluorescence intensity	MFI
Methanol-acetic acid	MeAc
Mesenchymal stem cells	MSCs
microRNA	miRNA
Mitogen-activated protein kinases	MAPKs
Multidrug resistance-like protein 1	MDR1
Myosin regulatory light chain 2, ventricular/cardiac muscle isoform	MLC2v
Paraformaldehyde	PFA
Particularly interesting new cysteine-histidine rich protein	PINCH
Phosphate buffered saline	PBS
Phosphoinositide 3-kinase	PI3K
Plasminogen activator inhibitor type 1	PAI-1
Poly(A) binding protein	PABP
Polymerase chain reaction	PCR
Precursor miRNAs	pre-miRNAs
Protein kinase C	PKC
Ras-related C3 botulinum toxin substrate 1	RAC1
RNA helicase A	RHA
RNA-induced silencing complex	RISC
Short hairpin RNAs	shRNAs

Stem cells antigen 1	SCA-1
Transactivation response RNA-binding protein	TRBP
Tumour necrosis factor α	TNFα
Untranslated region	UTR
Vascular endothelial growth factor	VEGF
VEGF receptor 2	VEGFR2
Wilms tumour protein homolog	Wt-1

Chapter 1: Introduction

1.1 Coronary heart disease and heart failure

Cardiovascular diseases are a group of heart and blood vessel related diseases, which include coronary heart disease, stroke, peripheral artery disease and congenital heart disorders. Cardiovascular diseases are the leading cause of death in the UK and worldwide, with coronary heart disease being the UK's single biggest cause of death [1, 2]. Within the UK, coronary heart disease is responsible for approximately 80,000 deaths each year [2].

Coronary heart disease involves the occlusion of coronary arteries preventing blood from reaching areas of the heart. This occurs due to the build-up of fatty deposits, forming an atherosclerotic plaque, which narrows the vessel (Figure 1.1). Pieces of these plaques may break off leading to formation of blood clots which can become stuck in a coronary artery, blocking it completely and causing a myocardial infarction. The end result is a failure in the blood supply to the affected region of the heart, leading to death of cardiomyocytes due to a lack of oxygen (Figure 1.1). This causes permanent tissue damage, as the human heart lacks the endogenous regenerative capacity to repair itself. Instead of replacement of dead cardiomyocytes with new ones, the heart is remodelled through formation of non-functional, fibrous scar tissue (Figure 1.1).

Extensive damage to the myocardium can in turn lead to heart failure: a clinical diagnosis defined by an inability of the heart to effectively pump blood around the body (Figure 1.1). Heart failure is not only caused by coronary heart disease but can also be caused by a range of cardiovascular problems including high blood pressure and congenital heart disease.

There are thought to be over 25,000 new cases of heart failure in the UK each year [2] and the 5-year survival rate is only 58% in prevalent cases [3]. Currently there is no cure for heart failure short of having a heart transplant and the supply of suitable donor hearts does not meet demand. However, the field of regenerative medicine is exploring potential future therapies for repairing the failing heart.

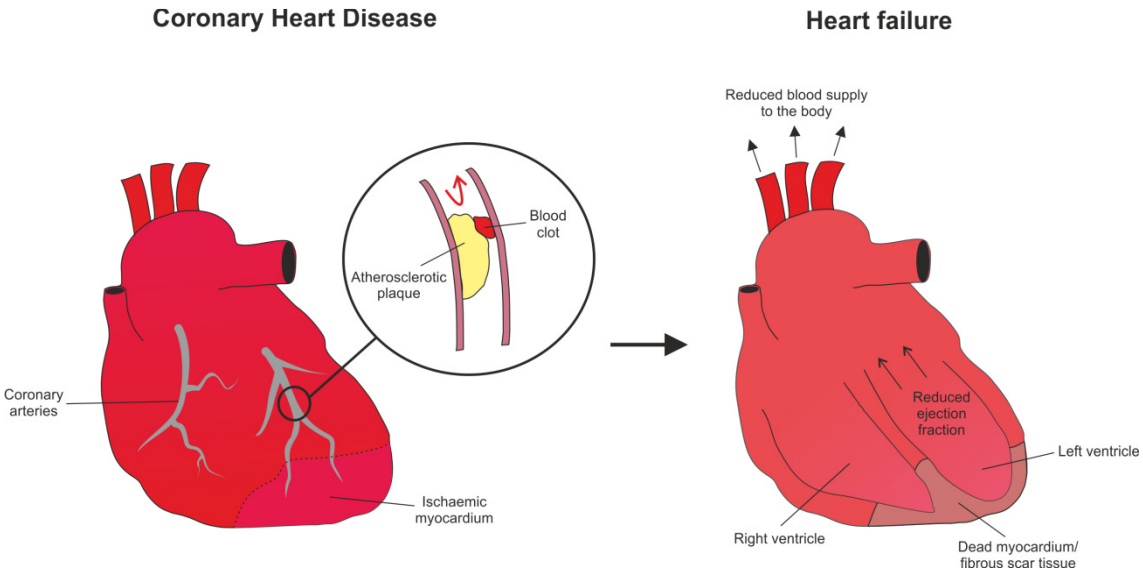

Figure 1.1 Diagrammatic representation of coronary heart disease leading to heart failure

Coronary heart disease occurs when coronary vessels become blocked leading to a loss of blood supply to areas of myocardium which become ischaemic. Extensive damage to the myocardium can prevent its ability to pump blood around the body, a condition known as heart failure.

1.2 Regenerative medicine in the heart

Until recently it was thought that the human heart did not produce new cardiomyocytes during adult life. It has now been shown that there is a low turnover of cardiomyocytes within the human heart, throughout life [4, 5]. This renewal capacity lessens with age, with replacement of 1% of cells per year at 25 years reduced to 0.45% by 75 years [4]. Research has suggested that there is some increase in this endogenous capacity to generate new cardiomyocytes following damage to the heart [6]. However, it is evident that the human heart is incapable of endogenously replacing the large numbers of cardiomyocytes which are lost following a myocardial infarction. As such, clinically-focussed strategies have been sought to replace dead cardiomyocytes following heart injury. To date such studies have primarily focussed on cell-based therapies, in which cells are transplanted into the damaged heart.

1.2.1 Early studies into transplantation of differentiated cells

Differentiated cardiomyocytes are perhaps the most logical cell type to transplant into the heart to directly replace lost cardiomyocytes. However, this strategy requires a large supply of viable, mature cardiomyocytes. While recent advances are addressing this issue (sections 1.2.4 and 1.2.5), early animal studies looked at transplanting foetal cardiomyocytes into the adult heart. Foetal cardiomyocytes stably integrate into the host heart, forming new myocardium and providing functional improvement [7, 8]. However, the number of cells retained in the heart is low and gradually decreases over time, rather than leading to substantial re-population of the heart [9]. These studies provided proof-of-concept for transplantation of differentiated cardiomyocytes into the damaged heart, while also highlighting issues such as cell retention and survival in cell-based therapies. However, human foetal cells are not used therapeutically for both ethical and logistical reasons.

1.2.2 Cell therapy using non-cardiac adult stem cells

1.2.2.1 Skeletal myoblasts

The first studies into cell-based therapies for the heart used skeletal myoblasts, which are activated satellite cells; the precursor cells to skeletal myocytes [10, 11]. Skeletal myoblasts could be expanded in culture from a small muscle biopsy to give significant numbers of cells, while the ability of skeletal muscle to regenerate suggested these cells had a superior regenerative capacity compared with cells resident in the heart [10, 11]. The heart was thought not to contain resident stem cells at the time, making skeletal myoblasts an attractive and logical cell type for cardiac cell therapy.

Unfortunately skeletal myoblasts were found not to differentiate into cardiomyocytes, instead forming myotubes, which do not integrate electrophysiologically with cardiomyocytes of the host heart [12–14]. Despite these caveats, transplantation of skeletal myoblasts elicit beneficial effects in animal models [15–17], which led to clinical trials in humans [18, 19]. However, the largest of these trials found limited beneficial effects and also highlighted the potential of skeletal myoblast transplantation to cause arrhythmias [20]. Such arrhythmias were seen in a previous clinical trial and also in animal studies [18, 21]. These arrhythmias are likely caused by the lack of electrical coupling between the myotubes and resident cardiomyocytes and are a noteworthy safety concern for cell-based therapy in the heart [21].

1.2.2.2 Bone marrow and blood-derived stem cells

To date, the cells that have had most interest for cardiac cell therapy are bone marrow-derived mononuclear cells, which include haematopoietic stem cells (HSCs) and mesenchymal stem cells (MSCs). These cells are clinically attractive due to their availability and the option of using unfractionated populations of mononuclear cells to reduce processing time and costs. Unfractionated cells, however, contain only small percentages of HSCs and MSCs [22, 23].

The major appeal of HSCs and MSCs comes from studies which suggest they have the ability to differentiate into cardiomyocytes [24-26]. However, other studies show that bone marrow cells do not generate new cardiomyocytes, but instead undergo cell fusion with existing cardiomyocytes [27-29]. This point remains in contention [30].

Importantly, bone marrow-derived HSCs and MSCs elicit beneficial effects in animal models [24, 31-33], resulting in bone marrow cell therapies moving quickly into clinical trials, which have demonstrated their safety [34, 35]. Larger clinical trials have now been carried out with mixed results, which may be due to differences in trial design, including the specific cell types used [36, 37]. Notably, one of the most promising trials to date used MSCs, rather than unfractionated bone marrow mononuclear cells [38]. While other trials have also shown modest improvements in cardiac function [39-42], two of the largest studies to be carried out have shown no benefit [43, 44].

More recently, work has been done using human umbilical cord blood mononuclear cells, which similarly contain HSC and MSC populations [45, 46]. Initial animal studies have shown improvements in cardiac function [45, 46]. It seems likely, however, that the progress of these therapies will depend on the success of clinical trials with bone marrow-derived cells.

It is becoming increasingly accepted that improvements in cardiac function elicited by HSCs and MSCs are unlikely to be due to direct regeneration of cardiac tissue. Clinical studies indicate that only a small percentage of transplanted cells are retained in the heart, with this number declining over the first 24 hours [47-49]. This suggests that, rather than becoming stably engrafted, these cells are having transient effects, which bestow long-term benefit on resident cells. The prevailing hypothesis is that blood and marrow-derived stem cells release paracrine factors which have effects that include promotion of angiogenesis and cell survival [50-52].

1.2.3 Cardiac progenitor cells

While direct regeneration of the heart may not be possible with HSCs and MSCs, the more recently discovered resident progenitor cells of the heart may

be able to achieve this goal. Several different populations of multipotent cardiac progenitor cells (CPCs) have been described in the mammalian adult heart.

1.2.3.1 C-Kit$^+$ CPCs

The first studies to identify CPCs did so using c-Kit; a cell surface tyrosine kinase receptor [53] which is a receptor for stem cell factor [54]. C-Kit was originally used as a marker of HSCs [55], however c-Kit-expressing, blood lineage-negative cells resident in the rat heart were found to be a distinct population of cardiac, rather than haematopoietic, progenitor cells [56]. These c-Kit+ CPCs were shown to be multipotent; capable of producing endothelial cells, smooth muscle cells and cardiomyocytes, which are the three main cell lineages of the heart [56]. Further to this, the ability of these c-Kit+ CPCs to promote regeneration of the rat heart, following induced myocardial infarction, was demonstrated [56, 57]. C-Kit$^+$ CPCs were soon identified in the human heart and their regenerative potential in rodent models of myocardial infarction was also demonstrated [58].

1.2.3.2 Insulin gene enhancer protein ISL-1$^+$ CPCs

Insulin gene enhancer protein ISL-1 (islet-1), a LIM homeodomain transcription factor, has been identified as a marker of a distinct CPC population [59]. Islet-1 was initially shown to be important in the developing murine heart and was demonstrated to be a marker of early CPCs, from which only specific portions of the heart arise [60]. Islet-1$^+$ cells have since been shown to persist, though in low numbers, into the post-natal stage of both rodents and humans and are present in the human heart over a week after birth [59]. These islet-1$^+$ cells do not express c-Kit and are therefore a distinct population of CPCs [59], however islet-1$^+$ CPCs are equally capable of differentiating into the three main cardiac lineages of cardiomyocytes, smooth muscle cells and endothelial cells [59, 61, 62]. Islet-1$^+$ cells are difficult to isolate for transplantation, as islet-1 is not a surface molecule like c-Kit, which may account for the lack of preclinical studies testing this CPC population in animal models of myocardial infarction. Islet-1$^+$ CPCs have been generated from pluripotent cells, however, and these cells could be used in such studies in future as well as clinically [63].

1.2.3.3 Cardiosphere cells

Perhaps the third most important CPC population identified to date are the cardiosphere and cardiosphere-derived cells. These cells spontaneously arise from explanted heart biopsy tissue and are formed from small, round, phase-bright cells that migrate away from the biopsy and begin to divide in suspension to form small, spherical clusters of cells, termed 'cardiospheres' [64]. When cardiospheres are dissociated and the cells are plated in a monolayer, they are termed cardiosphere-derived cells [64]. Though cardiospheres are a mixed population of CPCs and more differentiated cells, they are comprised of cells that are clonally derived from individual CPCs [64, 65]. Like other CPCs, cardiosphere cells can produce both cardiomyocytes and vascular cells, and have additionally been shown to differentiate into mesenchymal cells [64, 65]. Cardiospheres contain c-Kit$^+$ cells, which are primarily present in the centre of the spheres, suggesting c-Kit$^+$ CPCs are responsible for cardiosphere formation [64, 65]. However, cardiospheres themselves are a clinically attractive source of CPCs as they are easily obtained without the need for selection with xenogeneic antibodies, in the way that c-Kit$^+$ populations are. Cardiosphere-derived cells elicit beneficial effects in mouse models of myocardial infarction [66], and pre-clinical studies have shown the safety and potential efficacy of cardiosphere-derived cell therapy in large animal models of myocardial infarction [67, 68].

1.2.3.4 Side population cells

Another population of CPCs are the cardiac side population cells [69]. These cells express the molecules ATP-binding cassette subfamily G member 2 (ABCG2) and multidrug resistance-like protein 1(MDR1), which remove toxic substances from the cell, including the DNA-binding dye Hoechst 33342 [70]. As such, cells expressing these molecules appear as a side population on a scatter plot of their Hoechst staining, giving them their name [70, 71]. Side population cells were first identified in bone marrow as HSCs [71], however side population cells which lack hematopoietic markers were later found in the murine heart and these have the capacity to produce cardiomyocytes [69].

The regenerative potential of cardiac side population cells has been demonstrated in rats, where they produce endothelial cells and smooth muscle cells *in vivo*, as well as cardiomyocytes [72]. Cardiac side population cells have recently been identified in the human heart, though they appear to be limited to the left atria [73].

Cardiac side population cells are thought to be a heterogeneous population that may contain differentiated cells and non-cardiac progenitors such as MSCs, as they have the ability to produce osteocytes and adipocytes [72, 74]. Therefore, it should be noted that true CPCs may exist as only a fraction of side population cells.

1.2.3.5 SCA-1$^+$ CPCs

Another marker which has been used to identify CPCs in mice is stem cell antigen 1 (SCA-1) [69, 75]. While SCA-1 was independently identified as a marker of CPCs, it is also expressed by murine cardiac side population cells and the two populations may largely overlap [69, 75]. Like cardiac side population cells, SCA-1$^+$ cells may be a heterogenous population, as they also produce osteocyte and adipocyte lineages in addition to cardiomyocytes [75]. However, studies suggest that neither side population cells nor SCA-1$^+$ populations contain significant numbers of c-Kit+ cells [74, 76, 77], suggesting they may contain a population of CPCs that is distinct from c-Kit+ CPCs.

SCA-1$^+$ cells elicit beneficial effects when transplanted in mouse models of myocardial infarction [76–78], however there is no known human orthologue of Sca1, which limits its use as a marker of CPCs in terms of clinical regenerative medicine.

1.2.3.6 Clinical trials

Further research is still required to identify and define the resident stem and progenitor cell populations within the mammalian heart, with recent studies suggesting over-lap between the main CPC markers [79–82]. The best CPC population for use in cell therapy is still very much open for debate.

Despite this, clinical trials have begun using both c-Kit+ CPCs, in the SCIPIO trial [83, 84], and cardiosphere-derived CPCs, in the CADUCEUS trial [85, 86], likely due to the relative ease of obtaining these two cell populations. The CADUCEUS trial has reported final 1 year results, demonstrating the safety of cardiosphere-derived cells and showing reduced scar sizes, increases in viable myocardial tissue and improved regional left ventricular function in treated patients [86]. The SCIPIO trial is on-going and also reports increases in viable myocardial tissue at the 1 year time point, as well as reduced infarct sizes and improved global and regional left ventricular function in treated patients [84].

1.2.4 Pluripotent stem cells as a source of differentiated cardiomyocytes

1.2.4.1 Embryonic stem cells

The primary goal of regenerative medicine in the heart is to introduce new, functional cardiomyocytes into the damaged heart and early animal studies using foetal cardiomyocytes have demonstrated the potential of this technique [7, 8]. While the rare nature of adult CPCs currently limits their use in the production of mature cardiomyocytes, pluripotent stem cells represent a potential, clinically practical source of large numbers of differentiated cardiomyocytes for transplantation.

Pluripotency refers to the capacity of a cell to produce all the cells of the three embryonic germ layers. Human embryonic stem cells (ESCs) are pluripotent and have the ability to self-renew indefinitely as well as to differentiate into committed cell lineages [87]. As such, the utility of these cells as a source of various differentiated cells for regenerative medicine is clear.

Initial studies with human ESCs have shown the feasibility of generating functional cardiomyocytes from pluripotent stem cells [88, 89]. These human ESC-derived cardiomyocytes successfully engraft when introduced into the rodent heart and elicit medium-term improvements in cardiac function in rodent models of myocardial infarction [90-92]. Furthermore, studies in guinea pigs have shown that human ESC-derived cardiomyocytes can couple electrophysiologically with host cells, reducing the risk of arrhythmias [93]. A recent non-human primate study has demonstrated the ability of human ESC-

derived cardiomyocytes to remuscularise the heart on a clinically-relevant scale [94]. Grafted cells electrically coupled with host cells, though unfortunately arrhythmias were nonetheless seen [94].

The clinical use of ESCs is surrounded by ethical concerns, however the invention of induced pluripotent stem cells (iPSCs) has provided an alternative source of pluripotent stem cells.

1.2.4.2 Induced pluripotent stem cells

Creation of murine iPSCs was first described in 2006, followed a year later by human iPSCs [95, 96]. Through the introduction of only three factors, fibroblasts can be de-differentiated into pluripotent cells, which resemble ESCs [97]. Work is on-going in this new field of research and improved variations on iPSCs are emerging [98-100]. This technology could allow cells, such as skin fibroblasts, to be taken from a patient and de-differentiated into iPSCs. These autologous cells could then be differentiated into cardiomyocytes and transplanted back into the same patient, without risk of immune rejection.

Functional cardiomyocytes have been derived from both human and murine iPSCs [96, 101, 102] and mouse studies show long-term integration and electrophysiological coupling of murine iPSCs transplanted into recipient hearts [103]. If cells derived from iPSCs are to be used clinically, however, they must be a pure population of differentiated cells, , as introduction of pluripotent cells could lead to teratoma formation [104, 105].

1.2.4.3 Tissue engineering

The generation of mature cardiomyocytes from iPSCs is being utilised in tissue engineering strategies to develop cardiac patches which can be transplanted onto the damaged area of the heart [106, 107]. These cardiac patches have been shown to induce functional improvements in both rodent models of myocardial infarction [106] and in large animal studies which used human iPSC-derived cardiac patches [107]. Further to this, 3D patches with improved characteristics have been created using hydrogel scaffolds [108].

Arguably, the ultimate goal of such tissue engineering strategies is to create a whole replacement heart for transplantation. Research is moving forward in this area with the successful de-cellularisation of a mouse heart followed by re-population with human iPSC-derived cells [109]. In future, de-cellularised porcine heart scaffolds may be utilised clinically [110]. Advances in 3D printing technology have opened up avenues in a broad spectrum of fields, including biology. 3D bio-printing brings the possibility of printing defined layers of extracellular matrix, biological factors and cells to create transplantable 3D tissues and perhaps, in the longer term, even whole organs [111].

1.2.5 Direct reprogramming into cardiomyocytes

Further to the generation of iPSCs, recent research has found it possible to transdifferentiate cells directly from one lineage to another through the introduction of specific factors. In this manner, both mouse and human fibroblasts have been directly 'reprogrammed' into cardiomyocytes [112-116]. Direct reprogramming removes pluripotent cells from the process, removing fears of introducing tumour-generating pluripotent cells into patients.

Transdifferentiation also introduces the possibility of gene therapy, by which the dividing fibroblasts that begin to form scar tissue during cardiac remodelling are transfected with genes that will reprogram them to cardiomyocytes [117, 118]. Such *in vivo* reprogramming has been successfully carried out in mouse models of myocardial infarction, with reprogrammed cardiomyocytes not only surviving in the heart up to one month after treatment, but also functionally coupling with existing cardiomyocytes [117, 118]. These gene treatments led to reduced remodelling and improved cardiac function [117, 118]. While these initial findings show promise, it should be noted that the field of direct cardiac reprogramming is still very much in its infancy.

1.2.6 Cell cycle re-entry of resident cardiomyocytes

Recent research into cardiac regeneration seems to be focussing less on cell transplantation therapies. While direct *in vivo* cardiac reprogramming is one new area of interest, other researchers are investigating the possibility of

stimulating resident cardiomyocytes to re-enter the cell cycle and proliferate to produce new cardiomyocytes [119-122].

1.2.6.1 Lower vertebrates

Recent interest in this field has been prompted by studies in zebrafish which, like certain amphibians, are capable of regenerating the adult heart following damage [123, 124]. The regenerative capabilities of these lower vertebrates have been studied in the hope of uncovering regenerative mechanisms that can guide clinical therapies. Indeed, the zebrafish heart is capable of regenerating in response to both ventricular resection and cryo-injury; a model of myocardial infarction [124-126]. Importantly, recent studies have shown that regeneration in the zebrafish occurs through activation and proliferation of existing mature cardiomyocytes in the heart and not through differentiation of a CPC population [127, 128].

1.2.6.2 Mammals

A recent ground-breaking study has shown that cardiac regeneration is not limited to lower vertebrates [129]. The study found that the neonatal mouse heart has the ability to regenerate following resection of around 15% of the ventricle and, as in the zebrafish, this repair was mediated by proliferation of existing cardiomyocytes [129]. This regenerative capacity, while present in 1 day old mice, is lost within 7 days [129].

When the mammalian heart was found to generate a low turn-over of cardiomyocytes throughout life, one major question was whether new cardiomyocytes arise from CPCs or existing cardiomyocytes. Consistent with the mechanism of cardiac regeneration in the zebrafish and neonatal mouse, a recent study has indicated that new cardiomyocytes in the healthy adult murine heart, and following myocardial infarction, arise primarily from existing cardiomyocytes, not CPCs [130].

Together these studies suggest that stimulating resident cardiomyocytes in the human heart to re-enter the cell-cycle may be a viable clinical strategy. Indeed, in mouse models of myocardial infarction, forcing cardiomyocytes into the cell

cycle through transgenic cyclin D2 expression leads to improved cardiac function [119].

Mechanisms which govern the cell cycle and proliferation of cardiomyocytes are now being studied in the hope that cell-cycle re-entry and enhanced proliferation can be induced [120-122, 131-134]. Of note, a transcription factor called homeobox protein Meis1 (Meis1) has been identified as responsible for cell-cycle exit in murine cardiomyocytes [121]. When Meis1 was over-expressed in cardiomyocytes, neonatal heart regeneration was inhibited [121]. Furthermore, knock-down of Meis1 allowed adult cardiomyocytes to re-enter the cell cycle [121].

1.2.7 Protein-based therapies

An alternative therapeutic approach to cell-based therapies is protein-based therapy, including use of the paracrine factors which are released from transplanted cells. The idea that these factors are the key mediators of the beneficial effects seen in cell-based therapies has led to an increase in research seeking to identify these factors, as well as other cardioprotective proteins, in order to directly utilise them as therapeutics. Such cell-free treatments are more straightforward than cell-based therapies, removing issues of immune rejection of allogeneic cells or the need to expand large numbers of cells and process them, for example to obtain pure populations of pluripotent cell-derived differentiated cells

Studies have indicated that release of paracrine factors from cells including bone marrow-derived cells [135, 136]; in particular MSCs [51, 137-139]; and CPCs [140-142] are responsible for some of the effects of such cell-based therapies. The effects of the released factors include neovascularisation [137, 139], attenuation of fibrosis [138], cardiomyocyte survival [143, 144], and even the activation of resident CPCs [145-148]. Thus, the introduction of specific proteins into the heart could lead to the generation of new cardiomyocytes from resident CPCs, without the need to transplant cells. Equally, studies aiming to stimulate proliferation of mature cardiomyocytes have identified factors with this capacity [120, 149].

Several specific proteins with potential therapeutic use have now been identified, including growth factors such as hepatocyte growth factor (HGF), insulin-like growth factor-1 (IGF1) and fibroblast growth factor 2 (FGF2) [142-144, 146, 147, 150]. High mobility group protein B1 (HMGB1) has been shown to activate resident CPCs [148, 151], while periostin and neuregulin are both factors that have been demonstrated to stimulate proliferation of mature cardiomyocytes [120, 149].

Another such protein which has been identified for its therapeutic potential in the heart is thymosin β4.

1.3 Thymosin β4

1.3.1 Discovery of thymosin β4

Thymosin β4 is a small, 43 amino acid protein with a molecular weight of approximately 4.9 kDa [152]. Expression of thymosin β4 is conserved across vertebrate species from humans down to zebra fish. In humans, thymosin β4 is coded by the *TMSB4X* gene.

The isolation and identification of thymosin β4 from calf thymus extract was first described in 1981 [152]. Earlier studies looking at the role of the thymus gland in lymphocyte development led to the identification of a biologically active, protein component within the calf thymus, which was named “thymosin” [153]. Further characterisation of thymosin led to a partially purified preparation termed “thymosin fraction 5”, which was found to contain several small, acidic, heat-stable polypeptides [154]. These proteins have been categorised into three families based on their isoelectric points; the α-thymosins, β-thymosins, and γ-thymosins; and then numbered in chronological order of isolation [152].

Thymosin β4 was one of the individual, biologically active proteins to be isolated from thymosin fraction 5 and as indicated by its name is part of the β-thymosin family [152]. The β-thymosins are a family of functionally related proteins with high amino acid sequence homology. In addition to thymosin β4, thymosin β10 and thymosin β15 are present in human tissues, however thymosin β4 is the most highly expressed and, to date, the most extensively studied [155, 156].

Coupled with the original isolation of thymosin β4 from the thymus gland was an assumption that thymosin β4 played a role specific to the immune system. This idea was reinforced by the observation that thymosin β4 could induce the activity of an enzyme involved in the maturation of T-cells in immunosuppressed mice [152]. However, it was later found that there is little variation in endogenous levels of thymosin β4 mRNA in rat T-cell populations at different stages of development [157]. This suggested that thymosin β4 does not have an endogenous role in T-cell maturation.

In addition, thymosin β4 was later found to be expressed in a wide range of tissues and cell types including leukocytes, platelets, brain, testis, ovary, spleen, intestine, liver, lung, kidney and heart; though it is not present in red blood cells [157-159]. This widespread expression suggested that thymosin β4 has a much more general role than originally postulated.

1.3.2 Distribution and mechanisms of action

1.3.2.1 Thymosin β4 and actin

In the early 1990's, research attempting to understand how cells maintain high concentrations of free, globular actin (G-actin) and prevent polymerisation of that G-actin into actin filaments, uncovered one of the major physiological roles of thymosin β4: the sequestration of unpolymerised G-actin molecules [160, 161]. Thymosin β4 was found at high concentrations in both human platelets and polymorphonuclear leukocytes where it sequesters the majority of free G-actin, leading to the suggestion that thymosin β4 is the major actin sequestering protein in mammals [162, 163]. Thymosin β4 and other members of the β-thymosin family contain a conserved LKKTET sequence which is an actin-binding motif [164]. Through this motif, thymosin β4 targets and binds G-actin in 1:1 complexes and then undergoes conformational changes which provide steric hindrance, preventing incorporation of the G-actin molecule into actin filaments [164-166].

G-actin molecules are bound by either ATP or ADP and actin polymerisation is more efficient with ATP-bound G-actin [167]. Thymosin β4 has a higher affinity for ATP-bound G-actin and is thus able to maintain a pool of sequestered ATP-

bound G-actin [167, 168]. Under such conditions polymerisation occurs at a reduced rate using ADP-bound G-actin [167]. If thymosin β4 levels are lowered, ATP-bound G-actin is released and the rate of actin polymerisation increases [167]. Through this actin sequestering role, thymosin β4; alongside other actin-binding proteins, such as profilin; is able to control actin dynamics leading to polymerisation or depolymerisation of actin filaments, thus regulating a cell's actin cytoskeleton [167-169].

1.3.2.2 Intracellular signalling of thymosin β4

More recently, thymosin β4 has been shown to act as a signalling molecule. The signalling network which thymosin β4 has been most prominently implicated in is that of integrin-linked protein kinase (ILK), a major component of focal adhesion complexes [170-173]. ILK is involved in several different signalling pathways and has many binding partners [174]. Thymosin β4 has been shown to interact with ILK and 'particularly interesting new cysteine-histidine rich protein' (PINCH), a direct binding partner of ILK, leading to recruitment of ILK to the focal adhesion complex [170]. Once recruited to the focal adhesion complex, ILK is activated by phosphoinositide 3-kinase (PI3K), allowing ILK to phosphorylate Akt, which leads to downstream signalling [170]. One downstream signalling pathway which is induced by thymosin β4 via the PI3K-ILK-Akt pathway is the endothelial nitric oxide synthase (eNOS) pathway [171, 175, 176].

Thymosin β4 has also been implicated in other ILK signalling pathways, such as the activation of Ras-related C3 botulinum toxin substrate 1 (RAC1); a Rho GTPase involved in actin dynamics [173]. This activation of RAC1 occurs via IQ motif containing GTPase activating protein 1 (IQGAP1), which is another direct binding partner of ILK [173].

Another intracellular binding partner of thymosin β4 is Ku80, a subunit of ATP-dependent DNA helicase II [177]. When partnered with Ku80, thymosin β4 induces increased plasminogen activator inhibitor type 1 (PAI-1) expression in endothelial cells [177, 178]. This effect on PAI-1 expression occurs via activation of the c-Jun N-terminal kinase (JNK) signalling pathway [178]. JNK is one of several mitogen-activated protein kinases (MAPKs) and thymosin β4 has

additionally been found to signal through other MAPKs including p38 MAPK [179, 180] and extracellular signal regulated kinase (ERK) [180-182]. In particular, thymosin β4-induced phosphorylation of ERK has been shown to initiate diverse downstream signalling pathways including regulation of glycogen synthase kinase-3 (GSK-3) signalling [182], as well as the phosphorylation and stabilisation of hypoxia inducible factor 1α (HIF1α) [181]. Whether Ku80 is involved in thymosin β4 signalling through p38 MAPK or ERK is unknown.

More recently the Notch signalling pathway has been implicated in thymosin β4-mediated effects [183]. While thymosin β4 was demonstrated to up-regulate protein expression of the Notch1 and Notch4 receptors [183], little else is known about the mechanisms which link thymosin β4 to the Notch signalling pathway.

1.3.2.3 Nuclear thymosin β4

As well as being present in the cytoplasm of cells, thymosin β4 has been found in the cell nucleus [184, 185]. While thymosin β4 does not have a canonical nuclear localisation signal and is unable to localise to the nucleus alone [185-187], it has been shown to interact with human mutL homolog 1 (hMLH1), an enzyme primarily involved in DNA repair [187]. hMLH1 does contain a nuclear localisation signal and when thymosin β4 is bound to hMLH1, the two proteins are transported to the nucleus where they appear to remain colocalised [187].

The role of thymosin β4 in the nucleus remains unclear, though actin is present in the nucleus, where it is found in both its polymerised and unpolymerised forms [188]. Thus, it is logical to speculate that thymosin β4 within the nucleus acts in its actin-sequestering capacity. This does not preclude additional roles for thymosin β4 in the nucleus however. hMLH1 is able to up-regulate thymosin β4 expression, suggesting the two molecules may have a functional relationship, beyond transport to the nucleus [187]. Interestingly, while hMLH1 has a role in DNA repair, so too does Ku80; one of thymosin β4's other binding partners. Furthermore, thymosin β4-Ku80 complexes are detected in the nuclear extracts of endothelial cells [177]. Therefore, while thymosin β4 has not been directly implicated in DNA repair, its relationship with hMLH1 and Ku80 suggests it may play a role in this process.

1.3.2.4 Extracellular signalling of thymosin β4

Thymosin β4 is also found in the extracellular environment, suggesting it may signal between cells. Specifically, thymosin β4 has been found in human serum [189] and in wound fluid [190]; and its release from certain cultured cell types has been demonstrated [170, 191]. The mechanism of thymosin β4's release is unknown; it does not have a signal sequence [192], suggesting it is not actively secreted by conventional pathways. This does not, however, rule out active secretion by unconventional pathways, as has been demonstrated with other small proteins [193]. Alternatively, the small size of thymosin β4 may allow for passive diffusion out of the cell or it may only be released from damaged or dead cells.

Extracellular thymosin β4 can be taken up into cells [170, 184], through an unknown mechanism, which allows it to participate in intracellular signalling and G-actin-binding roles. Additionally, a recent study has identified an extracellular receptor for thymosin β4 [194]. Freeman and colleagues found that thymosin β4 interacts with cell surface F1F0 ATP synthase, leading to generation of ATP which in turn elicits downstream effects via P2X4 purinergic receptors [194]. This signalling pathway was demonstrated to be important for thymosin β4-induced migration of endothelial cells [194].

1.3.2.5 Derivatives of thymosin β4

Evidence also suggests that some of thymosin β4's effects may be mediated by derivatives of thymosin β4. Thymosin β4 sulfoxide, which may be formed by autoxidation of thymosin β4's methionine residue, may be responsible for many of thymosin β4's cell signalling activities [195, 196]. Studies indicate that thymosin β4 sulfoxide has a lower affinity for actin monomers but has increased biological activity in terms of extracellular signalling, compared to thymosin β4 [195, 196]. Thus oxidation of thymosin β4 may facilitate a switch between the actin-sequestering and the cell signalling roles of thymosin β4.

Some of thymosin β4's activities may also be due to formation of Ac-SDKP. Ac-SDKP is a naturally occurring tetrapeptide which can be formed through the breakdown of thymosin β4 [197, 198]. This has been demonstrated to occur

endogenously through a two-step cleavage at the N-terminal region of thymosin β4, involving the serine peptidase, prolyl oligopeptidase [198, 199].

1.3.3 Physiological and clinical roles

1.3.3.1 Cell migration

One of the major physiological functions which thymosin β4 is involved in is cell migration. This role was first demonstrated with human umbilical vein endothelial cells (HUVECs), which have increased motility when treated with thymosin β4 [200, 201]. Thymosin β4 has also been shown to increase migration of keratinocytes and epithelial cells [202, 203], as well as certain cancer cells [173, 204]. The effect is not general however, as migration of primary fibroblasts, smooth muscle cells and leukocytes is not affected by thymosin β4 treatment [201]. Thymosin β4 has been shown to stimulate directional migration of HUVECs and endothelial progenitor, indicating it can act as a chemoattractant [175, 201].

The mechanism of action through which thymosin β4 promotes migration is likely to be complex, with ILK signalling, Ku80 and F1F0 ATP synthase (sections 1.3.2.2 and 1.3.2.4) all implicated in thymosin β4-induced cell migration [173, 194, 205, 206]. In particular, the recruitment and activation of ILK at the focal adhesion complex has been found to coordinate with the actin-sequestering role of thymosin β4 to induce migration of endothelial cells [205]. At the leading edge of migrating cells, thymosin β4 dissociates from G-actin, which both frees up G-actin for filament elongation, a requirement of cell migration, and also allows thymosin β4 to interact with PINCH and ILK [205]. This leads to initiation of the PI3K-ILK-Akt signalling pathway, inducing downstream expression of matrix metalloproteinase-2 (MMP-2); an enzyme which promotes migration through the degradation of matrix proteins [205]. Thymosin β also up-regulates expression of other MMPs, including MMP-1, MMP-7 and MMP-9, to promote cell migration [203, 206, 207].

1.3.3.2 Angiogenesis

A major role of thymosin β4, which is of clinical interest, is its ability to promote angiogenesis. The ability of thymosin β4 to promote endothelial cell migration is evidently important in this respect, however thymosin β4 is further implicated in the function of endothelial cells. Thymosin β4 mRNA levels are up-regulated in HUVECs that are plated on Matrigel basement membrane matrix, concurrent with enhanced tubule formation [200]. This tubule formation is an *in vitro* process involving endothelial cell differentiation, which is used to model angiogenesis [200]. Exogenous thymosin β4 treatment further enhances tubule formation, illustrating thymosin β4's ability to promote endothelial cell differentiation [184]. Additionally, exogenous thymosin β4 treatment was found to increase proliferation of HUVECs and increase HUVEC attachment to matrix proteins, including laminin and collagen [184].

Thymosin β4's role in the promotion of angiogenesis has been further demonstrated in *ex vivo* and *in vivo* models of angiogenesis. Thymosin β4 increases capillary sprouting in an *ex vivo* chick aortic ring assay [208] and pig coronary artery ring assay [184], as well as increasing endothelial cell invasion into subcutaneous Matrigel plugs in mice, which is an *in vivo* model of angiogenesis [201].

Thymosin β4 has been found to up-regulate expression of vascular endothelial growth factor (VEGF), a pro-angiogenic growth factor, suggesting this may be part of the mechanism by which thymosin β4 promotes angiogenesis [209]. Recently, Notch signalling has been implicated in thymosin β4-induced VEGF expression and thymosin β4's promotion of angiogenesis, though the mechanism of this is unknown [183].

1.3.3.3 Wound healing

The ability of thymosin β4 to promote angiogenesis, along with the knowledge of its presence in human wound fluid [190], prompted investigations into the ability of thymosin β4 to enhance dermal wound healing [202]. Thymosin β4 treatment was been demonstrated to increase re-epithelialisation and enhance wound contraction *in vivo*, in a full thickness cutaneous wound model in rats, as

well as promoting angiogenesis [202]. Thymosin β4 stimulates keratinocyte migration *in vitro*, accounting for its ability to enhance re-epithelialisation [202]. Increases in collagen deposition were observed with thymosin β4 treatment in the *in vivo* wound model and this may contribute to the enhanced wound contraction [202].

Thymosin β4 has also been implicated in wound healing in the eye [203, 210]. Thymosin β4 is able to promote migration of human corneal epithelial cells *in vitro* [203, 207]. Further to this, thymosin β4 enhances re-epithelialisation *in vivo*, thus promoting healing, in rodent models of mild and severe corneal wounds [203, 210].

Thymosin β4 is present in human tears and saliva [211], as well as in wound fluid [190], suggesting it may act as an endogenous healing agent. Thymosin β4 also has antimicrobial properties [212], which may complement its role in wound healing.

1.3.3.4 Anti-inflammatory effects

In relation to its wound healing abilities, thymosin β4 also has anti-inflammatory effects. Thymosin β4 was first implicated as an anti-inflammatory agent when its oxidised form, thymosin β4-sulfoxide, was found to reduce neutrophil chemotaxis *in vitro* and attenuate footpad swelling in an *in vivo* mouse model of inflammation [196]. Further to this, thymosin β4 has been shown to reduce levels of inflammatory cytokines and chemokines, such as MIP-2, in a mouse model of severe corneal injury [210, 213]. In turn, thymosin β4 suppresses the infiltration of polymorphonuclear leukocytes, for which macrophage inflammatory protein-2 (MIP-2) is a known chemoattractant [213].

The mechanisms of thymosin β4's anti-inflammatory effects have since been investigated. In human corneal epithelial cells, thymosin β4 interferes with the p65 subunit of NFκB, preventing it from translocating to the nucleus [214]. This prevents NFκB from binding to and activating the promoter regions of genes for pro-inflammatory cytokines, including interleukin-8 (IL-8); the human homologue of MIP-2 [214, 215].

Thymosin β4's anti-inflammatory role has been extended to include septic shock in a study which observed decreased levels of thymosin β4 in the blood of septic shock patients [216]. In both rats and humans, lipopolysaccharide (LPS) treatment elicits a decrease in thymosin β4 blood levels [216]. Furthermore, mice pre-treated with thymosin β4 in LPS-induced septic shock models have reduced levels of tumour necrosis factor α (TNFα) and IL-1α, an indication of reduced inflammation [216]. This leads to increased survival of thymosin β4-treated animals compared to controls [216].

1.3.3.5 Anti-fibrotic effects

Ac-SDPK, the small peptide derived from thymosin β4 (section 1.3.2.5), has long been known to have anti-fibrotic effects [217-219]. More recently, thymosin β4 itself was noted to have anti-fibrotic effects in studies of dermal wound healing in rats [220]. Thymosin β4 treatment reduced the appearance of myofibroblasts in incisional wounds leading to minimal scarring once the wound had healed [220]. Recent studies have suggested that thymosin β4 could be utilised as an anti-fibrotic agent in the treatment of liver [221, 222], kidney [223] and lung diseases [224, 225].

1.3.3.6 Anti-apoptotic effects

Anti-apoptotic effects of thymosin β4 have been observed in a wide range of cell types, including human corneal epithelial cells [226-228], rat astrocytes [229], chick motor neurone cells [230], human intervertebral annulus cells [231], human gingival fibroblasts [232] and a human colon carcinoma cell line [233].

In human corneal epithelial cells, thymosin β4 treatment leads to reductions in activity of caspases-2, -3, -8 and -9, thus inhibiting apoptosis [226-228]. Exogenously applied thymosin β4 is internalised by these cells where it causes up-regulation of the anti-apoptotic protein, Bcl-2, and elicits a reduction in release of cytochrome C, the intrinsic initiator of apoptosis, from the mitochrondia [226, 227]. Thymosin β4 also inhibits apoptosis via increased Bcl-2 expression and decreased caspase-3 activity in rat astrocytes [229].

Furthermore, activity of caspase-3 and -9 are inhibited by thymosin β4 in human endothelial progenitor cells [171]. Thymosin β4 also increases expression of

Bcl-2 in human endothelial progenitor cells and additionally reduces expression of the pro-apoptotic protein, Bax [171]. These effects were found to be mediated by the PI3K-ILK pathway (section 1.3.2.2), leading to downstream eNOS signalling [171].

In SW480 colon carcinoma cells, over-expression of thymosin β4 has been demonstrated to reduce Fas ligand (FasL)-mediated apoptosis via production of MMP-7, which breaks down FasL itself [233]. Furthermore, thymosin β4 was found to up-regulate expression of survivin, which directly inhibits caspase 9 [233].

1.3.3.7 Thymosin β4 and stem cells

Thymosin β4 has been noted to stimulate certain effects by activating stem and progenitor cells. Thymosin β4 is endogenously present in rat hair follicle stem cells and exogenous application of thymosin β4 simulates the migration and differentiation of these cells *in vitro* [234]. When applied topically in rodent models of both normal and impaired hair growth, thymosin β4 treatment elicits increased hair growth [234].

Further to this thymosin β4 induces the differentiation of rat neural progenitor cells to form oligodendrocytes, which occurs through activation of p38 MAPK signalling. Thymosin β4 also inhibits apoptosis of these neural progenitor cells [179].

More recently, thymosin β4 has been found to stimulate murine omental progenitor cells to form smooth muscle and endothelial cells and to promote the migration and proliferation of these cells [235]. Furthermore, thymosin β4 has been shown to stimulate the differentiation of human dental pulp stem cells [236] and to enhance proliferation of human adipose tissue-derived stem cells [237].

1.3.3.8 Thymosin β4 in cancer

While many of the physiological roles of thymosin β4 are beneficial in terms of healing and tissue regeneration, the same roles have an undesirable impact in cancer. Thymosin β4 is present in primary tumours and metastases of various

cancers and is associated with increased metastatic potential, enhanced tumour growth and tumour recurrence [204, 209, 238-241]. However, clinical safety trials suggest thymosin β4 treatment does not itself cause cancer [242].

In mouse metastatic lung tumour cells, thymosin β4 increases cell migration *in vitro* and enhances angiogenesis *in vivo*, though it has no effect in *in vitro* cell invasion assays or on *in vitro* cell proliferation [209].

In SW480 human colon carcinoma cells on the other hand, thymosin β4 enhances growth rate and cell invasion both *in vitro* and *in vivo* in mice, in addition to increasing cell migration [239, 243]. Thymosin β4-induced migration in SW480 cells involves ILK signalling [173], while Ku80 (section 1.3.2.2) has been shown to be important in migration of other colon carcinoma cells [206]. As previously mentioned, thymosin β4 also protects SW480 cells from apoptosis [233].

More recently, thymosin β4 has been implicated in induction of epithelial to mesenchymal transition (EMT) of cancer cells, a process which involves the loss of E-cadherin, allowing cells to detach from the primary tumour and metastasise [244, 245]. Signalling of thymosin β4 through PINCH and ILK has been implicated in thymosin β4-induced EMT [244, 245].

While in solid tumours, thymosin β4 is pro-tumorigenic, in multiple myeloma, thymosin β4 has tumour suppressive effects, including decreased proliferation and migration of murine multiple myeloma cells [246].

1.3.3.9 Thymosin β4 as a therapeutic agent

The effects of thymosin β4 have prompted clinical investigations into thymosin β4 treatment in several models of disease.

Following the discovery of thymosin β4's ability to promote wound repair in the skin and eye (section 1.3.3.3), thymosin β4 has been shown to enhance healing of skeletal muscle injury in mice [247], ligament injury in rats [248], and following tooth extraction in rats [249]. Furthermore, thymosin β4 has been demonstrated to enhance bone formation in rats [249, 250].

In terms of dermal wound healing, thymosin β4 is now in clinical trials for treatment of venous stasis ulcers and pressure ulcers and has been shown to promote accelerated wound healing in phase II trials [251, 252].

Neuroprotective effects of thymosin β4 have also been demonstrated in models of excitotoxicity [253], multiple sclerosis [254], traumatic brain injury [255, 256], and stroke [257].

One of the first organs in which thymosin β4 was found to have therapeutic potential was the heart.

1.4 Thymosin β4 in the heart

1.4.1 Thymosin β4 in heart development

Thymosin β4 mRNA and protein are expressed in the developing murine heart [170]. Smart and colleagues have illustrated the importance of thymosin β4 in the heart during development by performing cardiac-specific knock-downs of thymosin β4 in mice [258]. Transgenic mice were created to conditionally express thymosin β4-targeting short hairpin RNAs (shRNAs) in either Nkx2-5 expressing cells, to target the majority of cardiomyocytes, or in myosin regulatory light chain 2, ventricular/cardiac muscle isoform (MLC2v) expressing cells, to specifically target ventricular cardiomyocytes [258]. Both knock-downs resulted in heart defects from around embryonic day 10 and in severe cases led to death and resorbtion of the embryo, illustrating the importance of endogenous thymosin β4 in the heart during development [258].

Knock-down of thymosin β4 led to defects in the epicardium, the outer layer of the heart, followed by defects in the myocardium [258]. The coronary vasculature is derived from the epicardium through the differentiation of epicardial progenitors into endothelial and smooth muscle cells which migrate into the myocardium to form the coronary vasculature. In thymosin β4 knock-down mice, however, epicardium-derived endothelial and smooth muscle cells fail to migrate into the myocardium to form vessels [258]. The subsequent defects seen in the myocardium were suggested to be due to this lack of vasculogenesis [258].

Furthermore, thymosin β4 mRNA was not detected in the epicardium, suggesting the epicardial phenotype seen upon cardiomyocyte-specific knock-down of thymosin β4 is due to release of thymosin β4 from cardiomyocytes acting in a paracrine fashion on epicardial cells [258]. In support of this, thymosin β4 treatment elicited increases in the outgrowth of smooth muscle and endothelial cells from *in vitro* epicardial explant cultures, taken from wild-type embryonic mouse hearts [258].

A recent study has presented findings contrary to those of Smart and colleagues, showing no essential role for thymosin β4 in murine heart development [259]. Banerjee and colleagues generated both global and cardiomyocyte-specific knockout mice by homologous recombination of the thymosin β4 gene and found no phenotype compared to controls [259]. The authors suggest that off-target effects of the shRNAs used by Smart and colleagues could account for the phenotype previously seen [259].

However, an alternative conclusion is that compensatory effects account for the lack of phenotype in the Banerjee study. Since 100% knock-down was not achieved by the shRNAs used by Smart and colleagues, such compensatory mechanisms may not have been activated. The effects of thymosin β4 knock-down reported in their study are supported by the observation of disrupted filamentous actin in the hearts of knock-down mice, an effect consistent with thymosin β4's established role in actin sequestration (section 1.3.2.1) [258]. Additionally, the epicardial phenotype seen in Smart and colleagues' knock-down mice is consistent with their *in vitro* data demonstrating the ability of thymosin β4's to stimulate epicardial cells [258]. Furthermore they confirmed the expression of thymosin β10, which has high homology with thymosin β4, was unaffected by their knock-downs, suggesting off-target effects are unlikely, though not ruling them out completely [258].

1.4.2 Activation of adult epicardial progenitor cells

Further to the endogenous role of thymosin β4 in activating the epicardium during development of the murine heart, Smart and colleagues demonstrated the ability of thymosin β4 to activate adult murine epicardial progenitor cells

[258, 260]. This led to differentiation of these progenitor cells into endothelial cells, smooth muscle cells and fibroblasts both *in vitro* and *in vivo*, where the mature cells contributed to new vessel growth [258, 260].

The ability of thymosin β4 to activate the adult epicardium has been supported by a study which showed that, in adult mice, systemic thymosin β4 treatment enhances levels of blood vessel epicardial substance (BVES), a protein associated with epicardial-derived cells [261]. Concurrently, epicardial thickness was enhanced and vessel growth from the epicardium was stimulated [261]. This activation of the epicardium and stimulation of vessel growth by thymosin β4 was found to be dependent on activation of the protein kinase C (PKC) signalling pathway [261]. Thymosin β4 treatment also increased expression of Wilms tumour protein homolog (Wt-1) and T-box transcription factor TBX18, markers of epicardial progenitor cells, again in a PKC dependent manner [261].

During development, epicardial progenitor cells have the capacity to produce cardiomyocytes in addition to producing cells that contribute to the heart vessels [262, 263]. While Smart and colleagues originally demonstrated the ability of adult epicardial progenitors to produce endothelial, smooth muscle and fibroblast cell types upon treatment with thymosin β4, they later found that if thymosin β4 is used to prime epicardial progenitors prior to heart injury, in an *in vivo* mouse model, then upon injury the progenitors will additionally produce cardiomyocytes [264]. This contributes to increased heart function post-injury with thymosin β4 pre-treatment compared to controls [264]. However, if thymosin β4 treatment is given post-injury, it does not stimulate epicardial cells to produce cardiomyocytes, though the beneficial effects, including increased vessel density and reduced infarct size, are still seen [265].

1.4.3 Cardioprotective effects of thymosin β4

While studies have demonstrated the ability of thymosin β4 to induce vessel growth through activation of progenitor cells in the heart, other cardioprotective effects of thymosin β4 have also been described.

As well as inducing vessel growth through progenitor cell activation, thymosin β4 stimulates migration of endothelial cells in *ex vivo* murine heart explants and

enhances Matrigel-induced tube formation of human coronary endothelial cells, as it does with HUVECs (section 1.3.3.2), indicating thymosin β4 is pro-angiogenic in the heart [170, 261].

Following a myocardial infarction, healthy myocardial tissue is replaced by non-functional fibrous, scar tissue. Ac-SDKP, the short peptide derived from thymosin β4 (section 1.3.2.5), has an inhibitory effect on inflammation and fibrosis in a rat model of myocardial infarction-induced heart failure [266]. Ac-SDKP was found to reduce macrophage infiltration and inhibit deposition of collagen, but did not have an effect on cardiac function in this *in vivo* model [266]. More recently, thymosin β4 itself has been found to reduce expression of pro-fibrotic genes, including collagen type-1 and collagen type-3, under conditions of oxidative stress [267]. Further to this, thymosin β4 enhanced survival of rat neonatal cardiac fibroblasts and neonatal cardiomyocytes under oxidative stress by reducing levels of reactive oxygen species as well as inhibiting apoptosis, as indicated by a decrease in caspase-3 and Bax expression and an increase in Bcl2 expression [267, 268]. Thymosin β4 also reduced expression of pro-inflammatory genes in rat neonatal cardiomyocytes [268].

In the first study to assess the effects of thymosin β4 in an *in vivo* mouse model of myocardial infarction, thymosin β4 treatment reduced cardiomyocyte cell death and reduced scarring, leading to improved cardiac function post-infarction [170, 269]. Thymosin β4 was demonstrated to improve cardiomyocyte survival *in vitro* [170, 269], suggesting the reduced cardiomyocyte death seen *in vivo* is not an indirect effect due to increased angiogenesis, for example. Thymosin β4 also enhanced cardiomyocyte migration *in vitro* [170, 269]. These *in vitro* effects of thymosin β4 were demonstrated to be dependent on recruitment of the PINCH-ILK complex and activation of Akt (section 1.3.2.2). *In vivo*, thymosin β4 treatment increased levels of ILK and phosphorylated Akt, supporting the role of this signalling pathway in thymosin β4's cardioprotective effects [269]. More recently, the ability of thymosin β4 to improve cardiac function in mouse models of myocardial infarction have been corroborated by other groups [264, 265].

1.4.4 Thymosin β4 in endothelial progenitor cell therapy

Thymosin β4 has been further implicated in cardioprotection in a series of investigations which identified thymosin β4 as a key modulator of the cardioprotective effects of embryonic endothelial progenitor cells (eEPCs). eEPCs have been considered as a cell therapy for ischemic injury of the heart [270]. The effects of transplanted eEPCs were found to occur via the PI3K/Akt pathway [271, 272]. As thymosin β4 is known to activate the PI3K/Akt pathway (section 1.3.2.2), its expression in eEPCs was assessed; these cells were found to express high levels of thymosin β4 [271, 272]. Studies utilising a shRNA against thymosin β4 demonstrated that the cardioprotective effects of eEPCs are thymosin β4-dependent and can be mimicked by application of thymosin β4 itself [273, 274].

The thymosin β4-dependent effects of eEPCs are consistent with the roles of thymosin β4 reported in other studies and include the ability to increase cardiomyocyte survival and reduce endothelial cell apoptosis *in vitro*; increase endothelial cell activation *in vitro* and angiogenesis *in vivo*; reduce infarct size and improve cardiac output in *in vivo* models of myocardial infarction; and suppress the activity of inflammatory cells both *in vitro* and *in vivo* [273, 274]. A recent study has found that endothelial progenitor cells derived from peripheral blood of adult rats have similar protective effects in models of myocardial infarction, which are also mediated by the release of thymosin β4 [275].

1.5 Regulation of thymosin β4 protein expression

While several physiological roles for thymosin β4 are now well-established and the mechanisms of action of thymosin β4 are starting to be elucidated, less is known about regulation of thymosin β4 expression.

Several factors, both endogenous and synthetic, have been found to up- or down-regulate thymosin β4 mRNA and protein levels when exogenously applied to various mammalian cell types. Factors including nerve growth factor [276], hepatocyte growth factor [277], growth hormone [278], IL-18 [279], dexamethasone [280], and certain non-steroidal anti-inflammatory drugs [281]

have all been shown to up-regulate thymosin β4 levels. Interferon-γ [192], 1,25-dihydroxyvitamin D3 [280], and several anti-tumour drugs [282, 283] have been shown to down-regulate thymosin β4 levels. However the mechanisms by which these different factors regulate thymosin β4 expression have not been explored.

hMLH1 has been identified as an endogenous upstream regulator of thymosin β4 protein expression and localisation in human cells (section 1.3.2.3) [187]. hMLH1 up-regulates thymosin β4 protein levels, but whether its effect is direct or indirect has not been reported [187].

1.5.1 Post-translational regulation

The activity of thymosin β4 may be regulated post-translationally to some extent through formation of thymosin β4 sulphoxide and generation of the Ac-SDKP peptide (section 1.3.2.5). While thymosin β4 does contain amino acid residues that can be acetylated and phosphorylated, studies have not been carried out to assess whether these post-translational modifications have any functional effect [284].

1.5.2 Transcriptional regulation

The primary level of regulation of a protein's expression is at the transcriptional level; that is control over expression of the gene that codes for the protein, leading to production of mRNA transcript. Transcription factors are molecules which bind to *cis*-acting regulatory sequences of DNA known as response elements, located in promoter regions. These response elements are termed enhancers or silencers depending on whether they lead to up- or down-regulation of transcription.

Androgen receptor is a transcription factor which is activated when bound by androgens. In human prostate cancer cells, androgens, including dihydrotestosterone, were found to down-regulate transcription of the thymosin β4 gene in an androgen receptor-dependent manner [285]. However, no steroid response element, the site recognised by androgen receptor, was found upstream of the thymosin β4 gene [285]. This may suggest that androgen

receptor, which has known interactions with other transcription factors [286, 287], down-regulates transcription of thymosin β4 in an indirect manner [285].

The transcription factor NFκB has been implicated in the up-regulation of thymosin β4 protein and mRNA levels in a murine melanoma cell line [288]. However, whether this is a direct effect of NFκB on transcription of thymosin β4 has not been explored [288].

More recently, heart- and neural crest derivatives-expressed protein 1 (HAND1), a basic helix-loop-helix transcription factor, has been identified as a direct regulator of the thymosin β4 gene in mice [289]. HAND1 was demonstrated to bind directly to the upstream promoter region of the murine thymosin β4 gene [289]. Furthermore, HAND1 could bind to different response elements, thus eliciting either activation or repression of transcription of the thymosin β4 gene [289].

Further to this, Nanog, a transcription factor of importance in maintenance of pluripotency, has recently been found to down-regulate transcription of the thymosin β4 gene in human cell lines [290]. A Nanog binding site was predicted to be present in the promoter of the thymosin β4 gene by *in silico* analysis, however direct binding of Nanog to the promoter of the thymosin β4 gene was not experimentally demonstrated [290].

1.5.3 Post-transcriptional regulation

The secondary level of regulation of protein expression is post-transcriptional and involves mechanisms which act upon mRNA transcript to prevent translation to protein.

For translation to occur the m^7GpppG cap which characterises the 5' end of an mRNA molecule must be bound by the cap-binding complex, which is formed of several molecules called eukaryotic initiation factors (eIF). The m^7GpppG cap itself is recognised by eIF4E, while the poly(A) tail found at the 3' end of a mature mRNA is bound by poly(A) binding protein (PABP) if the poly(A) tail is of a suitable length [291]. eIF4G, another member of the cap-binding complex, interacts with both eIF4E and PAPB, leading to recruitment of eIF4A, the final

member of the cap-binding complex, and causing circularisation of the mRNA molecule [291].

These events facilitate the attachment of the 40S ribosomal subunit, which is part of the pre-initiation complex, to the mRNA molecule. Once the 40S ribosomal subunit is bound, other members of the pre-initiation complex, including the 60S ribosomal subunit, are recruited. The pre-initiation complex then scans the 5'-UTR for an initiation codon (AUG), from which translation is commenced. The cap-binding complex and pre-initiation complex are illustrated in Figure 1.2.

RNA-binding proteins are proteins with many functions including post-transcriptional control. They can target either the 5'- or 3'- untranslated region (UTR) of an mRNA molecule, typically down-regulating or inhibiting translation. Different RNA-binding proteins regulate translation in different ways.

5'-UTR repressor proteins bind to secondary structures in the 5'-UTR, leading to steric hindrance of either the interaction between the 40S ribosomal subunit and the cap-binding complex or of the pre-initiation complex during 5'-UTR scanning [292, 293].

Other RNA-binding proteins act on the 3'-UTR. One of the most well characterised of these is cytoplasmic polyadenylation-element binding protein (CPEB). CPEB binds to RNAs which contain a specific sequence called the cytoplasmic polyadenylation-element (CPE) in their 3'-UTR. When bound, CPEB recruits additional molecules which compete with EIF4G for binding of EIF4E, thus preventing formation of the cap-binding complex [294]. This leads to repression of translation [295]. Other RNA-binding proteins have been found to repress translation in a similar manner [296, 297].

Interestingly, if CPEB is phosphorylated, it is also capable of mediating extension of the poly(A) tail, which leads to activation of translation [298, 299]. Thus, CPEB has the potential to both activate and supress translation.

No RNA-binding molecules have been reported to specifically regulate thymosin β4 expression.

More recently, microRNAs (miRNAs) have been described as a group of major endogenous post-transcriptional regulators in eukaryotic cells, through a process known as RNA interference.

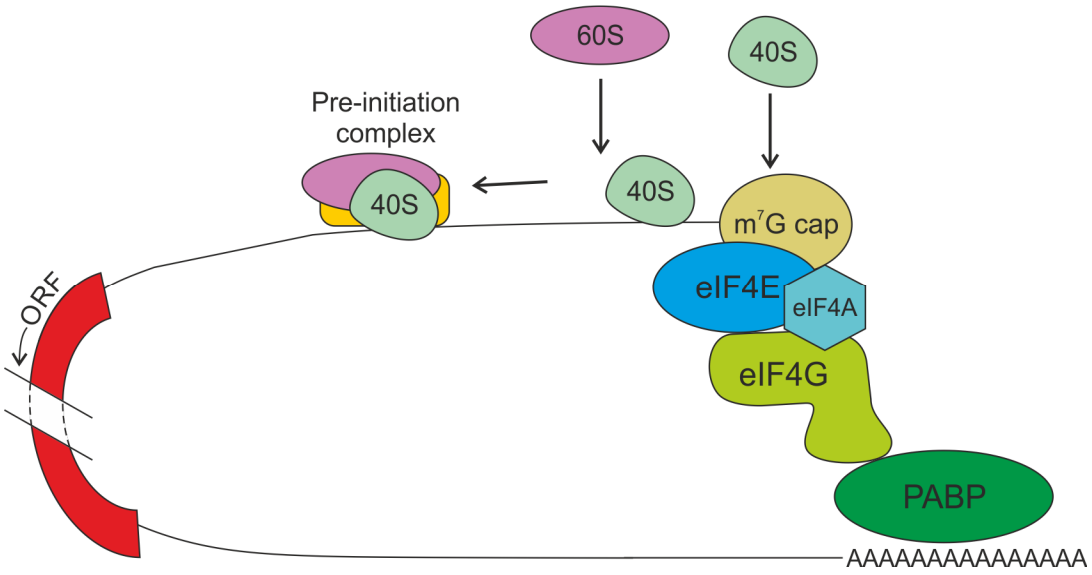

Figure 1.2 – Diagrammatic representation of initiation of translation

The m7G cap is bound by eukaryotic initiation factor (eIF) 4E, while the poly(A) tail is bound by poly(A) binding protein (PABP). These factors are bound by eIF4G leading to recruitment of eIF4A and circularisation of the mRNA molecule. Once this cap-binding complex has formed the 40S ribosomal subunit is recruited to the m7G cap and once it is bound to the mRNA molecule the 60S ribosomal subunit and other members of the pre-initiation complex are recruited. The pre-initiation complex scans for an initiation codon, leading to translation of the mRNA molecule. ORF; Open reading frame.

1.6 microRNAs

1.6.1 microRNA synthesis and processing

miRNAs are endogenous small RNAs of approximately 22 nucleotides [300-302]. They are transcribed from the genome as long primary precursors or 'pri-miRNAs', the sequences of which may be found in the introns of protein-coding genes or in intergenic regions [303, 304]. These pri-miRNAs are processed within the nucleus into approximately 70 nucleotide-long, stem-loop structured precursor miRNAs (pre-miRNAs) by Drosha, an RNAse III enzyme which functions as part of a multi-protein complex [302, 303, 305]. The pre-miRNAs are transported to the cytoplasm by Exportin 5 where they are further processed by another RNAse III enzyme, Dicer, into mature miRNAs duplexes [303, 306].

miRNA duplexes, which consist of what are known as the miRNA and miRNA* strands, are unwound and the two strands separated. The miRNA strand is the strand which then becomes incorporated into what is known as an RNA-induced silencing complex (RISC), while the miRNA* strand is discarded. Strand selection is determined by characteristics such as the thermodynamic stability of the miRNA duplex ends and the nucleotide content of each strand [307]. In some cases both the miRNA and miRNA* strands can form functioning RISC complexes [308]. In these cases miRNAs are named with a '-5p' or '-3p' suffix indicating whether they are derived from the 5' or 3' arm of the duplex.

The process of strand separation and incorporation of the miRNA strand into RISC appears to be directly coupled to pre-miRNA processing by Dicer and is mediated by the proteins which constitute RISC itself [309, 310]. Key proteins, in addition to Dicer, are recruited to the pre-miRNA, leading to generation of a mature miRNA and formation of a functional RISC complex [309-312]. These proteins include RNA helicase A (RHA), which promotes association of the miRNA with other RISC members and may be responsible for unwinding the miRNA duplex; transactivation response RNA-binding protein (TRBP), which associates with Dicer and other members of RISC to facilitate RISC assembly; and Argonaute 2, which is the mediator of RISC-induced RNA cleavage [309-312]. miRNA processing and formation of RISC are illustrated in Figure 1.3.

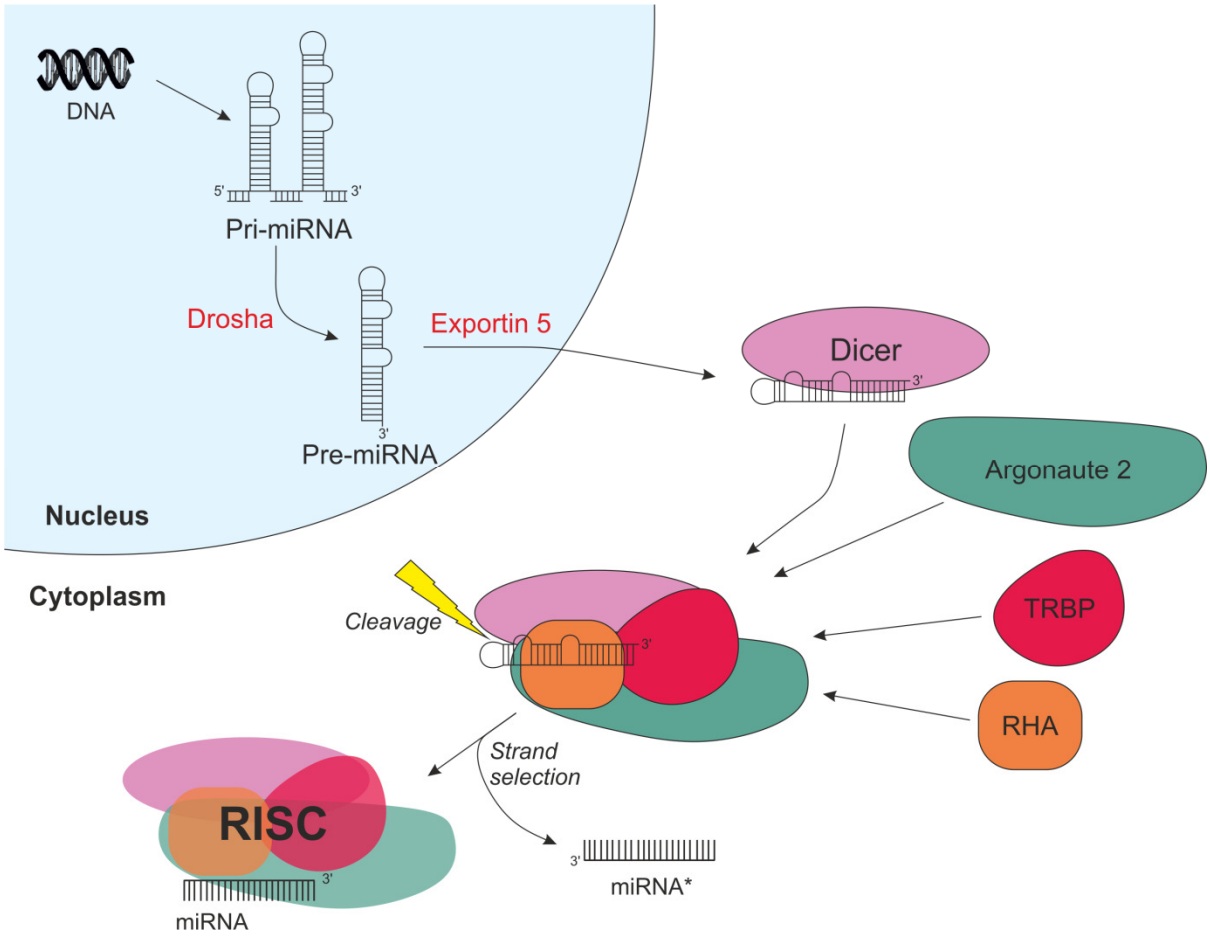

Figure 1.3 – Diagrammatic representation of miRNA processing and the formation of RISC

Primary precursor miRNAs (pri-miRNA) are transcribed from DNA and processed by Drosha within the nucleus to form precursor miRNAs (pre-miRNA). Exportin 5 transports the pre-miRNAs across the nuclear membrane and into the cytoplasm where the pre-miRNA is cleaved by Dicer, as part of RNA Induced Silencing Complex (RISC) formation, to form a single-stranded miRNA, which becomes part of RISC, and a single-stranded miRNA*, which is discarded. RHA; RNA Helicase A, TRBP; transactivation response RNA-binding protein. Adapted from Jeffrey [313].

1.6.2 Mechanism of action of microRNAs

Within the RISC complex, the miRNA acts through complimentary base pairing to direct the RISC to its target. miRNAs typically bind with imperfect complementarity to the 3'-UTR of an mRNA leading to down-regulation of expression, though exceptions have been reported [302, 314, 315]. miRNAs may lead to down-regulation of protein expression by either repressing translation of the mRNA or simply degrading the mRNA. In cases where miRNAs bind with perfect complementarity to their target, it is thought that the RISC complex will simply lead to cleavage by Argonaute 2 and degradation of the target mRNA [312, 316].

The mechanisms by which miRNAs that bind with imperfect complementarity cause suppression of mRNA expression are more contentious. Evidence has been provided for both mechanisms of translational repression and degradation of mRNA, independently of Argonaute 2-mediated cleavage. Argonaute 2 has a motif capable of binding the m7GpppG cap of mRNA (Figure 1.2) and as such may be able to compete with eIF4E (Figure 1.2) for cap-binding and thus prevent the initiation of translation [317, 318]. The miRNA RISC complex may also act by recruiting eIF6, which is known to inhibit the binding of the 60S ribosomal subunit to the pre-initiation complex, again preventing initiation of translation [319]. A third study suggests that inhibition of translation can occur post-initiation through induction of premature dissociation of the ribosomes from the mRNA [320].

In terms of mRNA degradation, a protein called GW182, which is implicated in miRNA-induced RNA interference, has been reported to mediate the deadenylation and decapping of mRNA, leading to its degradation [321, 322]. While some miRNAs appear to act purely at the level of translational repression, a reduction in mRNA levels through mRNA degradation has been reported to be the major mechanism by which miRNAs reduce protein levels endogenously [323-325].

1.6.3 Roles of microRNAs

miRNAs have many physiological roles including cell differentiation and determination of cell identity. In this respect many tissue-specific miRNAs have been identified [326, 327]. Furthermore, certain individual miRNAs have the ability to down-regulate hundreds of target mRNAs, when introduced to cells in *in vitro* systems, leading to changes in cell phenotype [323, 324]. While many different mRNAs may be targeted by a single miRNA the magnitude of the effect differs, with little change in expression seen for the majority of targets [324].

One of the first miRNAs to be identified in the heart was miR-1 [326]. Both miR-1 and mirR-499 are up-regulated in differentiated cardiomyocytes compared to foetal CPCs [328]. Introduction of miR-499 into CPCs leads to their differentiation into cardiomyocytes [328, 329]. No doubt due to this role in determining cell identity and differentiation, miRNAs have been found to be important in development, including within the heart [330].

Other miRNAs are involved in regulation of cellular processes such as proliferation [331, 332] and apoptosis [333, 334]. miRNAs regulate these processes effectively by regulating the expression of multiple proteins that have related functions. For example, miR-34 targets several genes involved in cell cycle progression to inhibit proliferation [335, 336].

While some miRNAs are part of large regulatory networks, others have much more specific physiological roles that are restricted by their expression in specific tissues or cells. For example miR-375 is only expressed in pancreatic islet cells, where it has a role in regulating insulin secretion [337].

Several miRNAs have also been associated with pathological conditions, including heart failure, in which expression of several miRNAs is dysregulated [338, 339]. In this respect, miRNAs may make good therapeutic targets, as they are easy to down-regulate in a highly specific manner. This can be done through use of anti-miRNA molecules which bind through complimentary base pairing and utilise endogenous RNA interference mechanisms to break down the target miRNA.

1.6.4 miRNAs and thymosin β4

An early study looking at thymosin β4 expression in thymocytes found that thymosin β4 protein levels could be rapidly increased with no change in mRNA levels and in the presence of actinomycin D, an inhibitor of transcription [340]. This may be an indication of a miRNA-mediated effect on thymosin β4 mRNA molecules.

The 3'-UTR of thymosin β4 contains highly conserved regions, which indicate that they may be of evolutionary importance. This supports the idea that thymosin β4 is regulated by the targeting of its 3'-UTR by miRNAs.

However, to date no thymosin β4-targeting miRNAs have been confirmed. Sequence complementarity for miR-1, a miRNA associated with heart and skeletal muscle, has been identified in the 3'-UTR of thymosin β4 [330]. However, while miR-1 can act upon the 3'-UTR of thymosin β4 in a luciferase reporter assay, thymosin β4 protein levels in the hearts of transgenic mice over-expressing miR-1 do not change, demonstrating that thymosin β4 is not a genuine target of miR-1 [330]. The authors attributed this finding to the fact that the complementary sequence of miR-1 within the 3'-UTR of thymosin β4 is in a relatively stable region, with low levels of free energy [330]. Authentic miRNA binding sites, however, are located in unstable regions where they are accessible to the miRNA, in addition to having a sequence complementarity to the miRNA [330]. This indicates that while *in silico* predictions provide a good starting point, experimental evidence is required to confirm the ability of miRNAs to down-regulate a given target, as well as providing physiological context.

In summary, thymosin β4 is a protein involved in endogenous repair mechanisms that is important in mammalian heart development and has multiple cardioprotective effects when applied exogenously in models of myocardial infarction. Furthermore, thymosin β4 has the capacity to activate progenitor cells within the heart, leading to production of new, functional cells. As such, elevating thymosin β4 levels within the heart may be an effective therapeutic strategy for regeneration and protection of the heart.

Identifying physiologically relevant thymosin β4-targeting miRNAs in the heart will not only improve understanding of how thymosin β4 is endogenously regulated but may also provide therapeutic miRNA targets, which may be down-regulated in order to enhance thymosin β4 expression in the failing heart.

1.7 Hypothesis

It was hypothesised that thymosin β4 is expressed in the foetal human heart and its expression is regulated by miRNAs.

1.8 Aims

The aims of this study were as follows:

1. To assess the expression and localisation of thymosin β4 within the foetal human heart.
2. To develop an experimental system in which thymosin β4-targeting miRNAs can be identified.
3. To identify putative thymosin β4-targeting miRNAs and demonstrate the ability of candidate miRNAs to down-regulate thymosin β4 levels.

Chapter 2: Methods

2.1 Foetal tissue and cells

2.1.1 Foetal tissue

Human foetal tissue was obtained with informed consent and full ethical approval (Southampton and West Hampshire Local Research Ethics Committee) from women undergoing termination of pregnancy at Royal South Hants Hospital, Southampton. Human foetal material was also provided by the Joint MRC/Wellcome Trust (grant #099175/2/12/2) Human Developmental Biology Resource (www.hdbr.org).

Foetal tissues obtained locally were collected, aged according to foot length and dissected by David Wilson, Kate Parry and Kelly Wilkinson.

Tissues to be used for RNA extraction were placed in RNase-free vials containing RNALater (Ambion) and stored at -20°C. Tissues to be used for protein extraction were placed in cryovials and stored at -80°C.

Heart tissue to be cultured was chopped into approximately 1 mm x 1 mm pieces using a McIlwain tissue chopper (Intracell). Pieces of tissue were placed into 6-well plates at an air-liquid interface: 1 ml cardiac medium (Table 2.1) was pipetted into each well, a tissue culture insert (PICM03050, Millipore) placed on top and the tissue placed on the membrane of the culture insert. Heart tissue was maintained in a 37°C in 5% CO_2/air incubator unless otherwise stated.

2.1.2 HeLa cells

HeLa cells (kindly provided by Ita O'Kelly's lab) were cultured in T75 tissue culture flasks in high glucose Dulbecco's Modified Eagle Medium (DMEM) containing 10% foetal bovine serum (FBS) and 1% penicillin/streptomycin antibiotics. Cells were maintained in a 37°C in 5% CO_2/air incubator unless otherwise stated.

Cells were passaged when 80-90% confluent: 0.05% Trypsin-EDTA was used to release cells from the plate, trypsin was neutralised using DMEM containing 10% FBS and the cell suspension collected and centrifuged at 1300 RPM for 3 mins to form a cell pellet. Supernatant was aspirated and the cell pellet re-suspended in an appropriate volume of medium; the cell suspension was then dispensed into the desired number of new T75 flasks. Cells were typically passaged at between 1:3 and 1:10 dilution. To collect HeLa cells for experiments, cell pellets were created in the same manner as when passaging the cells.

2.1.3 Human umbilical vein endothelial cells

2.1.3.1 HUVEC isolation

Human umbilical vein endothelial cells (HUVECs) were isolated from umbilical cords by Stefanie Inglis. Umbilical cords were first washed clean of blood. Umbilical veins were cannulated and perfused with phosphate buffered saline (PBS) to remove blood cells. The cord was tied off at the opposite end to the cannula and the umbilical veins perfused with 2 mg/ml pre-warmed (37°C) collagenase type II (Sigma) and incubated for 45-60 mins at room temperature. The collagenase was removed along with the detached endothelial cells and placed in HUVEC medium (Table 2.2) before being centrifuged at 400 G for 10 mins. The cells were re-suspended in HUVEC medium and seeded in a T25 tissue culture flask and placed in a 37°C in 5% CO_2/air incubator. The cells were washed with HUVEC medium the following day to remove contaminating blood cells.

2.1.3.2 HUVEC culture

HUVECs were provided in culture by Stefanie Inglis, typically at passage 4 or beyond. The cells were cultured in HUVEC medium (Table 2.2) and maintained in a 37°C in 5% CO_2/air incubator.

Cells were passaged when 80-90% confluent: 0.05% Trypsin-EDTA was used to release cells, trypsin was neutralised using HUVEC medium and the cell suspension collected and centrifuged at 1000 RPM for 5 mins to form a cell

pellet. Supernatant was aspirated and the cell pellet re-suspended in an appropriate volume of medium; the cell suspension was then dispensed into the desired number of new T75 flasks. Cells were typically passaged at a 1:3 dilution. To collect HUVECs for experiments, cell pellets were created in the same manner as when passaging the cells.

Table 2.1 – Cardiac medium

List of components, given at their final concentrations, used to make up cardiac medium. Media and supplements were from Gibco, unless otherwise stated.

Components (at final concentration)
High glucose DMEM
5% Foetal bovine serum
1X MEM non-essential amino acids
0.1 mM Vitamin C (Sigma)
0.1 nM Insulin (Sigma)
1X Penicillin/streptomycin

Table 2.2 – HUVEC medium

List of components, given at their final concentrations, used to make up HUVEC medium. Media and supplements were from Gibco, unless otherwise stated. Additional instructions are shown in italics.

Components (at final concentration)
Medium 199
0.4% Endothelial cell growth supplement/Heparin (Promocell)
1X Penicillin/streptomycin
10% Foetal bovine serum *(added on day of use)*

2.2 RNA extraction and reverse transcription

2.2.1 RNA extraction using TRIzol

Total RNA was isolated from tissue or cell pellets using TRIzol reagent (Invitrogen) or from cells in suspension using TriFast LS (peqGOLD).

For extraction from tissue, the tissue was removed from RNALater, placed in 1 ml TRIzol and ground up with a plastic tissue grinder.

For extraction from cell pellets, TRIzol reagent was added directly to the cell pellet and homogenised by passing through a micropipette tip several times.

For extraction from cells in suspension, the volume of cell suspension was measured and TriFast LS was added to give a 1:3 ratio of sample:TriFast LS and the solution mixed. The volumes of regents used throughout the rest of the RNA extraction protocol are per ml of the total volume of cell suspension/TriFast LS mixture.

Once samples were in TRIzol or TriFast LS they were incubated for 5 mins at room temperature. Samples were then centrifuged at 12,000 G for 10 mins and the supernatant transferred to a new RNase-free tube in order to remove any tissue or cell debris.

200 µl chloroform was added to each sample and the tubes were shaken vigorously for 30 secs. The samples were then left to stand at room temperature for 15 mins. The samples were next centrifuged at 12,000 G for 15 mins. The clear aqueous phase at the top of the tube contains the RNA and was transferred to new RNase-free tubes. 500 µl isopropanol and 1 µl glycogen was added to each sample and the samples incubated at -80°C for 30 mins.

The samples were next allowed to stand at room temperature for 15 mins and then centrifuged at 12,000 G for 15 mins at 4°C, so that an RNA pellet is formed. Keeping all samples on ice, the supernatant was removed and each cell pellet washed twice in 75% ethanol, which had been chilled at -20°C. Washing was carried out by adding the ethanol to each tube, leaving it to stand for 10 mins on ice and then centrifuging at 7,500 G for 10 mins at 4°C.

Finally, all the ethanol was removed and the pellets left to air dry for between 5 and 10 mins. The pellets were then re-suspended in 30 µl DEPC-treated water and treated with rRNasin RNase inhibitor (Promega). RNA concentrations and purity were assessed using a Nanodrop spectrophotometer. RNA samples were stored at -80°C.

2.2.2 RNA extraction from paraformaldehyde-fixed cells

2.2.2.1 Modified TriFast LS protocol

RNA extraction of paraformaldehyde (PFA)-fixed cells in suspension was carried out as in section 2.2.1, except after TriFast LS was added to the sample, 10 µl proteinase K (10 mg/ml) was added to each ml of sample/TriFast LS mixture. The samples were then heated using a dry heat block to 56°C for 15 mins, followed by 80°C for 15 mins. RNA extraction was then continued, omitting the 5 min room temperature incubation.

2.2.2.2 RecoverAll kit

RNA was extracted using a RecoverAll Total Nucleic Acid Isolation Kit for FFPE (Ambion). PFA-fixed cells in suspension were first centrifuged at 12,000 G for 5 mins to pellet the cells. The supernatant was removed, leaving a little behind to minimise the loss of cells. The manufacturer's protocol for the RecoverAll kit was followed, omitting steps relating to deparaffinization and beginning from the Protease Digestion steps, using 100 µl of digestion buffer. At the end of the protocol samples were eluted in 60 µl DEPC-treated water and stored at -80°C.

2.2.3 Reverse transcription of mRNA to cDNA

Between 200 ng and 1000 ng of each RNA sample to be reverse transcribed was treated with RQ1 RNase-free DNase (Promega), according to the manufacturer's instructions. Equal amounts of RNA were used for any samples to be compared in a quantitative manner. Samples were then reverse transcribed to cDNA using M-MLV Reverse Transcriptase (Promega) with Random Primers (Promega), according to the manufacturer's instructions. 'No reverse transcriptase' controls were created for each RNA sample by using

water in place of the reverse transcriptase enzyme. For each set of reverse transcription reactions carried out, a 'no template' negative control was carried out by adding water in place of template RNA. Once complete the reverse transcription products were stored at -20°C.

2.2.4 Reverse transcription of miRNAs to cDNA

Aliquots of RNA samples to be used in reverse transcription reactions for miRNAs were diluted down in DEPC-treated water to create 10 ng/µl aliquots. Reverse transcription was carried out using M-MLV Reverse Transcriptase reagents (Promega) along with specially designed stem-loop RT primers designed to reverse transcribe specific mature miRNAs, which are supplied in TaqMan MicroRNA Assays (Applied Biosystems) (Table 2.9).

Reaction mixtures were made up as indicated in Table 2.3 using the desired RNA template and specific RT primers for the miRNA to be reverse transcribed (Table 2.9). Reactions were carried out using the temperature steps indicated in Table 2.4. The reverse transcription products were then stored at -20°C.

2.2.5 Extraction of genomic DNA

Genomic DNA was extracted from foetal placental tissue by Kelly Wilkinson. This was done by adding 750 µl of DNA digestion buffer (50 mM Tris-HCl, pH 8.0; 100 mM EDTA, pH 8.0; 100 mM NaCl; 1% SDS) and 40 µl proteinase K to the tissue and incubating at 56°C overnight in a water bath. The following day the tissue was vortexed and agitated for 5 mins on a rocker before adding 250 µl of saturated NaCl solution. This was followed by 5 mins agitation on a rocker.

The sample was next centrifuged at 12,000 G for 10 mins and 1 ml of the supernatant transferred to a new tube. 500 µl isopropanol was added to the tube which was inverted several times before being centrifuged at 12,000 G for 10 mins. The supernatant was discarded and 500 µl of 70% ethanol was added to the DNA pellet. The sample was centrifuged at 12,000 G for 10 mins, the supernatant removed and the DNA pellet dried for 10 mins at 37°C. The pellet was then suspended in 100 µl Tris-EDTA buffer and the sample stored at -20°C.

Table 2.3 – miRNA reverse transcription reaction mixture

List of reagents used in reaction mixtures for the reverse transcription of miRNAs to cDNA. The volumes of each reagent are given per reaction. Reagents were from Promega, unless otherwise stated.

Reagents	Volume (µl)
10 mM dNTPs	0.075
M-MLV Reverse Transcriptase	0.125
5X RT Buffer	1.5
rRNasin RNase Inhibitor	0.047
DEPC-treated H_2O	3.753
RNA sample (10 ng/µl)	0.5
5X RT primers (TaqMan assays)	1.5

Table 2.4 – miRNA reverse transcription reaction temperature steps

The temperature steps used to carry out miRNA reverse transcription reactions are shown. Reactions were carried out using a G-Storm GS1 thermocycler.

Temperature	Time
16°C	30 min
42°C	30 min
85°C	5 min
10°C	Hold

2.3 PCR

Polymerase chain reaction (PCR) was carried out on cDNA or genomic DNA samples for the amplification and detection of specific DNA sequences. GoTaq polymerase (Promega) was used in combination with dNTPs and specifically designed primers (Table 2.5) in order to amplify the desired transcript or region of genomic DNA. Primers were designed using PrimerSelect (Lasergene 8; DNASTAR Inc.).

PCR was carried out using a G-Storm GS1 thermocycler, using the temperature cycles indicated in Table 2.6, with the appropriate annealing temperature for the primers being used (Table 2.5).

The PCR products obtained were separated by running them on 100 ml, 2% agarose gels, made up in Tris-acetate-EDTA buffer and containing 5 µl of Nancy-520 (Sigma Aldrich). An in-house 100 bp ladder or 1kb HyperLadder (Bioline) was also run on each gel. Gels were run in Tris-acetate-EDTA buffer at between 70 and 80 V, until the products and ladder were resolved. Gels were imaged using a High Performance Ultraviolet Transilluminator (UVP) and the associated DocIT software (UVP).

2.3.1 Purification of PCR products

To extract resolved PCR products for sequencing or downstream protocols, the appropriate product band was excised and the DNA purified. To do this, the DNA bands were visualised using a High Performance Ultraviolet Transilluminator (UVP), keeping exposure to the UV light to a minimum. The band of interest was excised using a clean scalpel and taking as little of the surrounding agarose as possible. The DNA in the excised band was then purified using a Wizard SV gel and PCR clean-up system (Promega), according to the manufacturer's instructions. Once purified the DNA samples were quantified using a Nanodrop spectrophotometer.

2.3.1.1 Sanger sequencing

Purified PCR products or plasmid DNA samples were sent to Source Bioscience LifeSciences for Sanger sequencing, along with custom primers if required. DNA samples were diluted down to the specifications of the sequencing company where possible, as were primers that were sent for use in sequencing. The pCR2.1-TOPO vector was sequenced using M13 reverse primers, which Source Bioscience LifeSciences keep in stock.

2.3.1.2 Sequence alignment analysis

MegAlign software (Lasergene 8; DNASTAR Inc.) was used to carry out *in silico* sequence alignment analysis. Sequences were aligned using the Clustal W method.

2.4 Quantitative PCR

Relative gene expression of samples was determined by carrying out quantitative PCR (qPCR) on cDNA, using TaqMan Gene Expression Assays (Applied Biosystems) (Table 2.7) with TaqMan Universal PCR Master Mix (Applied Biosystems). All reactions were carried out in triplicate.

A Roche LightCycler 480 machine was used to perform the reactions, using the temperature cycles shown in Table 2.8. The fluorescence of each sample, which relates to the quantity of cDNA in that sample, was detected by the machine after each cycle. The software used plots of fluorescence at each cycle to generate cycle threshold (Ct) values: the cycle number at which a threshold level of fluorescence is reached. The average Ct value of triplicates was used in further analysis, unless an outlier was present within the triplicates, in which case it was excluded. The lower the Ct value, the more starting template was present in the sample.

To assess the expression of a gene of interest, the Ct value for the gene of interest was normalised to the mean Ct value of the endogenous control genes for each sample. The normalised gene expression of each sample was then expressed as a fold change compared to the average normalised value of the

experimental control samples. By comparing each individual sample to the average of the experimental control samples, the variation in individual experimental control samples can still be seen.

As Ct values are logarithmic values they must be transformed to give linear data. The following equation describes how the data is transformed, normalised against the housekeeping genes and expressed relative to the experimental control samples:

$$\text{Relative expression} = 2^{-\Delta\Delta Ct}$$

Where:

$$\Delta\Delta Ct = \Delta Ct_{(\text{target sample})} - \Delta Ct_{(\text{mean of control samples})}$$

$$\Delta Ct = Ct_{(\text{target gene})} - \text{mean } Ct_{(\text{endogenous control genes})}$$

For ease of use, the equation for relative expression can also be rearranged as follows:

$$\text{Relative expression} = 2^{-\Delta Ct(\text{target sample})} / \text{mean } (2^{-\Delta Ct(\text{control samples})})$$

2.4.1 TaqMan MicroRNA assays

Relative expression of miRNAs in samples was determined by qPCR, in a similar manner as above, using TaqMan MicroRNA assays (Applied Biosystems) (Table 2.9) with TaqMan Universal PCR Master Mix II, no UNG (Applied Biosystems). Specifically created cDNA samples for each miRNA to be assessed were used as template (section 2.2.4).

A Roche LightCycler 480 machine was used to perform the reactions, using the temperature cycles shown in Table 2.10. Ct values were obtained and used to calculate normalised expression relative to control samples, as above.

Table 2.5 – PCR primers

The primer pairs used in PCR are listed, including the full primer sequences and the annealing temperature used for PCR.

Primer pair	Primer	Sequence	Annealing temperature
TMSB4X primers	Forward	5'- GAAGACAGAGACGCAAGAGAAAAA -3'	58°C
	Reverse	5'- TGCCAGCCAGATAGATAGACAGAT -3'	
Long 3'UTR primers	Forward	5'- GGCGAATCGTAATGAGGC -3'	45°C
	Reverse	5'- TTTTTTTTTTTTTTTTTTTTA -3'	
Short 3'UTR primers	Forward	5'- GGCGAATCGTAATGAGGC -3'	49°C
	Reverse	5'- TTTTTTTTTTTTTTTTTTTC -3'	
OAZ1 primers	Forward	5'- GGCGAGGGAATAGTCAGAGG -3'	58°C
	Reverse	5'- GGACTGGACGTTGAGAATCC -3'	
TMSB4X 3'UTR primers	Forward Reverse	5'- GCTAGCCGCCAATATGCACTGTACATTCC -3' 5'- GCGGCCGCAGAAACCAAACAGACACACCAGC -3'	63°C
pRL-TK 3'UTR primers	Forward	5'- TCGGACCCAGGATTCTTTTC -3'	58°C
	Reverse	5'- CTGCATTCTAGTTGTGGTTTGTC -3'	

Table 2.6 – PCR temperature steps

Details of the temperature steps performed on a G-Storm GS1 thermocycler for the amplification of cDNA by PCR.

	Temperature	Time
Step 1	95°C	5 mins
Step 2	94°C	1 min
Step 3	Annealing temp. (Table 2.5)	1 min
Step 4	72°C	1 min
Repeat steps 2-4 35 times		
Step 5	72°C	10 min
Step 6	10°C	Hold

Table 2.7 – TaqMan Gene Expression Assays

List of TaqMan Gene Expression assays (Applied Biosystems) used in qPCR to detect expression of the genes listed.

Gene	TaqMan Assay ID
TMSB4X	Hs03407480_gH
GNB2L1	Hs00272002_m1
PGK1	Hs00943178_g1

Table 2.8 – qPCR temperature steps

Details of the temperature steps performed on a Roche LightCycler 480 machine for the amplification and relative quantification of cDNA by qPCR.

	Temperature	Time
Step 1	50°C	2 mins
Step 2	95°C	10 mins
Step 3	95°C	15 secs
Step 4	60°C	1 min
Repeat steps 3-4 50 times		

Table 2.9 – TaqMan MicroRNA Assays

List of TaqMan MicroRNA assays (Applied Biosystems) used in qPCR to detect expression of miRNAs or the endogenous control.

TaqMan MicroRNA Assay Name
hsa-miR-148b
hsa-miR-199a-3p
hsa-miR-217
hsa-miR-495
RNU48

Table 2.10 – MicroRNA assay qPCR temperature steps

Details of the temperature steps performed on a Roche LightCycler 480 machine for the relative quantification of miRNA expression by qPCR.

	Temperature	Time
Step 1	95°C	10 mins
Step 2	95°C	15 secs
Step 3	60°C	1 min
Repeat steps 2-3 50 times		

2.5 Immunohistochemistry

2.5.1 Tissue fixation and embedding

Tissue fixation and embedding was carried out by David Wilson, Kelly Wilkinson and Kate Parry. Tissue collected for sectioning and staining was fixed in either PFA or methanol-acetic acid (MeAc). The tissue was incubated at room temperature overnight in either 4% PFA or a 2:2:1 mixture of methanol, acetic acid and DEPC-treated water, as appropriate.

The following day the fixative was discarded and the tissue was dehydrated by treating with 70%, then 80%, then 90% and finally 100% ethanol for 2 hours each. The tissue was then left in 100% chloroform overnight.

The following day the tissue was embedded in wax, by placing in a tube of paraffin wax for 2 hours at 72°C. The wax was replaced and the tissue left for a further 2 hours at 72°C. The wax was replaced again and left for a further 2 hours at 72°C, this time under vacuum. The tissue was then placed in a metal cassette which was filled with wax and left on a cold plate to set for 30 mins. Embedded tissue blocks were stored at 4°C.

2.5.2 Tissue sectioning and mounting

Ribbons of embedded tissue blocks were cut using a Leica rotary microtome. The sections were mounted onto cleaned, aminoalkylsilane-coated slides. This was done by floating the sections on the slides with water and placing the slides on a surface heated to 42°C, removing any wrinkles from the sections. The water was then removed using a vacuum pump and the slides were incubated at 37°C overnight. The mounted sections were stored at 4°C. Four sections were mounted on each slide and every ninth section was placed on a ‘H&E slide’, specifically set aside for haematoxylin and eosin (H&E) staining.

2.5.3 Immunofluorescent staining

Sections were de-paraffinised and rehydrated by treatment for 2 mins each with two xylene washes, 100% ethanol, 90% ethanol, 70% ethanol and finally

distilled water. If required, antigen retrieval was then carried out. The antigen retrieval treatment involved boiling slides in 0.01M sodium citrate solution (pH 6.0) plus 0.05% Tween 20, for between 5 and 20 mins. Slides were then allowed to cool for 20 mins before being washed in PBS.

Sections were then stained by incubating with the appropriate primary antibodies (see Table 2.11) diluted in PBS with 0.1% Triton X-100 and 3% goat serum, overnight at 4°C. The following day, sections were treated with the appropriate secondary antibodies (see Table 2.11), diluted in PBS + 0.1% Triton X-100, for 1 hour at room temperature. For triple staining, secondary antibody incubations were carried out consecutively, if required, to prevent cross-reactivity. Again, slides were washed with PBS before and after antibody treatment. Finally the sections were dehydrated by 2 min treatments in 70%, 90% and then 100% ethanol followed by two 2 min treatments in xylene. Sections were placed in 100% ethanol before being mounted and the nuclei counterstained using Vectashield Mounting Medium with DAPI (Vector Laboratories) and the slides sealed with a coverslip. The stained slides were stored at 4°C. Secondary antibody alone negative controls were stained only with the appropriate secondary antibodies and were treated with PBS plus 0.1% Triton X-100 during the primary antibody treatment step.

2.5.3.1 Blocking of thymosin β4 antibody

In order to ensure the anti-thymosin β4 antibody used was detecting thymosin β4, it was blocked with synthetic thymosin β4. This was done by incubating the desired amount of antibody with 0.0125 µg/µl of synthetic thymosin β4 (Immundiagnostik, A9522AG.1) for 30 mins on ice. The solution was then centrifuged to pellet immune complexes and the supernatant collected and made up in the same manner as the usual primary antibody solutions.

2.5.4 Haematoxylin and eosin staining

Sections were deparaffinised and rehydrated by treating twice with xylene for 3 mins and for 2 mins each in 100% ethanol, 90% ethanol and distilled water. The slides were then placed in filtered haematoxylin for 5 mins before washing in copious amounts of running water for 5 mins, to remove excess haematoxylin.

The sections were then stained with eosin for 2 mins, washed twice for 2 mins in water and finally dehydrated by 2 min treatments in each of 90% ethanol, 100% ethanol and two xylene washes. Sections were mounted in Entellan (Merck Millipore), sealed with a cover slip and left to dry for 1 hour. The stained slides can be stored at 4°C.

2.5.5 Imaging

Fluorescence and bright field images were captured using a Zeiss fluorescence microscope with an axiocam colour camera and using Axiovision software (Carl Zeiss Imaging Solutions). For each image taken, a negative control image was taken of the same region of the tissue from an adjacent section treated with the secondary antibody alone.

Confocal fluorescence images were also taken using a Leica SP5 confocal microscope using the associated Leica Application Suite (Leica Microsystems). The confocal microscope was operated by David Johnston of the Biomedical Imaging Unit, University of Southampton.

Table 2.11- Antibodies used in immunohistochemistry

List of the primary antibodies and corresponding secondary antibodies used to stain tissue sections. The dilutions used for each antibody are shown in brackets next to the antibody name. The suppliers for each antibody are also shown in brackets.

Primary antibodies		Secondary antibodies	
Rabbit α-Thymosin β4 (Millipore, AB6019)	(1:1500)	Goat α -rabbit IgG-FITC (Sigma, F6005)	(1:200)
Mouse α-Troponin C (Novocastra, NCL-TROPC)	(1:200)	Goat α-mouse IgG – Alexa Fluor 594 (Invitrogen, A11005)	(1:200)
Mouse α-CD34 (Novocastra, NCL-END)	(1:50)	Goat α-mouse IgG – Alexa Fluor 594 (Invitrogen, A11005)	(1:200)
Sheep α-CD31 (R&D Systems, AF806)	(1:2000)	Donkey α-sheep IgG-AF555 (Molecular Probes, A-21436)	(1:400)

2.6 Protein extraction

Protein was extracted from tissue by disrupting the tissue in 40 µl of RIPA buffer (Table 2.12) using a glass homogenizer. The tissue homogenate was then incubated on ice for 30 mins followed by sonication for 30 seconds. Finally the samples were centrifuged at 500 G for 10 mins at 4°C and the cell lysate removed into a clean tube. Cell lysates were stored at -80°C.

Protein was extracted from cell pellets by first re-suspending the pellet in lysis buffer (1% NP40 in PBS). The cells were homogenised by passing through a fine micropipette tip, used for gel-loading, several times. The sample was then incubated on ice for 30 mins, homogenising the sample, as previously, every 10 mins. The sample was centrifuged at 5,000 G for 10 mins at 4°C and the cell lysate removed to a fresh tube, leaving behind any debris.

The concentration of protein samples were measured using a Protein DC assay (Bio-Rad). This assay is a colorimetric assay based on the protein Lowry assay. Known dilutions of bovine serum albumin, prepared in RIPA buffer, were used to create a standard curve. Samples were measured using a Nanodrop spectrophotometer and the associated software was used to extrapolate the protein concentration values of the samples, based on the standard curve created.

Table 2.12 – RIPA buffer

The components used to make up RIPA buffer are listed with their final concentrations given. Further instructions are given in italics.

Component	Final concentration
Tris	50 mM
NaCl	150 mM
SDS	0.10%
NaDeoxycholate	0.50%
NP40	1%
Made up in PBS	
Protease inhibitor cocktail added (Complete mini, Roche)	

2.7 SDS-PAGE and Western blotting

2.7.1 Laemmli SDS-PAGE

Protein lysates were prepared in 4X sample buffer A (Table 2.13) and RIPA buffer (Table 2.12) to give the required concentration of protein. Samples were then denatured at 95°C for 5 mins.

Once prepared, the samples were resolved on 12% SDS-polyacrylamide gels (Table 2.14) using tris-glycine running buffer (250 mM Tris, 1.92 M Glycine, 1% SDS in water). Proteins were run through the stacking gel at 50 V for approximately 30 mins and then through the resolving gel at 100 V for approximately 1 hour, until the dye front reached the bottom of the gel.

2.7.2 Tricine-SDS-PAGE

Protein lysates or 50 ng synthetic thymosin β4 (Immundiagnostik) were prepared in 4X sample buffer B (Table 2.15) and RIPA buffer to give the desired protein concentration. Samples were then denatured at 70°C for 10 mins.

Once prepared, the samples were resolved on 16% SDS-polyacrylamide gels (Table 2.16) using the appropriate anode and cathode buffers, designed for tris-tricine SDS-PAGE. The cathode buffer (0.1 M tris, 0.1 M tricine, 0.1% SDS in water) is placed in the top chamber of the gel running apparatus, while the anode buffer (2 M tris-HCl solution in water at pH 8.9) is placed in the lower chamber. Proteins were run through the stacking gel at 50 V for approximately 30 mins and then through the resolving gel at 110 V for approximately 1 hour 30 mins, until the dye front reached the bottom of the gel.

2.7.3 Western blotting

Prior to transfer of proteins, the stacking gel was removed and discarded and the resolving gel was washed with PBS 4 times for 15 mins, treated with 10% glutaraldehyde solution for 40 mins and again washed with PBS 4 times for 15 mins. The proteins were then transferred at 80 V for 40 mins to Hybond-ECL nitrocellulose membranes (GE Healthcare).

2.7.3.1 Instant Blue gel protein stain

In order to stain for proteins that remained within the gel, gels were treated with Instant Blue (Expedeon), a coomassie blue based protein stain. The staining was imaged using a Chemidoc XRS imaging system (Bio-Rad) with Quantity One 1-D analysis software (Bio-Rad).

2.7.3.2 Ponceau red membrane protein stain

Ponceau red solution (0.1% Ponceau S, 1% acetic acid in water) was used to treat the membrane in order to stain for the transferred proteins and to visualise the protein ladder, which was then marked onto the membrane. The staining was imaged using the Chemidoc XRS imaging system (Bio-Rad) with Quantity One 1-D analysis software (Bio-Rad). The ponceau stain was then washed from the membrane with 5% milk powder in TBS-T (Tris Buffered Saline with 0.05% Tween 20).

2.7.3.3 Antibody staining

Membranes were next blocked for 1 hour in the 5% milk/TBS-T solution. Following blocking, membranes were probed for detection of thymosin β4 by incubating with 1 µg/ml of rabbit anti-thymosin β4 antibody (Millipore, AB6019) in 5% milk/TBS-T solution at 4°C overnight. The following day the membrane was washed 3 times for 10 mins in 5% milk/TBS-T solution and then incubated with a HRP-conjugated goat anti-rabbit IgG secondary antibody (Dako, P0448) at 1:5000 dilution in 5% milk/TBS-T solution for 1 hour at room temperature. The membrane was washed 2 times for 10 mins in TBS-T and then treated for detection with ECL Ultra detection reagent (Lumigen). Detection was carried out using a Chemidoc XRS imaging system (Bio-Rad) with Quantity One 1-D analysis software (Bio-Rad).

As β-actin is a different molecular weight to thymosin β4, at 42 kDa, it is possible to detect β-actin on the same membrane without first stripping the membrane. Prior to staining for β-actin, blots were washed 3 times for 10 mins in TBS-T. They were then probed with a HRP-conjugated β-actin antibody (Sigma, A3854) at 1:50,000 dilution in 5% milk/TBS-T solution for 1 hour at

room temperature. The membrane was washed 3 times for 10 mins in TBS-T and then treated for detection with ECL Plus detection reagent (Lumigen). This reagent is less sensitive than ECL Advance and therefore is unable to detect proteins that are present in low quantities, such as thymosin β4, but is able to detect β-actin which is present in large quantities. This allows for detection of the β-actin bands alone, without detection of the thymosin β4 bands. Detection was carried out using a Chemidoc XRS imaging system (Bio-Rad) with Quantity One 1-D analysis software (Bio-Rad).

2.7.3.4 Densitometry analysis

Band density was measured using Image J (National Institutes of Health). For measurement of the density of thymosin β4 and β-actin bands, the 'Analyse gels' function within the software was used. This facilitates the selection of lanes and plots variations in density down each lane. The areas under peaks, which represent bands, were measured and these values used to represent the density of the bands.

Table 2.13 – 4X Sample Buffer A

The components used to make up 4X sample buffer A, used for Laemmli SDS-PAGE samples, are listed with their final concentrations given. Further instructions are given in italics.

Component	Final concentration
SDS	8% w/v
Tris-HCl (pH 6.8)	250 mM
Glycerol	40% v/v
Made up in water	
Pinch of bromophenol blue added	
200 µl 1M DTT added per 1 ml aliquot directly before use	

Table 2.14 – Polyacrylamide gels for Laemmli SDS-PAGE

List of the components required to make up a 12% resolving gel (acrylamide:bis-acrylamide, 36.5:1) and 4% stacking gel (acrylamide:bis-acrylamide, 37:1) for Laemmli SDS-PAGE.

Components (at final concentration)	
12% Resolving gel	**4% Stacking gel**
11.68% acrylamide	3.84% acrylamide
0.32% bis-acrylamide	0.104% bis-acrylamide
375 mM Tris-HCl (pH 8.45)	125 mM Tris-HCl (pH 6.8)
0.1% SDS	0.1% SDS
0.05% TEMED	0.1% TEMED
0.05% APS	0.05% APS

Table 2.15 – 4X Sample Buffer B

The components used to make up 4X sample buffer B, used for tricine-SDS-PAGE samples, are listed with their final concentrations given. Further instructions are given in italics.

Component	Final concentration
SDS	16% w/v
Tris-HCl (pH 6.8)	200 mM
Glycerol	48% v/v
Made up in water	
Add 0.04% Coomassie blue G-250	
200 µl 1M DTT added per 1 ml aliquot directly before use	

Table 2.16 – Polyacrylamide gels for tricine-SDS-PAGE

List of the components required to make up a 16% resolving gel (acrylamide:bis-acrylamide, 32:1) and 4% stacking gel (acrylamide:bis-acrylamide, 32:1) for tricine-SDS-PAGE.

Ingredients (at final concentration)	
16% Resolving gel	**4% Stacking gel**
15.52% acrylamide	3.87% acrylamide
0.48% bis-acrylamide	0.122% bis-acrylamide
1 M Tris-HCl (pH 8.45)	744 mM Tris-HCl (pH 6.8)
0.1% SDS	0.1% SDS
0.1% TEMED	0.1% TEMED
0.1% APS	0.1% APS

2.8 Hypoxia experiments

2.8.1 Heart tissue

Pieces of ventricle tissue were divided between two 6-well plates (section 2.1.1) and cultured under standard tissue culture conditions of 37°C in 5% CO_2/air (normoxia) for 6 days. One plate was then used for hypoxic treatment of the heart explants, while the other plate was used for normoxic treatment. The plate for normoxic treatment was kept at 37°C in 5% CO_2/air for a further 24 hours. The plate for hypoxic treatment was placed in a Modular Incubator Chamber (Billups-Rothenburg inc.) along with a dish of sterile water, to maintain the humidity of the chamber. The chamber was sealed and flushed with a 5% CO_2/Argon gas mixture for approximately 5 mins at a flow rate of approximately 45 L/min, to remove the oxygen. This chamber was then placed in an incubator to maintain the temperature at 37°C. The hypoxic treatment plate was kept under these conditions for 24 hours. Following 24 hours of normoxic or hypoxic treatment the tissue was collected and stored for protein extraction at a later date by placing the tissue in cryogenic vials, which were stored at -80°C.

2.8.2 HeLa cells

HeLa cells were cultured and cells from a single flask passaged into two new T75 flasks (section 2.1.2). One flask was returned to a 5% CO_2/air incubator at 37°C and cultured for 48 hours (normoxic treatment). The other flask was placed in a Modular Incubator Chamber (Billups-Rothenburg inc.) along with a dish of sterile water. The chamber was sealed and flushed with a 5% O_2, 5% CO_2, 90% N_2 gas mixture for approximately 5 mins at a flow rate of approximately 45 L/min. This chamber was then placed in an incubator to maintain the temperature at 37°C. The hypoxic chamber was flushed with the 5% O_2 gas mixture again after 24 hours. The cells were cultured under hypoxic conditions for a total of 48 hours. Following 24 hours of normoxic or hypoxic treatment the cells were collected as pellets (section 2.1.2) and stored at -20°C for protein extraction at a later date.

2.9 Flow cytometry

For analysis of cells from tissue by flow cytometry, tissue was disaggregated in 3 ml PBS using a gentleMACs Dissociator (Miltenyi Biotec). The cell suspension obtained was filtered through a 70 µm filter to remove large clumps of tissue.

For analysis of cultured cells by flow cytometry, cells were collected as cell pellets (sections 2.1.2 and 2.1.3.2).

Dissociated cells from tissue or cells collected from culture were washed twice in 1% FBS/PBS, centrifuging at 1400 RPM for 4 mins and removing the supernatant after each wash. Cells were then re-suspended in an appropriate volume of 1% FBS/PBS and divided up for antibody treatment. Cells that required fixation and permeabilisation were incubated in 1% PFA for 10 mins at room temperature to fix with PFA or were incubated in a pre-chilled (-20°C) 2:2:1 mixture of methanol, acetic acid and DEPC-treated water for 10 mins at 4°C for MeAc fixation, as desired. The cells were then washed in 1% FBS/PBS containing 0.05% saponin and incubated in 1% FBS/PBS containing 0.05% saponin for 20 mins at room temperature. For permeabilised cells, all washes then contained 0.05% saponin.

Cells were incubated, as required, with the appropriate primary antibody (Table 2.17), made up in 1% FBS/PBS for detection of surface antigens, or in 1% FBS/PBS containing 0.05% saponin for detection of intracellular antigens. Antibody treatment was carried out for 20 mins at room temperature. Cells were then washed three times, as previously, before treatment with an appropriate secondary antibody (Table 2.17), if required, made up in 1% FBS/PBS containing 0.05% saponin for intracellular antigens. Again, antibody treatment was carried out for 20 mins at room temperature. Finally, cells were washed a further three times and then resuspended in 300 µl 1% FBS/PBS before being filtered through a 35 µm filter cap.

For each experiment a sample of cells was left unstained as a negative control. For directly conjugated antibodies a sample of cells was also stained with an appropriate isotype control antibody (Table 2.17) as a negative control. For

indirect staining, a sample of cells was stained with the appropriate secondary antibody (Table 2.17) alone as a negative control.

Cells which were dual stained for detection of a surface antigen and an intracellular antigen were stained first for detection of the surface antigen and then fixed and permeabilised before subsequently staining for detection of the intracellular antigen.

Stained cell suspensions were analysed using a FACS Aria flow cytometer (BD Biosciences) and sorted if desired.

Table 2.17 – Antibodies used in flow cytometry

List of the primary and secondary antibodies used to stain cell suspensions for flow cytometry analysis.

Primary antibodies	Conjugated fluorophore	Manufacturer
Rabbit α-Thymosin β4	N/A	Millipore, AB6019
Mouse IgG1 α-CD31	Allophycocyanin (APC)	ImmunoTools, 21270316
Mouse IgG1 isotype control	Allophycocyanin (APC)	ImmunoTools, 21275516
Secondary antibodies	**Conjugated fluorophore**	**Manufacturer**
Goat α-rabbit IgG	Fluorescein isothiocyanate (FITC)	Sigma, F6005
F(ab')2 fragment of Goat α-rabbit IgG	Alexa Fluor 488	Invitrogen, A11070
Chicken α-rabbit IgG	Alexa Fluor 647	Invitrogen, A21443

2.10 microRNA microarray

Quantitative microRNA arrays were carried out by Mirella Spalluto. RNA extracted from human foetal heart tissue was used to create cDNA with Megaplex RT primers (Applied Biosystems), according to the manufacturer's instructions. The cDNA samples were used with TaqMan Low Density Arrays (Applied Biosystems), Card A and Card B, according to the manufacturer's instructions, to assess expression of miRNAs. The data were analysed with Sequence Detection System v2.4 Enterprise Edition (Applied Biosystems).

2.10.1 microRNA data mining

In order to identify potential thymosin β4-targeting miRNAs, miRNA target prediction software had to be chosen. There are many options, including miRanda [341, 342], TargetScan [343], DIANA-micro T [344], and miRWalk [345]. As each algorithm is different, the predicted targets they yield can vary. In order to limit the number of miRNAs identified, only one miRNA target prediction tool was used to identify candidate miRNAs in this study. www.microRNA.org, which uses the miRanda algorithm, was chosen as it uses a well-established prediction algorithm and incorporates the mirSVR target site scoring method [346], which provides a means of identifying the best putative miRNA candidates.

The' target mRNA' search function of the www.microRNA.org website was used to search for miRNAs that target thymosin β4 (*TMSB4X*) mRNA. This yielded a list of miRNAs predicted to target the 3'-UTR of thymosin β4 mRNA, along with their predicted target region(s). mirSVR scores were provided for each miRNA, indicating the miRNAs predicted ability to down-regulate thymosin β4 mRNA when bound at a specific target site. The more negative the mirSVR score the greater the predicted down-regulation of the target. 'Target sites of all miRNAs with good mirSVR scores' were viewed.

2.11 Molecular cloning

2.11.1 pCR2.1-TOPO vector

PCR product was inserted into a pCR2.1-TOPO vector using a TOPO TA cloning kit. 2 µl of the PCR product was mixed with 0.5 µl of the provided salt solution (1.2 M NaCl; 0.06 M $MgCl_2$) and 0.5 µl of the TOPO vector. The solution was then incubated at room temperature for approximately 15 mins.

2.11.2 Transformation of competent cells

Vectors were transformed into JM109 competent cells (Promega). 1-50 ng of vector were added to 50-100 µl of competent cells and mixed gently in a tube. The tube of cells was chilled immediately on ice for 30 mins before being heat-shocked for 15-20 secs in a 42°C water bath. The tube of cells was then returned to ice for 2 mins. 450-900 µl of LB medium was added to the cells, which were then incubated for 1 hour at 37°C with continuous agitation (225 RPM).

2.11.3 Bacterial cell culture

2.11.3.1 Culture on agar plates

Following transformation of competent cells, the cells were cultured at clonal density on ampicillin-containing agar plates. Cells were first centrifuged at 10,000 G for 5 mins to create a cell pellet. Cells were re-suspended in approximately 500 µl LB medium and using a sterile glass spreader the cell suspension was spread across the surface of an agar plate. Plates were incubated at 37°C overnight, leading to formation of bacterial colonies.

2.11.3.2 Culture in LB medium

Selected colonies were expanded up in liquid suspension culture. Each selected colony was scooped up from the agar plate and added to a 50 ml conical tube containing 10 ml LB medium plus 10 µl ampicillin. The cells were incubated at 37°C overnight.

Bacteria from glycerol stocks (see below) were similarly expanded up in liquid culture, as desired. This was done by scraping a small amount of frozen cells and adding it to the LB medium.

To create larger quantities of bacteria containing desired plasmids, 150 ml LB medium plus 150 µl ampicillin within a conical flask could be inoculated with the bacteria and also incubated at 37°C overnight.

Bacterial culture was carried out using a Bunsen flame to sterilise equipment and prevent contamination of cultures.

2.11.3.3 Storage of bacterial cultures

Stocks of bacterial cultures were stored by adding 100 µl bacterial cell suspension to 500 µl of sterile glycerol. Glycerol stocks were stored at -80°C,

2.11.4 Extraction of plasmid DNA

To extract small amounts of plasmid DNA from bacterial cultures, 1 ml of bacterial cell suspension was taken and the isolation of plasmid DNA carried out using a PureYield Plasmid Miniprep System (Promega), according to the manufacturer's instructions.

To extract larger amount of plasmid DNA from bacterial cultures, a cell pellet was created from 75 ml of bacterial cell suspension by centrifuging at 3,000 RPM for 5 mins and disposing of the supernatant. Plasmid DNA was then extracted from the cell pellet using a GenElute HP Plasmid Maxiprep kit (Sigma Aldrich) according to the manufacturer's instructions.

The concentrations of plasmid DNA samples were assessed using a Nanodrop spectrophotometer. Samples were stored at -20°C.

2.11.5 Restriction digests

50 µl restriction digest reactions were carried out on plasmid DNA using restriction enzymes with the appropriate NEB buffers (New England Biolabs).

Dual digests with *Nhe* I and *Not* I were carried out sequentially. 5 µl NEB Buffer 2, 2 µl *Nhe* I, 0.5 µl BSA (10mg/ml) and 5 µg plasmid DNA were mixed together and made up to 50 µl with water. The reaction mixture was incubated at 37°C for 2 hours. The Tris concentration of the solution was then increased from 10 mM to 50 mM and the NaCl concentration was increased from 50 mM to 100 mM, to facilitate *Not* I digestion. 2 µl *Not* I was added to the reaction mixture which was incubated at 37°C overnight.

Dual digests with *Xba* I and *Not* I were carried out simultaneously. 5 µl NEB Buffer 3, 2 µl *Xba* I, 2 µl *Not* I, 0.5 µl BSA (10mg/ml) and 5 µg plasmid DNA were mixed together and made up to 50 µl with water. The reaction mixture was incubated at 37°C overnight.

2.11.6 Ligation reactions

T4 DNA ligase (Promega) was used to ligate an insert into a vector. The following reactions were set up: vector alone (no ligase), vector alone (with ligase), vector + insert (1:3 molar ratio), vector + insert (1:1 molar ratio), vector + insert (3:1 molar ratio). 20 µl reactions were set up using 2 µl ligase, 2 µl of the supplied buffer, and appropriate volumes of insert and vector, based on their DNA concentrations. Reaction mixtures were made up to volume in water. The reactions were incubated at between 10°C to 16°C overnight.

2.12 Tubule formation assays

Matrigel (Corning) was defrosted overnight at 4°C. The following day 150 µl of Matrigel was pipetted into four wells of a 6-well plate, pre-chilled at 4°C. The plate was left at 4°C for 15 mins to allow the Matrigel to coat the plate evenly. The plate was then incubated at 37°C for at least 30 mins to allow the Matrigel to set.

HUVECs were passaged (section 2.1.3.2) on to the Matrigel-coated wells at between $1x10^5$ and $2x10^5$ cells/ml, calculated using a haemocytometer. HUVECs were similarly passaged onto four wells of an uncoated 6-well tissue culture plate. The cells were cultured for 4 hours at 37°C in a 5% CO_2/air incubator.

After 4 hours the HUVECs were collected off the plates. Two wells of cells were collected for staining for flow cytometry, while two wells of cells were collected for RNA extraction. To remove the cells, each well was washed with 1 ml PBS prior to adding 1 ml Dispase (5U/ml) in HBSS (StemCell Technologies). The plates were incubated at 37°C for 15-30 mins, until the cells had detached. The cells were washed off the wells with media and removed to a 15 ml conical tube. The tube was centrifuge at 1,000 RPM for 5 mins and the supernatant removed to remove the Dispase from the cells. Cells were washed twice more by re-suspending in media or PBS, centrifuging and removing the supernatant. The collected HUVECs were then used in downstream protocols.

Chapter 3: Results - Expression of thymosin β4 in the developing human heart

3.1 Introduction

There have been no previous reports on the distribution of thymosin β4 in the developing human heart, however thymosin β4 protein has been detected by tissue microarray in the adult human heart [347].

More is known about the presence of thymosin β4 in the developing murine heart. Bock-Marquette and colleagues used RNA *in situ* hybridisation to demonstrate that at embryonic day (E) 10.5-12.5 the endocardial cushions (precursors to the cardiac valves), outflow tract, compact myocardium of the ventricles and the interventricular septum are enriched with thymosin β4-expressing cells [170]. Notably thymosin β4 mRNA was not detected in the atria [170].

Smart and colleagues have similarly shown by RNA *in situ* hybridisation that thymosin β4 mRNA is present throughout the ventricles in E14.5 mice, with enhanced expression detected in the compact myocardium and interventricular septum [258]. They also detected thymosin β4 mRNA in the smooth muscle walls of the outflow tract vessels [258]. They did not report findings for thymosin β4 mRNA expression within the atria [258].

These studies do not report which cell types of the heart thymosin β4 is expressed in. However, the adverse phenotype observed in mice with cardiomyocyte-specific knock-down of thymosin β4 (section 1.4.1) indicates that thymosin β4 is produced by cardiomyocytes during early development and plays a key role in this context [258]. Thymosin β4 is released from eEPCs delivered exogenously as a cell therapy in pre-clinical studies (section 1.4.4). Therefore endogenous eEPCs and potentially other early progenitor cells could be important thymosin β4-producing cells within the developing heart.

At the protein level, Bock-Marquette and colleagues have illustrated, using immunohistochemistry, that thymosin β4 protein is localised to the outflow tract

of mice at E9.5 and the endocardial cushions at E11.5, in accordance with the expression of thymosin β4 mRNA in these structures [170]. However, they did not report protein localisation data for the ventricles or atria [170].

Smart and colleagues used immunohistochemistry to show thymosin β4 protein localises to the smooth muscle walls of the outflow tract vessels in E14.5 mice [258]. Further to this they presented dual stained images of the ventricle wall, using antibodies for detection of thymosin β4 and VEGF receptor 2 (VEGFR2), a marker of endothelial cells [258]. Low magnification images were presented in which the thymosin β4 staining looks relatively homogenous, but is absent in patches where VEGFR2 is present [258]. The authors conclude that thymosin β4 protein is localised within most cells of the ventricular myocardium, but is absent from VEGFR2-positive endothelial cells [258].

Four different mRNA isoforms can be transcribed from *TMSB4X*, the human thymosin β4 gene: *TMSB4X-001*, *TMSB4X-002*, *TMSB4X-003* and *TMSB4X-004*. This is significant to the current study because *TMSB4X-004* has a reduced length 3'-UTR compared to the other three isoforms (Figure 3.1) and may therefore be targeted by a reduced number of miRNAs. As such, it was important to assess the expression of the different isoforms of *TMSB4X* in this study.

Pseudogenes are non-functioning copies of genes found within the genome. There are two main types of pseudogene. Non-processed pseudogenes are created by duplication of genes at the genomic DNA level and usually contain the promoter region of their functional counterparts, allowing them to be transcribed to mRNA. Processed pseudogenes are created when an endogenously reverse transcribed mRNA becomes integrated into the chromosomal DNA and will only produce transcript if the gene was inserted into the genome downstream of a promoter by chance.

In the Ensembl annotation of the most recent human genome assembly (GRCh38), there are eight different pseudogenes of *TMSB4X* listed (Table 3.1). As such it was important to ensure that no pseudogene transcripts were detected in place of *TMSB4X* mRNA in this study.

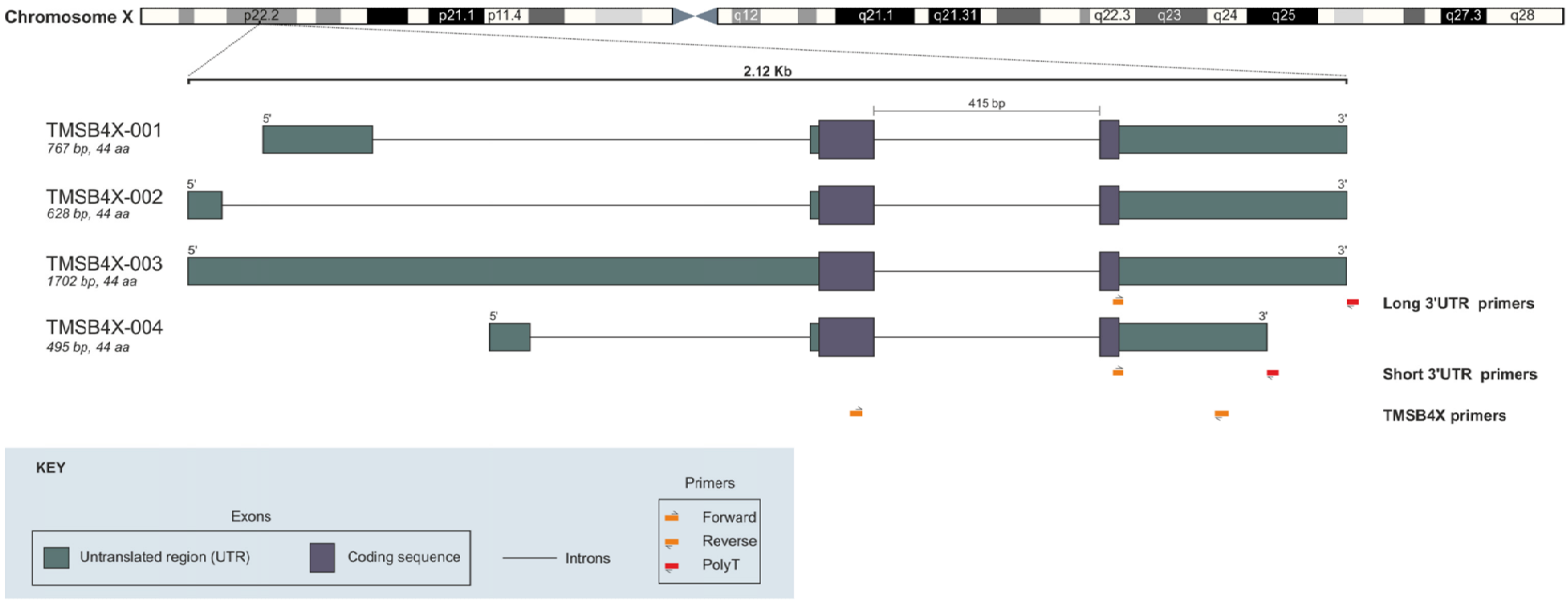

Figure 3.1 – Exonic structures of TMSB4X isoforms with primer binding locations

Diagrammatic representation of the exon usage of *TMSB4X* isoforms. The position of the PCR primer binding sites are shown: the 'TMSB4X primers' detect all isoforms, the 'Long 3'UTR primers' detect only TMSB4X-001, -002 and -003 and the 'Short 3'UTR primers' detect only TMSB4X-004.

Table 3.1 – Pseudogenes of TMSB4X

List of pseudogenes of TMSB4X based on the Ensembl annotation of human genome assembly GRCh38.

Gene	Synonyms	Size	Location
TMSB4XP1	TMSL1	135	6p34.2
TMSB4XP2	TMSL2	210	2p25.3
TMSB4XP3	-	114	7p14.3
TMSB4XP4	TMSL4	618	9q34.11
TMSB4XP5	TMSL5	522	11q12.3
TMSB4XP6	TMSL6, TMSB4L	135	20q13.13
TMSB4XP7	TMSL7	587	Xq23
TMSB4XP8	TMSL3	135	4q22.1

Figure 3.2 – Alignment of TMSB4X-002 and TMSB4XP4 sequences

In silico sequence alignment analysis was carried out on the sequences of *TMSB4X-002* and TMSB4XP4. The bases which are matched or mis-matched with *TMSB4X-002* are highlighted in the *TMSB4XP4* sequence.

3.2 Results

3.2.1 Detection of thymosin β4 mRNA in the developing human heart

To assess the presence of thymosin β4 mRNA in the developing human heart, primers were designed to be able to amplify any of the four isoforms of *TMSB4X* (TMSB4X primers) (Figure 3.1). These primers were intron-spanning and could therefore discriminate between amplification from genomic *TMSB4X* and *TMSB4X* cDNA based on product size (Figure 3.1). The sequence of the TMSB4X primers is shown in Table 2.5.

In silico sequence alignment analysis (section 2.3.1.2) found that of the known pseudogenes of *TMSB4X*, *TMSB4XP4* has high sequence consensus with TMSB4X transcripts, especially so with *TMSB4X-002* (Figure 3.2). As such the TMSB4X primers are predicted to detect *TMSB4XP4*, if present, as well as *TMSB4X* isoforms.

PCR (section 2.3) was used to determine whether the TMSB4X primers amplify the *TMSB4XP4* pseudogene and confirm detection of *TMSB4X* transcript. mRNA was extracted from foetal human hearts and reverse transcribed to cDNA, (sections 2.2.1 and 2.2.3). Genomic DNA was extracted from foetal placental tissue (section 2.2.5). The TMSB4X primers were then used to amplify the heart cDNA and genomic DNA samples using PCR (section 2.2).

The TMSB4X primers amplified a product of 278 base pairs from heart cDNA template, which is the expected product length from both *TMSB4X* and *TMSB4XP4* transcripts (Figure 3.3A). When genomic DNA was used as template two products were detected (Figure 3.3A). A product was again detected at 278 base pairs (Figure 3.3A). This is the expected length of a product derived from genomic *TMSB4XP4*, which lacks introns. A product was also detected at 693 base pairs, the expected length of a product derived from genomic *TMSB4X* (Figure 3.3A).

To ascertain whether the product amplified from heart cDNA was derived from *TMSB4X* transcripts or from *TMSB4XP4* transcript, the product was isolated and sent for Sanger sequencing (section 2.3.1). The sequence obtained was

aligned *in silico* with the expected sequences for products derived from *TMSB4X* and *TMSB4XP4* transcripts (section 2.3.1.2). The obtained sequence matches that for *TMSB4X* transcripts, indicating this is the major product being amplified by the TMSB4X primers within the foetal human heart (Figure 3.3B).

Using PCR to amplify reverse transcribed mRNA from foetal human heart tissue with the TMSB4X primers (section 2.3), *TMSB4X* mRNA was found to be present within the ventricle, atria and outflow tract (Figure 3.4). The absence of a genomic, 693 base pair product and the absence of bands in the 'no reverse transcriptase' control lanes indicate that there was no genomic DNA contamination (Figure 3.4).

3.2.2 Detection of TMSB4X transcripts in the developing human heart

The *TMSB4X-004* isoform of the *TMSB4X* gene contains a shortened 3'-UTR region (Figure 3.1). Primers were designed to assess the presence of this transcript within the developing human heart, compared to the other three transcripts, all of which have a longer 3'-UTR. The reverse primers were designed to bind the polyA tail and the forward primers to bind the 5' end of the 3'-UTR region. The sequence of the 'long 3'UTR primers', which detect *TMSB4X-001*, *-002* and *-003* and the 'short 3'UTR primers', which detect *TMSB4X-004* are shown in Table 2.5.

mRNA was extracted from dissected ventricle and atria from foetal human hearts and reverse transcribed to cDNA (sections 2.2.1 and 2.2.3). The 'long 3'UTR primers' and 'short 3'UTR primers' were each used to amplify the cDNA samples by PCR (section 2.2). Transcripts containing the long 3'-UTR; *TMSB4X-001*, *-002* or *-003*; were present within both the ventricle and atria, as indicated by the presence of a 447 base pair product (Figure 3.5A). *TMSB4X-004*, which has a shorted 3'-UTR, was also present within both the ventricle and atria, as indicated by the presence of a 300 base pair product (Figure 3.5B).

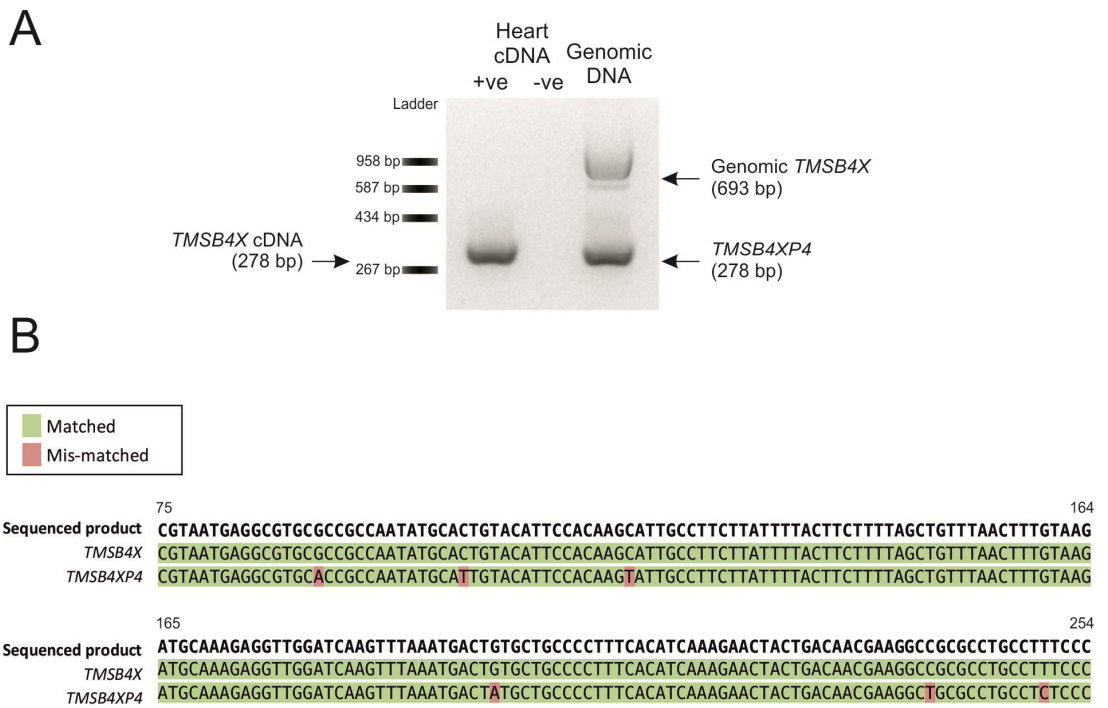

Figure 3.3 – Detection of TMSB4X transcripts in the human foetal heart

A) PCR products from reactions using the TMSB4X primers are shown, resolved on a 2% agarose gel. cDNA synthesised from mRNA from foetal heart tissue or genomic DNA from foetal placental tissue were used as templates. Alongside the heart cDNA sample (+ve), a corresponding 'no reverse transcriptase' negative control sample (–ve) was used as template. The expected sizes of products derived from *TMSB4X* cDNA, genomic *TMSB4X* and from *TMSB4XP4* (both genomic and transcript) are indicated. B) The sequence of the amplified product from heart cDNA, obtained by Sanger sequencing, is shown aligned with the sequences of *TMSB4X* and *TMSB4XP4*.

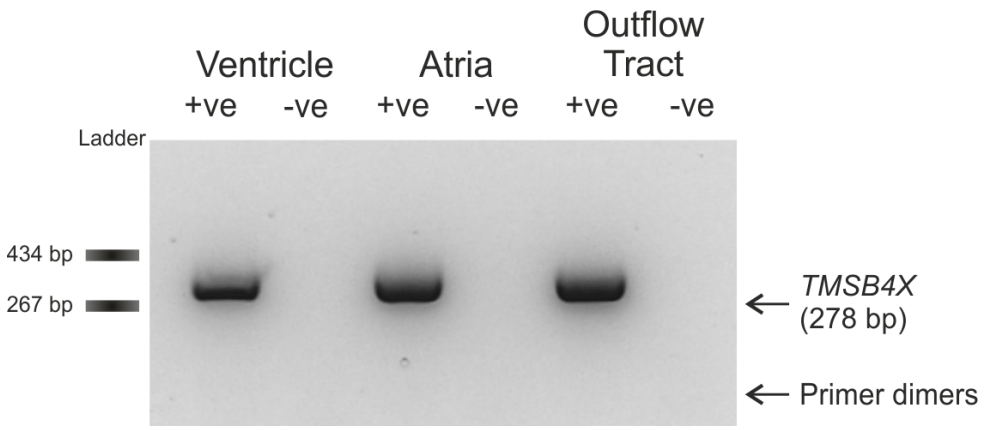

Figure 3.4 – Detection of TMSB4X transcripts in the ventricles, atria and outflow tract of the foetal human heart

PCR products from reactions using the TMSB4X primers are shown, resolved on a 2% agarose gel. cDNA synthesised from mRNA from separated ventricle, atria and outflow tract tissue from foetal heart were used as template. Alongside each cDNA sample (+ve), a corresponding 'no reverse transcriptase' negative control sample (-ve) was used as template. Bands indicating the presence of TMSB4X transcripts were seen in all three samples. The faint, low molecular weight bands are primer dimers.

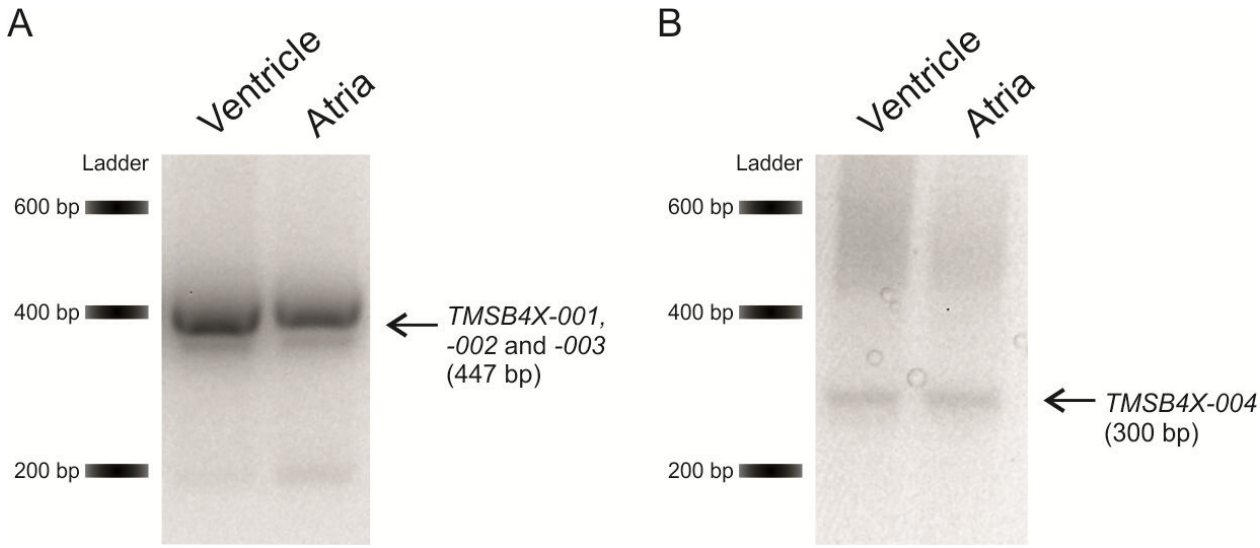

Figure 3.5 – Detection of TMSB4X transcripts with differing 3'-UTR lengths

PCR products from reactions using the 'long 3'UTR primers' (A) and 'short 3'UTR primers' (B) are shown, resolved on a 2% agarose gel. cDNA synthesised from mRNA from separated ventricle and atria were used as template. Bands indicating the presence of transcripts containing both the full length and shortened 3'-UTR were seen in both ventricle and atria.

3.2.3 Detection of thymosin β4 protein in the developing human heart

In order to confirm the presence of thymosin β4 protein in the developing human heart and to assess its localisation, fluorescence immunohistochemistry was carried out (section 2.5). An anti-thymosin β4 antibody was used with an appropriate FITC-conjugated secondary antibody (Table 2.11) to stain sections of foetal hearts aged between 7 and 9 post-conception weeks (n = 6).

During optimisation of this antibody, it was found to produce a distinct, well-defined staining pattern in PFA-fixed heart sections which were subjected to 15 mins pre-treatment in boiling sodium citrate solution (Figure 3.6B & E). Pre-incubating the anti-thymosin β4 antibody with synthetic thymosin β4 peptide (section 2.5.3.1) abolished the staining pattern (Figure 3.6C & F), indicating the primary antibody is detecting thymosin β4 protein. The staining pattern was also absent in sections treated with the secondary antibody alone (Figure 3.6D & G).

Some cells, thought to be red blood cells, were autofluorescent, as indicated by their detection in both the red and green spectrums in negative control sections (Figure 3.6H-J).

Figure 3.6 - Immunolocalisation of thymosin β4 protein in the human foetal heart

A) An H&E-stained human foetal heart section is shown; the rectangle indicates the area shown in panels B-G. The right atria (RA), interventricular septum (IVS), right ventricle (RV) and left ventricle (LV) are indicated.
B-G) Sections were stained for thymosin β4 (B), probed with the primary antibody after blocking by pre-incubation with synthetic thymosin β4 (C) or incubated with the secondary antibody alone (D). The nuclei were counterstained with DAPI (E-G). A distinct staining pattern is seen with the thymosin β4 but not in negative controls.
H-J) High powered images of sections stained with the secondary antibody alone show autofluorescence in the green (H) and red (I) spectrums, as highlighted by the white arrows.
Scale bars = 500 μm (A), 200 μm (B-G), 25 μm (H-J).

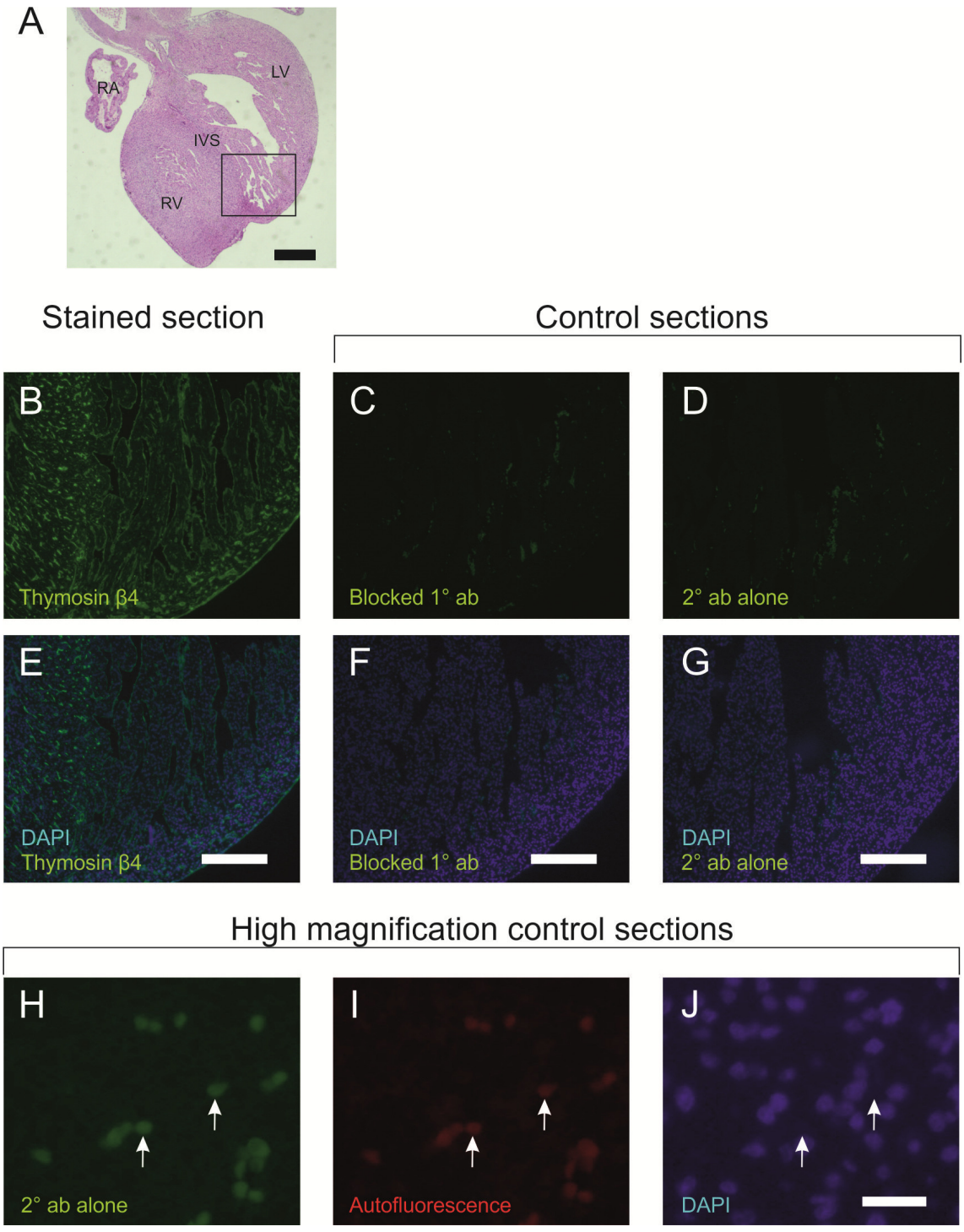
A
RA
LV
IVS
RV
Stained section
Control sections
B
Thymosin β4
C
Blocked 1° ab
D
2° ab alone
E
DAPI
Thymosin β4
F
DAPI
Blocked 1° ab
G
DAPI
2° ab alone
High magnification control sections
H
2° ab alone
I
Autofluorescence
J
DAPI

3.2.4 Localisation of thymosin β4 protein in structures of the foetal heart

Using fluorescence immunohistochemistry (section 2.5), localisation of thymosin β4 was demonstrated within various regions of the foetal human heart in 6 independent hearts, aged 7 to 9 post-conception weeks (Figures 3.7 and 3.8).

Thymosin β4 staining was detected throughout the ventricles, including in the ventricle walls (Figure 3.7B-D), the interventricular septum (Figure 3.7E-G), the epicardium (Figure 3.7B, white arrow) and the endocardial lining of the chambers (Figure 3.7B, yellow arrow). Thymosin β4 staining was more intense within the compact layer of the ventricle wall (CL) and interventricular septum (IVS), compared with the trabecular layer of the ventricle wall (TL) (Figure 3.7B, C, E & F).

In order to quantify the difference in staining intensity between the compact and trabecular layers of the ventricle wall, images were taken on a confocal microscope. Using the software associated with the confocal microscope (section 2.5.5), the mean fluorescence intensity was measured in selected regions of interest within both the compact and trabecular layer (Figure 3.7H, white boxes). Nine measurements were taken from each of the compact layer and trabecular layer, using images from three different foetal hearts. The mean fluorescence intensity (arbitrary units; a.u.) of thymosin β4 staining in the trabecular myocardium was 20.41 a.u. and 45.04 a.u. in the compact myocardium (Figure 3.7I).

Thymosin β4 staining was also detected in the atria (Figure 3.8), where staining was seen within the chamber walls (Figure 3.8B-D), the epicardium (white arrow) and endocardium (yellow arrow). Thymosin β4 staining was present throughout the walls of the outflow tract vessels (Figure 3.8E-G) as well as in the endothelial linings of small coronary vessels (Figure 3.8H-J, red arrow) and medium coronary vessels (Figure 3.8H-J, orange arrow).

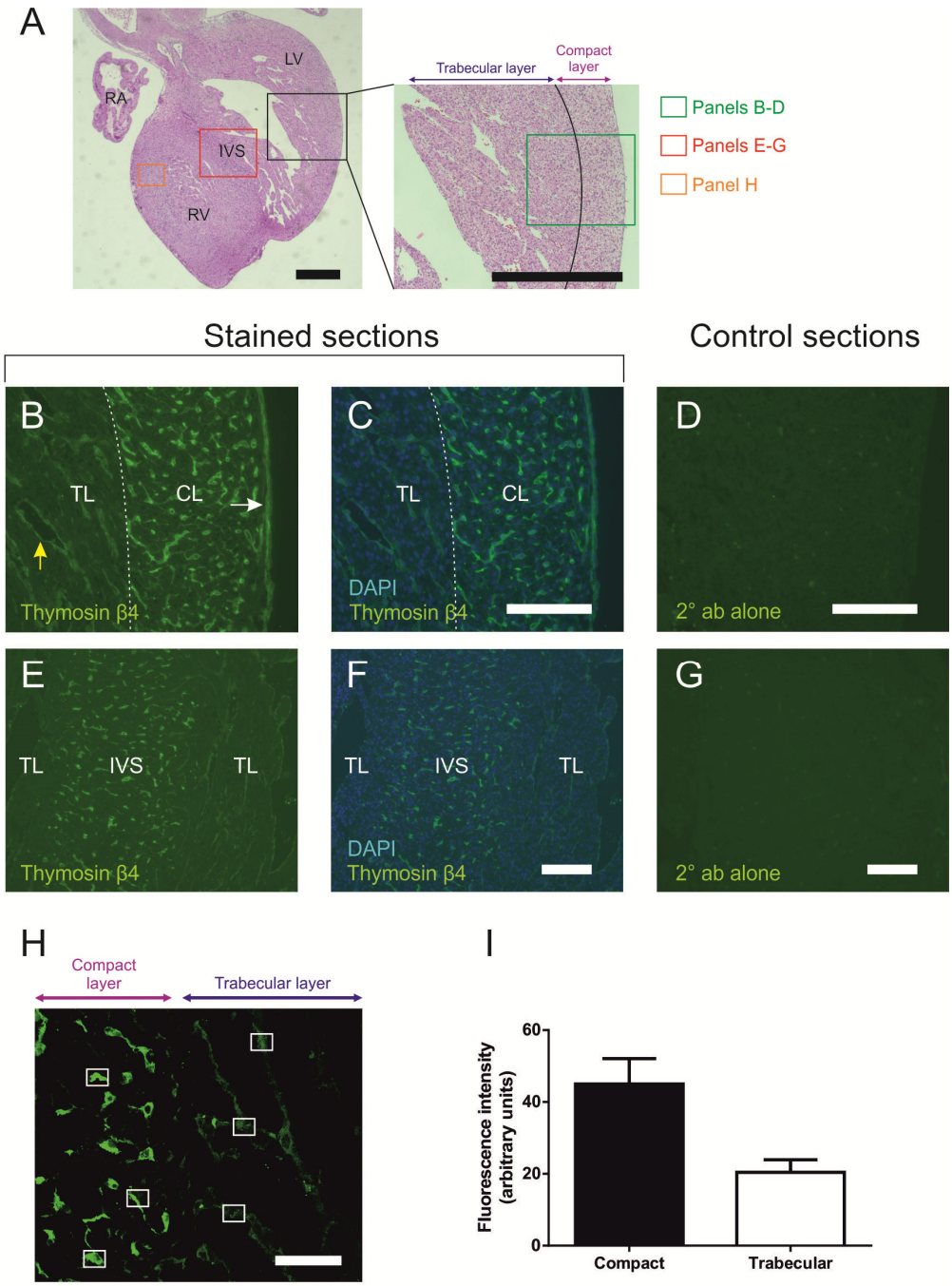

Figure 3.7 – Immunolocalisation of thymosin β4 in the ventricle walls and interventricular septum

A) An H&E-stained human foetal heart section is shown; the rectangles indicate the areas shown in the indicated panels. The right atrium (RA), interventricular septum (IVS), right ventricle (RV) and left ventricle (LV) are indicated. B-G) Sections stained for thymosin β4 (B, E) plus DAPI nuclear stain (C, F) or with the secondary antibody alone (D, G) are shown. The compact layer (CL), trabecular layer (TL), IVS, epicardium (white arrow) and endocardium (yellow arrow) are indicated. n=6. H) An example of the selection of regions of interest within the compact and trabecular myocardium from confocal microscopy images. I) The mean fluorescence intensity of these regions of interest is shown in a bar graph. Bars represent the mean ± standard error of the mean (n= 9). Scale bars = 500 μm (A), 150 μm (B-G), 50 μm (H).

Figure 3.8 – Immunolocalisation of thymosin β4 in the atria, outflow tract and coronary vessels

A) An H&E-stained human foetal heart section is shown; the rectangles indicate the areas shown in the indicated panels. The right atria (RA), left atria (LA), outflow tract (OFT), interventricular septum (IVS), right ventricle (RV) and left ventricle (LV) are indicated. B-J) Sections stained for thymosin β4 (B, E, H), plus DAPI nuclear stain (C, F & I), or with the secondary antibody alone (D, G, J) are shown. Thymosin β4 staining is present in the atria (B-D), including the epicardium (white arrow) and endocardium (yellow arrow). Thymosin β4 staining is also present in the outflow tract (E-G) and small (red arrow) and medium (orange arrow) coronary vessels (H-J). Images are representative of staining seen in 6 different hearts, ages 7 to 9 post-conception weeks. Scale bars = 500 μm (A), 150 μm (B-G), 50 μm (H-J).

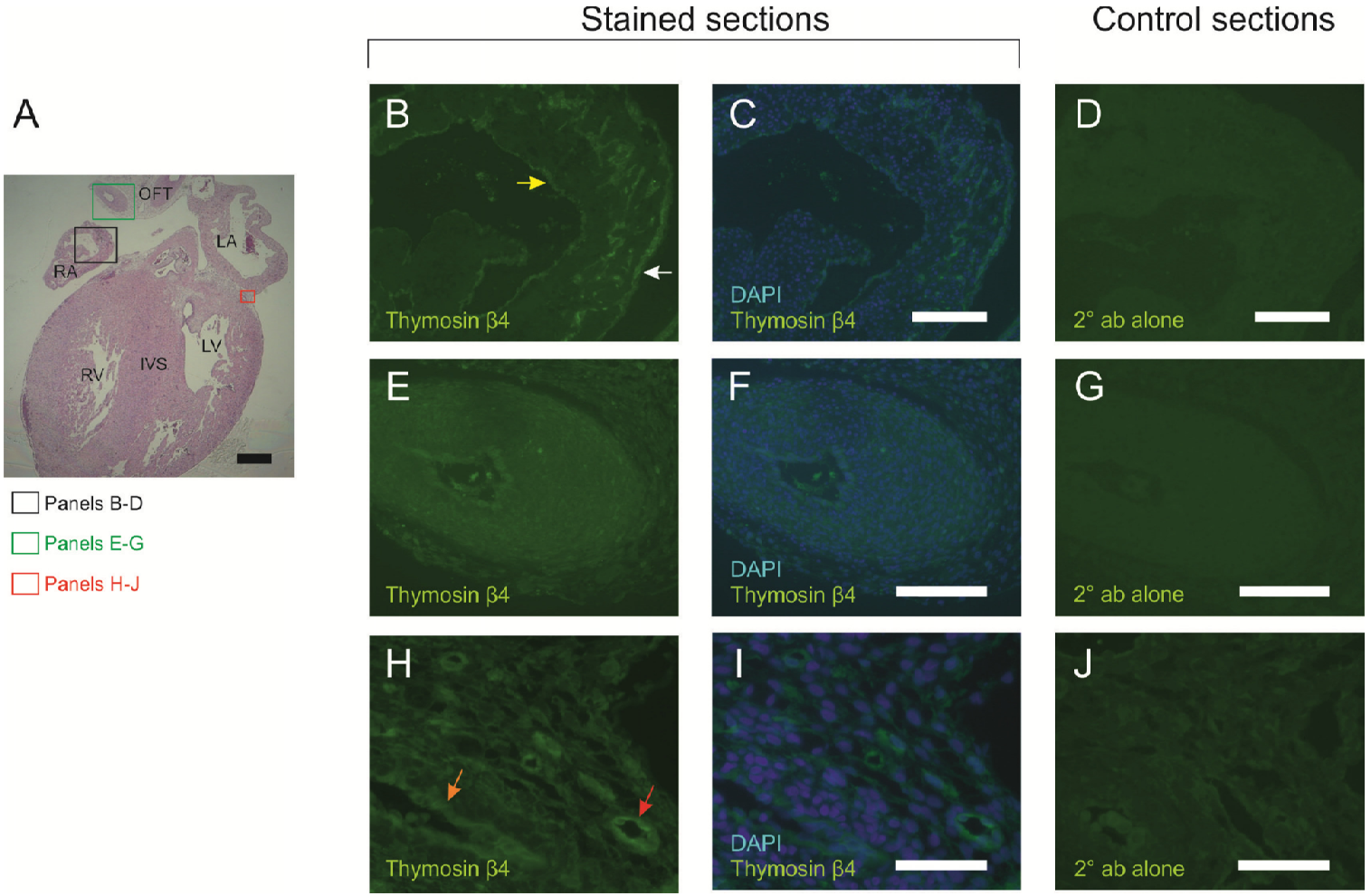
Stained sections
Control sections
A
OFT
LA
RA
LV
RV
IVS
Panels B-D
Panels E-G
Panels H-J
B
Thymosin β4
C
DAPI
Thymosin β4
D
2° ab alone
E
Thymosin β4
F
DAPI
Thymosin β4
G
2° ab alone
H
Thymosin β4
I
DAPI
Thymosin β4
J
2° ab alone

3.2.5 Intracellular localisation of thymosin β4 within cells of the ventricle wall

To ascertain the intracellular localisation of thymosin β4, foetal heart sections stained for thymosin β4 by fluorescence immunohistochemistry were imaged at multiple focal planes (z slices) using a confocal microscope (section 2.5) (n = 3). Figure 3.9 shows images from individual z-slices of a thymosin β4-stained cell located in the compact myocardium of the ventricle (panels A-C, G-I and M-O). The fluorescence intensity of thymosin β4 staining and the DAPI nuclear stain were measured along a transect across the cell, allowing co-localisation of the two stains to be assessed (Figure 3.9; blue lines). This quantification is illustrated by line graphs below each image panel within Figure 3.9, showing fluorescence intensity on the y axis and distance along the transect on the x axis (panels D-F, J-L and P-R).

Co-localisation of thymosin β4 staining with DAPI is an indication of localisation to the nucleus, while thymosin β4 staining that is not co-localised with DAPI is outside the nucleus. Thymosin β4 staining was present at high levels in areas of the cell where it was not co-localised with the DAPI nuclear stain (Figure 3.9A-L). However, low intensity thymosin β4 staining was also detected to be co-localised with DAPI (Figure 3.9I, L, M, N, P, Q).

Figure 3.10 shows single z slice images, along with quantification of transects, through the nucleus from four different thymosin β4-positive cells within the ventricle wall. The intensity of thymosin β4 staining was consistently greater on either side of the DAPI-stained nucleus, i.e. within the cytoplasm (Figure 3.10). As in the cell shown in Figure 3.9, low level thymosin β4 staining was seen co-localised with DAPI in some cells (Figure 3.10C & G), though it was not in others (Figure 3.10D & H).

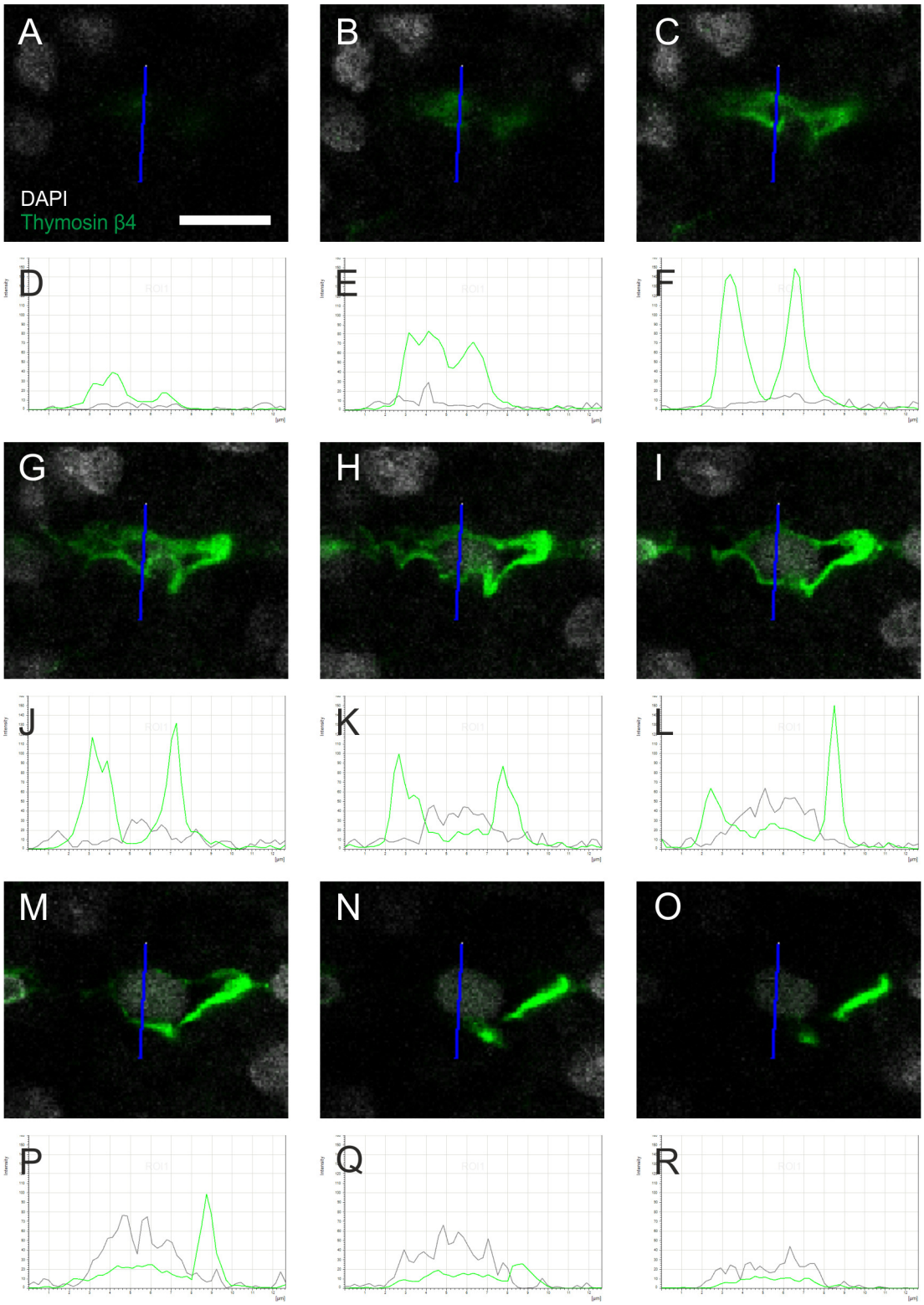

Figure 3.9 – Intracellular localisation of thymosin β4 protein throughout a cell

Confocal z-slice images of a single cell, stained for thymosin β4 and DAPI, are shown (A–C, G–I, M–O). Fluorescence intensities across transects (blue lines) were measured and are illustrated as line graphs (D–F, J–L, P–R); green lines represent thymosin β4 fluorescence and grey lines represent DAPI stain. Scale bars = 10 μm.

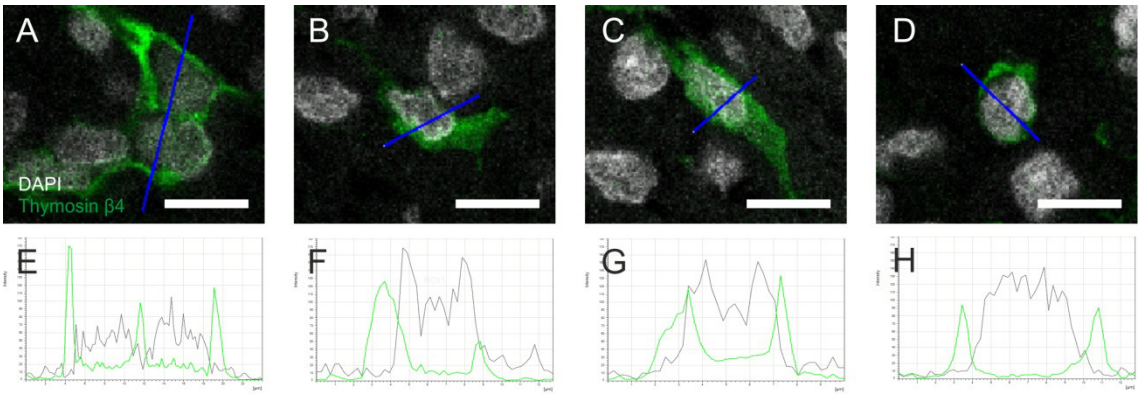

Figure 3.10 – Intracellular localisation of thymosin β4 in relation to the nucleus

A–D) Confocal images of z–slices through the nuclei of four different cells from within the ventricle wall of thymosin β4 and DAPI stained sections are shown.
E–H) Fluorescence intensities across transects (blue lines) were measured and illustrated as line graphs; green lines represent thymosin β4 fluorescence and grey lines represent DAPI fluorescence. Images are representative of staining seen in 3 different hearts, ages 7 to 9 post–conception weeks. Scale bars = 10 μm

3.2.6 Localisation of thymosin β4 protein with troponin C-positive cells within the ventricle wall

Thymosin β4 has a distinctive staining pattern within the ventricle walls, suggesting it is present in specific types of cells (section 3.2.4). Further immunofluorescent staining was carried out to determine which cells thymosin β4 protein is localised in. Staining was carried out on sections from 6 foetal hearts, aged 7 to 9 post-conception weeks.

Sections of foetal heart tissue were dual-stained for detection of thymosin β4 and troponin C, which is a sarcomeric protein and therefore a marker of cardiomyocytes (section 2.5).

The staining pattern of thymosin β4 differed to that of troponin C, with troponin C staining detected throughout the ventricle wall, compared to the more specific staining pattern of thymosin β4 (Figure 3.11A-D). At higher magnification it was evident that thymosin β4 staining did not co-localise with troponin C (Figure 3.11E-H, yellow arrows).

The presence of thymosin β4 in the epicardium, which surrounds the myocardium can also be seen (Figure 3.11A & B, white arrows).

Figure 3.11 – Immunolocalisation of thymosin β4 and troponin C within the ventricle wall

A–D) Images of the ventricle wall from foetal heart sections dual-stained for thymosin β4 and troponin C are shown. The individual stains are shown (A & B) alongside the merged image (C), plus DAPI nuclear stain (D). White arrows highlight the epicardium.

E–H) High magnification images of the region indicated by the white box in panel D are similarly shown. Yellow arrows highlight the lack of co-localisation between thymosin β4 staining and troponin C staining.

I–L) Images of sections stained with each secondary antibody alone are shown at low magnification (I & J) and high magnification (K & L). Images are representative of staining seen in 6 different hearts, ages 7 to 9 post-conception weeks. Scale bars = 150 μm (A–D, I, J), 25 μm (E–H, K, L).

Stained sections
Control sections
A
Thymosin β4
B
Troponin C
C
Troponin C
Thymosin β4
D
DAPI
Troponin C
Thymosin β4
E
Thymosin β4
F
Troponin C
G
Troponin C
Thymosin β4
H
DAPI
Troponin C
Thymosin β4
I
2° ab alone
J
2° ab alone
K
2° ab alone
L
2° ab alone

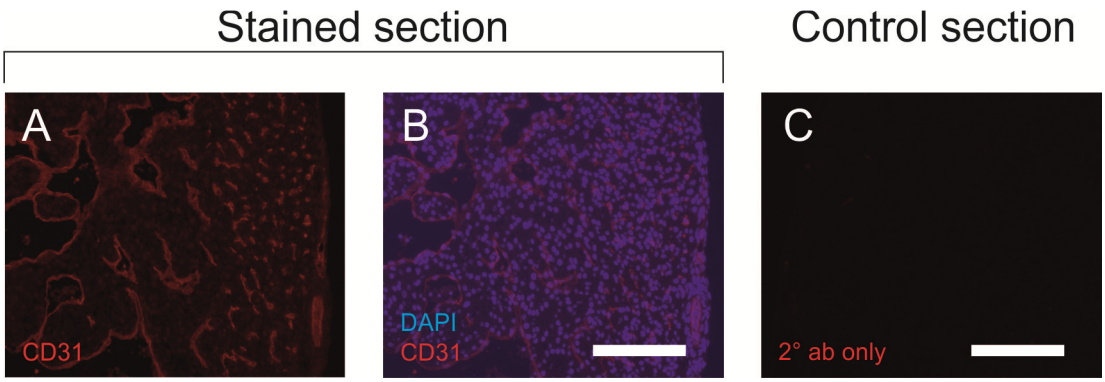

Figure 3.12 – Immunolocalisation of CD31 protein within the ventricle wall

Images of the ventricle wall from a foetal heart section stained for CD31 (A) and with the DAPI nuclear stain (B) are shown. An image of an adjacent section stained with the secondary antibody alone is also shown (C). Images are representative of staining seen in 6 different hearts, ages 7 to 9 post-conception weeks. Scale bars = 150 µm.

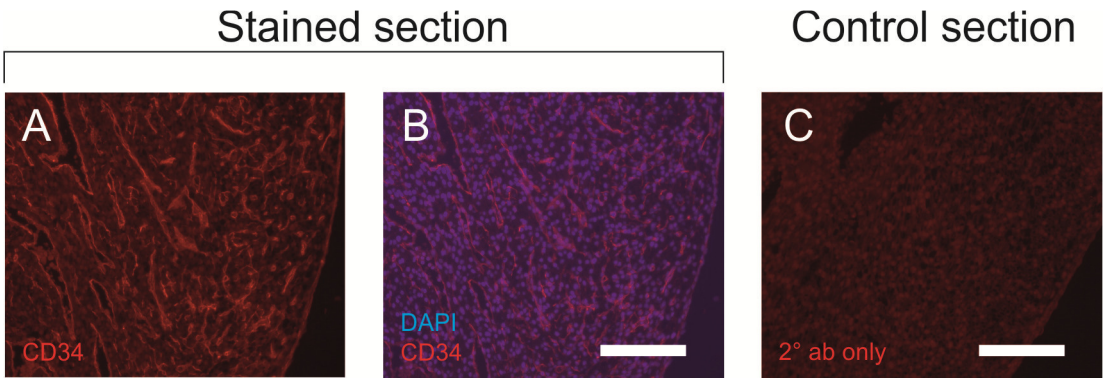

Figure 3.13- Immunolocalisation of CD34 protein within the ventricle wall

Images of the ventricle wall from a foetal heart section stained for CD34 (A) and with the DAPI nuclear stain (B) are shown. An image of an adjacent section stained with the secondary antibody alone is also shown (C). Images are representative of staining seen in 6 different hearts, ages 7 to 9 post-conception weeks. Scale bars = 150 μm.

3.2.7 Localisation of thymosin β4 protein with CD31 and CD34-positive cells within the ventricle wall

CD31 and CD34 are cell adhesion molecules found on the surface of endothelial cells and were therefore used as endothelial cell markers.

Fluorescence immunohistochemistry (section 2.5) was used to demonstrate the staining pattern of CD31 in the ventricle wall of the human foetal heart (Figure 3.12). Similarly, the staining pattern of CD34 in the ventricle wall of the human foetal heart was demonstrated (Figure 3.13).

Sections of foetal heart tissue were triple stained for detection of thymosin β4, CD31 and CD34 and images were taken using a confocal microscope (section 2.5). Images were taken of the ventricle wall and are shown as a sum of multiple z-slices. CD34 staining was more widespread than CD31 staining (Figure 3.14B & C). CD31 staining was always co-localised with thymosin β4 staining, however thymosin β4 staining not co-localised with CD31 was also present (Figure 3.14A, B & E). Thymosin β4 and CD34 largely co-localised, though there was some CD34 staining not co-localised with thymosin β4 staining (Figure 3.14A, C & F, white arrows).

Figure 3.15 shows higher magnification images of selected areas from within the field of view shown in Figure 3.14; this field of view is at the junction of the compact and trabecular myocardium of the ventricle (Figure 3.15A). Measurements of fluorescence intensity of each stain across transects demonstrate the co-localisation of thymosin β4, CD31 and CD34 in the different areas (Figure 3.15C-V).

Within the compact layer of the ventricle wall thymosin β4 staining co-localised with both CD31 and CD34 staining (Figure 3.15B-H). Within the trabecular layer of the ventricle wall, thymosin β4 staining co-localised with CD31 and CD34 staining, but thymosin β4 staining was less intense than in the compact layer (Figure 3.15I-O), consistent with data shown in section 3.2.4. Less intense thymosin β4 staining was also present in the compact myocardium and co-localised with CD34, in the absence of CD31 (Figure 3.15P-V).

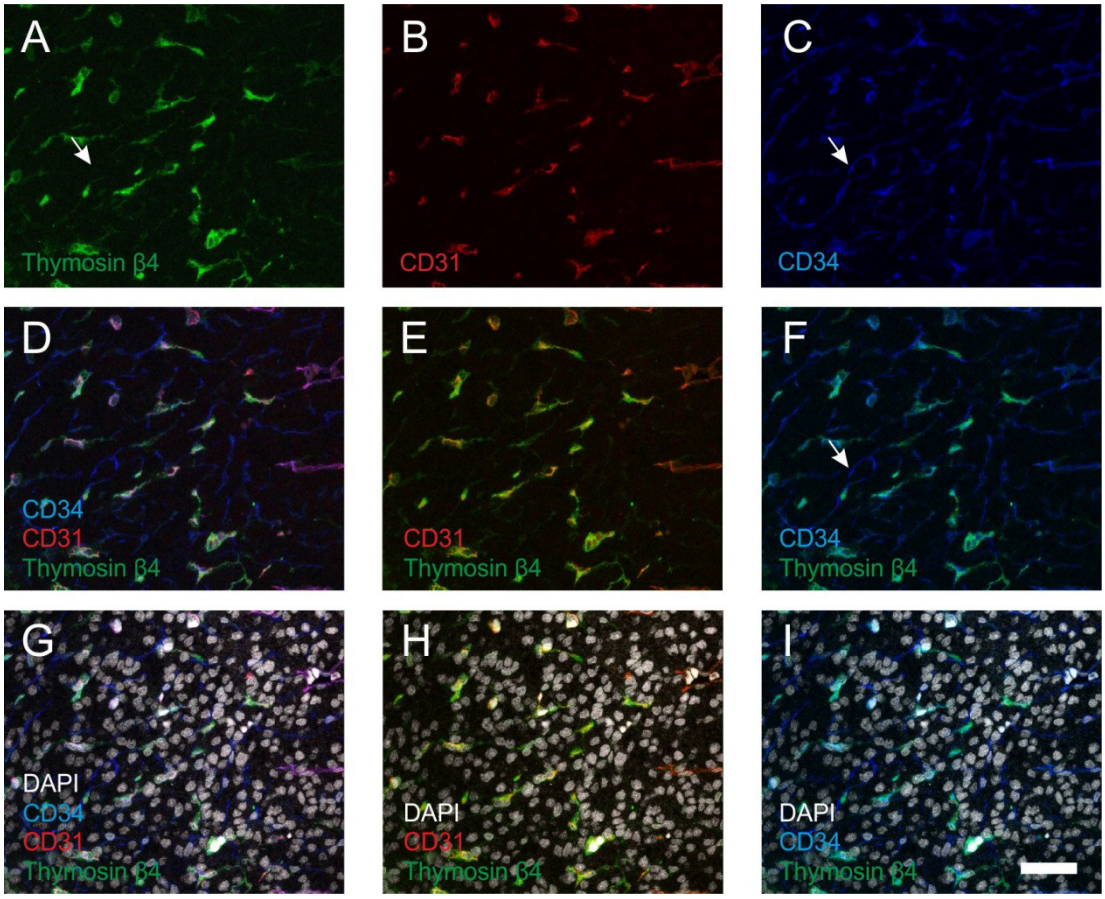

Figure 3.14 – Immunolocalisation of thymosin β4, CD31 and CD34 within the ventricle wall

Images of the ventricle wall from foetal heart sections triple-stained for thymosin β4, CD31 and CD34 are shown. The individual stains for thymosin β4 (A), CD31 (B) and CD34 (C) are shown along with the merged images of all three stains (D), thymosin β4 with CD31 (E) and thymosin β4 with CD34 (F). Merged images with the DAPI nuclear stain are also shown (G–I). The white arrows highlight an area in which CD34 staining is present, but thymosin β4 staining is absent. Images are representative of staining seen in 6 different hearts, ages 7 to 9 post-conception weeks. Scale bars = 40 μm.

Figure 3.15 – Localisation of thymosin β4 protein to individual cells expressing CD31 and CD34

A) An image of the ventricle wall from a foetal heart section triple-stained for thymosin β4, CD31 and CD34 is shown; the compact and trabecular layers of the myocardium are indicated. Rectangles indicate the locations of the high magnification images in the panels indicated.
B-V) The high magnification images show the thymosin β4 stain (C, J, Q), CD31 stain (D, K, R) and CD34 stain (E, L, S) individually, as well as merged and with the DAPI nuclear stain (B, I, P). Fluorescence intensities across transects (yellow lines) were measured and are illustrated as line graphs for each stain individually (F-H, M-O, T-V). Images are representative of staining seen in 6 different hearts, ages 7 to 9 post-conception weeks. Scale bar = 40 μm.

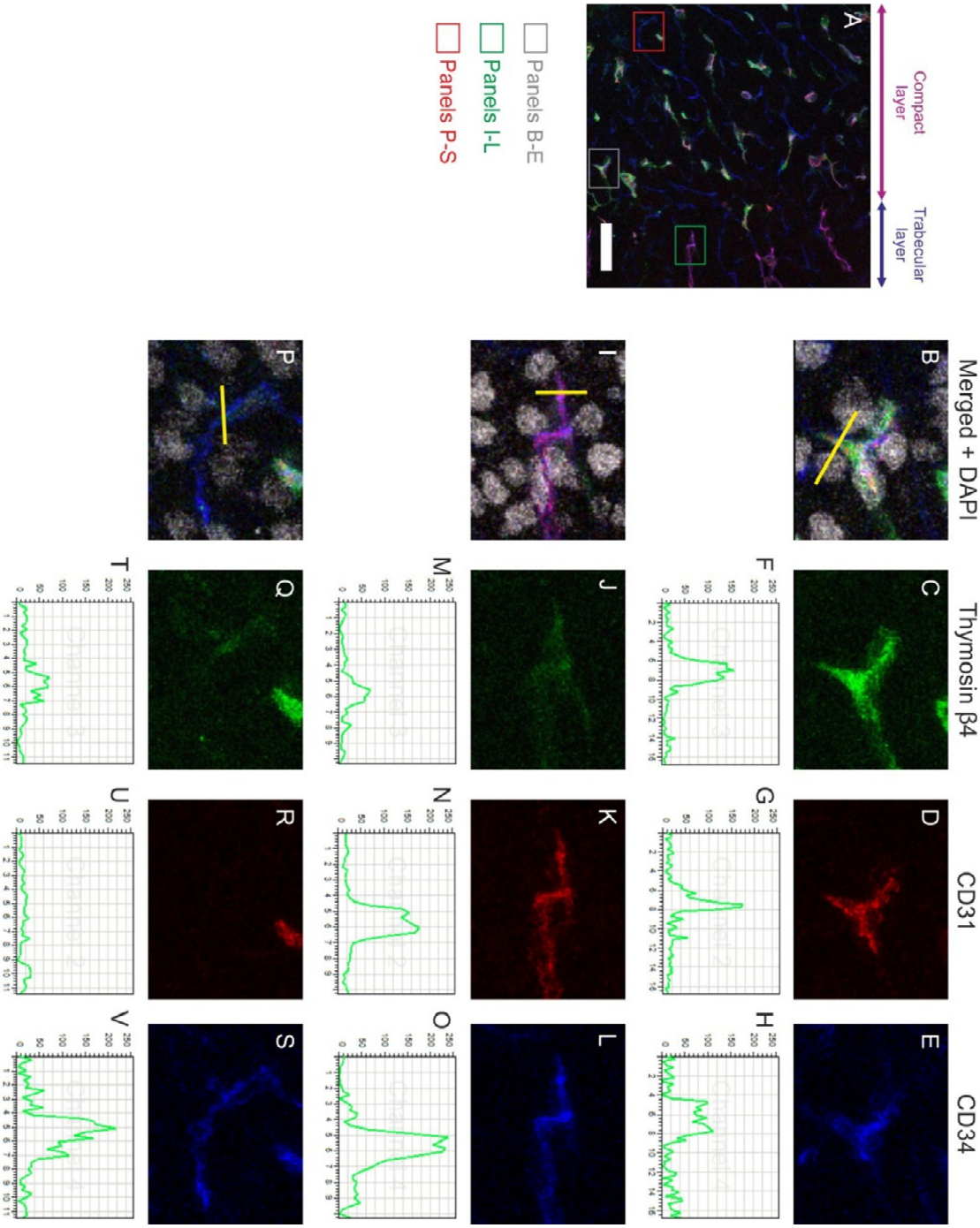
A
Compact layer
Trabecular layer
Panels B-E
Panels I-L
Panels P-S
Merged + DAPI
Thymosin β4
CD31
CD34
B
C
D
E
F
G
H
I
J
K
L
M
N
O
P
Q
R
S
T
U
V

3.3 Discussion

The results presented here demonstrate the expression of thymosin β4 transcripts within the human foetal heart and show the localisation of thymosin β4 protein at the tissue and cellular level.

3.3.1 Thymosin β4 mRNA expression

Thymosin β4 mRNA was found to be expressed in the human foetal heart using PCR. Sanger sequencing was used to confirm that the PCR product detected was amplified from thymosin β4 mRNA rather than transcript produced by the *TMSB4XP4* pseudogene. This suggests that the *TMSB4XP4* gene is not expressed in the foetal heart, at least not at detectable levels. As *TMSB4XP4* is a known pseudogene and does not produce protein, any transcript it does produce is likely expressed transiently before being degraded by nonsense mediated decay.

Thymosin β4 mRNA was expressed in ventricle, atria and outflow tract tissue. The presence of thymosin β4 transcript in the ventricle and outflow tract is consistent with previous reports of thymosin β4 mRNA expression in mice, based on *in situ* hybridisation data. However, Bock-Marquette and colleagues did not detect thymosin β4 mRNA in the atria of mice [170], contrary to the data presented here. This may be due to a difference in the methods of detection. Here, the heart chambers were dissected apart, total RNA extracted and cDNA created which was used as template in PCR reactions. This may be more sensitive to low levels of thymosin β4 mRNA expression than the *in situ* hybridisation used by Bock-Marquette and colleagues [170]. An alternative explanation is the developmental stage at which expression was measured. In the mouse studies the hearts were from E12.5 mice, which is Carnegie stage 18/19 of the embryonic development period. In the current study, human foetuses were between 7 and 9 post-conception weeks, which ranges between Carnegie stage 20 of embryonic development and into the early foetal development period. This could suggest that cells in the atria only begin expressing thymosin β4 in the late stages of the embryonic development period.

As this study seeks to identify thymosin β4-targeting miRNAs it was also important to assess the presence of the different thymosin β4 isoforms, due to the different lengths of 3'-UTR. Due to high sequence similarities between the four isoforms, this was done using primers designed to amplify the 3'-UTR region itself. In this way the PCR products amplified from the three isoforms which have a long 3'-UTR could be differentiated from products amplified from *TMSB4X-004*, which has a short 3'UTR, purely based on product size. Isoforms containing the long 3'-UTR and *TMSB4X-004* were both detected. Had only *TMSB4X-004* been detected, this would have suggested that miRNAs predicted to target the region of thymosin β4's 3'-UTR which is absent from *TMSB4X-004* are not of physiological relevance to regulation of thymosin β4 in the developing heart.

3.3.2 Thymosin β4 protein expression

Using fluorescence immunohistochemistry thymosin β4 protein was demonstrated to be localised to the ventricle, atria and outflow tract, in agreement with the mRNA data. At the intracellular level, thymosin β4 protein was primarily localised to the cytoplasm and was absent from the nuclei of some cells, but present at low levels in the nuclei of other cells.

Within the ventricle wall, co-staining with troponin C demonstrated that thymosin β4 protein is not present within cardiomyocytes. The staining pattern of thymosin β4 suggested that it may be present in the capillaries of the myocardium. To assess whether thymosin β4 was present in endothelial cells, CD31 and CD34 were used as endothelial cell markers. CD34 was found to have a much more widespread staining pattern than CD31, however, indicating it may not only be staining endothelial cells. Cells which dual stained for CD31 and CD34 are concluded to be endothelial cells and as such the data presented here indicates that the majority of thymosin β4-positive cells in the developing human heart are endothelial cells. This is consistent with the presence of thymosin β4 protein in the endothelial cells of the coronary vessels and in the endocardial lining of the chambers.

Notably, endothelial cells in the compact layer of the ventricle wall and interventricular septum were found to express higher levels of thymosin β4 protein than endothelial cells in the trabecular layer of the ventricle wall. This differential expression of thymosin β4 protein between the compact and trabecular layers of the myocardium, as well as the localisation of thymosin β4 primarily to endothelial cells, is in contrast to the immunofluorescent staining of thymosin β4 protein in the mouse heart reported by Smart and colleagues [258]. They reported homogenous thymosin β4 staining throughout the ventricle wall, except in endothelial cells, identified by VEGFR2 staining [258]. Staining was carried out on heart sections from an E14.5 or Carniege stage 20 embryo [258]. As this is in the same developmental period as the human hearts used in the present study, the difference in this result is not due to the developmental stage of the heart.

While genuine differences in species may be one explanation, the homogenous staining seen in the mouse heart may simply be due to poor specificity of the antibody used. Smart and colleagues did not block the antibody they used with thymosin β4 peptide, as was done in the present study, to demonstrate that the antibody is indeed binding thymosin β4 [258]. The data they present does not indicate that the experiment was carried out more than once [258]. They also do not provide any high magnification images or use confocal microscopy, both of which may yield better defined images [258]. The staining pattern seen in the present study, in which the compact layer and interventricular septum have higher expression of thymosin β4 protein than the trabecular layer, is in fact consistent with the enhanced mRNA expression in the same regions of the mouse heart reported not only by Smart and colleagues but also by Bock-Marquette and colleagues [170, 258]. Since the anti-thymosin β4 antibody used in the present study reacts with mouse as well as human thymosin β4, the antibody could be used to stain sections of foetal mouse heart to determine whether the discrepancies in the results seen between the two studies are indeed due to the different antibodies used.

The differential expression of thymosin β4 between the compact and trabecular layers of the myocardial tissue is not unique. The same pattern of expression, as well as the opposite pattern of expression; high in the trabecular layer and

low in the compact layer; is seen with numerous other genes during cardiac development [348]. The formation of the compact myocardial tissue is an important step in cardiac development and is associated with the initial migration of epicardium-derived coronary vessels into the ventricle wall [349]. The trabecular tissue is formed earlier in development and is lined by endocardial endothelial cells, which migrate into the heart at a much earlier stage of development [349]. Therefore the different levels of thymosin β4 protein expression in the endothelial cells of the compact layer compared to the trabecular layer may be due to the different developmental origins of these cells.

As well as being expressed in endothelial cells thymosin β4 was present in a minority of cells which were positive for CD34 but negative for CD31. The identity of these cells is unknown. CD34 is known to be a marker of haematopoietic progenitor cells [350]. However these cells are a rare population even within the blood [351] and are therefore likely to make a negligible contribution to the population of CD34-positive cells seen in foetal heart sections. Studies in rodents suggest that second to cardiomyocytes the most abundant type of cells within the developing heart are cardiac fibroblasts [352]. Fibrocytes are fibroblast progenitor cells that are derived from the bone marrow, and thus express CD34, but which are able to enter tissues and mature into myofibroblasts [353, 354]. The presence of CD34-positive fibrocytes in the adult human heart has recently been reported in relation to fibrosis of the heart [355]. The presence of fibrocytes in the foetal heart has not previously been reported, however the CD34-positive, CD31-negative cells seen in this study may represent a fibrocyte population.

Additionally, thymosin β4 protein was demonstrated to localise to the epicardium. Thymosin β4 mRNA was notably absent from the epicardium of murine hearts at a similar developmental stage, in the study by Smart and colleagues [258]. However, in that study, the authors suggested that thymosin β4 protein released from cardiomyocytes may act in a paracrine fashion on epicardial cells [258]. The immunohistochemistry results shown here may be explained by the internalisation of thymosin β4 protein into epicardial cells,

though it should be noted that the absence of thymosin β4 mRNA in the epicardium of the developing human heart has not been confirmed in this study.

Similarly, the mouse knock-down studies which indicate that thymosin β4 is produced by cardiomyocytes is not contradicted by the data shown here, demonstrating the absence of thymosin β4 protein in cardiomyocytes. Thymosin β4 may be produced by cardiomyocytes but if it is then released in a paracrine fashion, as described, thymosin β4 protein may not localise to cardiomyocytes themselves at significant levels. Another possibility is that cardiomyocytes may express thymosin β4 only in the early stages of heart development, leading to the phenotypes seen in mouse knock-down studies. They may then lose expression later in development, once the epicardium has been activated and the coronary vessels and myocardial capillaries have formed.

Chapter 4: Results – Experimental systems for the identification of thymosin β4-targeting miRNAs in the human heart

4.1 Introduction

In order to identify miRNAs that regulate the expression of a specific protein, it is typical to identify an inverse correlation between expression of the miRNAs and expression of the protein of interest. Studies have often achieved this by identifying miRNAs that are regulated during a particular physiological process or in a particular disease phenotype and further to this identifying the specific target of the miRNAs that are identified.

For example, studies have identified miRNAs which are involved in the inflammatory response in macrophages by inducing an inflammatory response with pro-inflammatory cytokines and using a miRNA microarray to identify miRNAs which are up-regulated [356]. Further studies have then identified the specific factors which the identified miRNAs regulate; in the case of the macrophage inflammatory response, miR-155 was found to be up-regulated while a later study found it directly targets IL-13 and SMAD2 mRNA [357, 358]. Similarly, members of the miR-29 family are down-regulated in lung cancer and have an inverse correlation with DNA methyltransferase 3A and 3B in this context, leading to their identification as targets of miR-29 [359].

Alternatively, conditions may first be identified in which the protein of interest is up- or down-regulated. In the current study, two experimental strategies were explored for the identification of thymosin β4-targeting miRNAs.

In the first strategy, culture of foetal heart explants under hypoxic conditions was used as a model of ischaemic insult in the human heart. Previous research has shown that in the adult murine heart, thymosin β4 protein levels, measured by Western blot, increase following myocardial infarction, from as early as 1 hour, and up to 1 week, post-infarction [258].

In a porcine model of acute heart ischemia, blood samples were taken from the right atria at 5-min intervals during ischaemia and during a resuscitation period which followed the onset of spontaneous ventricular fibrillation [360]. Using an enzyme-linked immunosorbent assay (ELISA), thymosin β4 plasma levels were found to increase over time, becoming significantly greater than control levels at the 15 min time-point post-onset of ischaemia [360]. Furthermore, the rate of increase in thymosin β4 plasma levels accelerated during the resuscitation period [360].

Using *in situ* hybridisation and fluorescence immunohistochemistry, thymosin β4 mRNA and protein levels have also been found to increase with transient ischaemia in the rat brain. 12 hours post-ischaemia, thymosin β4 mRNA was up-regulated in specific regions of the brain. mRNA levels remained enhanced in some regions of the brain, but returned to basal levels in others, by 72 hours. Additionally, fluorescence intensity of thymosin β4 protein staining was enhanced in specific cells in one region of the brain 48 hours post-ischaemia compared to controls.

Studies on cancer cell lines, including HeLa human cervical tumour cells and B16F10 mouse melanoma cells, have further implicated thymosin β4 in hypoxic signalling [181, 361]. They indicate that hypoxia leads to an increase in thymosin β4 expression which in turn leads to stabilisation of hypoxia inducible factor (HIF)1α, a transcription factor well established in hypoxic signalling [181, 361].

These studies suggest that hypoxia may elicit increased thymosin β4 expression within the human foetal heart. Identification of miRNAs that are down-regulated under such conditions would provide a list of candidates that may directly target thymosin β4 mRNA.

The second approach used was based on the results of Chapter 3, which suggest that CD31-positive endothelial cells within the compact layer of the ventricle wall express higher levels of thymosin β4 than CD31-positive endothelial cells in the trabecular layer of the ventricle wall (section 3.2.7). As miRNAs are involved in cell differentiation and determination of cell identity, many miRNAs will differ between two different cell types. This makes it difficult

to identify physiologically relevant miRNAs that may target a specific protein of interest by looking at two different cell types that express differing levels of the protein. However, the two endogenous populations of endothelial cells that were identified in the heart, which differ in their thymosin β4 protein expression, provide an opportunity to identify potential thymosin β4-targeting miRNAs with physiological relevance to the human heart.

Flow cytometry measures the fluorescence of individual cells that are in suspension, enabling the detection of a cell's protein expression through the use of fluorophore-conjugated antibodies. Further to this the cells can be physically sorted and collected according to their fluorescence and light scattering properties by a process known as fluorescence activated cell sorting (FACS). If populations of thymosin β4-high and thymosin β4-low expressing cells can be detected within a population of CD31-positive cells, then it should be possible to separate out these cells by FACS. miRNA levels can then be assessed in each population with the aim of identifying miRNAs that differ in expression between the two populations. Candidate thymosin β4-targeting miRNAs would have expression levels that inversely correlate with thymosin β4 levels.

In order to assess the miRNA content of the cells, RNA will have to be extracted. As thymosin β4 is present within the cell, rather than on the membrane, cells will need to be fixed and permeabilised prior to staining. PFA is most typically used to fix cells for flow cytometry studies and good staining was obtained with the anti-thymosin β4 antibody using PFA-fixed tissue sections for immunohistochemistry in Chapter 3. However, PFA is a cross-linking fixative and is thought to cause RNA fragmentation as well as affecting RNA isolation [362].

In studies assessing the effects of fixative on RNA extraction from tissue slices, alcohol-based fixatives have been shown to yield higher quantities of RNA and result in better RNA quality than cross-linking fixatives [363, 364]. In particular one study found that fixing with a mixture of methanol and acetic acid resulted in extraction of both a high quantity of RNA that was also of good quality [363]. RNA has been successfully extracted from formalin-fixed tissue, however, using

proteinase K to facilitate solubilisation of the tissue and by heating the sample to remove cross-links [362]. Notably short mRNAs were less affected by formalin-fixation [362], suggesting that extraction of intact miRNAs, which are short RNA molecules, from cells fixed with PFA is likely to be successful, using this technique.

The process of cell sorting by FACS, including the need to dissociate tissue into a single cell suspension, is another factor that may affect RNA-extraction from cells. Cells in suspension are likely to be more susceptible to degradation by ribonucleases which may be released from damaged cells. However, in a recent study RNA was successfully extracted from PFA-fixed, FACS-sorted differentiated human ESCs [365].

Another factor that must be taken into account in this study is the potential need to extract RNA from low numbers of cells. The number of thymosin β4-high expressing endothelial cells and thymosin β4-low expressing endothelial cells within a single heart may be relatively low. The percentage of endothelial cells within the human foetal heart is unknown. However, during late development of the mouse heart, at E18.5, the percentage of cells that are neither myocytes nor fibroblasts has been calculated to be approximately 20% [352]. Endothelial cells will only make up a portion of that 20%. Further to this, cells will be lost during tissue dissociation and the wash steps associated with staining cells in suspension. As such, the number of sorted cells in each of the desired populations may be limited.

4.2 Results

4.2.1 Detection of thymosin β4 protein by Western blotting

The detection of thymosin β4 protein by Western blotting was optimised in order to quantify thymosin β4 protein levels in tissue and cells cultured under hypoxic and normoxic conditions.

Protein extracted from foetal placental and skin tissue (section 2.6) was resolved by Laemmli SDS-PAGE (section 2.7.1). The polyacrylamide gel was treated with glutaraldehyde prior to transfer of protein to a nitrocellulose

membrane (section 2.7.3). Glutaraldehyde treatment was used to facilitate the transfer and retention of low molecular weight proteins on to the membrane.

Using a coomassie blue based stain to stain protein that was retained in the gel (section 2.7.3.1) and ponceau red to stain protein that was transferred to the membrane (section 2.7.3.2), it was demonstrated that low molecular weight proteins had been transferred to the membrane while high molecular weight proteins were largely retained in the gel (Figure 4.1A & B).

Staining of the membrane with an anti-thymosin β4 antibody (section 2.7.3.3) revealed detection of thymosin β4 protein in broad smears ranging from approximately 6.5 kDa to 15 kDa (Figure 4.1C). The thymosin β4 stain partially overlapped with the thick bands detected by the ponceau red total protein stain (Figure 4.1B & C). This suggested that while low molecular weight proteins, including thymosin β4, were transferred and retained on the membrane using this protocol, they had not fully separated from each other.

Therefore, tricine-SDS-PAGE (section 2.7.2) was used in place of Laemmli SDS-PAGE to achieve better resolution of low molecular weight proteins. Protein extracted from foetal placental and heart tissue was resolved by tricine-SDS PAGE alongside synthetic thymosin β4 and Western blotting was carried out for detection of thymosin β4 (sections 2.6 and 2.7). Narrow, well-defined bands were detected at 11.5 kDa in placental and heart tissue (Figure 4.2). This is approximately twice the expected weight of thymosin β4, which is a 5 kDa protein; however, synthetic thymosin β4 was detected as a double band, with the highest band also at 11.5 kDa (Figure 4.2).

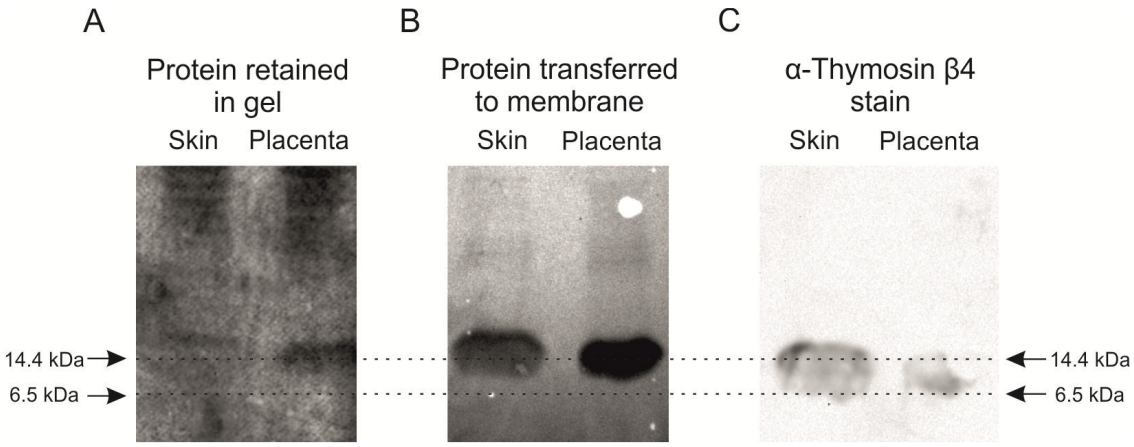

Figure 4.1 – Laemmli SDS-PAGE for detection of thymosin β4 protein

A & B) Protein samples from foetal placental and skin tissue were resolved by Laemmli SDS-PAGE and blotted onto membranes. A total protein stain of the gel post-transfer shows proteins retained in the gel (A). A total protein stain of the membrane post-transfer shows proteins transferred to the membrane (B). C) The blot was stained with an α-thymosin β4 antibody.

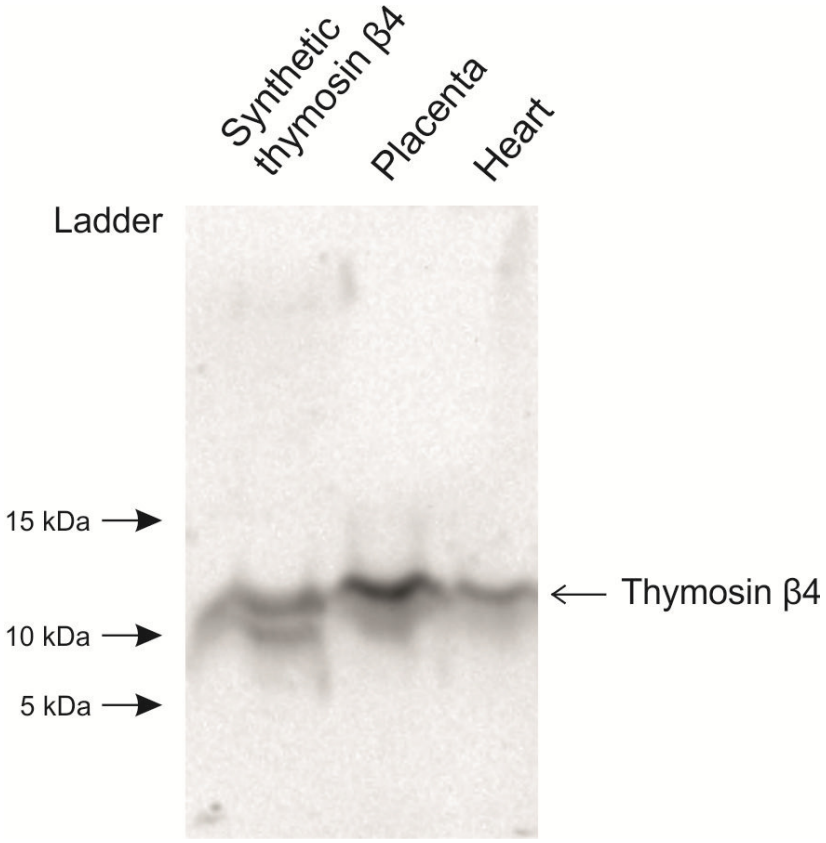

Figure 4.2 – Tricine-SDS-PAGE for detection of thymosin β4 protein

A Western blot for detection of thymosin β4 is shown. Synthetic thymosin β4 or protein samples from foetal placental and heart tissue were resolved by tricine-SDS-PAGE and Western blotting performed using an α-thymosin β4 antibody.

4.2.2 Effect of hypoxia on thymosin β4 protein

The optimised Western blotting technique was used to assess the effect of hypoxia on foetal ventricle explants. Foetal ventricle explants were cultured for 24 hours under normoxic or hypoxic conditions (section 2.8). Protein was extracted and Western blotting carried out (sections 2.6 and 2.7). Densitometry was carried out on bands to quantify protein levels (section 2.7.3.4).

This experiment was carried out six times; three representative blots demonstrate that no consistent trend in thymosin β4 protein expression was detected (Figure 4.3). Thymosin β4 expression normalised to β-actin levels, used as a loading control, showed a 30% decrease in expression in one experiment (Figure 4.3D), a 5% decrease in another (Figure 4.3E) and a 140% increase in a third (Figure 4.3F). However poor band uniformity, as seen in the hypoxic thymosin β4 band in experiment 1 (Figure 4.3A) and the hypoxic β-actin band in experiment 3 (Figure 4.3C) may skew densitometry measurements and the differences in expression seen.

As previous studies demonstrating an effect of hypoxia on thymosin β4 expression have primarily been carried out on cancer cell lines, HeLa cells were used in an attempt to validate this approach. HeLa cells were cultured for 48 hours under normoxic or hypoxic conditions and thymosin β4 protein levels assessed by Western blotting (sections 2.8, 2.6 and 2.7). Three independent experiments were carried out; one experiment showed a 20% increase in normalised thymosin β4 expression (Figure 4.4D), one showed a 90% decrease in expression (Figure 4.4E) and the third showed a 30% decrease in expression (Figure 4.4F).

The differences in the results obtained in the three independent experiments demonstrated an unreliability of this method. In the first experiment, the normoxic thymosin β4 band was smeared and non-uniform, which may affect densitometry (Figure 4.4A). In the second experiment the normoxic thymosin β4 band had an abnormally large densitometry value which may have been due to the band being smeared (Figure 4.4B). Additionally, the lane loading appeared to be unequal in this experiment (Figure 4.4B). The normoxic β-actin band was very faint and non-uniform (Figure 4.4B); if this measurement was unreliable it

would have skewed the normalised data in this experiment, making the difference in experimental conditions appear larger. In experiment 3, lane loading was also unequal (Figure 4.4C), which could again skew the results.

Therefore, while no differences in expression of thymosin β4 were detected under hypoxic conditions by Western blotting, the technique was considered unreliable as a means for quantification.

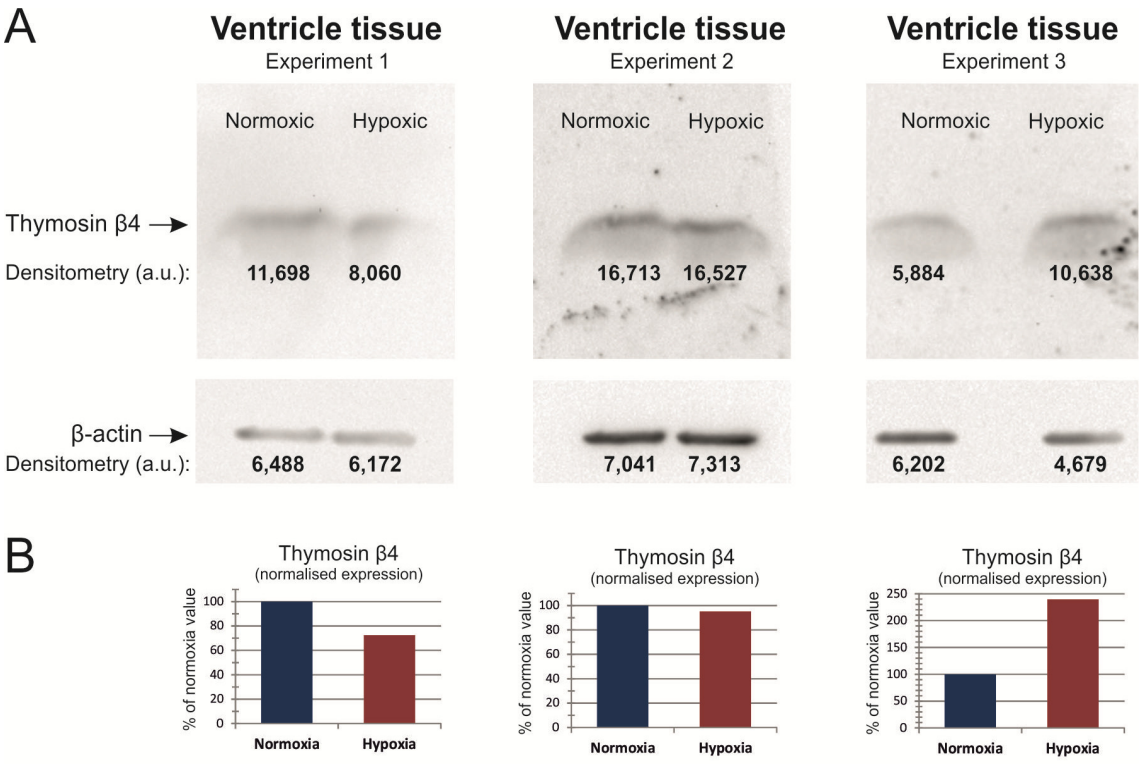

Figure 4.3 –Thymosin β4 protein expression in foetal ventricle tissue cultured under hypoxic and normoxic conditions

Thymosin β4 protein expression in ventricle tissue cultured under normoxic or hypoxic conditions was assessed by Western blot. A–C) Blots of the thymosin β4 stain and β-actin stain, which was used as a loading control, are shown from 3 representative experiments. Band densities were quantified to give densitometry values (arbitrary units, a.u.) as an indication of protein expression and are shown below each band. D–F) Thymosin β4 expression was normalised to β-actin expression. Normalised thymosin β4 expression in hypoxic samples is represented as a percentage of the expression under normoxic conditions.

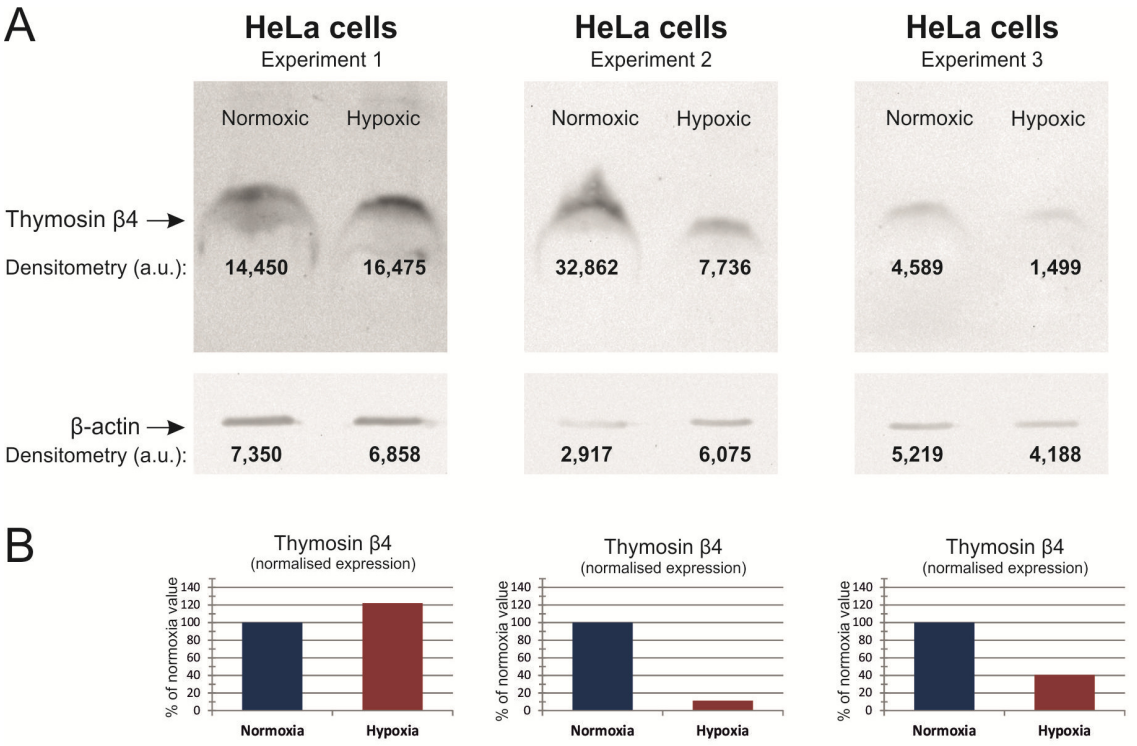

Figure 4.4 – Thymosin β4 protein expression in HeLa cells cultured under hypoxic and normoxic conditions

Thymosin β4 protein expression in HeLa cells cultured under normoxic or hypoxic conditions was assessed by Western blot. A–C) Blots of the thymosin β4 stain and β-actin stain, which was used as a loading control, are shown from 3 representative experiments. Band densities were quantified to give densitometry values (arbitrary units, a.u.) as an indication of protein expression and are shown below each band. D–F) Thymosin β4 expression was normalised to β-actin expression. Normalised thymosin β4 expression in hypoxic samples is represented as a percentage of the expression under normoxic conditions.

4.2.3 Detection of individual cell fluorescence by flow cytometry

A second experimental system used was based on the results of section 3.2.7 which demonstrated by immunohistochemistry the existence of populations of CD31-expressing cells which express high levels of thymosin β4 and low levels of thymosin β4. Experiments were carried out in order to confirm the existence of these populations by flow cytometry, specifically with the aim of sorting cells by FACS and then extracting RNA from sorted cells.

Figure 4.5 shows a diagrammatic representation of flow cytometry data. Scatter plots of forward scattered light, an indication of size, and side scattered light, an indication of granularity are used to characterise the 'events' detected by the flow cytometer (Figure 4.5A). Events include any particle that is detected by the flow cytometer and can include whole cells, damaged cells and debris. Debris tends to have low forward scattered and side scattered light properties and is therefore detected in the bottom left corner of the plot (Figure 4.5A). Homogenous cell populations, such as cell lines, tend to form distinct populations on a plot of forward scattered light against side scattered light (Figure 4.5A). The events that represent cells can be selected with a 'gate' so that only the events in that gate are displayed in further plots (Figure 4.5A).

The fluorescence of each cell can be represented in a scatter plot of fluorescence intensity against forward scattered light. In a sample of stained cells the positive-stained cells will display a rightwards shift on the plot, indicative of an increase in their fluorescence intensity (Figure 4.5B & C). The same data can be summarised in histograms, with peaks representing populations of cells (Figure 4.5D & E). A rightwards shift in the peak (i.e. an increase in fluorescence intensity) of stained cells can be seen compared to unstained cells (Figure 4.5D & E). In an ideal experiment this shift will be in the form of a distinct peak representing positively-stained cells compared to unstained cells (Figure 4.5D & E).

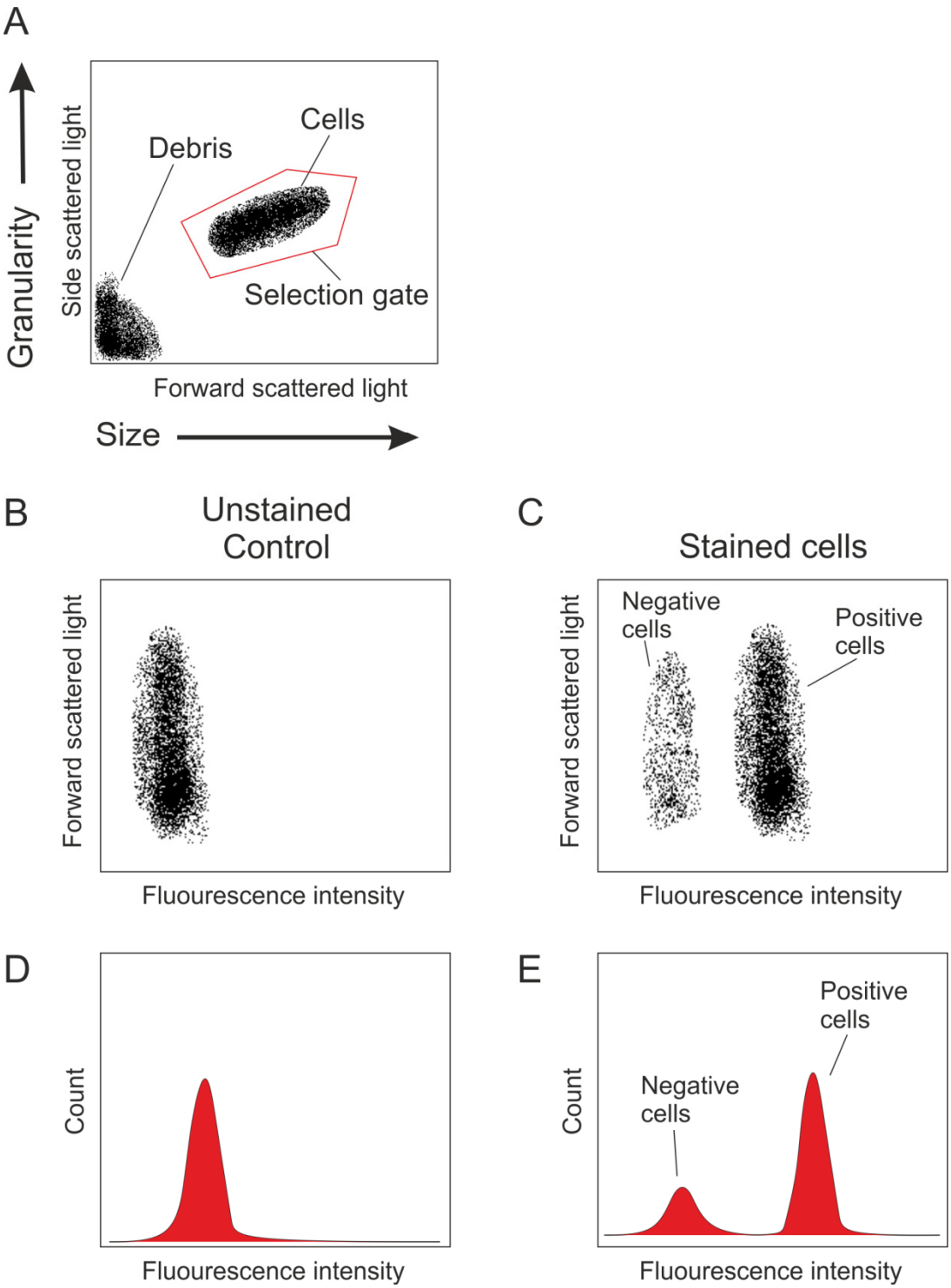

Figure 4.5 – Diagrammatic representation of flow cytometry data

A) Scatter plots of forward scattered light, a measure of size, versus side scattered light, a measure of granularity, were used to define cell populations. B & C) Cells were then characterised in scatter plots of their fluorescence intensity versus forward scattered light. Positively stained cells shift right on the x axis. D & E) The same data was also summarised in histograms of fluorescence intensity.

4.2.4 Detection of CD31-positive cells by flow cytometry

4.2.4.1 Validation of CD31 antibody

Human umbilical vein endothelial cells (HUVECs) were used as a positive control to validate a directly conjugated CD31 antibody for detection of endothelial cells by flow cytometry. The HUVECs were stained with a CD31 antibody directly conjugated to APC (Table 2.17), stained with a matched isotype control antibody (Table 2.17), used as a negative control, or were left unstained; the fluorescence of the cells was measured by flow cytometry (section 2.9).

Unstained cells had a baseline mean fluorescence intensity (MFI) of 48 (Figure 4.6B). On the histogram of fluorescence intensity, a gate was used to select the region to the right of the peak representing unstained cells, including 1.0% of the cell population, to facilitate detection of a rightwards shift in stained cells (Figure 4.6B; P2). Cells stained with a 1:2 dilution of the isotype negative control had an MFI of 106 and displayed a small rightwards shift, placing 5.7% of cells in the P2 gate (Figure 4.6C). Cells stained with a 1:2 dilution of the CD31 antibody had an MFI of 20,734 and displayed a large rightwards shift, placing 98.3% of cells in the P2 gate (Figure 4.6D). Similarly, at 1:100 dilution the isotype control-stained cells had an MFI of 62 and 2.5% of cells in P2 compared with the CD31-stained cells, which had an MFI of 4,744 and 99.3% of cells in P2 (Figure 4.6E & F).

While the MFI of HUVECs was lower when stained with the CD31 antibody at 1:100 dilution compared to 1:2 dilution, the population still undergoes a rightwards shift, forming a distinct peak on the histogram, indicating the antibody successfully stains CD31-positive cells even at low concentration.

4.2.4.2 Detection of CD31-positive cells in foetal heart

Dissociated foetal heart cells were stained with the CD31 antibody, the matched isotope control antibody or left unstained, to assess the detection of CD31-positive cells in dissociated heart tissue (section 2.9). The unstained cells had an MFI of 18. As previously a gate was used to facilitate the identification of a

rightward shift of positive cells (Figure 4.7B; P2). Cells stained with the isotype negative control had an MFI of 94 with 9.3% of cells appearing in the P2 gate (Figure 4.7C). Cells stained with the CD31 antibody had an MFI of 170 with 40% of cells appearing in the P2 gate (Figure 4.7D).

The histogram of the CD31-stained cells had a sharp peak of negative cells and an over-lapping broader peak of positive cells (Figure 4.7D). To better distinguish the positive cells from the negative cells, scatter plots of fluorescence intensity against forward scattered light were plotted (Figure 4.7E-G). The scatter plot of unstained cells showed a distinct population of cells; a gate was used to select the region to the right of this population and denoted the ‘positive gate’ (Figure 4.7E). In the unstained sample, 2.6% of cells were in the positive gate and this increased to 10.5% in the isotype control sample, indicating there was a degree of non-specific, background staining (Figure 4.7E & F). In the CD31-stained sample this increased to 47.5% of cells (Figure 4.7G). The ability to select out the positive cells is important for sorting cells by FACS. The separate populations of CD31-negative and -positive cells were further illustrated on histograms (Figures 4.7H-J).

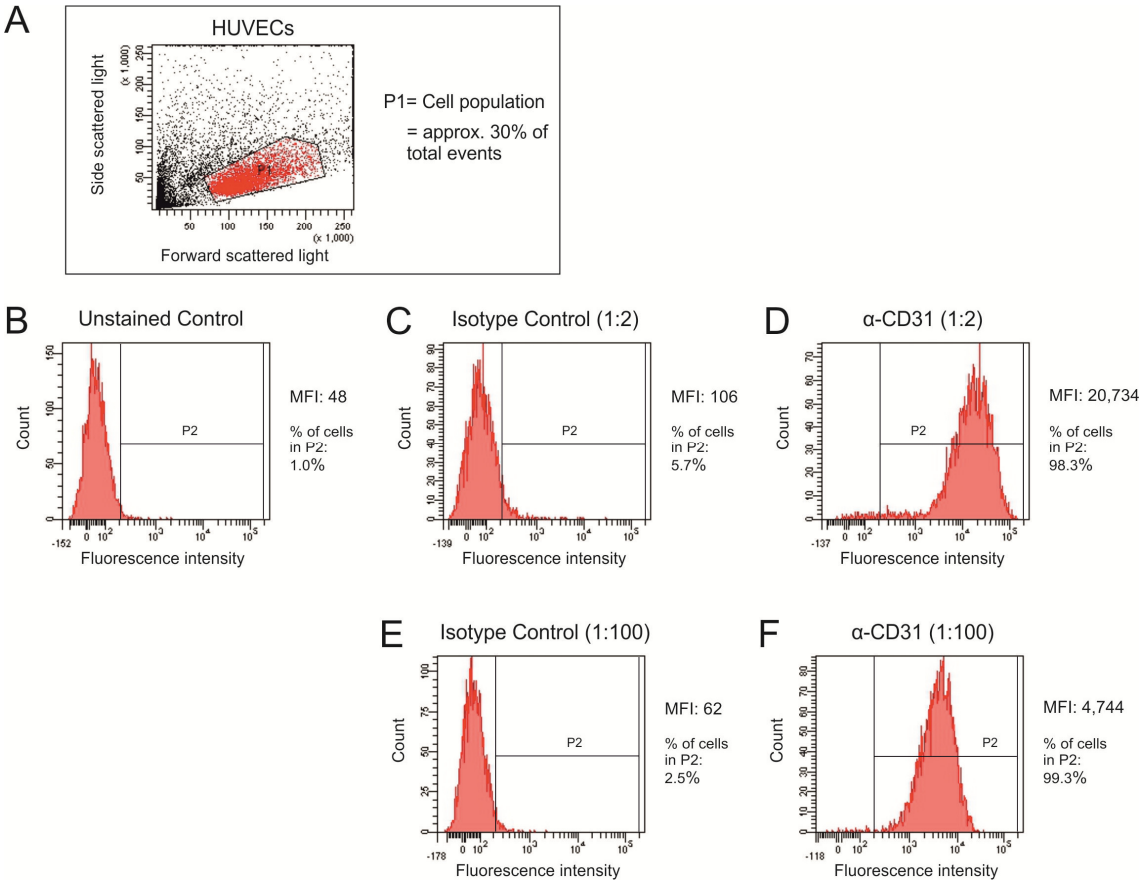

Figure 4.6 – Validation of α-CD31 antibody for flow cytometry using HUVECs

A) The scatter plot used to characterise the sample and select the HUVEC population (P1) is shown. B-F) Histograms of fluorescence intensity are shown for an unstained control sample (B), samples stained at 1:2 dilution with the isotype control antibody (C) or α-CD31 antibody (D), and for samples stained at 1:100 dilution with the isotype control antibody (E) or α-CD31 antibody (F). A gate (P2) was selected, based on the unstained control sample, to assess positive shifts in fluorescence intensity. The mean fluorescence intensity (MFI) of each sample is shown, alongside the percentage of cells in the P2 gate.

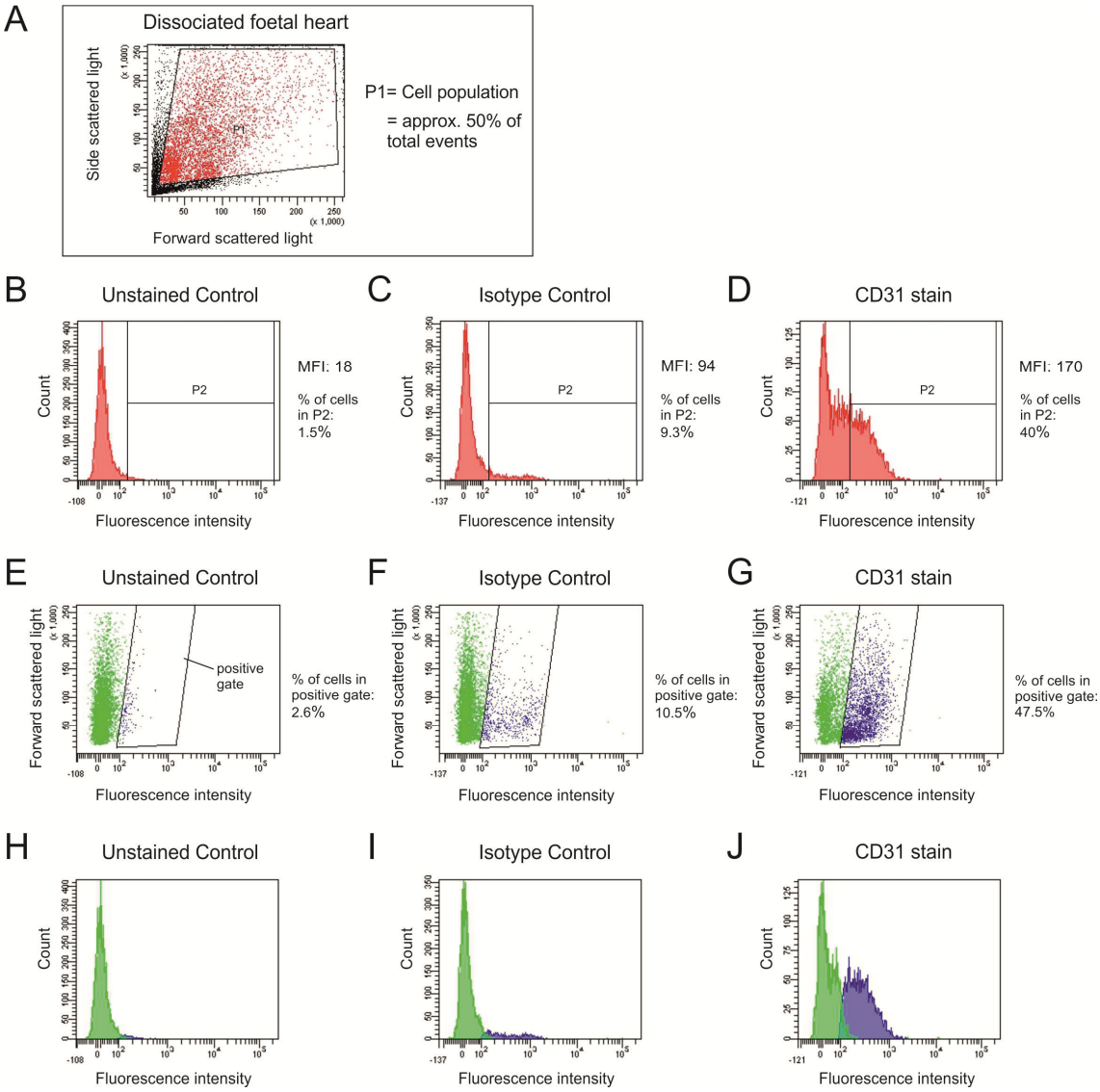

Figure 4.7 – Detection of CD31-positive cells in the human foetal heart

A) The scatter plot used to characterise the sample is shown. The cell population (P1) was selected by omitting events with low forward scattered or side scattered light properties. B-D) Histograms of fluorescence intensity are shown for the unstained control sample (B), the isotype control sample (C) and the CD31 stained sample (D). A gate (P2) was selected, based on the unstained control sample, to assess positive shifts in fluorescence intensity. The mean fluorescence intensity (MFI) of each sample is shown, alongside the percentage of cells in the P2 gate. E-G) Scatter plots of fluorescence intensity against forward scattered light are shown; a 'positive gate' was selected, based on the unstained control, to facilitate identification of CD31-positive cells. Percentage of cells in the positive gate is shown. H-J) Histograms are shown illustrating cells inside and outside the positive gate as separate populations.

4.2.5 Detection of thymosin β4-positive cells by flow cytometry

4.2.5.1 Optimisation of secondary antibody

For detection of thymosin β4-positive cells by flow cytometry, the same anti-thymosin β4 primary antibody was used as in immunohistochemistry and Western blotting. As this antibody is not directly conjugated to a fluorochrome, a secondary antibody had to be used in conjunction with the primary antibody. In flow cytometry, indirect staining can lead to high background signals due to non-specific binding of the secondary antibody and this can mask genuine positive signals. Therefore, several secondary antibodies were tested to find one that produced a low background signal.

The secondary antibodies used were chicken α-rabbit IgG conjugated to Alexa Fluor 647, goat α-rabbit IgG conjugated to FITC and F(ab')2 fragment of goat α-rabbit IgG conjugated to Alexa Fluor 488, which is spectrally similar to FITC (Table 2.17). F(ab')2 fragment antibodies lack the Fc portion of the antibody, preventing non-specific binding of the secondary antibody to Fc receptors, which can be found on the membranes of cells from primary tissue.

PFA-fixed HUVECs were stained with the anti-thymosin β4 primary antibody (Table 2.17) plus each of the secondary antibodies (Table 2.17), stained with each secondary antibody alone, as negative controls, or left unstained (section 2.9). The fluorescence of the cells was then measured by flow cytometry (section 2.9).

The unstained sample had a baseline Alexa Fluor 647 MFI of 13. On the histogram of fluorescence intensity, a gate was used to select the region to the right of the peak representing unstained cells, including approximately 1% of the cell population (Figure 4.8B; P2a). Cells stained with the Alexa Fluor 647 secondary antibody alone had an MFI of 278 and displayed a large rightwards shift, placing 92.87% of cells in the P2a gate (Figure 4.8C). A new gate based on the fluorescence profile of the secondary antibody alone was used to facilitate the detection of any further rightward shift in the positively stained sample (Figure 4.8C; P2b). Cells stained with the anti-thymosin β4 antibody in conjunction with the Alexa Fluor 647 secondary antibody had an MFI of 1351

and displayed a further rightwards shift , placing 99.8% of cells in P2a and 92.8% of cells in P2b (Figure 4.8D). This indicates that while this secondary antibody produced a large amount of background staining, it was possible to detect positive staining above this level.

The baseline FITC/Alexa Fluor 488 MFI in unstained cells was 25 (Figure 4.8E). Gates were used, as previously, to detect rightwards shifts in relation to the unstained sample (Figure 4.8E; P3a), in relation to background staining with the FITC secondary antibody (Figure 4.8F; P3b) and in relation to background staining with the Alexa Fluor 488 secondary antibody (Figure 4.8H; P3c).

Cells stained with the FITC secondary antibody alone had an MFI of 106 and displayed a moderate rightwards shift, placing 33.4% of cells in the P3a gate (Figure 4.8F). Cells stained with the anti-thymosin β4 antibody in conjunction with the FITC secondary antibody had an MFI of 575 and displayed a further rightwards shift , placing 98.9% of cells in P3a and 92.8% of cells in P3b (Figure 4.8G).

Cells stained with the Alexa Fluor 488 secondary antibody alone had an MFI of 63 and displayed a small rightwards shift, placing 5.9% of cells in the P3a gate (Figure 4.8H). Cells stained with the anti-thymosin β4 antibody in conjunction with the Alexa Fluor 488 secondary antibody had an MFI of 674 and displayed a large rightwards shift compared to the secondary antibody alone, placing 99.1% of cells in P3a and 98.0% of cells in P3c (Figure 4.8I).

The Alexa Fluor 488 secondary antibody produced the least background staining, with a distinct shift in fluorescence intensity detected in the stained sample. Therefore this secondary antibody was used in further experiments.

Figure 4.8 – Optimisation of secondary antibody for detection of thymosin β4 by flow cytometry using HUVECs

A) The scatter plot used to characterise the sample and select the HUVEC population (P1) is shown. B–I) Histograms of fluorescence intensity are shown for unstained controls (B & E) and samples stained with each of the following secondary antibodies alone as controls (C, F, H) or in conjunction with an α-thymosin β4 antibody (D, G, I): chicken α-rabbit IgG conjugated to Alexa Fluor 647 (C & D), goat α-rabbit IgG conjugated to FITC (F & G), F(ab')2 fragment of goat α-rabbit IgG conjugated to Alexa Fluor 488 (H & I). Gates were used to assess positive shifts in fluorescence intensity. Gates were selected based on fluorescence of the unstained control (P2a and P3a) or on fluorescence of samples stained with secondary antibodies alone (P2b, P3b, P3c). The mean fluorescence intensity (MFI) of each sample is shown, alongside the percentage of cells in each gate.

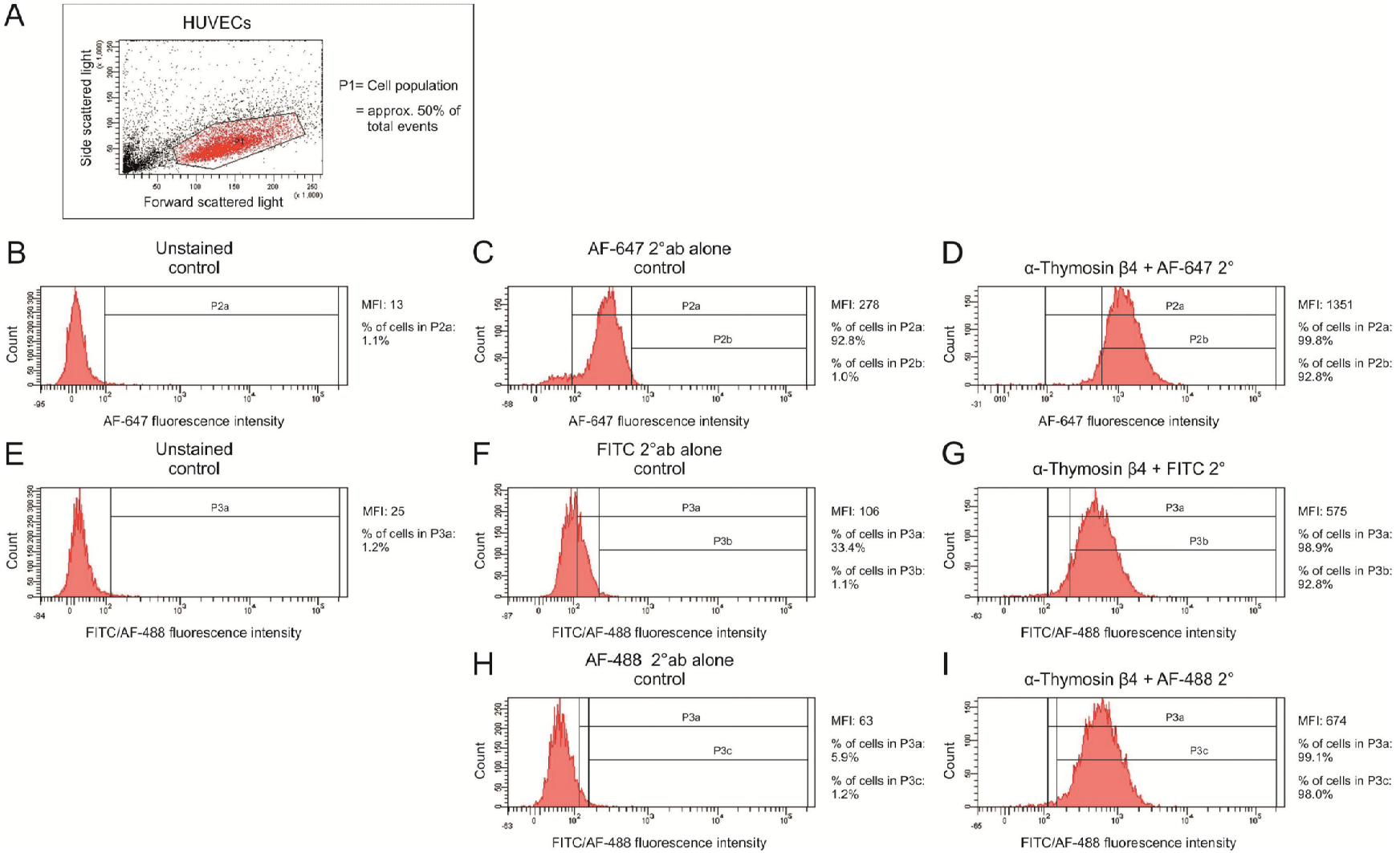
A
HUVECs
Side scattered light
Forward scattered light
P1= Cell population
= approx. 50% of total events
B
Unstained control
P2a
MFI: 13
% of cells in P2a: 1.1%
Count
AF-647 fluorescence intensity
C
AF-647 2°ab alone control
P2a
P2b
MFI: 278
% of cells in P2a: 92.8%
% of cells in P2b: 1.0%
Count
AF-647 fluorescence intensity
D
α-Thymosin β4 + AF-647 2°
P2a
P2b
MFI: 1351
% of cells in P2a: 99.8%
% of cells in P2b: 92.8%
Count
AF-647 fluorescence intensity
E
Unstained control
P3a
MFI: 25
% of cells in P3a: 1.2%
Count
FITC/AF-488 fluorescence intensity
F
FITC 2°ab alone control
P3a
P3b
MFI: 106
% of cells in P3a: 33.4%
% of cells in P3b: 1.1%
Count
FITC/AF-488 fluorescence intensity
G
α-Thymosin β4 + FITC 2°
P3a
P3b
MFI: 575
% of cells in P3a: 98.9%
% of cells in P3b: 92.8%
Count
FITC/AF-488 fluorescence intensity
H
AF-488 2°ab alone control
P3a
P3c
MFI: 63
% of cells in P3a: 5.9%
% of cells in P3c: 1.2%
Count
FITC/AF-488 fluorescence intensity
I
α-Thymosin β4 + AF-488 2°
P3a
P3c
MFI: 674
% of cells in P3a: 99.1%
% of cells in P3c: 98.0%
Count
FITC/AF-488 fluorescence intensity

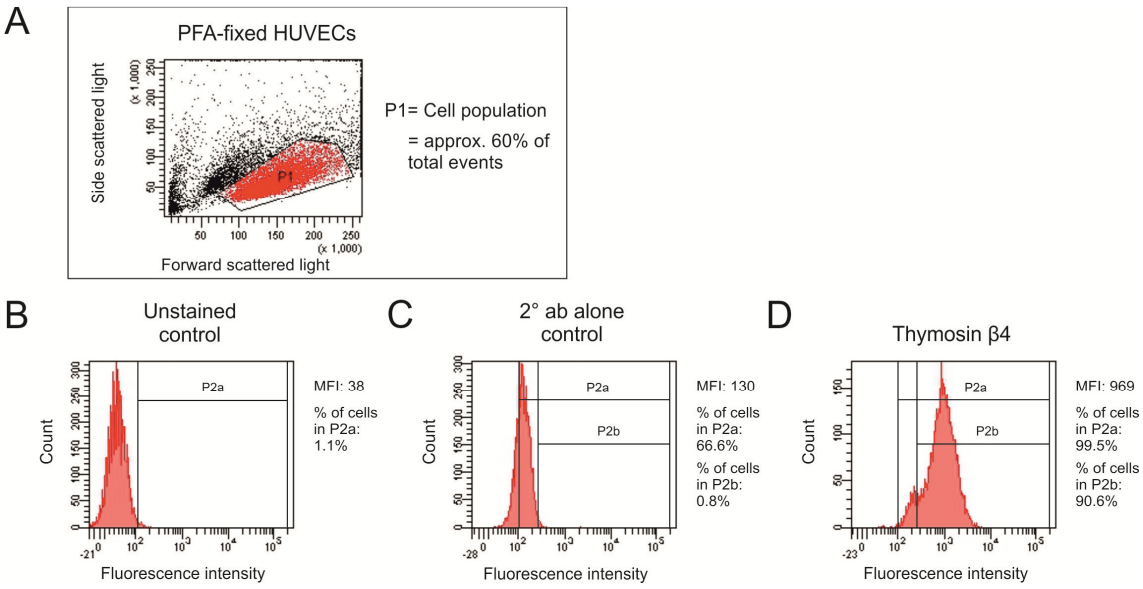

Figure 4.9 – Thymosin β4 staining of PFA-fixed HUVECs

A) The scatter plot used to characterise the sample and select the HUVEC population (P1) is shown. B-D) Histograms of fluorescence intensity are shown for an unstained control sample (B), control sample stained with the secondary antibody alone (C) and thymosin β-stained sample (D). Gates were selected based on fluorescence of the unstained control sample (P2a) and the secondary antibody-stained control sample (P2b), to assess positive shifts in fluorescence intensity. The mean fluorescence intensity (MFI) of each sample is shown, alongside the percentage of cells each gate.

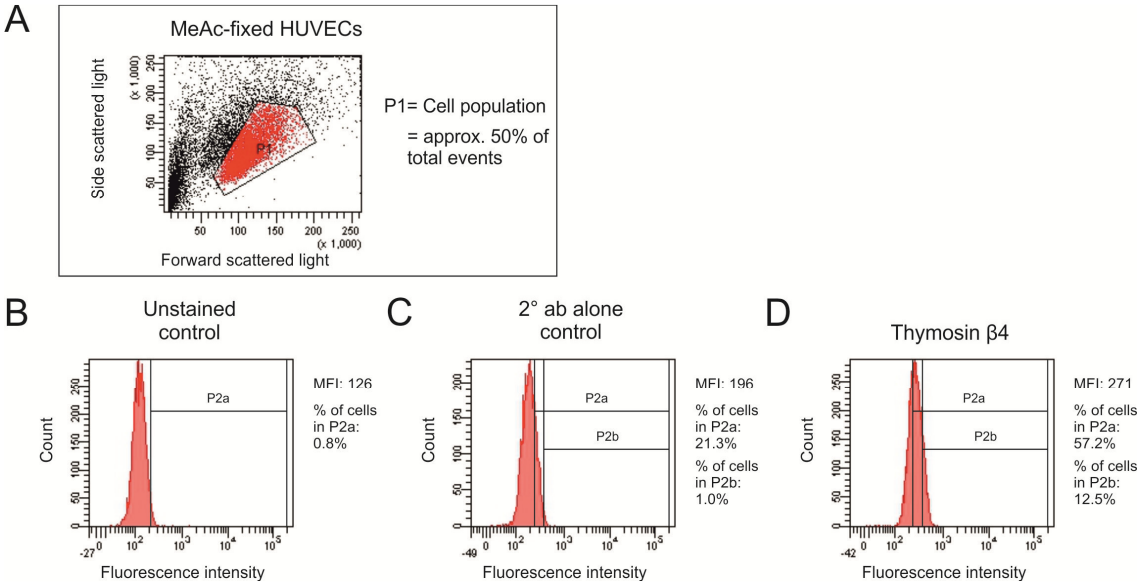

Figure 4.10 – Thymosin β4 staining of MeAc-fixed HUVECs

A) The scatter plot used to characterise the sample and select the HUVEC population (P1) is shown. B-D) Histograms of fluorescence intensity are shown for an unstained control sample (B), control sample stained with the secondary antibody alone (C) and thymosin β-stained sample (D). Gates were selected based on fluorescence of the unstained control sample (P2a) and the secondary antibody-stained control sample (P2b), to assess positive shifts in fluorescence intensity. The mean fluorescence intensity (MFI) of each sample is shown, alongside the percentage of cells each gate.

4.2.5.2 Optimisation of cell fixative for flow cytometry

MeAc may be a preferential fixative for the extraction of RNA from cells following sorting. Therefore, HUVECs were fixed with MeAc or 4% PFA prior to staining for thymosin β4 in order to compare the quality of staining, as detected by flow cytometry (section 2.9).

The unstained PFA-fixed cells had an MFI of 38 (Figure 4.9B). Negative control cells stained with secondary antibody alone had an MFI of 130 with 66.6% of cells appearing in the P2 gate (Figure 4.9C). The cells stained for detection of thymosin β4 had an MFI of 969 and underwent a large rightwards shift, with 99.5% of cells appearing in the P2 gate (Figure 4.9D).

For the MeAc-fixed cells, the unstained cells had an MFI of 124 (Figure 4.10B). The cells stained with the secondary antibody alone had an MFI of 193 with 30.9% of cells in P2 while the thymosin β4-stained cells had an MFI of 267 and underwent only a small rightward shift, with 70.1% of cells in P2 (Figure 4.10C & D). While positively-stained cells could be identified as a distinct population from the negative control cells when PFA was used as a fixative (Figure 4.9), the population of positively-stained MeAc-fixed cells over-lapped with the population seen in the negative control (Figure 4.10). Therefore, PFA was used to fix cells in subsequent experiments.

4.2.5.3 Detection of thymosin β4-positive cells in foetal heart

Dissociated foetal heart cells were stained for detection of thymosin β4, with the secondary antibody alone as a negative control, or left unstained in order to assess the detection of thymosin β4-positive cells in dissociated heart tissue (sections 2.9). The unstained cells had an MFI of 21 and 4.9% of cells were included in the P2 gate (Figure 4.11B). Cells stained with the secondary antibody alone had an MFI of 33 with 8.6% of cells appearing in the P2 gate (Figure 4.11C). Cells stained for detection of thymosin β4 had an MFI of 214 with 30.2% of cells appearing in the P2 gate (Figure 4.11D). The thymosin β4-positive cells did not appear as a separate population on the histogram, but over-lapped with the negative population (Figure 4.11D).

Scatter plots of fluorescence intensity against forward scattered light were used to better distinguish thymosin β4-positive and -negative cells (Figure 4.11E-G). A 'positive gate' was placed based on the fluorescence of the cell populations in the unstained and negative control samples (Figure 4.11E & F). In the unstained sample, 2.9% of cells were in the positive gate and this increased to 3.6% in the secondary antibody alone control, indicating non-specific, background staining was low (Figure 4.11E & F). In the thymosin β4-stained sample this increased to 19.8% of cells (Figure 4.11G). The populations of thymosin β4-postive and –negative cells were further illustrated on histograms, illustrating successful detection of a small population of thymosin β4-postive cells in the stained sample, largely over-lapping with the thymosin β4-negative population (Figures 4.11H-J).

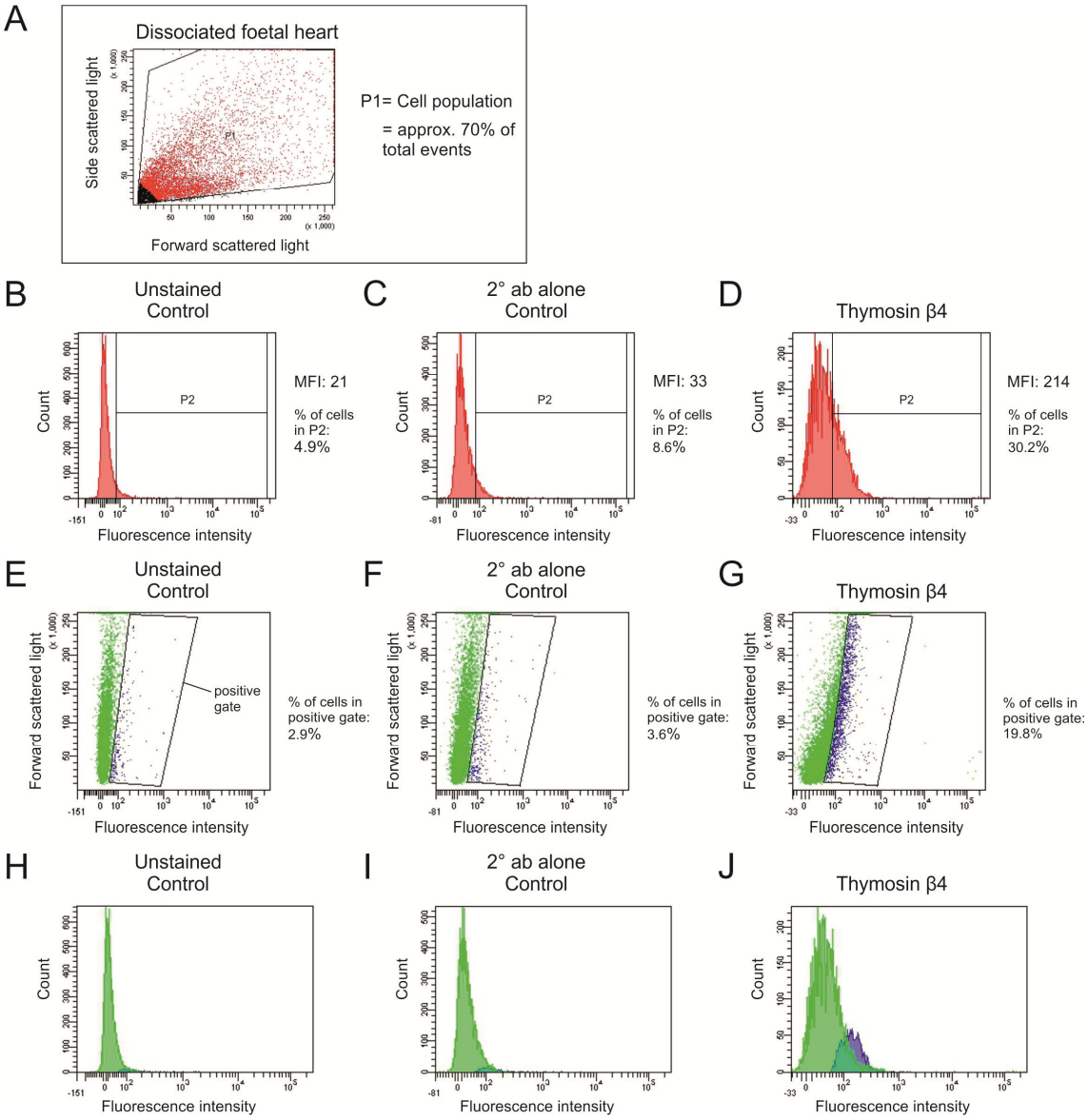

Figure 4.11 – Detection of thymosin β4-positive cells in the human foetal heart

A) The scatter plot used to characterise the sample is shown. The cell population (P1) was selected by omitting events with low forward scattered and side scattered light properties. B-D) Histograms of fluorescence intensity are shown for the unstained control sample (B), the control sample stained with secondary antibody alone (C) and the thymosin β4 stained sample (D). A gate (P2) was selected, based on the unstained control sample, to assess positive shifts in fluorescence intensity. The mean fluorescence intensity (MFI) of each sample is shown, alongside the percentage of cells in the P2 gate. E-G) Scatter plots of fluorescence intensity against forward scattered light are shown; a 'positive gate' was selected, based on the unstained control, to facilitate identification of thymosin β4-positive cells. Percentage of cells in the positive gate is shown. H-J) Histograms are shown illustrating cells inside and outside the positive gate as separate populations.

4.2.6 Detection of thymosin β4-positive cells within the CD31-positive population

Dissociated heart cells were dual stained for CD31 and thymosin β4 detection by flow cytometry (section 2.9). Scatter plots of Alexa Fluor 488 fluorescence against APC fluorescence were plotted and divided into quadrants to detect shifts in fluorescence (Figure 4.12B-D). Shifts into Q1 and Q2 are indicative of increases in APC fluorescence while shifts into Q2 and Q4 are indicative of increases in Alexa Fluor 488 fluorescence (Figure 4.12B-D).

The unstained cells had an APC MFI of 73 with 3.9% of cells in Q1 and Q2 (Figure 4.12B). In the negative control sample, APC MFI increased to 156 with 20.7% of cells in Q1 and Q2, indicative of some non-specific background staining (Figure 4.12C). In the stained sample the APC MFI increased to 244 with 34.2% of cells in Q1 and Q2, indicating the detection of CD31-positive cells (Figure 4.12D).

Similarly, the unstained cells had an Alexa Fluor 488 MFI of 83 with 7.2% of cells in Q2 and Q4, with the MFI increasing to 241 in the negative control sample, with 25.4% of cells in Q2 and Q4 (Figure 4.12B & C). In the stained sample the Alexa Fluor 488 MFI increased to 351 with 37.2% of cells in Q1 and Q2, indicating the detection of thymosin β4-positive cells (Figure 4.12D).

In order to determine the presence of distinct thymosin β4-negative and thymosin β4-positive populations of CD31-expressing cells, the CD31-expressing cells were selected out (Figure 4.13A). Approximately 40,000 cells were predicted to be in this population. The fluorescence intensity of thymosin β4 within only the CD31-expressing population was plotted in scatter plots of fluorescence intensity against forward scattered light (Figure 4.13B & C). Distinct populations of thymosin β4-negative and thymosin β4-positive cells could be selected, with the thymosin β4-positive cells comprising 18.4% of the CD31-expressing population (Figure 4.13D & E).

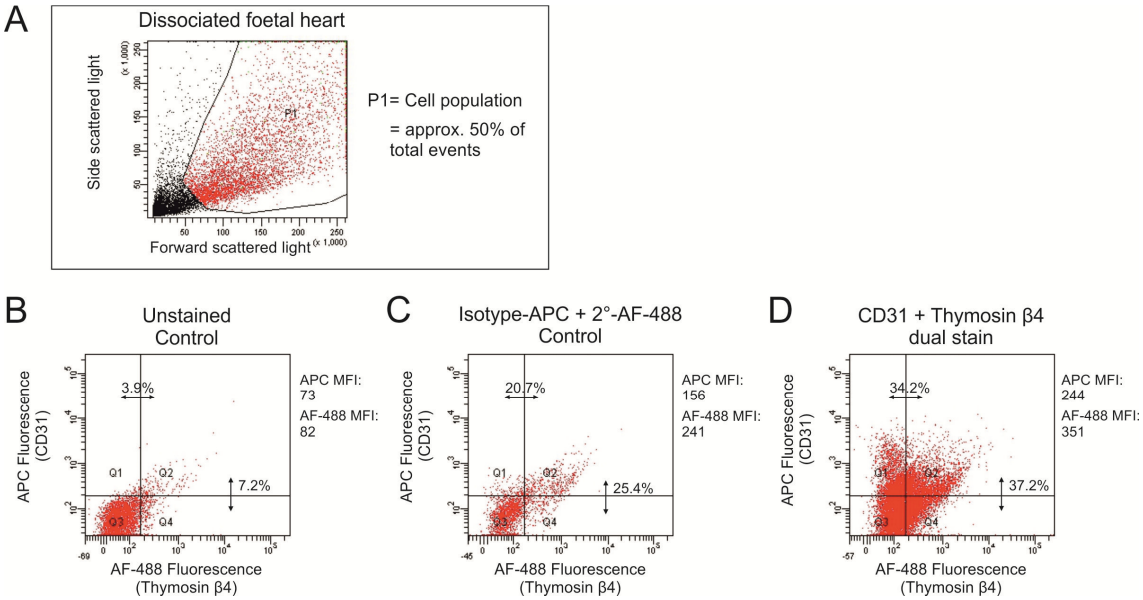

Figure 4.12 – Thymosin β4 and CD31 dual-stain of human foetal heart cells

A) The scatter plot used to characterise the sample is shown. The cell population (P1) was selected by omitting events with low forward scattered and side scattered light properties. B–D) Scatter plots of FITC fluorescence against APC fluorescence are shown for an unstained sample (B), a control sample stained with the APC-conjugated isotype control antibody and the Alexa Fluor-488-conjugated secondary antibody (C), and a sample dual-stained for detection of CD31 and thymosin β4 (D). The mean fluorescence intensity (MFI) of each fluorophore is given for each sample. The plots are divided into quadrants based on the fluorescence of the unstained control, to help assess positive shifts in fluorescence (Q1 – Q4). The percentage of cells in Q1 plus Q2 (positive for APC fluorescence) and the percentage of cells in Q2 plus Q4 (positive for Alexa Fluor-488 fluorescence) are indicated for each sample.

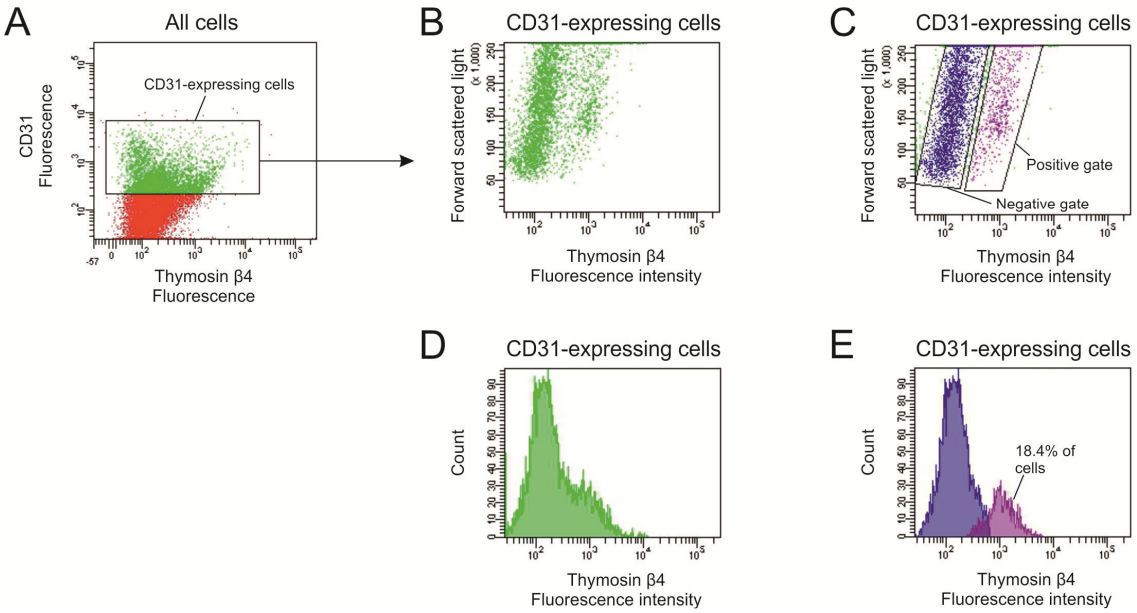

Figure 4.13 – Detection of thymosin β4-positive and -negative cells within the CD31-expressing population of a human foetal heart sample

A) The scatter plot of thymosin β4 fluorescence against CD31 fluorescence for the dual-stained sample of dissociated foetal heart cells is shown. A gate was used to select only CD31-positive cells. B & C) Scatter plots of thymosin β4 fluorescence intensity against forward scattered light for the CD31-expressing cells are shown. The thymosin β4-positive and -negative cells were selected with gates (C). D & E) Histograms of thymosin β4 fluorescence intensity are shown for all CD34-expressing cells (D) and for the separate populations of thymosin β4-positive and -negative cells (E).

4.2.7 Extraction of RNA from PFA-fixed cells

To ensure that RNA could be extracted from PFA-fixed cells, foetal placental tissue was dissociated and fixed as it would be prior to staining for flow cytometry (section 2.9). RNA was extracted using a modified TriFast LS extraction involving addition of proteinase K and heating of the sample, and using a RecoverAll kit designed for the extraction of RNA from PFA-fixed, paraffin-embedded tissue sections (section 2.2.2). 735 ng of RNA was extracted using TRIzol and 1464 ng using the RecoverAll kit (Table 4.1). Following reverse transcription to cDNA, PCR was carried out using primers designed for detection of *OAZ1*, a housekeeping gene (sections 2.2.3 and 2.3 and Table 2.5). Bands representing detection of *OAZ1* were present in both samples, indicating that cDNA could be created from RNA extracted from PFA-fixed cells by both methods (Figure 4.14A).

Similarly, to ensure that RNA could be extracted from relatively low numbers of PFA-fixed cells that had been sorted by FACS, HeLa cells were PFA-fixed and approximately 90,000 cells were sorted by a FACS machine into two separate tubes (section 2.9). The TriFast RNA extraction yielded 1012 ng of RNA and the RecoverAll kit yielded 897 ng (Table 4.1). Using PCR on reverse transcribed samples (sections 2.2.3 and 2.3), *OAZ1* was detected in both samples (Figure 4.14B).

Table 4.1 – RNA extraction from PFA-fixed cells

The amounts of RNA extracted by two different methods from PFA-fixed cells from dissociated foetal placental tissue and from PFA-fixed, FACS-sorted HeLa cells are shown.

		Extraction technique	
		TriFast	RecoverAll kit
Sample	Dissociated foetal placental tissue	735 ng	1464 ng
	FACS-sorted HeLa cells	1012 ng	897 ng

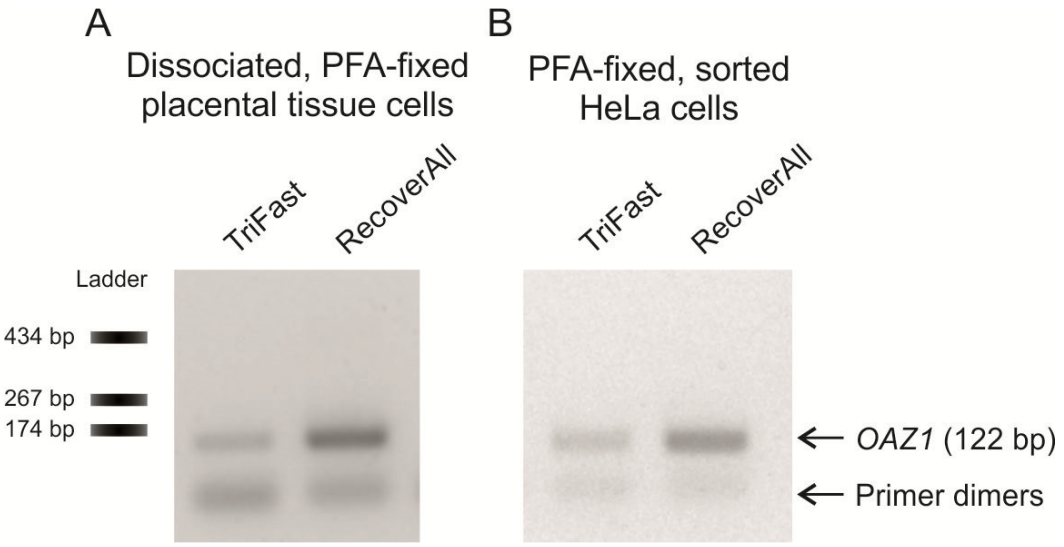

Figure 4.14 – Detection of cDNA derived from RNA extracted from PFA-fixed cells

cDNA was synthesised from mRNA extracted from PFA-fixed cells using TriFast LS or a RecoverAll kit. The cDNA was used as template and amplified with OAZ1 primers by PCR; the products, resolved on a 2% agarose gel, are shown. Bands indicating the detection of OAZ1 cDNA were seen in all four samples. The faint, low molecular weight bands are primer dimers.

4.3 Discussion

4.3.1 Effect of hypoxia on thymosin β4 measured by Western blotting

The data presented here demonstrates that thymosin β4 protein could be detected by Western blotting. This was achieved by using tricine-SDS-PAGE to resolve low molecular weight proteins and then using glutaraldehyde to cross-link protein molecules to ensure transfer and retention of low molecular weight proteins on the membrane. Despite thymosin β4 being a 5 kDa protein it was detected at approximately twice this weight; this band was confirmed to be thymosin β4 by running synthetic thymosin β4 alongside tissue samples. This indicates that the size discrepancy is not due to post-translational modifications, but does not exclude the possibility of dimerization. The synthetic thymosin β4 ran as a double band, which may be explained by oxidation or degradation of the molecule.

No consistent differences in thymosin β4 protein levels in ventricle tissue explants cultured under normoxic and hypoxic conditions were detected by Western blotting. However, this may have been due to the inconsistent appearance of the bands, making quantification unreliable.

Thymosin β4 protein levels have previously been shown to increase in both murine and porcine models of heart ischemia [258, 360]. However, *in vivo* ischemia is induced by the restriction of the blood supply to tissue. This affects multiple factors in addition to reducing oxygen levels, including reductions in glucose levels, for example. Therefore, hypoxia alone may not have an effect on thymosin β4 levels in foetal heart explants.

As studies on cancer cell lines have specifically linked hypoxia to increases in thymosin β4 levels [181, 361], the expression of thymosin β4 in HeLa cells under hypoxic conditions was assessed using Western blotting. Cultured cells represent a simpler experimental system than tissue explant cultures and any effect of hypoxia on thymosin β4 may have been more evident.

Unfortunately, the Western blots obtained from experiments in which HeLa cells were cultured under normoxic and hypoxic conditions were also variable, with

no consistent trend in expression seen. The non-uniform and smeared appearance of the bands suggest they may not be representative of protein levels. In conclusion, thymosin β4 levels could not be reliably assessed by Western blotting, indicating a better method of quantification would be beneficial.

While hypoxia has not directly been shown to up-regulate thymosin β4 in HeLa cells, treatment of HeLa cells with thymosin β4 mimics hypoxia and leads to stabilisation of HIF-1α. Thymosin β4 expression has been reported to increase under hypoxic conditions in B16F10 murine melanoma cells, however the study used end-point PCR with agarose gels to assess thymosin β4 mRNA levels and observed less than a 4-fold increase in expression [361]. It is also unclear how many independent experiments were carried out [361]. End-point PCR can produce variable results from the same starting sample and is not believed to be sensitive enough to reliably detect changes less than 10-fold in magnitude. Using qPCR would produce much more reliable and sensitive results. The study also presents Western blotting data, however only one blot is shown [361]. Additionally, the lane loading is not consistent as indicated by the large variability in band density of the loading control they used [361]. As in the present study this leads to difficulty in interpreting the results.

Hypoxia has also been shown to up-regulate thymosin β4 mRNA expression in MSCs, however only a 2-fold increase was observed [366]. While qPCR was used, the number of independent experiments carried out is not given [366].

4.3.2 Detection of thymosin β4-positive and -negative populations of CD31-postive endothelial cells by flow cytometry

Using HUVECs as a positive control, the staining of cells for detection of CD31 and thymosin β4 by flow cytometry was confirmed.

In order to minimise background staining associated with the thymosin β4 stain, three different secondary antibodies were tested. An F(ab')2 fragment of a goat α-rabbit IgG antibody conjugated to Alexa Fluor 488 produced the least background staining, suggesting that binding of the other secondary antibodies to Fc receptors on the cells contributed to the non-specific background binding.

The potential to use MeAc as a fixative in place of PFA was assessed, as RNA extraction from MeAc-fixed cells is easier and has been shown to yield higher quantities of good quality RNA [363]. The thymosin β4 staining was lower in MeAc-fixed cells however, with little increase in fluorescence intensity between the secondary antibody alone control and the stained sample.

When dissociated heart cells were stained for detection of CD31 it was possible to detect a distinct population of positive cells. This would be important for selecting out only positive CD31 cells in dual-stained samples so that thymosin β4 expression could be assessed only within the endothelial cell population.

Thymosin β4 staining of dissociated heart cells did not result in such a distinct population of positive cells, however. Despite this, a thymosin β4-positive population of cells was detected, which over-lapped with the thymosin β4-negative population.

As the aim was to detect thymosin β4-expressing cells within a selected CD31-postive endothelial cell population, dissociated heart cells were dual stained for detection of CD31 and thymosin β4. The CD31-positive cells were first gated out and the expression of thymosin β4 was assessed only in this population of cells. In this experiment the distinction between CD31-positive and -negative cells was not clear. However, once the CD31-positive cells were selected it was possible to detect a distinct population of thymosin β4-positive cells and a population of thymosin β4-negative cells. Negative, low and high populations of thymosin β4 expressing cells could not be distinguished, however.

Given the low levels of fluorescence of thymosin β4-positive cells it may be that cells with low levels of thymosin β4 expression were indistinguishable from the thymosin β4-negative cells. However, separation of thymosin β4-negative/low and thymosin β4-positive cells would still provide a means of identifying potential thymosin β4-targeting miRNAs. In addition, using a directly conjugated anti-thymosin β4 primary antibody, may produce a stronger positive signal without increasing background staining, as would occur if the secondary antibody concentration were increased.

Further studies could be carried out to assess the purity of the CD31-positive population by sorting the cells, extracting the RNA and assessing the presence of CD31 mRNA in the CD31-positive and negative populations. The thymosin β4-positive and negative populations could be verified in a similar way. An alternative approach would be to initially select out the CD31-positive endothelial cells by magnetic-activated cell sorting. These cells could then be stained for thymosin β4 detection and their fluorescence assessed by flow cytometry. The presence of different thymosin β4-expressing populations may be clearer and allow for purer sorting by FACS if the starting cell population is already a selected population of endothelial cells.

As PFA was the preferential fixative in terms of thymosin β4 staining, the ability to extract intact RNA from PFA-fixed cells was assessed. RNA was successfully extracted from dissociated tissue and was also successfully extracted from a low number of cultured HeLa cells that had been sorted through a FACS machine. cDNA was successfully created from both RNA samples, as demonstrated by the detection of *OAZ1* cDNA by PCR. miRNAs are thought to be less susceptible to the fragmentation that occurs with PFA-fixing due to their small size. As such, these results strongly suggest that miRNAs will also be intact in RNA extracted from PFA-fixed cells by the methods used.

The data presented here suggests that sorting CD31-positive endothelial cells which have differential thymosin β4 expression and then extracting RNA from the sorted cells is possible. Unfortunately, due to limited availability of foetal heart tissue it was not possible to continue with this experimental strategy. With access to tissue the next steps would have been to physically sort the cells by FACS to give samples of thymosin β4-positive endothelial cells and thymosin β4-negative/low endothelial cells. RNA would then be extracted from the cells and the miRNAs in each sample assessed either by TaqMan miRNA assay, to look at individual candidate miRNAs, or by miRNA microarray, to assess the miRNA profile of each cell population. This choice would depend on the amount of RNA that could be extracted from the cells.

As this was not possible an alternative strategy was developed to establish a system that would allow investigation of thymosin β4 regulation.

Chapter 5: Results – Assessment of thymosin β4 and microRNA expression in a model of endothelial cell differentiation

5.1 Introduction

As thymosin β4 was localised to endothelial cells in the human foetal heart (section 3.2.7), an endothelial cell line may provide an alternative cell source in which to explore the miRNA-mediated regulation of thymosin β4 in the absence of foetal tissue.

As described in sections 1.4.1 and 1.4.2, thymosin β4 has been implicated in the activation of murine epicardial progenitor cells within the heart leading to differentiation into vessel-forming cells, including endothelial cells [258, 260]. The importance of thymosin β4 in the formation of mature endothelial cells was first suggested in the *in vitro* HUVEC tubule formation assay studies described in section 1.3.3.2.

When cultured on Matrigel basement membrane, HUVECs form networks and differentiate into mature tubule-forming cells, in a process which is used as a model of angiogenesis. In these studies HUVECs plated on Matrigel were found to start forming networks by 4 hours after plating, but not by 2 hours [200]. Using Northern analysis, mRNA levels of thymosin β4 were found to increase 5-fold in HUVECs cultured on Matrigel between the 2 hour and 4 hour time points, concurrent with formation of tubule networks [200]. These levels of thymosin β4 mRNA were maintained at the 6 hour time point [200]. HUVECs cultured on plastic, on the other hand, showed no differences in thymosin β4 mRNA levels across this time course [200].

The time frame in which thymosin β4 mRNA levels were reported to be up-regulated in the HUVEC tubule formation assay is consistent with regulation by miRNAs. If miRNAs are targeting thymosin β4 mRNA molecules within the cell and directing their degradation, then the down-regulation of those miRNAs would lead to a rapid increase in thymosin β4 mRNA levels. Studies have shown that miRNA levels can decrease rapidly, with certain brain-enriched

miRNAs having half-lives as short as 0.7 hours in cultured human neural cells [367]. Of five brain-enriched miRNAs assessed the most stable had a half-life of 3.4 hours, illustrating the rapid degradation of miRNA molecules [367]. Further to this, miRNA levels have been demonstrated to have a rapid response to external stimuli; levels of specific miRNAs in retinas of mice placed in the dark decrease in approximately 1.5 hours [368]. When the mice are returned to light conditions, these miRNAs rapidly increase within 0.5 hours [368].

The rapid degradation kinetics of miRNAs is consistent with a potential decrease in specific miRNAs being responsible for the up-regulation of thymosin β4 mRNA within 4 hours in HUVEC tubule formation assays. The baseline expression of miRNAs within endothelial cells has previously been assessed using miRNA microarray by McCall and colleagues [369]. Importantly they indicate that of 166 miRNAs expressed, only 3 differed significantly between types of endothelial cells [369]. The endothelial cells they investigated included HUVECs and human coronary artery endothelial cells, indicating that miRNAs identified to regulate thymosin β4 in HUVECs may also be of importance in endothelial cells of the heart.

Therefore the HUVEC tubule formation assay was used as a model of endothelial cell differentiation. Expression of thymosin β4 and candidate miRNAs would be assessed in tubule-forming HUVECs cultured on Matrigel and in control HUVECs cultured on tissue culture plastic. miRNAs found to be down-regulated concurrently with up-regulation of thymosin β4 would be potential thymosin β4-targeting miRNAs. Direct targeting of the 3'-UTR of thymosin β4 mRNA by miRNAs identified in this way could then be assessed in experiments such as luciferase assays in which the 3'-UTR of thymosin β4 is coupled to a fluorescent reporter gene. Assessment of miRNA levels in the HUVEC tubule formation assay may additionally identify miRNAs of importance in the process of angiogenesis.

5.2 Results

5.2.1 Identification of candidate thymosin β4-targeting miRNAs

In silico analysis was carried out in order to identify candidate thymosin β4-targeting miRNAs that may be of relevance within the heart, to be measured in the HUVEC tubule formation assays.

To identify putative thymosin β4-targeting miRNAs, the microRNA.org online database was searched for miRNAs predicted to target the 3'-UTR of thymosin β4 mRNA (section 2.10.1). This search yielded a list of 143 miRNAs (Appendix 1). Using raw data (available from Wilson and Sanchez-Elsner lab) from a miRNA array previously carried out using cDNA reverse transcribed from human foetal heart tissue RNA (section 2.10), 484 miRNAs were detected that are present in the foetal heart (Appendix 2). Comparing these two lists, 62 miRNAs were identified which are present in a human foetal heart and predicted to target thymosin β4 (Table 5.1). The cycle threshold (Ct) values of these miRNAs, taken from the microarray, are shown along with their mirSVR scores, obtained from microRNA.org. mirSVR scores are a prediction of a miRNAs ability to down-regulate a target. The more negative the score, the greater the predicted down-regulation.

The top 15 thymosin β4-targeting miRNA candidates detected in the heart, based on their mirSVR scores, are shown in Figure 5.1. Figure 5.1 indicates the binding locations on the 3'-UTR of thymosin β4, which is illustrated to be highly conserved across vertebrate species. The levels of conservation are based on phyloP conservation scores, as provided by the UCSC Genome Browser database.

As the chosen miRNAs were to be assessed within the HUVEC tubule formation assay, candidate miRNAs (Table 5.1) were further selected by cross-referencing with miRNAs reported to be expressed in endothelial cells by McCall and colleagues [369]. This resulted in a list of 15 miRNAs (Table 5.2). Based on their mirSVR scores, 4 of these miRNAs were selected for further study: miR-148b, miR-199a-3p, miR-217 and miR-495 (Figure 5.2).

5.2.2 Expression of candidate miRNAs in the human foetal heart

To confirm the results of the previously carried out microarray, the expression levels in foetal human heart of the four selected candidate miRNAs were assessed using TaqMan miRNA assays. RNA was extracted from foetal heart tissue and miRNA reverse transcription reactions were carried out for each for the four miRNAs (section 2.2.4). TaqMan miRNA assays were carried out using the cDNA samples obtained in order to quantify miRNA levels by real-time quantitative PCR (section 2.4.1). Plots of fluorescence measured after each cycle of a 50 cycle PCR amplification illustrate that miR-148b, miR-199a-3p, miR-217 and miR-495 were all amplified from foetal heart template, confirming their expression (Figure 5.3).

Table 5.1 – Candidate miRNAs present in human foetal heart

miRNAs predicted using miRNA.org to target the 3'-UTR of thymosin β4 which were detected in the human foetal heart are shown. Cycle threshold (Ct) values from the miRNA array are shown. The lower the Ct value, the higher the expression. mirSVR scores obtained from miRNA.org are shown. The more negative the value the greater the predicted ability of the miRNA to down-regulate thymosin β4.

miRNA	Ct	mirSVR score		miRNA	Ct	mirSVR score
hsa-miR-1	15.34	-1.3335		hsa-miR-96	27.55	-0.2624
hsa-miR-206	22.22	-1.3335		hsa-miR-130a	16.34	-0.2533
hsa-miR-579	25.90	-1.3203		hsa-miR-454	15.52	-0.2488
hsa-miR-520d-5p	29.56	-1.2741		hsa-miR-130b	17.93	-0.2488
hsa-miR-183	26.92	-1.2641		hsa-miR-301a	17.97	-0.2466
hsa-miR-152	16.89	-1.25		hsa-miR-301b	20.91	-0.2466
hsa-miR-148b	22.38	-1.25		hsa-miR-186	15.64	-0.2375
hsa-let-7g*	28.06	-1.2474		hsa-miR-106a*	29.71	-0.1729
hsa-miR-148a	19.79	-1.2406		hsa-miR-210	17.92	-0.1701
hsa-miR-200b*	30.68	-1.1068		hsa-miR-517a	23.73	-0.1552
hsa-miR-200a*	30.42	-1.0999		hsa-miR-517c	23.86	-0.1552
hsa-miR-29a*	26.48	-1.0425		hsa-miR-223*	28.53	-0.155
hsa-miR-199a-3p	15.67	-1.0268		hsa-miR-218	12.69	-0.1549
hsa-miR-217	31.74	-0.9327		hsa-miR-519a	24.67	-0.1373
hsa-miR-222*	23.34	-0.8831		hsa-miR-519c-3p	31.52	-0.1373
hsa-miR-302a*	24.66	-0.5734		hsa-miR-519b-3p	27.74	-0.1373
hsa-miR-450b-5p	22.53	-0.5234		hsa-miR-493*	24.43	-0.1278
hsa-miR-495	19.84	-0.4945		hsa-miR-550*	28.67	-0.1213
hsa-miR-7-2*	25.50	-0.4911		hsa-miR-30a	15.06	-0.1168
hsa-miR-488	25.76	-0.4846		hsa-miR-30e	16.46	-0.1168
hsa-miR-20a*	21.31	-0.4409		hsa-miR-30d	17.84	-0.1168
hsa-miR-656	23.20	-0.4091		hsa-miR-520g	31.80	-0.1161
hsa-miR-551b*	24.58	-0.397		hsa-miR-30c	11.92	-0.1157
hsa-miR-139-5p	17.86	-0.3571		hsa-miR-30b	12.57	-0.1157
hsa-miR-124	29.44	-0.3346		hsa-miR-944	29.62	-0.107
hsa-miR-15b*	19.81	-0.3329		hsa-miR-93	16.86	-0.1028
hsa-miR-506	29.17	-0.3319		hsa-miR-518d-5p	31.65	-0.102
hsa-miR-545*	27.05	-0.3218		hsa-miR-17	12.76	-0.1017
hsa-miR-522	27.28	-0.3034		hsa-miR-106a	12.85	-0.1017
hsa-miR-610	28.94	-0.3015		hsa-miR-20a	13.17	-0.1007
hsa-miR-128	21.53	-0.2708		hsa-miR-122	25.02	-0.1

Table 5.2 – Candidate miRNAs present in human foetal heart and in endothelial cells

The list of miRNAs shown in Table 5.1 was cross-referenced with a list of miRNAs detected in endothelial cells, published by McCall and colleagues [369]. The mirSVR scores obtained from miRNA.org are shown. The more negative the value the greater the predicted ability of the miRNA to down-regulate thymosin β4.

miRNA	mirSVR score
miR-148b	-1.25
miR-199a-3p	-1.0268
mIR-217	-0.9327
miR-495	-0.4945
miR-139-5p	-0.3571
miR-128	-0.2708
miR-130a	-0.2533
miR-130b	-0.2488
miR-30a	-0.1168
miR-30d	-0.1168
miR-30b	-0.1157
miR-30c	-0.1157
miR-93	-0.1028
miR-17	-0.1017
miR-20a	-0.1007

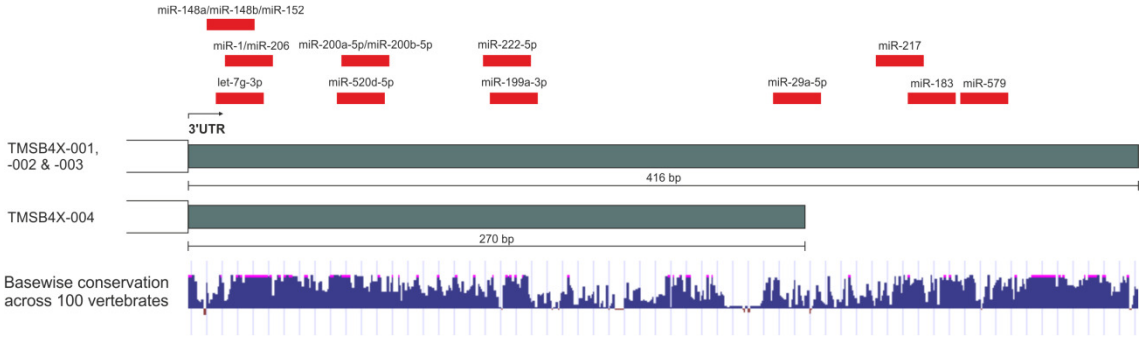

Figure 5.1 – 15 best predicted thymosin β4-targeting miRNAs present in human foetal heart

Diagrammatic representation of the 3'-UTR of thymosin β4 showing binding sites of the 15 miRNAs best predicted to target thymosin β4 that were detected in the human foetal heart. The basewise conservation (taken from UCSC Genome Browser database) are based on phyloP conservation scores.

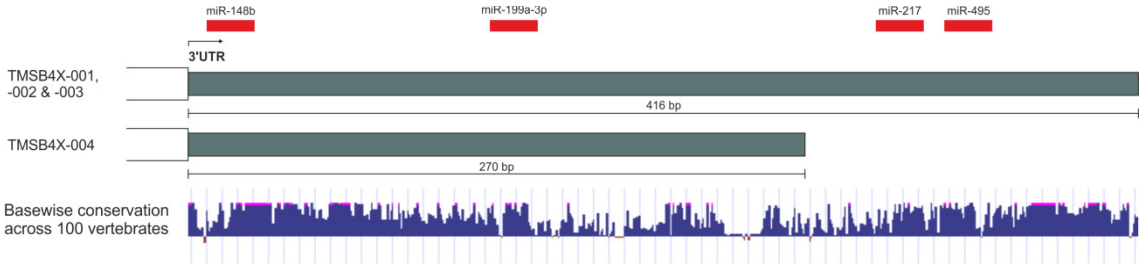

Figure 5.2 – 4 best predicted thymosin β4-targeting miRNAs present in human foetal heart and endothelial cells

Diagrammatic representation of the 3'-UTR of thymosin β4 showing binding sites of the 4 miRNAs best predicted to target thymosin β4 that were detected in the human foetal heart by miRNA array and indicated by McCall and colleagues [369] to be present in endothelial cells. The basewise conservation (taken from UCSC Genome Browser database) are based on phyloP conservation scores.

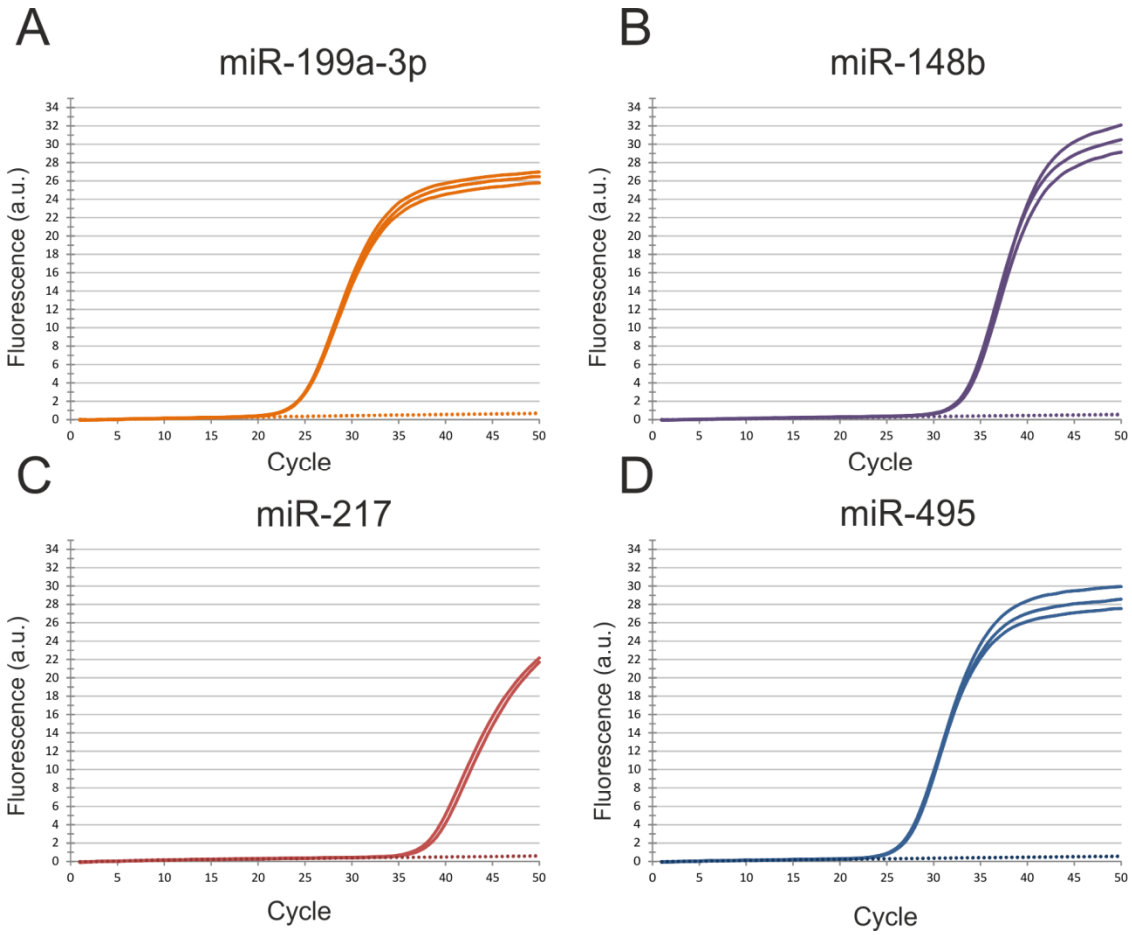

Figure 5.3 – Amplification of candidate miRNAs in human foetal heart

Plots of fluorescence (arbitrary units, a.u.) over 50 PCR cycles are shown from reactions carried out using TaqMan MicroRNA Assays for detection of miR-199a-3p (A), miR-148b (B), miR-217 (C) and miR-495 (D). Multiple technical repeats (A, B, D: n = 3; C: n = 2) are shown using cDNA from human foetal heart as template (solid lines) and using water as a 'no template' control (dotted lines).

5.2.3 Creation of a pRL-TK vector containing the 3'-UTR of *TMSB4X*

It was anticipated that of the four candidate miRNAs identified, one or more would prove to have a role in HUVEC tubule formation. The miRNAs could then be investigated further, using luciferase assays in order to assess a direct effect of the miRNA on the 3'-UTR of thymosin β4 mRNA. In anticipation of this, a pRL-TK vector was created in which the *Renilla* luciferase gene is under the control of the 3'-UTR of the thymosin β4 gene.

The cloning strategy for the creation of this vector involved the amplification of the 3'-UTR of *TMSB4X* by PCR from genomic DNA template using specifically designed primers (Table 2.5; TMSB4X 3'-UTR primers) (Figure 5.4A). The PCR product was to be inserted into a pCR2.1-TOPO vector, a vector designed to receive a PCR product amplified by *Taq* polymerase (Figure 5.4B). The primers to be used to amplify the 3'-UTR contained restriction sites at their 5' ends; the forward primer included an *Nhe* I restriction site, while the reverse primer included a *Not* I restriction site (Figure 5.4A). This would allow the cloned 3'-UTR to be removed from the pCR2.1-TOPO vector and ligated into a pRL-TK vector, following amplification of the plasmid in bacterial cultures (Figure 5.4C & D). The pRL-TK vector to be used (kindly provided by Tilman Sanchez-Elsner) contained the 3'-UTR of *SMAD2* following the cDNA sequence coding the *Renilla* luciferase enzyme (Figure 5.4F). An *Xba* I restriction site was located directly up-stream of the 3'-UTR of *SMAD2*, while a *Not* I restriction site was located directly down-stream (Figure 5.4F). As *Xba* I and *Nhe* I produce compatible cohesive ends, removal of the 3'-UTR of *SMAD2* by restriction digest with *Xba* I and *Not* I would allow for insertion of the 3'-UTR of thymosin β4, digested by *Nhe* I and *Not* I, into the same site and in the desired orientation (Figure 5.4D & E).

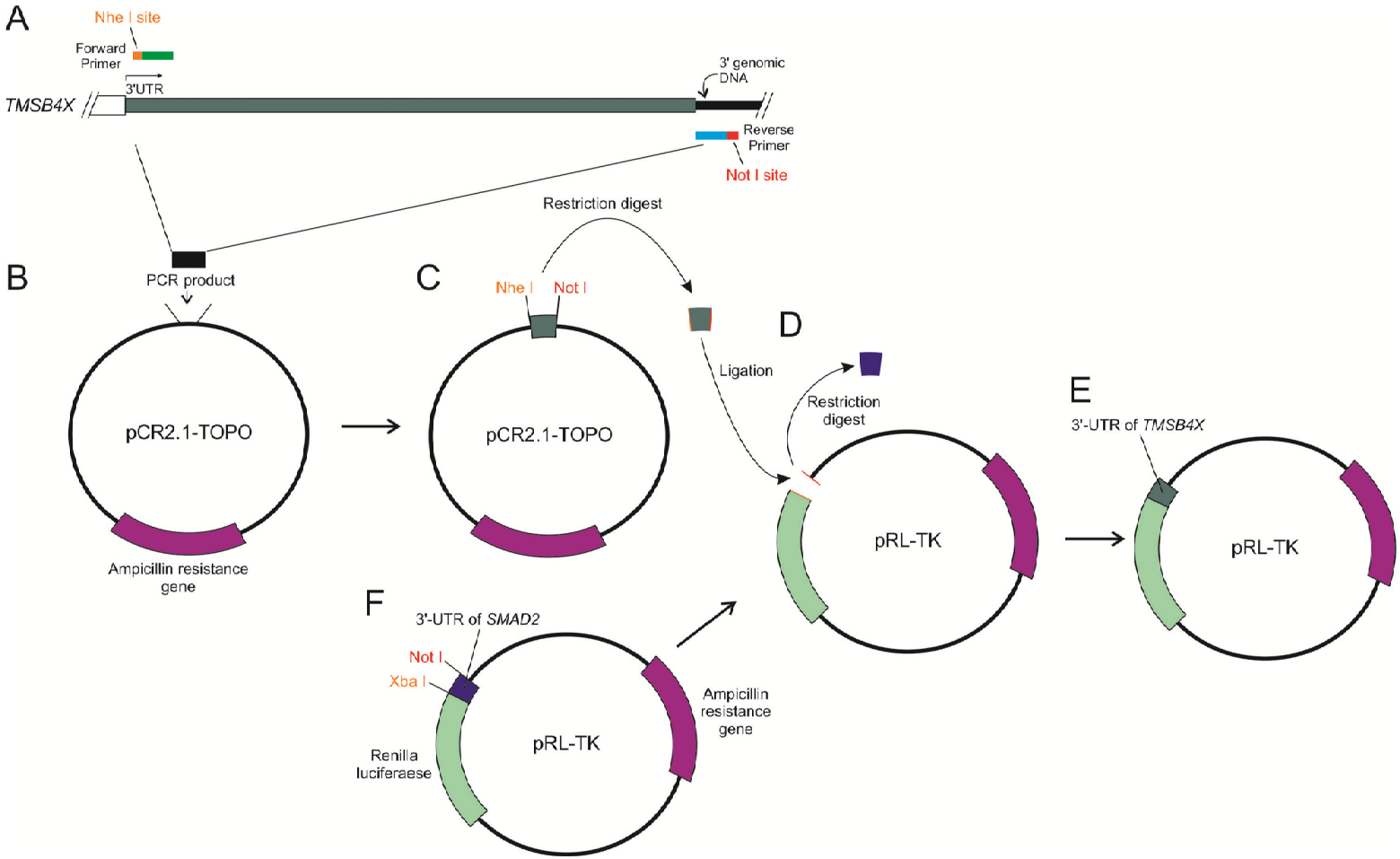

Figure 5.4 – Diagrammatic representation of the cloning strategy used

Diagrammatic representation of the amplification of the 3'-UTR of thymosin β4, insertion in a pCR2.1-TOPO vector and subcloning into a pRL-TK vector.

Amplification by PCR (section 2.3) of the 3'-UTR of *TMSB4X* from genomic DNA extracted from foetal placental tissue (section 2.2.5) was successful, as illustrated by the detection of a single 441 bp amplicon when the PCR products were resolved on an agarose gel (Figure 5.5). The PCR product was therefore inserted into the pCR2.1-TOPO vector (section 2.11.1) and the vector transformed into JM109 competent cells which were cultured on ampicillin-containing agar plates (sections 2.11.2 and 2.11.3). The pCR2.1-TOPO vector contains an ampicillin resistance gene (Figure 5.4B) so that all colonies that form must contain the vector, though the vector does not necessarily contain the insert.

Therefore, to assess the presence of the insert, individual colonies were cultured (section 2.11.3) and plasmid DNA extracted from each sample using plasmid miniprep systems (section 2.11.4). The presence of vector containing the 3'-UTR insert was assessed by carrying out PCR reactions with the same primers used to amplify the 3'-UTR of *TMSB4X* (Table 2.5). Of four colonies that were selected, the 3'-UTR was detected in two of them (Figure 5.6A).

Further to this, results of Sanger sequencing carried out on plasmid DNA from colony 4 confirmed the presence of the 3'-UTR of *TMSB4X* in the expected location within the pCR2.1-TOPO vector (Figure 5.6B). The restriction sites designed into the primers were present and intact (Figure 5.6B). Mutations were present within the sequence of the 3'-UTR itself, however, with deletion of two adenine bases and a substitution of a cytosine for a thymine (Figure 5.6B). These mutations are not listed as naturally occurring human polymorphisms (Ensembl) and likely occurred during cloning. These mutations were not located in binding regions of any of the miRNAs of interest, therefore this clone was used in further experiments.

The selected colony was cultured up in a flask and plasmid DNA extracted using a plasmid maxiprep system (sections 2.11.3 and 2.11.4). The plasmid DNA was treated with *Nhe* I and *Not* I to release the 3'-UTR of *TMSB4X* from the pCR2.1-TOPO vector. A restriction digest using *Xba* I and *Not* I was concurrently carried out on a sample of pRL-TK vector containing the 3'-UTR of *SMAD2* (supplied by Tilman Sanchez-Elsner). Resolving the restriction digest

products on an agarose gel alongside undigested vectors revealed the digests had been successful (Figure 5.7). The band containing the 3'-UTR of *TMSB4X* and the band containing the pRL-TK vector with the 3'-UTR of *SMAD2* removed were excised and the DNA extracted (section 2.3.1).

The 3'-UTR of *TMSB4X* was ligated into the pRL-TK vector (section 2.11.6) and transformed into competent cells which were cultured on ampicillin-containing agar plates (sections 2.11.2 and 2.11.3). Colonies were cultured up and PCR used to assess the presence of the pRL-TK vector containing the 3'-UTR of *TMSB4X* (sections 2.11.3, 2.11.4 and 2.3). Of four selected colonies, the 3'-UTR was detected in three (Figure 5.8A). Sanger sequencing, using primers designed to detect the 3'-UTR region of the pRL-TK vector (Table 2.5; pRL-TK 3'UTR primers), was carried out on plasmid DNA from colony 1 (section 2.3.1.1). The sequence obtained confirmed the presence of the 3'-UTR of *TMSB4X* in the correct location and orientation within the pRL-TK vector extracted from colony 1 (Figure 5.8B). This vector could be used in future luciferase assays to assess the effects of candidate miRNAs on expression of *Renilla* luciferase under the control of the 3'-UTR of *TMSB4X*.

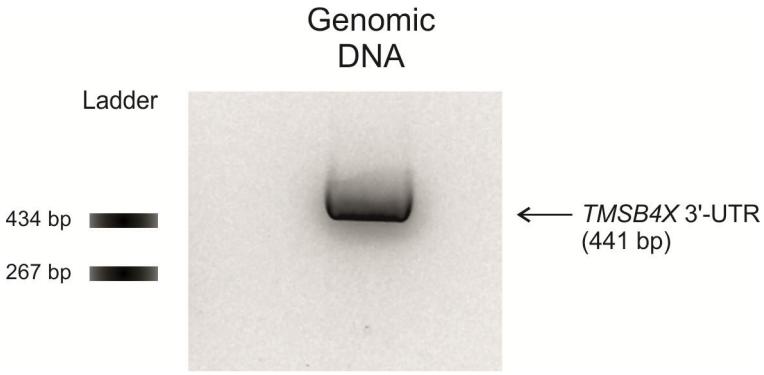

Figure 5.5 – Amplification of the 3'-UTR of TMSB4X

Primers designed to amplify the 3'-UTR region of TMSB4X were used with genomic DNA template in PCR; the PCR products, resolved on a 2% agarose gel, are shown.

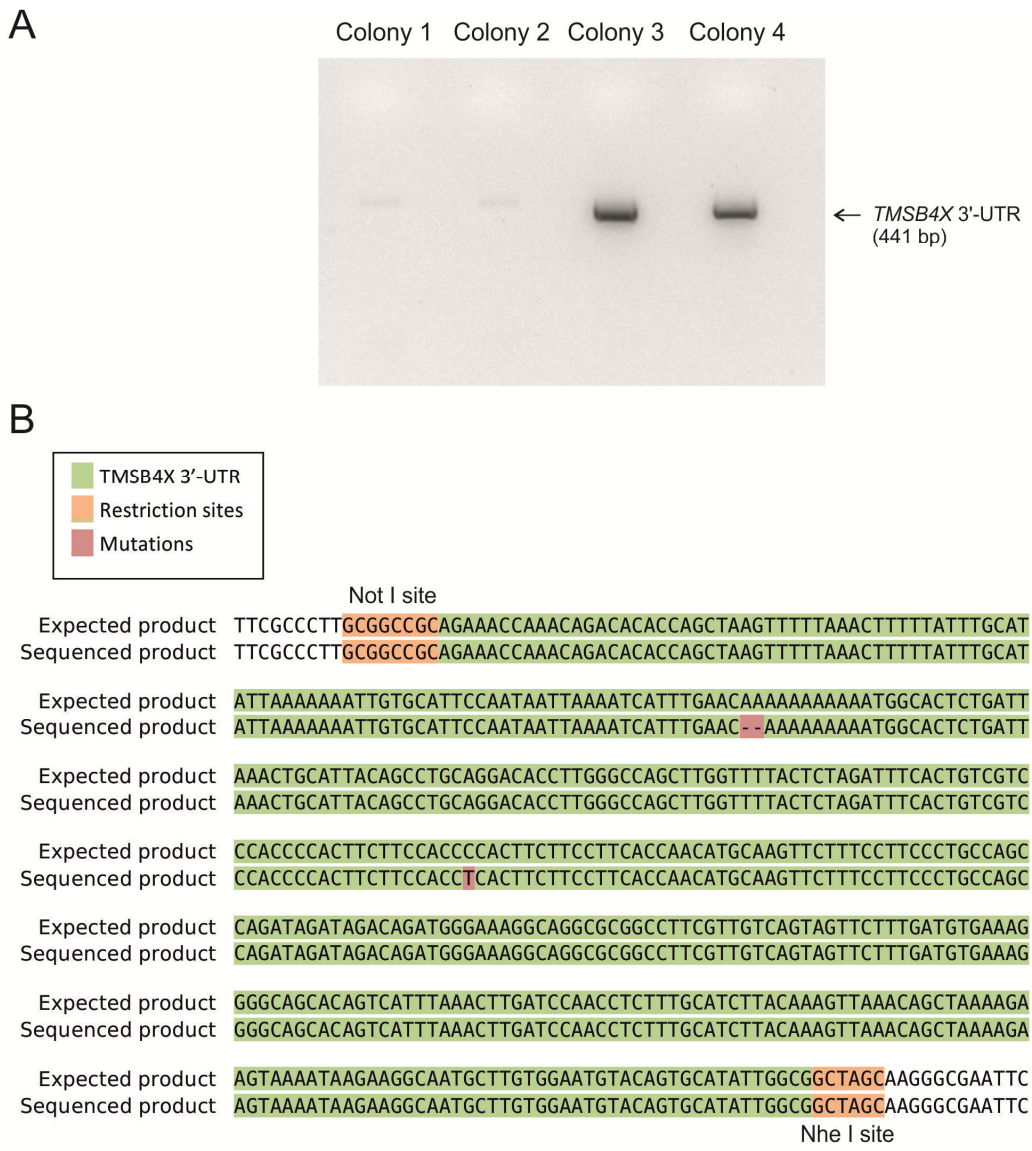

Figure 5.6 – Detection of pCR2.1 TOPO plasmid containing the 3'-UTR of TMSB4X in transformed colonies

A) PCR was carried out using the TMSB4X 3'-UTR primers and plasmid DNA from four different transformed colonies as template; the PCR products, resolved on a 2% agarose gel are shown. B) Plasmid DNA from Colony 4 was sequenced in the 3'-UTR region and the alignment to the expected product if the 3'-UTR of TMSB4X were inserted in the correct site is shown.

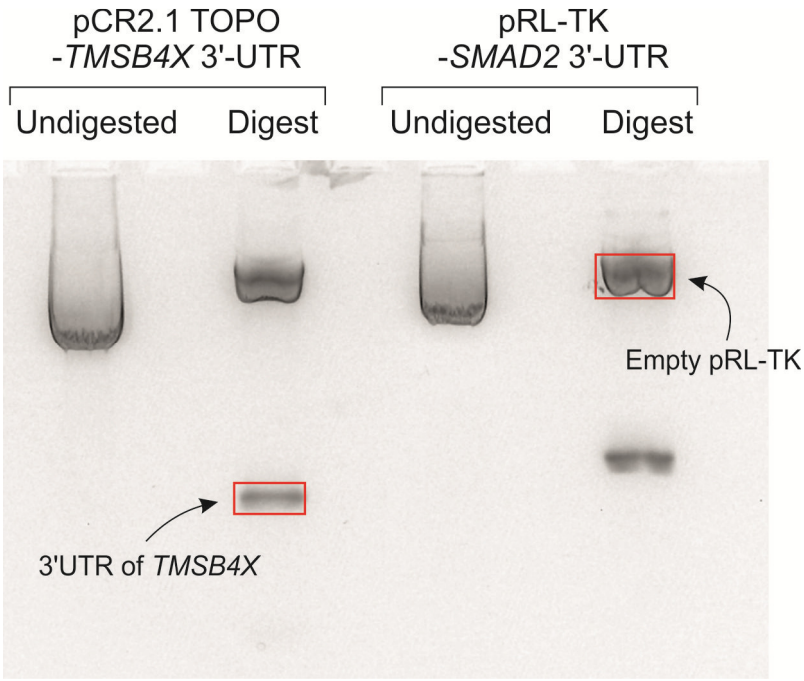

Figure 5.7 – Digestion of pCR2.1 TOPO vector containing the 3'-UTR of TMSB4X and of pRL-TK vector containing the 3'-UTR of SMAD2

The pCR2.1 TOPO vector containing the 3'-UTR of *TMSB4X* was digested with *Nhe I* and *Not I*. The pRL-TK vector containing the 3'-UTR of *SMAD2* was digested with *Xba I* and *Not I*. The digested products are shown resolved on a 1.5% agarose gel alongside the respective undigested vectors. The bands representing the 3'-UTR of *TMSB4X* and the empty pRL-TK vector are indicated.

A

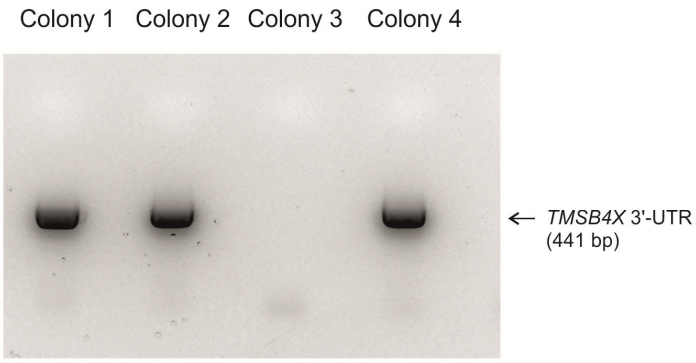

B

Renilla luciferase cDNA
TMSB4X 3'-UTR
Down-stream vector sequence

Expected product	TGAATTTGTCAAAGTAAAAGGTCTTCATTTTTCGCAAGAAGATGCACCTGATGAAATGGGAAAATATAT
Sequenced product	TGAATTTGTCAAAGTAAAAGGTCTTCATTTTTCGCAAGAAGATGCACCTGATGAAATGGGAAAATATAT
Expected product	CAAATCGTTCGTTGAGCGAGTTCTCAAAAATGAACAATAATTCTAGCCGCCAATATGCACTGTACATTC
Sequenced product	CAAATCGTTCGTTGAGCGAGTTCTCAAAAATGAACAATAATTCTAGCCGCCAATATGCACTGTACATTC
Expected product	CACAAGCATTGCCTTCTTATTTTACTTCTTTTAGCTGTTTAACTTTGTAAGATGCAAAGAGGTTGGATC
Sequenced product	CACAAGCATTGCCTTCTTATTTTACTTCTTTTAGCTGTTTAACTTTGTAAGATGCAAAGAGGTTGGATC
Expected product	AAGTTTAAATGACTGTGCTGCCCCTTTCACATCAAAGAACTACTGACAACGAAGGCCGCGCCTGCCTTT
Sequenced product	AAGTTTAAATGACTGTGCTGCCCCTTTCACATCAAAGAACTACTGACAACGAAGGCCGCGCCTGCCTTT
Expected product	CCCATCTGTCTATCTATCTGGCTGGCAGGGAAGGAAAGAACTTGCATGTTGGTGAAGGAAGAAGTGAGG
Sequenced product	CCCATCTGTCTATCTATCTGGCTGGCAGGGAAGGAAAGAACTTGCATGTTGGTGAAGGAAGAAGTGAGG
Expected product	TGGAAGAAGTGGGGTGGGACGACAGTGAAATCTAGAGTAAAACCAAGCTGGCCCAAGGTGTCCTGCAGG
Sequenced product	TGGAAGAAGTGGGGTGGGACGACAGTGAAATCTAGAGTAAAACCAAGCTGGCCCAAGGTGTCCTGCAGG
Expected product	CTGTAATGCAGTTTAATCAGAGTGCCATTTTTTTTTGTTCAAATGATTTTAATTATTGGAATGCACAAT
Sequenced product	CTGTAATGCAGTTTAATCAGAGTGCCATTTTTTTTTGTTCAAATGATTTTAATTATTGGAATGCACAAT
Expected product	TTTTTTAATATGCAAATAAAAAGTTTAAAAACTTAGCTGGTGTGTCTGTTTGGTTTCTGCGGCCGCTTC
Sequenced product	TTTTTTAATATGCAAATAAAAAGTTTAAAAACTTAGCTGGTGTGTCTGTTTGGTTTCTGCGGCCGCTTC
Expected product	GAGCAGACATGATAAGATACATTGATGAGTTTGGACAAACCACAACTAGAATGCAGTGAAAAAAATGCT
Sequenced product	GAGCAGACATGATAAGATACATTGATGAGTTTGGACAAACCACAACTAGAATGCAGTGAAAAAAATGCT

Figure 5.8 - Detection of pRL-TK plasmid containing the 3'-UTR of TMSB4X in transformed colonies

A) PCR was carried out using the TMSB4X 3'-UTR primers and plasmid DNA from four different transformed colonies as template; the PCR products, resolved on a 2% agarose gel are shown. B) Plasmid DNA from Colony 1 was sequenced in the 3'-UTR region and the alignment to the expected product if the 3'-UTR of TMSB4X were inserted in the correct site and orientation is shown.

5.2.4 HUVEC tubule formation

HUVEC tubule formation assays were carried out by passaging HUVECs on to either a thin gel layer of Matrigel or on to tissue culture plastic, as the control condition, in 6-well plates (section 2.12). HUVECs cultured on Matrigel began to form distinctive networks as early as 3 hours after plating (Figure 5.9B) and consistently by 4 hours (Figure 5.9D & F); four hours was used as the time point at which cells were collected. In comparison, HUVECs cultured on tissue culture plastic were distributed evenly across the surface in a monolayer and did not form tubules (Figure 5.9A, C & E).

5.2.5 Thymosin β4 mRNA expression in tubule-forming HUVECs

After seeding on either tissue culture plastic or Matrigel, HUVECs were cultured for 4 hours before being collected (section 2.12). In each of four independent experiments, half of the cells were used to assess thymosin β4 protein expression (section 5.2.6), while RNA was extracted from the remaining cells and reverse transcribed to cDNA (section 2.2).

Amplification of cDNA with the ‘TMSB4X primers’ (Table 2.5) by PCR was used to assess the presence of thymosin β4 transcript in HUVECs cultured under each condition from the four independent experiments (section 2.3). Separation of the PCR products on an agarose gel revealed bands representing the detection of *TMSB4X* expression in HUVECs cultured on both tissue culture plastic and Matrigel (Figure 5.10) The absence of bands in the 'no reverse transcriptase' negative controls indicate that there was no genomic contamination in the samples (Figure 5.10).

As miR-217 and miR-495, two of the candidate miRNAs that were to be assessed, were predicted not to target *TMSB4X-004* due to its short 3'-UTR (Figure 5.2), the expression of *TMSB4X* isoforms was assessed using the 'long 3'-UTR primers' and 'short 3'-UTR primer' (Table 2.5). Using these primers, PCR reactions were carried out on the cDNA samples obtained from the four independent experiments (section 2.3). Separation of the products on agarose gels revealed bands representing detection of isoforms of *TMSB4X* with the long 3'UTR in samples from both the tissue culture plastic and Matrigel culture

conditions (Figure 5.11A). No bands were detected in samples under either culture condition using the 'short 3'UTR primers' however (Figure 5.11B).

In order to quantify differences in levels of thymosin β4 transcript between the tissue culture plastic and Matrigel samples, qPCR analysis was carried out, using *GNB2L1* and *PGK1* as endogenous controls (section 2.4). The raw data from these experiments is show in Appendix 3. Average data from the four independent experiments showed no significant difference in thymosin β4 mRNA expression between HUVECs cultured on Matrigel compared to tissue culture plastic (Figure 5.12).

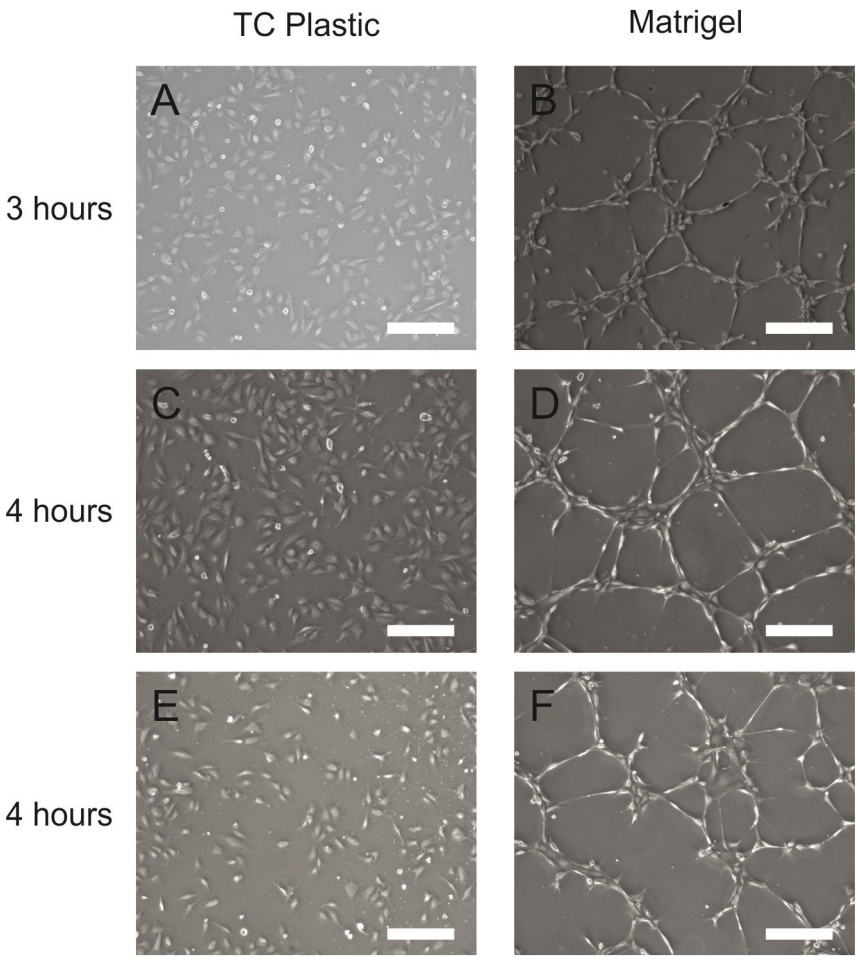

Figure 5.9 – Tubule formation of HUVECs on Matrigel

Representative phase contrast images from 3 independent experiments are shown, taken at 3 hours (A & B) or 4 hours (C–F) post-plating. Scale bars = 250 μm.

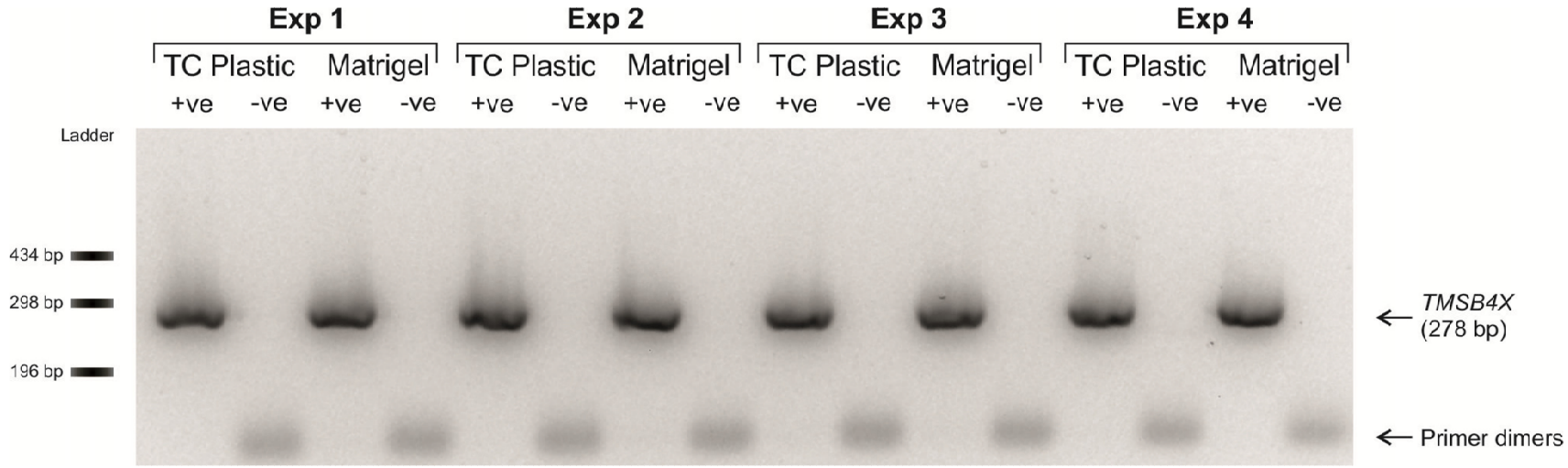

Figure 5.10 – Detection of TMSB4X transcripts in HUVECs cultured on Matrigel or plastic

PCR products from reactions using the TMSB4X primers are shown, resolved on a 2% agarose gel. cDNA synthesised from mRNA from HUVECs cultured on tissue culture plastic or Matrigel were used as template. Alongside each cDNA sample (+ve), a corresponding 'no reverse transcriptase' negative control sample (-ve) was used as template. Bands indicating the presence of TMSB4X transcripts were seen in all positive samples. The faint, low molecular weight bands are primer dimers.

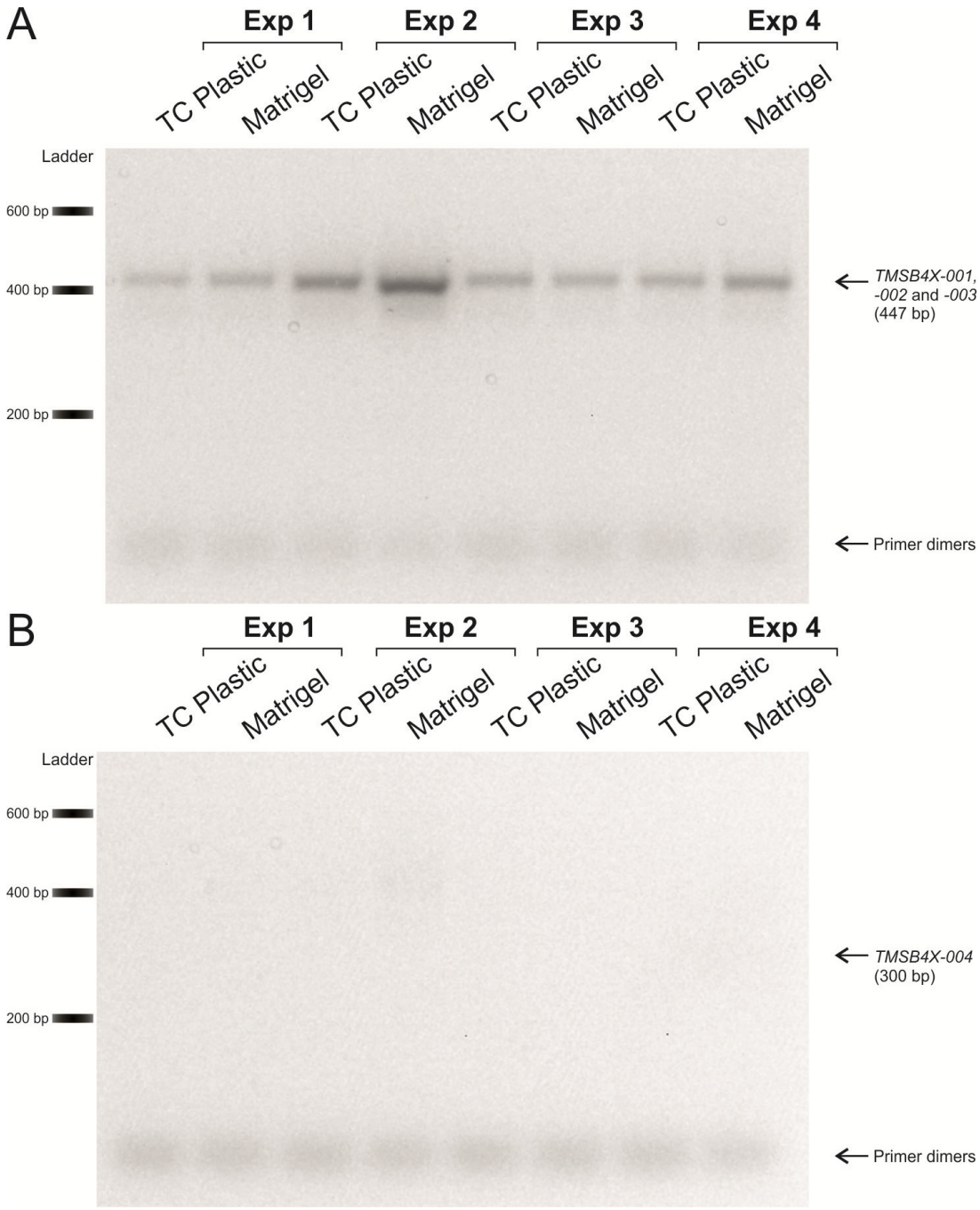

Figure 5.11 – Detection of TMSB4X transcripts with differing 3'-UTR lengths in HUVECs cultured on Matrigel or plastic

PCR products from reactions using the 'long 3'UTR primers' (A) and 'short 3'UTR primers' (B) are shown, resolved on a 2% agarose gel. cDNA synthesised from mRNA from HUVECs cultured on tissue culture plastic of Matrigel were used as template. Bands indicating the presence of transcripts containing the full length 3'-UTR were seen for both culture conditions, while a lack of bands indicated the absence of *TMSB4X-004* transcript in HUVECs cultured under both conditions.

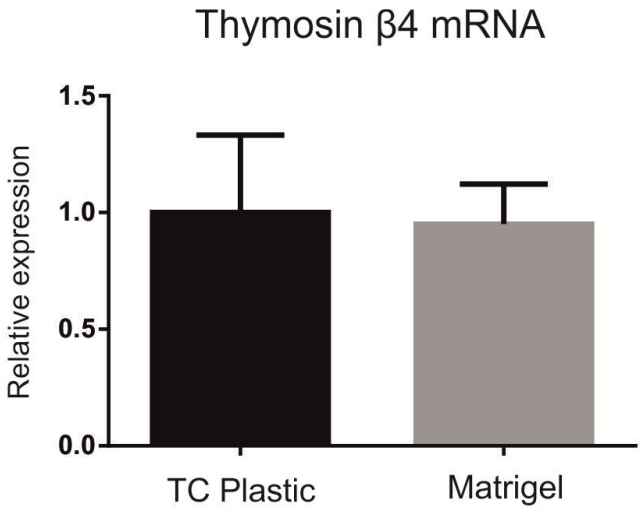

Figure 5.12 – Relative expression of thymosin β4 mRNA in HUVECs cultured on Matrigel or plastic

The average relative expression, assessed by qPCR, of thymosin β4 mRNA in HUVECs cultured on tissue culture plastic or Matrigel is shown. Data is from four independent experiments. Bars show the mean ± standard error of the mean.

5.2.6 Thymosin β4 protein expression in tubule-forming HUVECs

Thymosin β4 protein expression in HUVECs cultured on tissue culture plastic or Matrigel from the four independent experiments was assessed by flow cytometry (section 2.9). As demonstrated in histograms taken from one of the four independent experiments, the negative controls had little background staining with 0.7% and 2.1% of cells cultured on tissue culture plastic appearing in the positive gate in the unstained sample and secondary antibody alone control sample, respectively (Figure 5.13B & C). Similarly 1.0% and 2.1% of cells cultured on Matrigel appeared in the positive gate in the unstained sample and secondary antibody alone control sample, respectively (Figure 5.13E & F).

In samples stained for detection of thymosin β4, 60.1% of cells cultured on tissue culture plastic were positively stained compared to 68.4% of cells cultured on Matrigel (Figure 5.13D & G). The MFI of thymosin β4-positive cells cultured on tissue culture plastic was 276 compared to 264 for cells cultured on Matrigel (Figure 5.13D & G).

However, across the four independent experiments, no significant differences were seen in either the percentage of thymosin β4-positive cells (Figure 5.14A) or in thymosin β4 expression levels of the positive population, as assessed by the fluorescence intensity of the population (Figure 5.14B).

5.2.7 Expression of candidate miRNAs in tubule-forming HUVECs

Given the short time scale of the experiment, there was a possibility that miRNA levels had been regulated but changes in thymosin β4 mRNA and protein levels had not yet changed. Therefore, using RNA extracted from the HUVECs, TaqMan miRNA assays were carried out on cDNA samples reverse transcribed for detection of miR-199a-3p, miR-148b, miR-217 and miR-495, using RNU48 as an endogenous control (sections 2.2.4 and 2.4.1). The raw data from these experiments is shown in Appendix 4. The results of the real-time qPCR analysis using these TaqMan assays indicate that there was no significant difference in expression of any of the four miRNAs between HUVECs cultured on tissue culture plastic and HUVECs cultured on Matrigel (Figure 5.15).

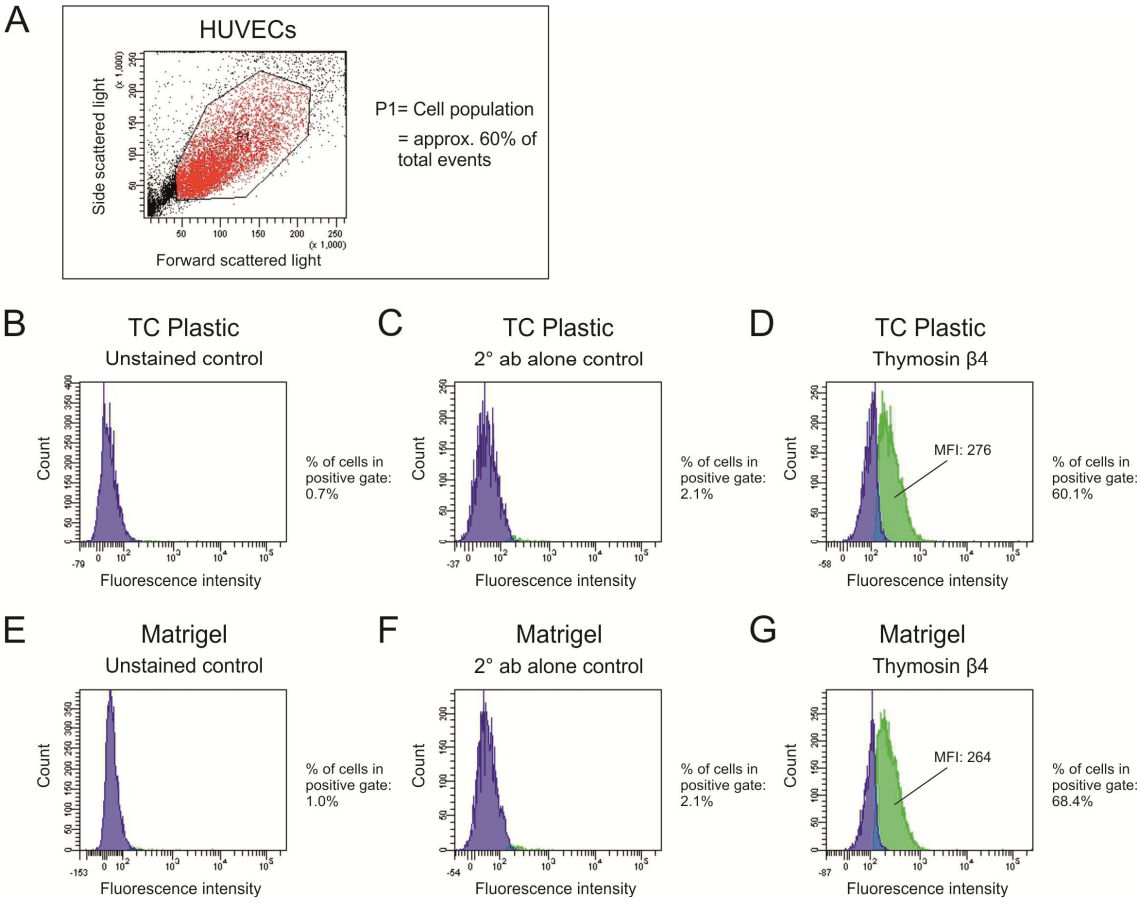

Figure 5.13 – Detection of thymosin β4-positive cells in HUVECs cultured on Matrigel or plastic

A) The scatter plot used to characterise the sample and select the HUVEC cell population (P1) is shown. B-G) Histograms of fluorescence intensity show the populations of cells in thymosin β4-positive (green) and -negative (purple) gates for unstained controls (B & E), secondary antibody alone controls (C & F) and thymosin β4 stained samples (D & G). These plots are shown for HUVECs cultured on tissue culture plastic (B-D) and on Matrigel (E-G). The percentage of cells in the positive gate is shown for each sample. The mean fluorescence intensity (MFI) of the thymosin β4-positive population in the stained sample is shown for HUVECs cultured on Matrigel and plastic.

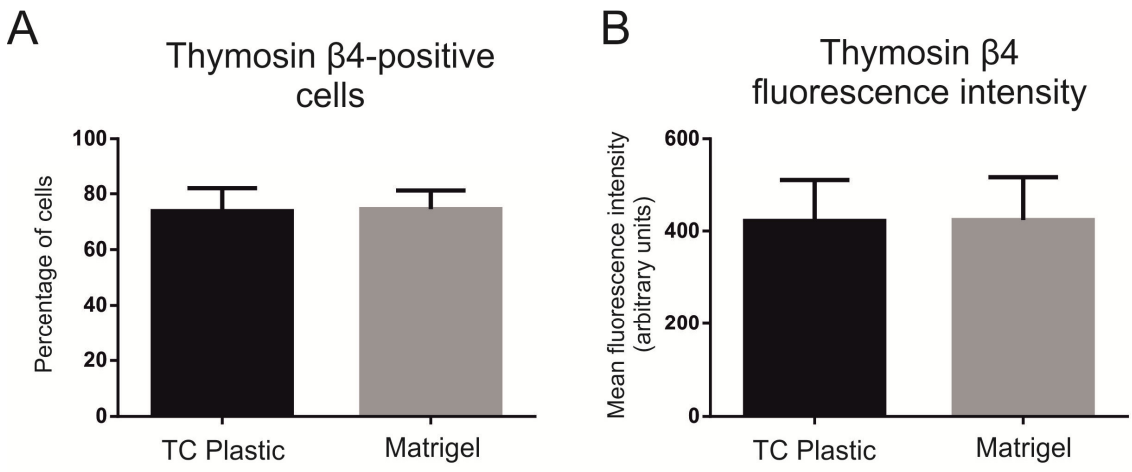

Figure 5.14 – Effect of culturing HUVECs on Matrigel on the expression of thymosin β4 protein

A) The average percentage of thymosin β4-positive HUVECs when cultured on tissue culture plastic or Matrigel is shown in a bar chart. B) The average mean fluorescence intensity (arbitrary units) of thymosin β4-positive HUVECs when cultured on tissue culture plastic or Matrigel is shown in a bar chart. Data is from four independent experiments. Bars show the mean ± standard error of the mean.

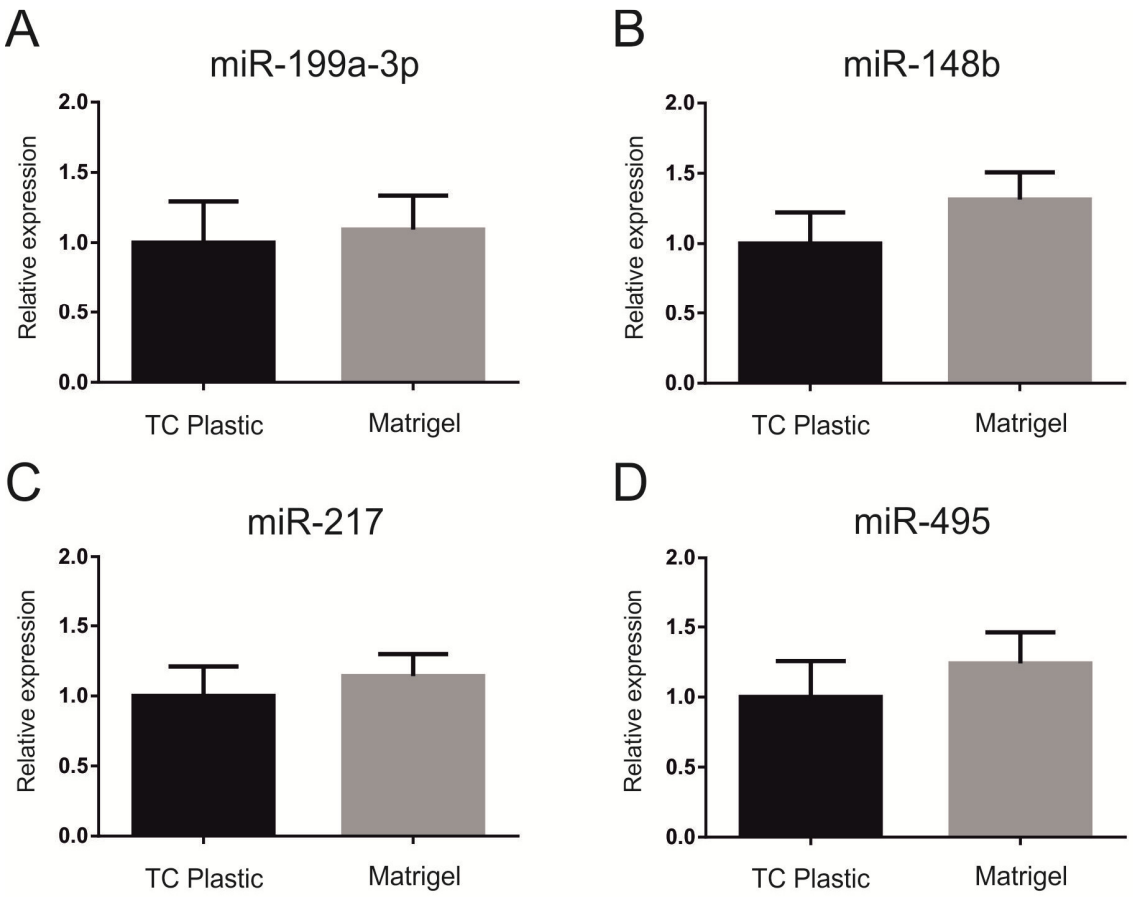

Figure 5.15 – Relative expression of miRNAs in HUVECs cultured on Matrigel or plastic

The average relative expression, assessed by qPCR using TaqMan MicroRNA Assays, of miR-199a-3p (A), miR-148b (B), miR-217 (C) and miR-495 (D) in HUVECs cultured on tissue culture plastic or Matrigel is shown. Data is from four independent experiments. Bars indicate mean ± standard error of the mean.

5.3 Discussion

Using *in silico* analysis combined with miRNA microarray data previously obtained (Wilson and Sanchez-Elsner lab), 62 miRNAs were identified that were present in the human foetal heart and are predicted to target thymosin β4. Of these miRNAs, 15 had previously been reported to be expressed in endothelial cells [369]. Using mirSVR scores to select the best candidates, miR-148b, miR-199a-3p, miR-217 and miR-495 were selected to be measured in HUVEC tubule forming assays. The expression of these four miRNAs in the foetal human heart was confirmed using TaqMan miRNA assays.

HUVEC tubule formation assays were successfully carried out; HUVECs cultured on Matrigel started to form tubule structures within 3 hours post-plating. Thymosin β4 mRNA was present in HUVECs cultured on both tissue culture plastic and Matrigel. Importantly isoforms of thymosin β4 with the long 3'-UTR were present in HUVECs cultured in both conditions. These isoforms are predicted to be targeted by all four candidate miRNAs, while only miR-148b and miR-199a-3p are predicted to target *TMSB4X-004*, which has a short 3'-UTR. TMSB4X-004 was not detected in HUVECs cultured in either condition; however no positive control for the primers was run alongside. This is in contrast to foetal heart tissue in which isoforms with both the long and short 3'-UTR were detected (section 3.2.2).

Using qPCR to quantify thymosin β4 mRNA levels, no difference in expression was seen between the two culture conditions. This was consistent with measurements of thymosin β4 protein expression by flow cytometry which showed no difference in either the percentage of positive cells or the fluorescence intensity of positive cells between the two conditions.

As HUVEC tubule formation had successfully occurred, the expression of the four candidate miRNAs was assessed between the two conditions. It is possible that changes in miRNAs had occurred but not yet resulted in detectable changes in thymosin β4 expression. However, no difference in expression of any of the four miRNAs was detected by TaqMan miRNA assay between HUVECs cultured on Matrigel compared to tissue culture plastic. From this it

can be concluded that tubule formation is not associated with altered levels of miR-148b, miR-199a-3p, miR-217 or miR-495.

However, different forms of a mature miRNA, called isomiRs, which differ by one or two base pairs can be produced [370]. These differences primarily occur due to slight variation in the location of cleavage by Drosha and Dicer, known as trimming, during miRNA processing (Figure 1.3) [370]. Differences in trimming can result in variation at both the 5' and 3' end of the mature miRNA in terms of loss or gain of nucleotides, compared to the canonical form [370]. Variation can also occur due to nucleotide substitutions within the sequence, though these are rare, or due to addition of extra nucleotides at the 3' end of the mature miRNA, following normal processing [370, 371].

The TaqMan stem-loop RT primers that are used to reverse transcribe miRNAs prior to qPCR are designed to detect specific mature miRNAs. However, they are designed to detect the canonical isomiR, as listed in miRBase, and will not efficiently detect all isomiRs of a given miRNA. Due to their design, stem-loop primers will not stably bind isomiRs that differ at the 3' end from the canonical form of the miRNA that they were designed to reverse transcribe (Figure 5.16). IsomiRs with variation at the 5' end of the mature miRNA will be reverse transcribed, however if isomiRs are present that have lost or gained nucleotides at their 3' end, compared to the canonical isomiR, then they will be unable to bind stably to the stem-loop primer and therefore will not be reverse transcribed efficiently or at all (Figure 5.16). This means that relevant isomiRs may not be detected when qPCR is carried out, though a recent study has shown that there is a significant degree of cross-detection between isomiRs when using stem-loop RT primers [372].

According to annotation by mIRBase (www.mirbase.org) [373-377] of deep sequencing data, the canonical isomiR of miR-217 is the most abundant [378-380]. However, for miR-148b, the vast majority of reads (over 100 times more) are for isomiRs with 3' variations compared to the canonical form [378-381]. There are 3 isomiRs of miR-199a-3p that have relative abundance similar to or greater than the canonical isomiR and which differ from it at the 3' end [378-

381]. For miR-495, there are 5 isomiRs with 3' variation that have relative abundance similar to or greater than the canonical isomiR [378, 379, 381].

Therefore, if any of the highly abundant isomiRs of miR-148b, miR-199a-3p or miR-495 are important in HUVECs, then changes in their expression levels may have occurred but may not have been detected in this study. To address this issue in future studies, next generation RNA sequencing could be used.

As no changes in any of the four miRNAs were seen in this study, it was concluded that they are unlikely to be involved in the regulation of the HUVEC tubule formation process. Had changes in the levels of these miRNAs correlated with either tubule formation or inversely to thymosin β4 expression, indicating a potential physiological role, luciferase assays would have been carried out to assess a direct effect of the miRNA on the 3'-UTR of thymosin β4. A construct containing the *Renilla* luciferase gene under the regulation of the 3'-UTR of thymosin β4 was created coincident with the HUVEC tubule assays in anticipation of these experiments. However, as the results indicated that thymosin β4 was not under the regulation of the candidate miRNAs during HUVEC tubule formation, experiments using the construct were not undertaken.

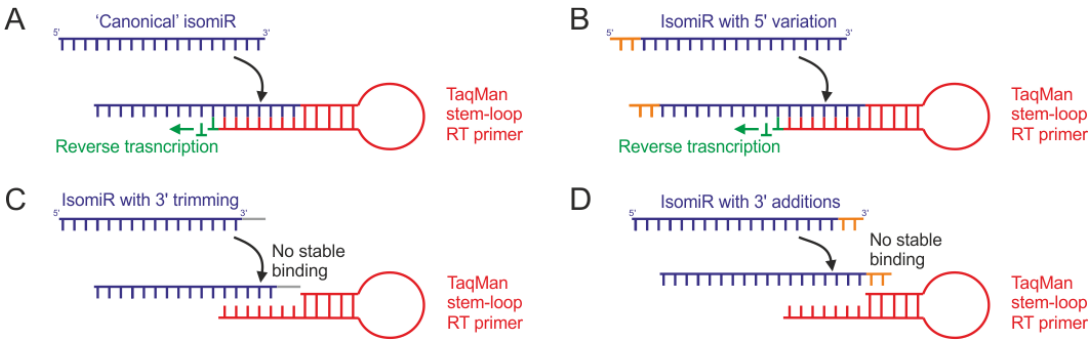

Figure 5.16 – Diagrammatic representation of reverse transcription using stem-loop RT primers designed for a canonical miRNA isomiR

TaqMan stem-loop RT primers are designed with an over-hang that is complimentary to the 3' end of the target miRNA, allowing the target miRNA to bind and elongation to proceed (A). However, these stem-loop primers are designed to bind the canonical variant of a mature miRNA (A). If an isomiR has variation at the 5' end due to 5' trimming, which may result in the presence of more or less bases compared to the canonical isomiR, then the isomiR is still able to bind to the stem-loop and reverse transcription proceeds (B). If, however, the isomiR has a reduced number of bases at the 3' end due to 3' trimming (C) or has additional bases either due to 3' trimming or 3' additions (D), then the ability of the miRNA to bind the stem-loop primer is impaired. This may reduce the efficiency of the reverse transcription or prevent it entirely.

The absence of any change in thymosin β4 mRNA levels in HUVECs cultured on Matrigel in the present study is in contrast to the study which these experiments were based on. In the study by Grant and colleagues, thymosin β4 mRNA expression was found to be increased 5-fold in HUVECs cultured for 4 and 6 hours on Matrigel compared to 1 and 2 hour time points on the same surface [200]. Cells cultured on tissue culture plastic showed no increase in expression across these time points [200]. However, the measurements were obtained by carrying out densitometry on Northern blots [200]. The difference in technique used may explain the differences in the results seen by Grant and colleagues compared to the current study. Northern blotting is considered to be a less sensitive method of detection compared to qPCR [382], therefore it is surprising that differences are detected by Northern blot analysis, but not by qPCR in the current study. However, Grant and colleagues only show data from a single experiment in their paper [200], therefore it is unclear whether the data they present is representative of a consistent effect.

Matrigel is a protein mixture derived from Engelbreth-Holm-Swarm mouse sarcoma cells. As such, the exact protein composition of Matrigel is not fully defined and lot to lot variation in the commercially available product used in the current study is noted by the manufacturers. In the study by Grant and colleagues they prepared Matrigel in-house. Therefore, the difference in the results reported here and seen in the previous study may be due to variations in the Matrigel used. Interestingly the images presented by Grant and colleagues suggest tubule formation had only just begun at the 4 hour time point [200]. In comparison, tubules were already starting to look well formed at 3 hours in the present study. This could indicate that the conditions used in the current study were perhaps more favourable for tubule formation and this may also affect the response of cells in terms of their thymosin β4 expression.

The results of the current study suggest that increased thymosin β4 expression is not a requirement of HUVEC tubule formation. The previous study used antisense oligos against thymosin β4 mRNA which were demonstrated to elicit an inhibition in tubule formation of approximately 50% [200]. Only two independent experiments were carried out however and no statistical tests were carried out to indicate whether the results are statistically significant [200]. If the

effect seen is real, it indicates that the presence of thymosin β4 may either be required for tubule formation or may simply promote tubule formation. However, the effect could be due to a reduction in baseline thymosin β4 levels and does not necessarily indicate that an increase in thymosin β4 expression is required for tubule formation. The ability of thymosin β4 to enhance tubule formation is illustrated in studies in which thymosin β4 was transfected into HUVECs and in studies in which HUVECs were treated with exogenous thymosin β4 protein [184, 200].

Therefore, it may be that upon initiation of tubule formation in sub-optimal conditions, HUVECs up-regulate thymosin β4 production, facilitating the formation of mature tubules. To test this hypothesis, future experiments could be carried out in which HUVECs are cultured on Matrigel at various dilutions. Assessing the state of tubule formation visually across a range of time points as well as assessing thymosin β4 expression at each time point would provide a clear picture of how thymosin β4 expression changes throughout the process of tubule formation under the different conditions.

miR-155, one of the miRNAs predicted to target thymosin β4 (Appendix 1), has been found to help promote HUVEC tubule formation when over-expressed in the cells [383]. Since down-regulation of thymosin β4 has been shown to inhibit tubule formation [200], this suggests that miR-155 does not target and down-regulate thymosin β4, as predicted by *in silico* analysis.

Chapter 6: Discussion

Thymosin β4 is an endogenous protein which has previously been reported to be present in the murine heart, where it had a key role in heart development. Furthermore, studies indicate that thymosin β4 has clinical potential as a regenerative and cardioprotective factor for the treatment of cardiovascular disease. Little is currently known about the endogenous regulation of thymosin β4 and in the present study it was hypothesised that miRNAs may play a role in its regulation.

The present study found that thymosin β4 was expressed in the developing human heart and primarily localised to endothelial cells but was not detected in cardiomyocytes. Notably the expression of thymosin β4 in endothelial cells in the compact layer of the myocardium, as well as the interventricular septum, was greater than in the endothelial cells of the trabecular myocardium.

Two different experimental strategies were developed in order to identify miRNAs with expression levels that are inversely correlated with expression of thymosin β4 in the developing human heart. The first of these involved culture of foetal heart explants under hypoxic conditions, which was hypothesised to up-regulate thymosin β4 expression. However, no differences in thymosin β4 protein levels were detected by Western blotting. Due to the inconsistency of the results seen in individual Western blots, which highlighted the potential inaccuracy of this system for quantification of thymosin β4 protein levels, this experimental system was not pursued further.

The second experimental system sought to separate out the endogenous populations of thymosin β4-high and low expressing endothelial cells by FACS, with the aim of measuring miRNA levels within these two populations. Thymosin β4-positive and negative cells were detected within the CD31-expressing endothelial cell population of a human foetal heart using flow cytometry. Further to this, intact RNA was successfully extracted from PFA-fixed cells. The experiments carried out here provide a proof of concept for the proposed experimental system. However, due to disruption in access to foetal tissue the experiments could not be developed further.

As an alternative model system for exploring the regulation of thymosin β4 by miRNAs, HUVEC tubule formation assays were carried out. However, despite previous reports of the up-regulation of thymosin β4 mRNA during HUVEC tubule formation on Matrigel, no changes in thymosin β4 mRNA or protein were detected in the present study. As HUVEC tubule formation itself was successful, the expression of four candidate thymosin β4-targeting miRNAs, identified by *in silico* analysis, was assessed between tubule forming and control conditions. However, levels of miR-148b, miR-199a-3p, miR-217 and miR-495 were found to be unchanged between the two conditions, indicating that regulation of these miRNAs is not associated with HUVEC tubule formation.

6.1.1 The role of *TMSB4X-004* in miRNA-mediated regulation of thymosin β4

Of the four reported isoforms of thymosin β4, *TMSB4X-004* has a reduced length 3'-UTR. As such, the target sites for certain miRNAs are absent, preventing miRNAs that are able to target the other three isoforms of thymosin β4 from targeting *TMSB4X-004*. In the present study *TMSB4X-004* was detected in human foetal heart tissue, along with isoforms containing the full length 3'-UTR, but was not detected in primary HUVECs. This is likely accounted for by the presence of multiple cell types within the heart, some of which may express *TMSB4X-004* and some of which may not. Therefore, there may be cells in the foetal heart in which there is a reduced level of miRNA regulation over thymosin β4 expression, due to the presence of *TMSB4X-004*.

It may be assumed that cells which express *TMSB4X-004* will have higher levels of thymosin β4 expression than cells which do not, however this is not necessarily the case. miRNAs provide a secondary level of regulation over the expression of a protein in a cell. Transcriptional regulation is the primary level of regulation and is likely to determine baseline protein levels in a cell.

Interestingly, if it is assumed that the endothelial cells of the developing heart do not express TMSB4X-004, in the way that HUVECs do not, then it is the cells which express the highest levels of thymosin β4, based on the data presented here, that have the highest level of regulation. A high degree of regulation over

a protein in a cell could be consistent with an important functional role of that protein. Levels of such proteins may need to be controlled in a precise and timely manner allowing them to carry out their functions. Therefore a high degree of regulation would be consistent with the known roles of thymosin β4 in regulating endothelial cell differentiation, migration and proliferation leading to promotion of vessel formation.

In contrast, other cells within the developing heart may express relatively low levels of thymosin β4 and may only express TMSB4X-004. In these cells thymosin β4 may carry out housekeeping functions which do not require levels of thymosin β4 to vary greatly beyond their baseline levels. Thymosin β4 levels in these cells would still be under the control of some miRNAs, but not others.

Another possibility is that the presence of TMSB4X-004 in some cells of the foetal heart but not others does account for differences in their thymosin β4 expression. For example, TMSB4X-004 may be expressed in the endothelial cells of the compact myocardium, while endothelial cells of the trabecular myocardium may only express isoforms with the long 3'-UTR. If miRNAs which only target isoforms with the long 3'-UTR are present in both populations of endothelial cells, then thymosin β4 expression would be down-regulated in endothelial cells of the trabecular myocardium, while thymosin β4 expression in endothelial cells of the compact myocardium would remain high.

This highlights the importance of understanding which isoforms of thymosin β4 different cells in the foetal heart are expressing. This is something that could be addressed in future work.

6.1.1.1 Potential role of TMSB4X-004 in cancer

The presence of the *TMSB4X-004* isoform may also be of clinical relevance in cancer. mRNA isoforms of proto-oncogenes with shortened 3'-UTRs have been found to be increased in cancer cells [384]. This leads to a loss of regulation by miRNAs leading to over-production of the protein. High levels of thymosin β4 are associated with tumour growth and metastasis (section 1.3.3.8). It's possible that this is due to the abnormal expression of *TMSB4X-004* in place of

other isoforms in cancer cells, leading to a loss of miRNA regulation and increased thymosin β4 expression.

6.1.2 Candidate thymosin β4-targeting miRNAs

The present study was unable to support physiological roles involving the targeting and down-regulation of thymosin β4 for the candidate miRNAs that were identified by *in silico* analysis. However, several of these candidate miRNAs have been reported to have functions which support a potential physiological role in targeting thymosin β4.

6.1.2.1 miR-199a-3p

miR-199a-3p, a good candidate thymosin β4-targeting miRNA selected in this study, has been shown to be down-regulated in cardiomyocytes under hypoxic conditions [385]. More importantly, miR-199a-5p, which is derived from the opposite strand of the same pre-miRNA hairpin, was down-regulated completely [385]. When present, miR-199a-5p was found to directly target and down-regulate levels of HIF1α, a major initiator of hypoxic responses [385]. If miR-199a-3p does down-regulate thymosin β4 as predicted, then the two miRNAs derived from the miR-199a pre-miRNA hairpin would have synergistic roles in the hypoxic response. Previous studies have shown that thymosin β4 levels increase under hypoxic conditions leading to stabilisation of HIF1α, thus contributing to the hypoxic response (section 4.1). Therefore, under hypoxic conditions the down-regulation of miR-199a-5p would allow for up-regulation of HIF1α, while the down-regulation of miR-199a-3p would allow for the up-regulation of thymosin β4. Thymosin β4 would in turn stabilise the HIF1α protein, allowing it to initiate downstream responses in its role as a transcription factor.

The potential down-regulation of thymosin β4 by miR-199a-3p is also supported by a reported role of miR-199a-3p in promoting apoptosis and inhibiting cell migration of human osteosarcoma cancer cells [386, 387]. Thymosin β4 has been reported to be anti-apoptotic and has a well-established role in promoting cell migration (sections 1.3.3.6 and 1.3.3.1). These functions have been associated with thymosin β4's role in promoting tumour growth and metastasis

(section 1.3.3.8). Therefore the ability of miR-199a-3p to promote apoptosis and inhibit cell migration may be partially mediated through down-regulation of thymosin β4. Interestingly, miR-199a-3p was implicated in activation of the p53 apoptosis pathway [386], while thymosin β4 has been implicated in modulating the same pathway in a recent study which implicated thymosin β4 in the malignancy of glioblastomas [388].

6.1.2.2 miR-495

miR-495 was one of the candidate thymosin β4-targeting miRNAs predicted to be of importance in endothelial cells. A recent study has implicated miR-495, along with other miRNAs in the same gene cluster, in regulating the formation of new blood vessels. Inhibition of miR-495 increased angiogenesis *in vivo* in a mouse model of hindlimb ischaemia [389]. Thymosin β4 is known to promote angiogenesis and may therefore be one of the proteins which is up-regulated when miR-495 is inhibited.

miR-495 has also been identified as a tumour suppressing miRNA and inhibits the proliferation and migration of cancer cells including gastric cancer, prostate cancer and, most recently, lung cancer cells [390-392].

6.1.2.3 miR-222

miR-222 has been reported to be anti-angiogenic *in vitro* and *in vivo* [393, 394], which is consistent with a potential ability to down-regulate thymosin β4. Interestingly, an indirect down-regulation of eNOS has been suggested to contribute to the anti-angiogenic effects of miR-222 [395]. As eNOS is activated down-stream of thymosin β4 (section 1.3.2.2), this could be due to down-regulation of thymosin β4 by miR-222.

miR-222 has also been found to down-regulate expression of several genes involved in cell migration [394], suggesting an ability to down-regulate thymosin β4, which promotes cell migration, may be part of the same regulatory network.

6.1.2.4 miR-200

A recently study has specifically identified a role for miR-200a and miR-200b in regulating genes involved in actin mechanics and regulation of cell migration

[396]. miR-200 was found to down-regulate cell migration and repress expression and activity of MMPs [396], both processes which are stimulated by thymosin β4. While thymosin β4 was not identified as a target of miR-200 in the study, which looked at miR-200 family targets in a breast cancer cell line, miR-200 may target thymosin β4 in other contexts, contributing to the effects of miR-200 on cell migration.

Further to this, miR-200a has been found to inhibit the process of EMT in cancers including pancreatic and colorectal cancer, leading to reduced cell migration and invasion [397, 398]. EMT is a process which thymosin β4 has been shown to promote in the context of cancer (section 1.3.3.8).

6.1.2.5 Tumour suppressor miRNAs

In addition to miR-199a-3p, miR-495 and miR-200a, a number of the other candidate thymosin β4-targeting miRNAs identified in this study have been shown to act as tumour suppressors in certain cancers.

miR-148b suppresses cell proliferation and migration and induces apoptosis in cancers including gastric cancer, colorectal cancer, pancreatic cancer and lung cancer [399-402].

miR-217 has been shown to inhibit proliferation, migration and invasion of lung cancer cells as well as promoting apoptosis [403]. miR-217 also inhibits the invasion of hepatocellular carcinoma cells [404]. Furthermore, inhibition of miR-217 promotes EMT in pancreatic cancer cells [405].

let-7g is down-regulated in lung cancer and has been shown to inhibit proliferation and promote death of lung cancer cells [406, 407].

miR-29a is down-regulated in neuroblastomas and is further associated with metastases and relapse in neuroblastoma patients [408]. In lung adenocarcinoma cells, miR-29a inhibits proliferation, migration and invasion [409].

6.1.3 The extended regulatory network of thymosin β4-targeting miRNAs

Any miRNA that does target thymosin β4 is likely to be part of a wider regulatory network. For example, miR-495 and other members of its gene cluster are predicted to target multiple genes involved in angiogenesis [389], while the miR-200 family targets genes involved in cell migration [396]. miR-199a-3p on the other hand targets multiple genes involved in apoptosis [386]. The potential regulation of thymosin β4 by any of these miRNAs would therefore be part of a larger network of targets.

Thymosin β4 may itself elicit the transcription of miRNAs, which may in turn contribute to the downstream effects of thymosin β4. Several miRNAs are known to have effects similar to those of thymosin β4 and it is possible that thymosin β4 up-regulates the expression of such miRNAs. For example, miR-126 has pro-angiogenic effects [410, 411]. These effects are mediated through the targeting of mRNAs which code for proteins that negatively regulate VEGF [411]. miR-146a is an anti-inflammatory miRNA, which has been shown to inhibit NFκB activity [412, 413], a function which thymosin β4 also carries out (section 1.3.3.4). Interestingly, increasing miR-146a expression in mouse models of myocardial infarction leads to a reduction in infarct size and improvement in post-infarct cardiac function due to these anti-inflammatory effects [414].

Thymosin β4 may elicit the up-regulation of miRNAs which suppress expression of thymosin β4 itself. Negative feedback loops such as this are important in the regulation of protein expression as they prevent exponential increases in protein production, allowing protein concentrations to be maintained at a steady level. Interestingly, miR-210, one of the miRNAs predicted to target thymosin β4 (Appendix 1), has been shown to be up-regulated in HUVECs cultured under hypoxic conditions [415]. If thymosin β4 is up-regulated by hypoxia and miR-210 is a genuine regulator of thymosin β4, then miR-210 could be a key mediator of negative feedback for thymosin β4 expression under hypoxic conditions.

The way in which miRNAs are themselves regulated is an interesting emerging question. Certain nucleases have been shown to degrade miRNAs and some have even been found to be selective in the miRNAs they degrade [416-418].

More recently it has been suggested that highly expressed, naturally occurring circular RNAs may act to sequester specific miRNAs, thus preventing the miRNA from binding its mRNA targets [419, 420]. One of these circular RNAs was found to consist of over 70 binding sites for miR-7, but was resistant to miRNA-mediated decay when miR-7 bound [420]. As such the circular RNA was able to sequester miR-7 molecules leading to a down-regulation in miR-7 activity [420].

6.1.4 Clinical potential of regulating thymosin β4-targeting miRNAs

The clinical potential of thymosin β4 is clear and RegeneRx Biopharmaceuticals was founded for the sole purpose of developing and marketing thymosin β4-based pharmaceutical products. Phase 2 clinical trials have already been carried out for certain skin and eye conditions based on thymosin β4's wound healing properties. A 0.02% or 0.03% thymosin β4 topical gel was found to accelerate wound healing in patients with pressure ulcers or venous stasis ulcers in two independent double-blind, placebo-controlled trials [251, 252]. In a more recent double blind, placebo-controlled trial for treatment of severe dry eye, a 0.1% thymosin β4 solution administered as eye drops was found to significantly improve symptoms including ocular discomfort and tear volume production [421].

A phase 2 trial to treat acute myocardial infarction using an injectable formulation of thymosin β4 is being planned [422]. The RegeneRx website also lists stroke and peripheral neuropathy as potential indications for phase 2 trials of their injectable formulation [423]. The issue of route of administration for a small peptide-based drug is highlighted by RegeneRx's clinical pipeline, with eye drop and topical formulations having already made it through phase 2 trials, while phase 2 trials of an injectable formulation are still being planned [423].

One issue may be ensuring that injected thymosin β4 has sustained, high bioavailability in the target organ. Recent studies have developed methods which may address such issues, allowing for a single treatment in place of multiple injections across several days. These techniques include incorporating thymosin β4 peptide into hydrogels or encapsulating thymosin β4 in synthetic

polymer microspheres, both of which release thymosin β4 over a number of days, between one and two weeks [424, 425].

Recent studies have also used gene therapy techniques to deliver the thymosin β4 gene into the rat heart, leading to long-term over-expression of thymosin β4 [426]. This led to stimulation of resident CPCs and induced the formation of new blood vessels as well as formation of new cardiomyocytes [426].

However, targeting miRNAs which negatively regulate the expression of thymosin β4 may be an alternative means of increasing thymosin β4 levels in a target organ.

6.1.4.1 Treatment with miRNA inhibitors

Inhibiting thymosin β4-targeting miRNAs may provide greater beneficial effects than simply introducing thymosin β4 itself, by up-regulating other proteins that are involved in healing or angiogenesis that are targeted by the same miRNA. miRNA inhibitors have been developed which can target and block the activity of specific miRNAs [427].

Using animal models, recent studies have demonstrated the benefit of inhibiting specific miRNAs in the injured heart. miR-25 is a miRNA associated with heart failure which inhibits calcium up-take in cardiomyocytes by targeting mRNA of sarcoplasmic/endoplasmic reticulum calcium ATPase 2, thus affecting contractility of the heart [428]. A miR-25 inhibitor was able to improve cardiac function in a mouse model of established heart failure [428]. miR-92a is an anti-angiogenic miRNA [429]. Treatment with a miR-92a inhibitor in a porcine model of myocardial infarction enhanced angiogenesis and decreased inflammation, resulting in reductions in infarct size and improved post-infarct function [430]. A recent study has shown that encapsulating the miR-92a inhibitor in microspheres enhances retention of the inhibitor in the cardiac tissue at the injection site, helping to prevent potential off-target effects [431].

It is possible to achieve long-term knock-down of miRNAs through stable expression of an shRNA which targets and binds to a specific miRNA, preventing it from binding to its target [432]. While the stable expression of a miRNA-targeting shRNA has not been demonstrated clinically, a potential future

gene therapy for the treatment of heart failure could involve the stable knock-down of thymosin β4-targeting miRNAs. If this treatment is provided following an initial myocardial infarction it would enhance levels of thymosin β4, and potentially other cardioprotective proteins, in the heart, thus providing enhanced protection in the event of a second myocardial infarction as well as improving cardiac repair.

6.1.4.2 Enhancing stem cells for cell therapy

An alternative to using thymosin β4-based therapies alone is to improve the efficacy of cells used in cell therapy by treating them with thymosin β4 or by enhancing their thymosin β4 production.

One of the benefits of using stem cells for cell therapy is that autologous cells taken from the patient can be used, preventing issues of immune rejection. However, myocardial infarction and heart failure are conditions which are prevalent in aging patients and it has been noted that stem cells of older patients have a reduced regenerative capacity compared to young patients [433]. Interestingly, thymosin β4 levels are reduced in the tears and saliva of subjects aged over 50 compared to subjects aged between 25 and 35 years, suggesting thymosin β4 production may decrease with age [211].

The reduced efficacy of stem cells from aged patients may be due to a decrease in the production of the paracrine factors, including thymosin β4, which confer benefit on the heart. Using miRNA inhibitors would be one way of increasing production of thymosin β4 and other proteins in these cells prior to transplantation into the heart. miR-377 is an anti-angiogenic miRNA which directly targets and down-regulates VEGF [434]. A recent study has demonstrated that knock-down of miR-377 in MSCs prior to implantation into infarcted rat hearts led to enhanced *in vivo* angiogenesis and improved cardiac function compared to control MSCs [434].

In a rat model of myocardial infarction, MSCs have been introduced to the heart in a fibrin patch containing thymosin β4 encapsulated in microspheres for sustained delivery [435]. The presence of thymosin β4 led to enhanced survival and retention of the MSCs and facilitated improved cardiac function post-infarct

[435]. This indicates that enhancing thymosin β4 levels in MSCs may be a beneficial strategy.

In a recent study, ESCs modified to over-express thymosin β4 were transplanted into the heart in a rat model of myocardial infarction [436]. Transplantation of these thymosin β4 over-expressing ESCs led to enhanced *in vivo* cardiomyocyte differentiation [436]. Further to this, apoptosis was reduced in cardiac myocytes within the infarcted heart, as were levels of cardiac fibrosis, leading to improved cardiac function compared with control ESCs [436]. While ESCs are unlikely to be used clinically, this suggests that increasing thymosin β4 expression in CPCs, for example, may increase their potential to form cardiomyocytes, enhancing their beneficial effects in repair of the damaged heart.

Thymosin β4 may also be beneficial for the *ex vivo* culture of cardiac patches prior to their implantation into the heart. A recent study found that coating a nanofibre scaffold with thymosin β4 facilitated the proliferation and differentiation of murine cardiomyocytes seeded on the scaffold [437]. Such a scaffold, containing mature, functional cardiomyocytes could then be implanted to replace damaged tissue following a myocardial infarction.

6.1.4.3 miRNA mimics for cancer treatment

As previously noted, while thymosin β4 has largely beneficial effects, it has been found to enhance growth and metastases in certain cancers. A number of miRNAs which are predicted to target thymosin β4 are tumour suppressors. Therefore synthetic versions of these miRNAs, known as miRNA mimics, may be of use in the treatment of certain cancers.

miR-34 was one of the first tumour suppressor miRNAs to be identified and its expression is lost in a wide variety of cancers [438]. In 2013 a miR-34 mimic became the first miRNA mimic to enter clinical trials, where it is being assessed for the treatment of liver-based cancers [438].

6.2 Future work

6.2.1 Identification of thymosin β4-targeting miRNAs

Future studies on thymosin β4-targeting miRNAs would initially continue on directly from the experiments of Chapter 4, using FACS to separate out endothelial cells expressing high and low levels of thymosin β4.

TaqMan miRNA assays or miRNA arrays would be used to assess levels of miRNAs in both populations and miRNAs which inversely correlate with thymosin β4 expression would be selected for further study.

It would also be important to assess the expression of different isoforms of thymosin β4 in the two populations of endothelial cells, to determine whether *TMSB4X-004* is more highly expressed in the thymosin β4-positive population compared to thymosin β4-negative/low cells.

miRNAs selected for further study would be over-expressed in thymosin β4-expressing cells to assess their effects on thymosin β4 mRNA and protein levels. Further to this, over-expressing candidate miRNAs in HUVECs cultured on Matrigel could provide evidence of a functional effect of the miRNA, if tubule formation was inhibited in parallel with decreased thymosin β4 expression. Equally miRNA inhibitors could be used to assess their ability to enhance tubule formation.

Having confirmed the ability of a miRNA to down-regulate thymosin β4 expression, luciferase assays would be carried out to assess the ability of the miRNA to directly target the 3'-UTR of thymosin β4.

6.2.2 Identification of miRNA networks in thymosin β4-mediated processes

Once thymosin β4-targeting miRNAs have been identified experiments could be carried out to identify the wider networks that thymosin β4 is part of.

In silico analysis of databases could be used to identify other potential targets of thymosin β4-targeting miRNAs. Targets which are involved in similar processes to thymosin β4, such as angiogenesis and wound healing, would be good

candidates for further study. The ability of the identified miRNAs to down-regulate predicted targets could then be assessed experimentally, as above.

To identify miRNAs which are regulated down-stream of thymosin β4, synthetic or recombinant thymosin β4 could be used to treat tissues, such as foetal heart explants, or cells, such as HUVECs. Assessing miRNA levels using miRNA arrays could identify miRNAs which are regulated by thymosin β4 either directly or indirectly.

6.2.3 Thymosin β4 expression and localisation throughout heart development

The data presented in this study regarding the expression of thymosin β4 in the developing heart compared with previous mouse studies, raises questions about the expression of thymosin β4 throughout heart development. There is also a question as to whether thymosin β4 protein is localised within the same cells which produce it.

Studies could be carried out using immunohistochemistry and *in situ* hybridisation to assess the expression and localisation of thymosin β4 at different stages of development in both the murine and human heart. Using FACS to isolate specific cell types and assessing the presence of thymosin β4 mRNA in these cells would be an alternative method of determining which cells of the heart produce thymosin β4.

Using *in situ* hybridisation it would also be possible to assess the localisation of thymosin β4-miRNAs in the developing heart.

Another area of interest which could be explored is the difference in expression of thymosin β4 between the developing heart, the healthy adult heart and the failing heart in humans. Comparison of foetal heart and adult heart biopsies, either taken during operations or using recent post-mortem biopsies could be used to address this question.

Thymosin β4-targeting miRNAs could also be assessed in these three situations. If thymosin β4-targeting miRNAs are up-regulated in the adult heart compared to the developing heart, this would support the proposal that

thymosin β4-targeting miRNAs are potential clinical targets for cardiovascular disease.

6.2.4 Effects of down-regulating thymosin β4-targeting miRNAs in pre-clinical models of myocardial infarction

Once thymosin β4-targeting miRNAs have been identified it would be important to assess the potential clinical benefit of targeting these miRNAs. Specific miRNA inhibitors could be used to down-regulate levels of a specific miRNA in the heart in rodent models of myocardial infarction. The effects of this treatment on recovery of the heart post-infarction based on parameters such as ejection fraction could be assessed alongside measurements of thymosin β4 expression.

Appendices

Appendix 1

miRNAs predicted to target TMSB4X			
hsa-miR-448	hsa-miR-488	hsa-miR-155	hsa-miR-507
hsa-miR-579	hsa-miR-3153	hsa-miR-940	hsa-miR-1205
hsa-miR-1279	hsa-miR-33a	hsa-miR-219-2-3p	hsa-miR-1244
hsa-miR-4286	hsa-miR-33b	hsa-miR-517a	hsa-miR-323b-3p
hsa-miR-1	hsa-miR-3185	hsa-miR-517c	hsa-miR-3154
hsa-miR-206	hsa-miR-586	hsa-miR-223*	hsa-miR-495
hsa-miR-613	hsa-miR-656	hsa-miR-218	hsa-miR-7-2*
hsa-miR-20a*	hsa-miR-1202	hsa-miR-3189	hsa-miR-635
hsa-miR-520d-5p	hsa-miR-551b*	hsa-miR-663	hsa-miR-548p
hsa-miR-524-5p	hsa-miR-2113	hsa-miR-650	hsa-miR-488*
hsa-miR-183	hsa-miR-1260	hsa-miR-519a	hsa-miR-452*
hsa-miR-148b	hsa-miR-1260b	hsa-miR-519b-3p	hsa-miR-106a*
hsa-miR-152	hsa-miR-548g	hsa-miR-519c-3p	hsa-miR-600
hsa-let-7g*	hsa-miR-596	hsa-miR-493*	hsa-miR-210
hsa-let-7a-2*	hsa-miR-1179	hsa-miR-3197	hsa-miR-450b-5p
hsa-miR-4282	hsa-miR-139-5p	hsa-miR-3190-5p	hsa-miR-3133
hsa-miR-148a	hsa-miR-124	hsa-miR-550*	hsa-miR-122
hsa-miR-29a*	hsa-miR-506	hsa-miR-200c*	
hsa-miR-3121	hsa-miR-15b*	hsa-miR-1252	
hsa-miR-200b*	hsa-miR-582-5p	hsa-miR-30a	
hsa-miR-200a*	hsa-miR-4307	hsa-miR-30d	
hsa-miR-3194	hsa-miR-545*	hsa-miR-30e	
hsa-miR-640	hsa-miR-128	hsa-miR-520g	
hsa-miR-3129	hsa-miR-224*	hsa-miR-520h	
hsa-miR-199a-3p	hsa-miR-522	hsa-miR-30b	
hsa-miR-199b-3p	hsa-miR-610	hsa-miR-30c	
hsa-miR-517*	hsa-miR-1469	hsa-miR-944	
hsa-miR-153	hsa-miR-3163	hsa-miR-518e*	
hsa-miR-217	hsa-miR-1197	hsa-miR-519a*	
hsa-miR-892a	hsa-miR-1271	hsa-miR-519b-5p	
hsa-miR-222*	hsa-miR-96	hsa-miR-519c-5p	
hsa-miR-548c-3p	hsa-miR-581	hsa-miR-522*	
hsa-miR-1286	hsa-miR-130a	hsa-miR-523*	
hsa-miR-561	hsa-miR-1825	hsa-miR-93	
hsa-miR-486-3p	hsa-miR-1248	hsa-miR-518d-5p	
hsa-miR-412	hsa-miR-130b	hsa-miR-518f*	
hsa-miR-517b	hsa-miR-454	hsa-miR-520c-5p	
hsa-miR-3065-5p	hsa-miR-301a	hsa-miR-526a	
hsa-miR-302a*	hsa-miR-301b	hsa-miR-106a	
hsa-miR-4328	hsa-miR-4295	hsa-miR-17	
hsa-miR-148a*	hsa-miR-186	hsa-miR-20a	
hsa-miR-557	hsa-miR-4289	hsa-miR-647	

Appendix 2

microRNAs detected in the human foetal heart				
miRNA	Ct		miRNA	Ct
hsa-miR-133a	10.290702		hsa-miR-483-5p	16.472288
hsa-miR-126	11.394829		hsa-miR-20b	16.484379
hsa-miR-30c	11.924925		hsa-miR-100	16.54913
hsa-miR-24	12.029309		hsa-let-7c	16.589756
hsa-miR-19b	12.511163		hsa-miR-19a	16.606133
hsa-miR-30b	12.570808		hsa-miR-197	16.606203
hsa-miR-218	12.694185		hsa-miR-99b	16.702168
hsa-miR-17	12.757605		hsa-miR-149	16.764196
hsa-miR-106a	12.845315		hsa-miR-376a	16.778376
hsa-miR-16	12.95662		hsa-let-7b	16.784008
hsa-miR-20a	13.171876		hsa-miR-376c	16.818108
hsa-miR-145	13.284618		hsa-miR-135a*	16.842562
hsa-miR-191	13.583757		hsa-let-7g	16.853168
hsa-let-7e	14.373441		hsa-miR-27a	16.862762
hsa-miR-320	14.479178		hsa-miR-93	16.863117
hsa-miR-204	14.684103		hsa-miR-146b-5p	16.88307
hsa-miR-331-3p	14.728112		hsa-miR-152	16.891895
hsa-miR-484	14.876382		hsa-miR-21	16.996578
hsa-miR-125b	14.933792		hsa-let-7a	17.008085
hsa-miR-92a	14.95699		hsa-miR-140-5p	17.036585
hsa-miR-26a	15.017699		hsa-miR-345	17.234398
hsa-miR-30a	15.059454		hsa-miR-28-5p	17.251253
hsa-miR-30e*	15.106466		hsa-miR-27b	17.313446
hsa-miR-143	15.165743		hsa-miR-223	17.37151
hsa-miR-126*	15.205937		hsa-miR-25	17.386225
hsa-miR-1	15.343493		hsa-miR-28-3p	17.420681
hsa-miR-342-3p	15.422452		hsa-let-7d	17.44666
hsa-miR-574-3p	15.486437		hsa-miR-411	17.476837
hsa-miR-374a	15.4966		hsa-miR-99a	17.585545
hsa-miR-193b	15.510811		hsa-miR-30d	17.839338
hsa-miR-214	15.511139		hsa-miR-139-5p	17.861586
hsa-miR-454	15.517092		hsa-miR-195	17.86178
hsa-miR-409-3p	15.606855		hsa-miR-151-3p	17.914036
hsa-miR-186	15.640066		hsa-miR-210	17.916645
hsa-miR-199a-3p	15.667425		hsa-miR-130b	17.928099
hsa-miR-30a*	15.671075		hsa-miR-30d	17.966143
hsa-miR-106b	15.712039		hsa-miR-301a	17.970165
hsa-miR-409-3p	15.937374		hsa-miR-432	18.21594
hsa-miR-374b	15.959167		hsa-miR-432	18.256857
hsa-miR-15b	16.028454		hsa-miR-590-5p	18.416796
hsa-miR-222	16.079903		hsa-miR-203	18.43938
hsa-miR-133b	16.15794		hsa-miR-801	18.4863
hsa-miR-768-3p	16.302326		hsa-miR-103	18.50664
hsa-miR-125a-5p	16.317953		hsa-miR-801	18.552015
hsa-miR-130a	16.338839		hsa-miR-532-5p	18.578568
hsa-miR-132	16.39696		hsa-miR-184	18.672396
hsa-miR-26b	16.404676		hsa-miR-382	18.68366
hsa-miR-127-3p	16.417238		hsa-miR-29a	18.721077
hsa-miR-768-3p	16.429914		hsa-miR-31	18.725533
hsa-miR-30e	16.45513		hsa-miR-324-5p	18.746523

Appendix 2

microRNAs detected in the human foetal heart				
miRNA	Ct		miRNA	Ct
hsa-miR-335	18.80735		hsa-miR-769-5p	20.627632
hsa-miR-150	18.859596		hsa-miR-769-5p	20.654566
hsa-miR-532-3p	18.88424		hsa-miR-194	20.696836
hsa-miR-744	18.917212		hsa-miR-494	20.735853
hsa-miR-370	18.942818		hsa-miR-9	20.74551
hsa-miR-539	18.972586		hsa-miR-193a-5p	20.756369
hsa-miR-766	19.056746		hsa-miR-23b	20.88566
hsa-miR-192	19.105175		hsa-miR-885-5p	20.900839
hsa-miR-181a	19.111889		hsa-miR-301b	20.911911
hsa-miR-766	19.11525		hsa-miR-136*	20.982573
hsa-miR-181a-2*	19.159533		hsa-miR-10b	20.987797
hsa-miR-328	19.188557		hsa-miR-886-3p	20.995333
hsa-miR-146a	19.271435		hsa-miR-598	21.034899
hsa-miR-379	19.349579		hsa-miR-363	21.037388
hsa-miR-365	19.414219		hsa-miR-98	21.044348
hsa-miR-378	19.445501		hsa-miR-145*	21.05617
hsa-miR-18a	19.445835		hsa-miR-15a	21.065567
hsa-miR-7-1*	19.4491		hsa-miR-135a	21.089243
hsa-miR-410	19.459064		hsa-miR-491-5p	21.100668
hsa-miR-106b*	19.535633		hsa-miR-138	21.12349
hsa-miR-708	19.537699		hsa-miR-425	21.189608
hsa-miR-142-3p	19.54661		hsa-miR-565	21.189709
hsa-miR-499-5p	19.561502		hsa-miR-212	21.197815
hsa-miR-660	19.618862		hsa-miR-95	21.199413
hsa-let-7f	19.623003		hsa-miR-675	21.222189
hsa-miR-451	19.673416		hsa-miR-675	21.292246
hsa-miR-335*	19.689217		hsa-miR-652	21.294155
hsa-miR-340	19.773384		hsa-miR-20a*	21.313854
hsa-miR-148a	19.785158		hsa-miR-424*	21.360243
hsa-miR-214*	19.802256		hsa-miR-425*	21.382336
hsa-miR-15b*	19.80741		hsa-miR-642	21.402098
hsa-miR-495	19.843716		hsa-miR-34a	21.448248
hsa-miR-99b*	19.88018		hsa-miR-93*	21.468248
hsa-miR-361-5p	19.89663		hsa-miR-452	21.485905
hsa-miR-923	19.938808		hsa-miR-29c	21.522892
hsa-miR-372	19.99262		hsa-miR-128	21.530079
hsa-miR-339-3p	19.99571		hsa-miR-323-3p	21.54159
hsa-miR-221	20.057768		hsa-miR-10a	21.548632
hsa-miR-324-3p	20.078339		hsa-miR-628-5p	21.572042
hsa-miR-302b	20.094265		hsa-miR-424	21.577202
hsa-miR-923	20.12211		hsa-miR-208	21.589996
hsa-miR-224	20.1563		hsa-miR-886-5p	21.61325
hsa-miR-487b	20.212036		hsa-miR-185	21.621655
hsa-miR-144*	20.25086		hsa-miR-22	21.697374
hsa-miR-455-3p	20.332441		hsa-miR-107	21.72986
hsa-miR-135b	20.339338		hsa-miR-422a	21.771442
hsa-miR-625*	20.392862		hsa-miR-362-5p	21.799175
hsa-miR-433	20.439903		hsa-miR-101	21.80387
hsa-miR-455-5p	20.524961		hsa-miR-512-3p	21.81058
hsa-miR-340*	20.595596		hsa-miR-302d	21.898201

microRNAs detected in the human foetal heart				
miRNA	Ct		miRNA	Ct
hsa-miR-9*	21.93061		hsa-miR-490-3p	23.279697
hsa-miR-302d	21.942945		hsa-miR-383	23.287693
hsa-miR-130b*	21.985044		hsa-miR-656	23.32069
hsa-miR-509-3p	21.995136		hsa-miR-222*	23.335268
hsa-miR-493	21.997902		hsa-miR-18b	23.360191
hsa-miR-30d*	22.001595		hsa-miR-770-5p	23.413559
hsa-miR-296-5p	22.018211		hsa-miR-744*	23.44341
hsa-miR-134	22.100597		hsa-miR-181a*	23.473919
hsa-miR-26b*	22.122326		hsa-miR-188-5p	23.50093
hsa-miR-543	22.123491		hsa-miR-10b*	23.587038
hsa-miR-208b	22.200642		hsa-miR-758	23.617994
hsa-miR-190	22.206678		hsa-miR-34a*	23.649477
hsa-miR-206	22.216806		hsa-miR-375	23.667109
hsa-miR-423-5p	22.231771		hsa-miR-16-1*	23.711205
hsa-miR-505*	22.290564		hsa-miR-517a	23.727024
hsa-miR-19b-1*	22.303858		hsa-miR-542-5p	23.76533
hsa-miR-503	22.32933		hsa-miR-935	23.772717
hsa-miR-337-5p	22.375141		hsa-miR-501-5p	23.797396
hsa-miR-148b	22.37727		hsa-miR-517c	23.86114
hsa-miR-485-3p	22.447958		hsa-miR-450a	23.869213
hsa-miR-27a*	22.457872		hsa-miR-33a*	23.885311
hsa-miR-32	22.46834		hsa-miR-362-3p	23.896763
hsa-miR-140-3p	22.492315		hsa-miR-302a	23.913326
hsa-miR-450b-5p	22.529545		hsa-miR-137	23.929958
hsa-miR-99a*	22.535856		hsa-miR-148b*	23.931643
hsa-miR-367	22.562801		hsa-miR-592	23.968454
hsa-miR-877	22.574924		hsa-miR-125a-3p	23.998823
hsa-miR-500	22.615295		hsa-miR-668	24.000854
hsa-miR-551b	22.650784		hsa-miR-545	24.083843
hsa-miR-199a-5p	22.667114		hsa-miR-668	24.08411
hsa-miR-655	22.785135		hsa-miR-629*	24.113781
hsa-miR-431	22.877382		hsa-miR-26a-1*	24.113945
hsa-miR-302c	22.884874		hsa-miR-331-5p	24.11421
hsa-miR-628-3p	22.94126		hsa-miR-760	24.117392
hsa-miR-454*	22.95767		hsa-miR-502-5p	24.138535
hsa-miR-15a*	22.972765		hsa-miR-597	24.189175
hsa-miR-628-3p	23.081615		hsa-miR-218-2*	24.218102
hsa-miR-654-5p	23.105444		hsa-miR-411*	24.305908
hsa-miR-27b*	23.12709		hsa-miR-200b	24.317041
hsa-miR-889	23.143		hsa-miR-519d	24.361595
hsa-miR-504	23.146128		hsa-miR-200c	24.369791
hsa-miR-22*	23.14751		hsa-miR-874	24.379766
hsa-miR-542-3p	23.168135		hsa-miR-193b*	24.404537
hsa-miR-942	23.184011		hsa-miR-337-3p	24.434013
hsa-miR-139-3p	23.195787		hsa-miR-493*	24.434813
hsa-miR-656	23.204138		hsa-miR-935	24.43734
hsa-miR-129-3p	23.225185		hsa-miR-618	24.526098
hsa-miR-199b-5p	23.263174		hsa-miR-502-3p	24.531847
hsa-miR-339-5p	23.272943		hsa-miR-551b*	24.577503
hsa-miR-671-3p	23.274572		hsa-miR-17*	24.579977

Appendix 2

microRNAs detected in the human foetal heart				
miRNA	Ct		miRNA	Ct
hsa-miR-576-3p	24.602106		hsa-miR-363*	25.927235
hsa-miR-200a	24.625708		hsa-miR-584	25.978025
hsa-miR-302a*	24.66243		hsa-miR-29c*	25.983843
hsa-miR-519a	24.672844		hsa-miR-499-3p	26.041725
hsa-miR-149*	24.787416		hsa-miR-29b	26.082129
hsa-miR-625	24.83909		hsa-miR-181c	26.149529
hsa-miR-508	24.863813		hsa-miR-489	26.205736
hsa-miR-380*	24.867151		hsa-miR-329	26.218367
hsa-miR-381	24.881437		hsa-miR-141	26.270912
hsa-miR-18a*	24.926281		hsa-miR-7	26.31704
hsa-miR-369-3p	24.926357		hsa-miR-190b	26.392445
hsa-miR-378*	24.95108		hsa-miR-142-5p	26.411804
hsa-miR-518f	24.97831		hsa-miR-215	26.42271
hsa-miR-654-3p	24.985971		hsa-miR-616*	26.450819
hsa-miR-92a-1*	25.01239		hsa-miR-29a*	26.48437
hsa-miR-122	25.020428		hsa-miR-7	26.49784
hsa-miR-589*	25.023409		hsa-let-7e*	26.530325
hsa-miR-182	25.068346		hsa-miR-20b*	26.530714
hsa-miR-518e	25.082762		hsa-miR-636	26.562765
hsa-miR-338-3p	25.119286		hsa-miR-125b-2*	26.583845
hsa-miR-497	25.14947		hsa-miR-429	26.616804
hsa-miR-497	25.18778		hsa-miR-21*	26.625452
hsa-miR-143*	25.196556		hsa-miR-487a	26.625658
hsa-miR-509-5p	25.19787		hsa-let-7i*	26.718792
hsa-miR-887	25.205393		hsa-miR-369-5p	26.73105
hsa-miR-299-5p	25.27234		hsa-miR-629	26.882998
hsa-miR-183*	25.28983		hsa-miR-373	26.88434
hsa-miR-511	25.317358		hsa-miR-374b*	26.89397
hsa-miR-138-1*	25.338324		hsa-miR-183	26.922203
hsa-miR-941	25.387598		hsa-miR-379*	26.94149
hsa-miR-125b-1*	25.436422		hsa-miR-891a	26.99367
hsa-miR-330-3p	25.481108		hsa-miR-100*	27.012196
hsa-miR-7-2*	25.502388		hsa-miR-938	27.039803
hsa-miR-409-5p	25.506851		hsa-miR-545*	27.054024
hsa-miR-376a*	25.529778		hsa-miR-520c-3p	27.115524
hsa-miR-486-5p	25.537403		hsa-miR-187	27.154427
hsa-miR-193a-3p	25.587582		hsa-miR-522	27.278902
hsa-miR-584	25.597273		hsa-miR-651	27.296276
hsa-miR-374a*	25.603252		hsa-miR-192*	27.408161
hsa-miR-154*	25.676752		hsa-miR-550	27.45985
hsa-miR-371-3p	25.686998		hsa-miR-146b-3p	27.473368
hsa-miR-525-3p	25.69435		hsa-miR-377*	27.512411
hsa-miR-518b	25.70809		hsa-miR-24-1*	27.52601
hsa-miR-485-5p	25.728807		hsa-miR-135b*	27.548721
hsa-miR-505	25.756039		hsa-miR-541	27.55105
hsa-miR-488	25.758015		hsa-miR-96	27.552614
hsa-miR-500*	25.762995		hsa-miR-888	27.641687
hsa-miR-26a-2*	25.765726		hsa-miR-519b-3p	27.73789
hsa-miR-181c*	25.838512		hsa-miR-19a*	27.799528
hsa-miR-579	25.895632		hsa-miR-449a	27.809761

microRNAs detected in the human foetal heart				
miRNA	Ct		miRNA	Ct
hsa-miR-519b-3p	27.84733		hsa-miR-124	29.441654
hsa-miR-769-3p	27.907148		hsa-miR-202*	29.44656
hsa-miR-661	27.90799		hsa-miR-515-5p	29.47523
hsa-miR-518a-3p	27.937042		hsa-miR-198	29.531965
hsa-miR-769-3p	27.942688		hsa-miR-520d-5p	29.563923
hsa-let-7f-2*	27.965673		hsa-miR-944	29.616228
hsa-miR-515-3p	27.997211		hsa-miR-496	29.643803
hsa-miR-92b*	28.005705		hsa-miR-548b-5p	29.660606
hsa-let-7g*	28.061562		hsa-miR-106a*	29.7089
hsa-miR-601	28.135082		hsa-miR-196b	29.794537
hsa-miR-361-3p	28.17243		hsa-miR-580	29.804726
hsa-miR-34c-5p	28.256565		hsa-miR-330-5p	29.822754
hsa-miR-346	28.405203		hsa-miR-132*	29.856882
hsa-miR-501-3p	28.450489		hsa-miR-296-3p	29.858383
hsa-miR-136	28.468962		hsa-miR-589	29.86808
hsa-miR-875-5p	28.473537		hsa-miR-524-3p	29.913477
hsa-miR-526b*	28.486063		hsa-miR-524-3p	29.980822
hsa-miR-219-1-3p	28.48984		hsa-miR-510	30.05457
hsa-miR-223*	28.534307		hsa-miR-523	30.093119
hsa-miR-513-3p	28.586588		hsa-miR-580	30.15898
hsa-let-7a*	28.605282		hsa-miR-23a*	30.21261
hsa-miR-937	28.606524		hsa-miR-376b	30.398365
hsa-miR-205	28.647457		hsa-miR-200a*	30.420048
hsa-miR-550*	28.67494		hsa-miR-641	30.454697
hsa-miR-564	28.7211		hsa-miR-216b	30.47035
hsa-miR-624*	28.75335		hsa-miR-130a*	30.475037
hsa-miR-10a*	28.7927		hsa-miR-302c*	30.667234
hsa-miR-548d-5p	28.842325		hsa-miR-200b*	30.680872
hsa-miR-202	28.873075		hsa-miR-876-3p	30.69808
hsa-miR-767-5p	28.879934		hsa-miR-873	30.705761
hsa-miR-551a	28.88676		hsa-miR-516a-3p	30.745874
hsa-miR-127-5p	28.898602		hsa-miR-491-3p	30.82275
hsa-miR-154	28.919556		hsa-miR-572	30.835035
hsa-miR-610	28.940102		hsa-miR-641	30.854567
hsa-miR-23b*	28.940386		hsa-miR-377	30.900827
hsa-miR-627	28.966063		hsa-miR-582-3p	30.922024
hsa-miR-548d-3p	28.979939		hsa-miR-129-5p	30.938515
hsa-miR-342-5p	29.018589		hsa-miR-155*	31.001978
hsa-miR-632	29.086575		hsa-miR-432*	31.00699
hsa-miR-30c-1*	29.088696		hsa-miR-516b	31.043427
hsa-miR-548c-5p	29.16466		hsa-miR-105	31.054342
hsa-miR-506	29.169548		hsa-miR-453	31.078701
hsa-miR-449b	29.235792		hsa-miR-216a	31.13224
hsa-miR-767-5p	29.241259		hsa-miR-939	31.251366
hsa-miR-219-5p	29.247997		hsa-miR-326	31.313868
hsa-let-7f-1*	29.254622		hsa-miR-605	31.3496
hsa-miR-361-3p	29.315828		hsa-miR-221*	31.408388
hsa-miR-544	29.35865		hsa-miR-548a-3p	31.432558
hsa-miR-570	29.410757		hsa-miR-380	31.438845
hsa-miR-29b-2*	29.44035		hsa-miR-519c-3p	31.51515

Appendix 2

microRNAs detected in the human foetal heart				
miRNA	Ct		miRNA	Ct
hsa-miR-638	31.548552			
hsa-let-7d*	31.613987			
hsa-miR-138-2*	31.64256			
hsa-miR-518d-5p	31.654938			
hsa-miR-217	31.736666			
hsa-miR-520g	31.79897			
hsa-miR-576-5p	31.85434			
hsa-miR-23a	31.868933			
hsa-miR-605	31.872032			

Appendix 3

The following table shows raw data in the form of Ct (cycle threshold) values obtained by qPCR for the detection of thymosin β4 (*TMSB4X*) and the endogenous controls, *GNB2L1* and *PGK1*, in endothelial cells cultured on tissue culture plastic or Matrigel.

Reaction code	Ct value	Average Ct of repeats		Reaction code	Ct value	Average Ct of repeats
A1	20.07			B8	21.76	
A1	20.51	20.3767		B8	21.81	21.7767
A1	20.55			B8	21.76	
A7	20.8			C6	28.09	
A7	20.8	20.8600		C6	28.18	28.1233
A7	20.98			C6	28.1	
B5	24.53			A5	22.84	
B5	24.5	24.5000		A5	22.81	22.8300
B5	24.47			A5	22.84	
C3	25.65			B3	22.1	
C3	25.71	25.7367		B3	22.32	22.2433
C3	25.85			B3	22.31	
A2	21.82			C1	25.97	
A2	21.96	21.9867		C1	25.9	25.8767
A2	22.18			C1	25.76	
A8	19.46			C7	25.13	
A8	19.6	19.2800		C7	25.66	25.5267
A8	18.78			C7	25.79	
B6	23.99			A6	22.83	
B6	24.07	24.1267		A6	22.95	22.9100
B6	24.32			A6	22.95	
C4	29.96			B4	25.01	
C4	29.93	29.9700		B4	25.2	25.1167
C4	30.02			B4	25.14	
A3	20.47			C2	27.24	
A3	20.58	20.5867		C2	27.3	27.3433
A3	20.71			C2	27.49	
B1	23.05			C8	24.27	
B1	23.17	23.2267		C8	24.58	24.4400
B1	23.46			C8	24.47	
B7	22.35			A9		
B7	22.34	22.4133		A9		
B7	22.55			A9	39.46	
C5	28.58			B9		
C5	28.68	28.5900		B9		
C5	28.51			B9		
A4	24.25			C9		
A4	23.72	23.8933		C9		
A4	23.71			C9		
B2	23.83					
B2	23.84	23.8800				
B2	23.97					

Appendix 3

The following table indicates, for each reaction code, expression of which gene is being detected and in which sample. It also summarises the average Ct values for each reaction.

Reaction code	Gene	Sample	Ct value
A1	TMSB4X	Exp 1 Control	20.377
A2	TMSB4X	Exp 1 Matrigel	21.987
A3	TMSB4X	Exp 2 Control	20.587
A4	TMSB4X	Exp 2 Matrigel	23.893
A5	TMSB4X	Exp 3 Control	22.830
A6	TMSB4X	Exp 3 Matrigel	22.910
A7	TMSB4X	Exp 4 Control	20.860
A8	TMSB4X	Exp 4 Matrigel	19.280
A9	TMSB4X	No template	N/A
B1	GNB2L1	Exp 1 Control	23.227
B2	GNB2L1	Exp 1 Matrigel	23.880
B3	GNB2L1	Exp 2 Control	22.243
B4	GNB2L1	Exp 2 Matrigel	25.117
B5	GNB2L1	Exp 3 Control	24.500
B6	GNB2L1	Exp 3 Matrigel	24.127
B7	GNB2L1	Exp 4 Control	22.413
B8	GNB2L1	Exp 4 Matrigel	21.777
B9	GNB2L1	No template	N/A
C1	PGK1	Exp 1 Control	25.877
C2	PGK1	Exp 1 Matrigel	27.343
C3	PGK1	Exp 2 Control	25.737
C4	PGK1	Exp 2 Matrigel	29.970
C5	PGK1	Exp 3 Control	28.590
C6	PGK1	Exp 3 Matrigel	28.123
C7	PGK1	Exp 4 Control	25.527
C8	PGK1	Exp 4 Matrigel	24.440
C9	PGK1	No template	N/A

Appendix 4

The following table shows raw data in the form of Ct values obtained by qPCR for the detection of miR-148b, miR-495, miR-199a-3p, miR-217 and RNU-48, the endogenous control, in endothelial cells cultured on tissue culture plastic or Matrigel.

Reaction code	Ct value	Average Ct of repeats		Reaction code	Ct value	Average Ct of repeats
A1	39.99			A6	36.92	
A1		39.165		A6	36.36	36.526667
A1	38.34			A6	36.3	
A7	35.48			B4	31.22	
A7	36.26	35.953333		B4	31.06	31.14
A7	36.12			B4	31.14	
B5	29.83			A9		
B5	30	29.976667		A9		
B5	30.1			A9		
A2	36.25			B9		
A2	37.05	36.666667		B9		
A2	36.7			B9		
A8	35.07			C1	32.62	
A8	34.98	35.116667		C1	32.61	32.74
A8	35.3			C1	32.99	
B6	30.07			C7	29.15	
B6	29.91	29.993333		C7	29.31	29.25
B6	30			C7	29.29	
A3	36.13			D5	31.98	
A3	34.96	35.556667		D5	31.51	31.826667
A3	35.58			D5	31.99	
B1	32.64			E3	24.21	
B1	32.79	32.916667		E3	24.16	24.24
B1	33.32			E3	24.35	
B7	29.86			C2	29.2	
B7	29.85	29.973333		C2	29.49	29.34
B7	30.21			C2	29.33	
A4	36.53			C8	28.33	
A4	36.46	36.366667		C8	28.47	28.43
A4	36.11			C8	28.49	
B2	30.95			D6	32.67	
B2	30.69	30.86		D6	32.55	32.696667
B2	30.94			D6	32.87	
B8	30.21			E4	25.69	
B8	29.94	30.09		E4	25.78	25.766667
B8	30.12			E4	25.83	
A5	36.36			C3	28.24	
A5	35.01	35.673333		C3	28.27	28.256667
A5	35.65			C3	28.26	
B3	30.49			D1	35.34	
B3	30.54	30.54		D1	34.91	35.09
B3	30.59			D1	35.02	

Appendix 4

Reaction code	Ct value	Average Ct of repeats		Reaction code	Ct value	Average Ct of repeats
D7	32.17	32.156667		E7	25.33	25.163333
D7	32.32			E7	24.86	
D7	31.98			E7	25.3	
E5	24.78	24.89		C6	29.21	29.213333
E5	24.81			C6	29.32	
E5	25.08			C6	29.11	
C4	30.26	30.23		D4	32.14	32.2
C4	30.16			D4	32.4	
C4	30.27			D4	32.06	
D2	32.48	32.42		E2	25.32	25.3
D2	32.13			E2	25.33	
D2	32.65			E2	25.25	
D8	31.6	31.756667		E8	24.61	24.71
D8	31.73			E8	24.76	
D8	31.94			E8	24.76	
E6	25.3	25.456667		C9		
E6	25.51			C9		
E6	25.56			C9		
C5	28.19	28.23		D9		
C5	28.32			D9		
C5	28.18			D9		
D3	30.88	30.886667		E9		
D3	30.77			E9		
D3	31.01			E9		
E1	26.63	26.636667				
E1	26.49					
E1	26.79					

The following table indicates, for each reaction code, expression of which miRNA is being detected and in which sample. It also summarises the average Ct values for each reaction.

Reaction code	miRNA	Sample	Ct value
A1	miR-148b	Exp 1 Control	39.165
A2	miR-148b	Exp 1 Matrigel	36.667
A3	miR-148b	Exp 2 Control	35.557
A4	miR-148b	Exp 2 Matrigel	36.367
A5	miR-148b	Exp 3 Control	35.673
A6	miR-148b	Exp 3 Matrigel	36.527
A7	miR-148b	Exp 4 Control	35.953
A8	miR-148b	Exp 4 Matrigel	35.117
A9	miR-148b	No template	N/A
B1	miR-495	Exp 1 Control	32.917
B2	miR-495	Exp 1 Matrigel	30.860
B3	miR-495	Exp 2 Control	30.540
B4	miR-495	Exp 2 Matrigel	31.140
B5	miR-495	Exp 3 Control	29.977
B6	miR-495	Exp 3 Matrigel	29.993
B7	miR-495	Exp 4 Control	29.973
B8	miR-495	Exp 4 Matrigel	30.090
B9	miR-495	No template	N/A
C1	miR-199a-3p	Exp 1 Control	32.740
C2	miR-199a-3p	Exp 1 Matrigel	29.340
C3	miR-199a-3p	Exp 2 Control	28.257
C4	miR-199a-3p	Exp 2 Matrigel	30.230
C5	miR-199a-3p	Exp 3 Control	28.230
C6	miR-199a-3p	Exp 3 Matrigel	29.213
C7	miR-199a-3p	Exp 4 Control	29.250
C8	miR-199a-3p	Exp 4 Matrigel	28.430
C9	miR-199a-3p	No template	N/A
D1	miR-217	Exp 1 Control	35.090
D2	miR-217	Exp 1 Matrigel	32.420
D3	miR-217	Exp 2 Control	30.887
D4	miR-217	Exp 2 Matrigel	32.200
D5	miR-217	Exp 3 Control	31.827
D6	miR-217	Exp 3 Matrigel	32.697
D7	miR-217	Exp 4 Control	32.157
D8	miR-217	Exp 4 Matrigel	31.757
D9	miR-217	No template	N/A
E1	RNU-48	Exp 1 Control	26.637
E2	RNU-48	Exp 1 Matrigel	25.300
E3	RNU-48	Exp 2 Control	24.240
E4	RNU-48	Exp 2 Matrigel	25.767
E5	RNU-48	Exp 3 Control	24.890
E6	RNU-48	Exp 3 Matrigel	25.457
E7	RNU-48	Exp 4 Control	25.163
E8	RNU-48	Exp 4 Matrigel	24.71
E9	RNU-48	No template	N/A

References

1. WHO. Fact sheet 317: Cardiovascular diseases. World Health Organization, 2012.
2. Townsend N WK, Bhatnagar P, Smolina K, Nichols M, Luengo-Fernandez R, Rayner M. Coronary heart disease statistics 2012 edition. London: British Heart Foundation, 2012.
3. Hobbs FD, Roalfe AK, Davis RC, Davies MK, Hare R. Prognosis of all-cause heart failure and borderline left ventricular systolic dysfunction: 5 year mortality follow-up of the Echocardiographic Heart of England Screening Study (ECHOES). *Eur Heart J* 2007;**28**:1128-1134.
4. Bergmann O, Bhardwaj RD, Bernard S, Zdunek S, Barnabe-Heider F, Walsh S*, et al.* Evidence for cardiomyocyte renewal in humans. *Science* 2009;**324**:98-102.
5. Mollova M, Bersell K, Walsh S, Savla J, Das LT, Park SY*, et al.* Cardiomyocyte proliferation contributes to heart growth in young humans. *Proc Natl Acad Sci U S A* 2013;**110**:1446-1451.
6. Beltrami AP, Urbanek K, Kajstura J, Yan SM, Finato N, Bussani R*, et al.* Evidence that human cardiac myocytes divide after myocardial infarction. *N Engl J Med* 2001;**344**:1750-1757.
7. Soonpaa MH, Koh GY, Klug MG, Field LJ. Formation of nascent intercalated disks between grafted fetal cardiomyocytes and host myocardium. *Science* 1994;**264**:98-101.
8. Li RK, Jia ZQ, Weisel RD, Mickle DA, Zhang J, Mohabeer MK*, et al.* Cardiomyocyte transplantation improves heart function. *Ann Thorac Surg* 1996;**62**:654-660; discussion 660-651.
9. Muller-Ehmsen J, Whittaker P, Kloner RA, Dow JS, Sakoda T, Long TI*, et al.* Survival and development of neonatal rat cardiomyocytes transplanted into adult myocardium. *J Mol Cell Cardiol* 2002;**34**:107-116.
10. Marelli D, Desrosiers C, el-Alfy M, Kao RL, Chiu RC. Cell transplantation for myocardial repair: an experimental approach. *Cell Transplant* 1992;**1**:383-390.
11. Chiu RC, Zibaitis A, Kao RL. Cellular cardiomyoplasty: myocardial regeneration with satellite cell implantation. *Ann Thorac Surg* 1995;**60**:12-18.
12. Koh GY, Klug MG, Soonpaa MH, Field LJ. Differentiation and long-term survival of C2C12 myoblast grafts in heart. *J Clin Invest* 1993;**92**:1548-1554.
13. Reinecke H, Poppa V, Murry CE. Skeletal muscle stem cells do not transdifferentiate into cardiomyocytes after cardiac grafting. *J Mol Cell Cardiol* 2002;**34**:241-249.
14. Leobon B, Garcin I, Menasche P, Vilquin JT, Audinat E, Charpak S. Myoblasts transplanted into rat infarcted myocardium are functionally isolated from their host. *Proc Natl Acad Sci U S A* 2003;**100**:7808-7811.
15. Taylor DA, Atkins BZ, Hungspreugs P, Jones TR, Reedy MC, Hutcheson KA*, et al.* Regenerating functional myocardium: improved performance after skeletal myoblast transplantation. *Nat Med* 1998;**4**:929-933.

16. Jain M, DerSimonian H, Brenner DA, Ngoy S, Teller P, Edge AS*, et al.* Cell therapy attenuates deleterious ventricular remodeling and improves cardiac performance after myocardial infarction. *Circulation* 2001;**103**:1920-1927.
17. Ghostine S, Carrion C, Souza LC, Richard P, Bruneval P, Vilquin JT*, et al.* Long-term efficacy of myoblast transplantation on regional structure and function after myocardial infarction. *Circulation* 2002;**106**:I131-136.
18. Smits PC, van Geuns RJ, Poldermans D, Bountioukos M, Onderwater EE, Lee CH*, et al.* Catheter-based intramyocardial injection of autologous skeletal myoblasts as a primary treatment of ischemic heart failure: clinical experience with six-month follow-up. *J Am Coll Cardiol* 2003;**42**:2063-2069.
19. Siminiak T, Fiszer D, Jerzykowska O, Grygielska B, Rozwadowska N, Kalmucki P*, et al.* Percutaneous trans-coronary-venous transplantation of autologous skeletal myoblasts in the treatment of post-infarction myocardial contractility impairment: the POZNAN trial. *Eur Heart J* 2005;**26**:1188-1195.
20. Menasche P, Alfieri O, Janssens S, McKenna W, Reichenspurner H, Trinquart L*, et al.* The Myoblast Autologous Grafting in Ischemic Cardiomyopathy (MAGIC) trial: first randomized placebo-controlled study of myoblast transplantation. *Circulation* 2008;**117**:1189-1200.
21. Fernandes S, Amirault JC, Lande G, Nguyen JM, Forest V, Bignolais O*, et al.* Autologous myoblast transplantation after myocardial infarction increases the inducibility of ventricular arrhythmias. *Cardiovasc Res* 2006;**69**:348-358.
22. Abkowitz JL, Catlin SN, McCallie MT, Guttorp P. Evidence that the number of hematopoietic stem cells per animal is conserved in mammals. *Blood* 2002;**100**:2665-2667.
23. Pittenger MF, Mackay AM, Beck SC, Jaiswal RK, Douglas R, Mosca JD*, et al.* Multilineage potential of adult human mesenchymal stem cells. *Science* 1999;**284**:143-147.
24. Orlic D, Kajstura J, Chimenti S, Jakoniuk I, Anderson SM, Li B*, et al.* Bone marrow cells regenerate infarcted myocardium. *Nature* 2001;**410**:701-705.
25. Toma C, Pittenger MF, Cahill KS, Byrne BJ, Kessler PD. Human mesenchymal stem cells differentiate to a cardiomyocyte phenotype in the adult murine heart. *Circulation* 2002;**105**:93-98.
26. Eisenberg LM, Burns L, Eisenberg CA. Hematopoietic cells from bone marrow have the potential to differentiate into cardiomyocytes in vitro. *Anat Rec A Discov Mol Cell Evol Biol* 2003;**274**:870-882.
27. Alvarez-Dolado M, Pardal R, Garcia-Verdugo JM, Fike JR, Lee HO, Pfeffer K*, et al.* Fusion of bone-marrow-derived cells with Purkinje neurons, cardiomyocytes and hepatocytes. *Nature* 2003;**425**:968-973.
28. Nygren JM, Jovinge S, Breitbach M, Sawen P, Roll W, Hescheler J*, et al.* Bone marrow-derived hematopoietic cells generate cardiomyocytes at a low frequency through cell fusion, but not transdifferentiation. *Nat Med* 2004;**10**:494-501.
29. Murry CE, Soonpaa MH, Reinecke H, Nakajima H, Nakajima HO, Rubart M*, et al.* Haematopoietic stem cells do not transdifferentiate into cardiac myocytes in myocardial infarcts. *Nature* 2004;**428**:664-668.

30. Rota M, Kajstura J, Hosoda T, Bearzi C, Vitale S, Esposito G*, et al.* Bone marrow cells adopt the cardiomyogenic fate in vivo. *Proc Natl Acad Sci U S A* 2007;**104**:17783-17788.
31. Kocher AA, Schuster MD, Szabolcs MJ, Takuma S, Burkhoff D, Wang J*, et al.* Neovascularization of ischemic myocardium by human bone-marrow-derived angioblasts prevents cardiomyocyte apoptosis, reduces remodeling and improves cardiac function. *Nat Med* 2001;**7**:430-436.
32. Tomita S, Mickle DA, Weisel RD, Jia ZQ, Tumiati LC, Allidina Y*, et al.* Improved heart function with myogenesis and angiogenesis after autologous porcine bone marrow stromal cell transplantation. *J Thorac Cardiovasc Surg* 2002;**123**:1132-1140.
33. Amado LC, Saliaris AP, Schuleri KH, St John M, Xie JS, Cattaneo S*, et al.* Cardiac repair with intramyocardial injection of allogeneic mesenchymal stem cells after myocardial infarction. *Proc Natl Acad Sci U S A* 2005;**102**:11474-11479.
34. Strauer BE, Brehm M, Zeus T, Kostering M, Hernandez A, Sorg RV*, et al.* Repair of infarcted myocardium by autologous intracoronary mononuclear bone marrow cell transplantation in humans. *Circulation* 2002;**106**:1913-1918.
35. Assmus B, Schachinger V, Teupe C, Britten M, Lehmann R, Dobert N*, et al.* Transplantation of Progenitor Cells and Regeneration Enhancement in Acute Myocardial Infarction (TOPCARE-AMI). *Circulation* 2002;**106**:3009-3017.
36. Clifford DM, Fisher SA, Brunskill SJ, Doree C, Mathur A, Watt S*, et al.* Stem cell treatment for acute myocardial infarction. *Cochrane Database Syst Rev* 2012;**2**:CD006536.
37. Trachtenberg B, Velazquez DL, Williams AR, McNiece I, Fishman J, Nguyen K*, et al.* Rationale and design of the Transendocardial Injection of Autologous Human Cells (bone marrow or mesenchymal) in Chronic Ischemic Left Ventricular Dysfunction and Heart Failure Secondary to Myocardial Infarction (TAC-HFT) trial: A randomized, double-blind, placebo-controlled study of safety and efficacy. *Am Heart J* 2011;**161**:487-493.
38. Chen SL, Fang WW, Ye F, Liu YH, Qian J, Shan SJ*, et al.* Effect on left ventricular function of intracoronary transplantation of autologous bone marrow mesenchymal stem cell in patients with acute myocardial infarction. *Am J Cardiol* 2004;**94**:92-95.
39. Wollert KC, Meyer GP, Lotz J, Ringes-Lichtenberg S, Lippolt P, Breidenbach C*, et al.* Intracoronary autologous bone-marrow cell transfer after myocardial infarction: the BOOST randomised controlled clinical trial. *Lancet* 2004;**364**:141-148.
40. Assmus B, Rolf A, Erbs S, Elsasser A, Haberbosch W, Hambrecht R*, et al.* Clinical outcome 2 years after intracoronary administration of bone marrow-derived progenitor cells in acute myocardial infarction. *Circ Heart Fail* 2010;**3**:89-96.
41. Leistner DM, Fischer-Rasokat U, Honold J, Seeger FH, Schachinger V, Lehmann R*, et al.* Transplantation of progenitor cells and regeneration enhancement in acute myocardial infarction (TOPCARE-AMI): final 5-year results suggest long-term safety and efficacy. *Clin Res Cardiol* 2011;**100**:925-934.

42. Heldman AW, DiFede DL, Fishman JE, Zambrano JP, Trachtenberg BH, Karantalis V*, et al.* Transendocardial mesenchymal stem cells and mononuclear bone marrow cells for ischemic cardiomyopathy: the TAC-HFT randomized trial. *JAMA* 2014;**311**:62-73.
43. Traverse JH, Henry TD, Pepine CJ, Willerson JT, Zhao DX, Ellis SG*, et al.* Effect of the use and timing of bone marrow mononuclear cell delivery on left ventricular function after acute myocardial infarction: the TIME randomized trial. *JAMA* 2012;**308**:2380-2389.
44. Perin EC, Willerson JT, Pepine CJ, Henry TD, Ellis SG, Zhao DX*, et al.* Effect of transendocardial delivery of autologous bone marrow mononuclear cells on functional capacity, left ventricular function, and perfusion in chronic heart failure: the FOCUS-CCTRN trial. *JAMA* 2012;**307**:1717-1726.
45. Henning RJ, Abu-Ali H, Balis JU, Morgan MB, Willing AE, Sanberg PR. Human umbilical cord blood mononuclear cells for the treatment of acute myocardial infarction. *Cell Transplant* 2004;**13**:729-739.
46. Henning RJ, Aufman J, Shariff M, Sawmiller D, DeLostia V, Sanberg P*, et al.* Human umbilical cord blood mononuclear cells decrease fibrosis and increase cardiac function in cardiomyopathy. *Regen Med* 2010;**5**:45-54.
47. Hofmann M, Wollert KC, Meyer GP, Menke A, Arseniev L, Hertenstein B*, et al.* Monitoring of bone marrow cell homing into the infarcted human myocardium. *Circulation* 2005;**111**:2198-2202.
48. Penicka M, Lang O, Widimsky P, Kobylka P, Kozak T, Vanek T*, et al.* One-day kinetics of myocardial engraftment after intracoronary injection of bone marrow mononuclear cells in patients with acute and chronic myocardial infarction. *Heart* 2007;**93**:837-841.
49. Silva SA, Sousa AL, Haddad AF, Azevedo JC, Soares VE, Peixoto CM*, et al.* Autologous bone-marrow mononuclear cell transplantation after acute myocardial infarction: comparison of two delivery techniques. *Cell Transplant* 2009;**18**:343-352.
50. Uemura R, Xu M, Ahmad N, Ashraf M. Bone marrow stem cells prevent left ventricular remodeling of ischemic heart through paracrine signaling. *Circ Res* 2006;**98**:1414-1421.
51. Nguyen BK, Maltais S, Perrault LP, Tanguay JF, Tardif JC, Stevens LM*, et al.* Improved function and myocardial repair of infarcted heart by intracoronary injection of mesenchymal stem cell-derived growth factors. *J Cardiovasc Transl Res* 2010;**3**:547-558.
52. Henning RJ, Sanberg P, Jimenez E. Human cord blood stem cell paracrine factors activate the survival protein kinase Akt and inhibit death protein kinases JNK and p38 in injured cardiomyocytes. *Cytotherapy* 2014;**16**:1158-1168.
53. Yarden Y, Kuang WJ, Yang-Feng T, Coussens L, Munemitsu S, Dull TJ*, et al.* Human proto-oncogene c-kit: a new cell surface receptor tyrosine kinase for an unidentified ligand. *EMBO J* 1987;**6**:3341-3351.
54. Williams DE, Eisenman J, Baird A, Rauch C, Van Ness K, March CJ*, et al.* Identification of a ligand for the c-kit proto-oncogene. *Cell* 1990;**63**:167-174.

55. Morrison SJ, Wandycz AM, Hemmati HD, Wright DE, Weissman IL. Identification of a lineage of multipotent hematopoietic progenitors. *Development* 1997;**124**:1929-1939.
56. Beltrami AP, Barlucchi L, Torella D, Baker M, Limana F, Chimenti S*, et al.* Adult cardiac stem cells are multipotent and support myocardial regeneration. *Cell* 2003;**114**:763-776.
57. Dawn B, Stein AB, Urbanek K, Rota M, Whang B, Rastaldo R*, et al.* Cardiac stem cells delivered intravascularly traverse the vessel barrier, regenerate infarcted myocardium, and improve cardiac function. *Proc Natl Acad Sci U S A* 2005;**102**:3766-3771.
58. Bearzi C, Rota M, Hosoda T, Tillmanns J, Nascimbene A, De Angelis A*, et al.* Human cardiac stem cells. *Proc Natl Acad Sci U S A* 2007;**104**:14068-14073.
59. Laugwitz KL, Moretti A, Lam J, Gruber P, Chen Y, Woodard S*, et al.* Postnatal isl1+ cardioblasts enter fully differentiated cardiomyocyte lineages. *Nature* 2005;**433**:647-653.
60. Cai CL, Liang X, Shi Y, Chu PH, Pfaff SL, Chen J*, et al.* Isl1 identifies a cardiac progenitor population that proliferates prior to differentiation and contributes a majority of cells to the heart. *Dev Cell* 2003;**5**:877-889.
61. Moretti A, Caron L, Nakano A, Lam JT, Bernshausen A, Chen Y*, et al.* Multipotent embryonic isl1+ progenitor cells lead to cardiac, smooth muscle, and endothelial cell diversification. *Cell* 2006;**127**:1151-1165.
62. Bu L, Jiang X, Martin-Puig S, Caron L, Zhu S, Shao Y*, et al.* Human ISL1 heart progenitors generate diverse multipotent cardiovascular cell lineages. *Nature* 2009;**460**:113-117.
63. Moretti A, Bellin M, Jung CB, Thies TM, Takashima Y, Bernshausen A*, et al.* Mouse and human induced pluripotent stem cells as a source for multipotent Isl1+ cardiovascular progenitors. *FASEB J* 2010;**24**:700-711.
64. Messina E, De Angelis L, Frati G, Morrone S, Chimenti S, Fiordaliso F*, et al.* Isolation and expansion of adult cardiac stem cells from human and murine heart. *Circ Res* 2004;**95**:911-921.
65. Davis DR, Zhang Y, Smith RR, Cheng K, Terrovitis J, Malliaras K*, et al.* Validation of the cardiosphere method to culture cardiac progenitor cells from myocardial tissue. *PLoS One* 2009;**4**:e7195.
66. Smith RR, Barile L, Cho HC, Leppo MK, Hare JM, Messina E*, et al.* Regenerative potential of cardiosphere-derived cells expanded from percutaneous endomyocardial biopsy specimens. *Circulation* 2007;**115**:896-908.
67. Johnston PV, Sasano T, Mills K, Evers R, Lee ST, Smith RR*, et al.* Engraftment, differentiation, and functional benefits of autologous cardiosphere-derived cells in porcine ischemic cardiomyopathy. *Circulation* 2009;**120**:1075-1083, 1077 p following 1083.
68. Lee ST, White AJ, Matsushita S, Malliaras K, Steenbergen C, Zhang Y*, et al.* Intramyocardial injection of autologous cardiospheres or cardiosphere-derived cells preserves function and minimizes adverse ventricular remodeling in pigs with heart failure post-myocardial infarction. *J Am Coll Cardiol* 2011;**57**:455-465.
69. Pfister O, Mouquet F, Jain M, Summer R, Helmes M, Fine A*, et al.* CD31- but Not CD31+ cardiac side population cells exhibit functional cardiomyogenic differentiation. *Circ Res* 2005;**97**:52-61.

70. Pfister O, Oikonomopoulos A, Sereti KI, Sohn RL, Cullen D, Fine GC*, et al.* Role of the ATP-binding cassette transporter Abcg2 in the phenotype and function of cardiac side population cells. *Circ Res* 2008;**103**:825-835.
71. Goodell MA, Brose K, Paradis G, Conner AS, Mulligan RC. Isolation and functional properties of murine hematopoietic stem cells that are replicating in vivo. *J Exp Med* 1996;**183**:1797-1806.
72. Oyama T, Nagai T, Wada H, Naito AT, Matsuura K, Iwanaga K*, et al.* Cardiac side population cells have a potential to migrate and differentiate into cardiomyocytes in vitro and in vivo. *J Cell Biol* 2007;**176**:329-341.
73. Sandstedt J, Jonsson M, Kajic K, Sandstedt M, Lindahl A, Dellgren G*, et al.* Left atrium of the human adult heart contains a population of side population cells. *Basic Res Cardiol* 2012;**107**:255.
74. Yamahara K, Fukushima S, Coppen SR, Felkin LE, Varela-Carver A, Barton PJ*, et al.* Heterogeneic nature of adult cardiac side population cells. *Biochem Biophys Res Commun* 2008;**371**:615-620.
75. Matsuura K, Nagai T, Nishigaki N, Oyama T, Nishi J, Wada H*, et al.* Adult cardiac Sca-1-positive cells differentiate into beating cardiomyocytes. *J Biol Chem* 2004;**279**:11384-11391.
76. Oh H, Bradfute SB, Gallardo TD, Nakamura T, Gaussin V, Mishina Y*, et al.* Cardiac progenitor cells from adult myocardium: homing, differentiation, and fusion after infarction. *Proc Natl Acad Sci U S A* 2003;**100**:12313-12318.
77. Matsuura K, Honda A, Nagai T, Fukushima N, Iwanaga K, Tokunaga M*, et al.* Transplantation of cardiac progenitor cells ameliorates cardiac dysfunction after myocardial infarction in mice. *J Clin Invest* 2009;**119**:2204-2217.
78. Wang X, Hu Q, Nakamura Y, Lee J, Zhang G, From AH*, et al.* The role of the sca-1+/CD31- cardiac progenitor cell population in postinfarction left ventricular remodeling. *Stem Cells* 2006;**24**:1779-1788.
79. Di Felice V, Ardizzone NM, De Luca A, Marciano V, Marino Gammazza A, Macaluso F*, et al.* OPLA scaffold, collagen I, and horse serum induce an higher degree of myogenic differentiation of adult rat cardiac stem cells. *J Cell Physiol* 2009;**221**:729-739.
80. Takamiya M, Haider KH, Ashraf M. Identification and characterization of a novel multipotent sub-population of Sca-1(+) cardiac progenitor cells for myocardial regeneration. *PLoS One* 2011;**6**:e25265.
81. Serradifalco C, Catanese P, Rizzuto L, Cappello F, Puleio R, Barresi V*, et al.* Embryonic and foetal Islet-1 positive cells in human hearts are also positive to c-Kit. *Eur J Histochem* 2011;**55**:e41.
82. Ye J, Boyle A, Shih H, Sievers RE, Zhang Y, Prasad M*, et al.* Sca-1+ cardiosphere-derived cells are enriched for Isl1-expressing cardiac precursors and improve cardiac function after myocardial injury. *PLoS One* 2012;**7**:e30329.
83. Bolli R, Chugh AR, D'Amario D, Loughran JH, Stoddard MF, Ikram S*, et al.* Cardiac stem cells in patients with ischaemic cardiomyopathy (SCIPIO): initial results of a randomised phase 1 trial. *Lancet* 2011;**378**:1847-1857.
84. Chugh AR, Beache GM, Loughran JH, Mewton N, Elmore JB, Kajstura J*, et al.* Administration of cardiac stem cells in patients with ischemic cardiomyopathy: the SCIPIO trial: surgical aspects and interim analysis

of myocardial function and viability by magnetic resonance. *Circulation* 2012;**126**:S54-64.
85. Makkar RR, Smith RR, Cheng K, Malliaras K, Thomson LE, Berman D*, et al.* Intracoronary cardiosphere-derived cells for heart regeneration after myocardial infarction (CADUCEUS): a prospective, randomised phase 1 trial. *Lancet* 2012;**379**:895-904.
86. Malliaras K, Makkar RR, Smith RR, Cheng K, Wu E, Bonow RO*, et al.* Intracoronary cardiosphere-derived cells after myocardial infarction: evidence of therapeutic regeneration in the final 1-year results of the CADUCEUS trial (CArdiosphere-Derived aUtologous stem CElls to reverse ventricUlar dySfunction). *J Am Coll Cardiol* 2014;**63**:110-122.
87. Thomson JA, Itskovitz-Eldor J, Shapiro SS, Waknitz MA, Swiergiel JJ, Marshall VS*, et al.* Embryonic stem cell lines derived from human blastocysts. *Science* 1998;**282**:1145-1147.
88. Kehat I, Kenyagin-Karsenti D, Snir M, Segev H, Amit M, Gepstein A*, et al.* Human embryonic stem cells can differentiate into myocytes with structural and functional properties of cardiomyocytes. *J Clin Invest* 2001;**108**:407-414.
89. Mummery C, Ward-van Oostwaard D, Doevendans P, Spijker R, van den Brink S, Hassink R*, et al.* Differentiation of human embryonic stem cells to cardiomyocytes: role of coculture with visceral endoderm-like cells. *Circulation* 2003;**107**:2733-2740.
90. Laflamme MA, Gold J, Xu C, Hassanipour M, Rosler E, Police S*, et al.* Formation of human myocardium in the rat heart from human embryonic stem cells. *Am J Pathol* 2005;**167**:663-671.
91. Laflamme MA, Chen KY, Naumova AV, Muskheli V, Fugate JA, Dupras SK*, et al.* Cardiomyocytes derived from human embryonic stem cells in pro-survival factors enhance function of infarcted rat hearts. *Nat Biotechnol* 2007;**25**:1015-1024.
92. van Laake LW, Passier R, Monshouwer-Kloots J, Verkleij AJ, Lips DJ, Freund C*, et al.* Human embryonic stem cell-derived cardiomyocytes survive and mature in the mouse heart and transiently improve function after myocardial infarction. *Stem Cell Res* 2007;**1**:9-24.
93. Shiba Y, Fernandes S, Zhu WZ, Filice D, Muskheli V, Kim J*, et al.* Human ES-cell-derived cardiomyocytes electrically couple and suppress arrhythmias in injured hearts. *Nature* 2012;**489**:322-325.
94. Chong JJ, Yang X, Don CW, Minami E, Liu YW, Weyers JJ*, et al.* Human embryonic-stem-cell-derived cardiomyocytes regenerate non-human primate hearts. *Nature* 2014;**510**:273-277.
95. Takahashi K, Yamanaka S. Induction of pluripotent stem cells from mouse embryonic and adult fibroblast cultures by defined factors. *Cell* 2006;**126**:663-676.
96. Takahashi K, Tanabe K, Ohnuki M, Narita M, Ichisaka T, Tomoda K*, et al.* Induction of pluripotent stem cells from adult human fibroblasts by defined factors. *Cell* 2007;**131**:861-872.
97. Nakagawa M, Koyanagi M, Tanabe K, Takahashi K, Ichisaka T, Aoi T*, et al.* Generation of induced pluripotent stem cells without Myc from mouse and human fibroblasts. *Nat Biotechnol* 2008;**26**:101-106.

98. Kim D, Kim CH, Moon JI, Chung YG, Chang MY, Han BS*, et al.* Generation of human induced pluripotent stem cells by direct delivery of reprogramming proteins. *Cell Stem Cell* 2009;**4**:472-476.
99. Yu J, Hu K, Smuga-Otto K, Tian S, Stewart R, Slukvin, II*, et al.* Human induced pluripotent stem cells free of vector and transgene sequences. *Science* 2009;**324**:797-801.
100. Warren L, Manos PD, Ahfeldt T, Loh YH, Li H, Lau F*, et al.* Highly efficient reprogramming to pluripotency and directed differentiation of human cells with synthetic modified mRNA. *Cell Stem Cell* 2010;**7**:618-630.
101. Narazaki G, Uosaki H, Teranishi M, Okita K, Kim B, Matsuoka S*, et al.* Directed and systematic differentiation of cardiovascular cells from mouse induced pluripotent stem cells. *Circulation* 2008;**118**:498-506.
102. Kuzmenkin A, Liang H, Xu G, Pfannkuche K, Eichhorn H, Fatima A*, et al.* Functional characterization of cardiomyocytes derived from murine induced pluripotent stem cells in vitro. *FASEB J* 2009;**23**:4168-4180.
103. Halbach M, Peinkofer G, Baumgartner S, Maass M, Wiedey M, Neef K*, et al.* Electrophysiological integration and action potential properties of transplanted cardiomyocytes derived from induced pluripotent stem cells. *Cardiovasc Res* 2013;**100**:432-440.
104. Swijnenburg RJ, Tanaka M, Vogel H, Baker J, Kofidis T, Gunawan F*, et al.* Embryonic stem cell immunogenicity increases upon differentiation after transplantation into ischemic myocardium. *Circulation* 2005;**112**:I166-172.
105. Nussbaum J, Minami E, Laflamme MA, Virag JA, Ware CB, Masino A*, et al.* Transplantation of undifferentiated murine embryonic stem cells in the heart: teratoma formation and immune response. *FASEB J* 2007;**21**:1345-1357.
106. Miki K, Uenaka H, Saito A, Miyagawa S, Sakaguchi T, Higuchi T*, et al.* Bioengineered myocardium derived from induced pluripotent stem cells improves cardiac function and attenuates cardiac remodeling following chronic myocardial infarction in rats. *Stem Cells Transl Med* 2012;**1**:430-437.
107. Kawamura M, Miyagawa S, Miki K, Saito A, Fukushima S, Higuchi T*, et al.* Feasibility, safety, and therapeutic efficacy of human induced pluripotent stem cell-derived cardiomyocyte sheets in a porcine ischemic cardiomyopathy model. *Circulation* 2012;**126**:S29-37.
108. Zhang D, Shadrin IY, Lam J, Xian HQ, Snodgrass HR, Bursac N. Tissue-engineered cardiac patch for advanced functional maturation of human ESC-derived cardiomyocytes. *Biomaterials* 2013;**34**:5813-5820.
109. Lu TY, Lin B, Kim J, Sullivan M, Tobita K, Salama G*, et al.* Repopulation of decellularized mouse heart with human induced pluripotent stem cell-derived cardiovascular progenitor cells. *Nat Commun* 2013;**4**:2307.
110. Wainwright JM, Czajka CA, Patel UB, Freytes DO, Tobita K, Gilbert TW*, et al.* Preparation of cardiac extracellular matrix from an intact porcine heart. *Tissue Eng Part C Methods* 2010;**16**:525-532.
111. Gaetani R, Doevendans PA, Metz CH, Alblas J, Messina E, Giacomello A*, et al.* Cardiac tissue engineering using tissue printing technology and human cardiac progenitor cells. *Biomaterials* 2012;**33**:1782-1790.

112. Ieda M, Fu JD, Delgado-Olguin P, Vedantham V, Hayashi Y, Bruneau BG*, et al.* Direct reprogramming of fibroblasts into functional cardiomyocytes by defined factors. *Cell* 2010;**142**:375-386.
113. Efe JA, Hilcove S, Kim J, Zhou H, Ouyang K, Wang G*, et al.* Conversion of mouse fibroblasts into cardiomyocytes using a direct reprogramming strategy. *Nat Cell Biol* 2011;**13**:215-222.
114. Protze S, Khattak S, Poulet C, Lindemann D, Tanaka EM, Ravens U. A new approach to transcription factor screening for reprogramming of fibroblasts to cardiomyocyte-like cells. *J Mol Cell Cardiol* 2012;**53**:323-332.
115. Jayawardena TM, Egemnazarov B, Finch EA, Zhang L, Payne JA, Pandya K*, et al.* MicroRNA-mediated in vitro and in vivo direct reprogramming of cardiac fibroblasts to cardiomyocytes. *Circ Res* 2012;**110**:1465-1473.
116. Nam YJ, Song K, Luo X, Daniel E, Lambeth K, West K*, et al.* Reprogramming of human fibroblasts toward a cardiac fate. *Proc Natl Acad Sci U S A* 2013;**110**:5588-5593.
117. Qian L, Huang Y, Spencer CI, Foley A, Vedantham V, Liu L*, et al.* In vivo reprogramming of murine cardiac fibroblasts into induced cardiomyocytes. *Nature* 2012;**485**:593-598.
118. Song K, Nam YJ, Luo X, Qi X, Tan W, Huang GN*, et al.* Heart repair by reprogramming non-myocytes with cardiac transcription factors. *Nature* 2012;**485**:599-604.
119. Hassink RJ, Pasumarthi KB, Nakajima H, Rubart M, Soonpaa MH, de la Riviere AB*, et al.* Cardiomyocyte cell cycle activation improves cardiac function after myocardial infarction. *Cardiovasc Res* 2008;**78**:18-25.
120. Bersell K, Arab S, Haring B, Kuhn B. Neuregulin1/ErbB4 signaling induces cardiomyocyte proliferation and repair of heart injury. *Cell* 2009;**138**:257-270.
121. Mahmoud AI, Kocabas F, Muralidhar SA, Kimura W, Koura AS, Thet S*, et al.* Meis1 regulates postnatal cardiomyocyte cell cycle arrest. *Nature* 2013;**497**:249-253.
122. Eulalio A, Mano M, Dal Ferro M, Zentilin L, Sinagra G, Zacchigna S*, et al.* Functional screening identifies miRNAs inducing cardiac regeneration. *Nature* 2012;**492**:376-381.
123. Oberpriller JO, Oberpriller JC. Response of the adult newt ventricle to injury. *J Exp Zool* 1974;**187**:249-253.
124. Poss KD, Wilson LG, Keating MT. Heart regeneration in zebrafish. *Science* 2002;**298**:2188-2190.
125. Gonzalez-Rosa JM, Martin V, Peralta M, Torres M, Mercader N. Extensive scar formation and regression during heart regeneration after cryoinjury in zebrafish. *Development* 2011;**138**:1663-1674.
126. Chablais F, Veit J, Rainer G, Jazwinska A. The zebrafish heart regenerates after cryoinjury-induced myocardial infarction. *BMC Dev Biol* 2011;**11**:21.
127. Jopling C, Sleep E, Raya M, Marti M, Raya A, Izpisua Belmonte JC. Zebrafish heart regeneration occurs by cardiomyocyte dedifferentiation and proliferation. *Nature* 2010;**464**:606-609.

128. Kikuchi K, Holdway JE, Werdich AA, Anderson RM, Fang Y, Egnaczyk GF*, et al.* Primary contribution to zebrafish heart regeneration by gata4(+) cardiomyocytes. *Nature* 2010;**464**:601-605.
129. Porrello ER, Mahmoud AI, Simpson E, Hill JA, Richardson JA, Olson EN*, et al.* Transient regenerative potential of the neonatal mouse heart. *Science* 2011;**331**:1078-1080.
130. Senyo SE, Steinhauser ML, Pizzimenti CL, Yang VK, Cai L, Wang M*, et al.* Mammalian heart renewal by pre-existing cardiomyocytes. *Nature* 2013;**493**:433-436.
131. Engel FB, Hsieh PC, Lee RT, Keating MT. FGF1/p38 MAP kinase inhibitor therapy induces cardiomyocyte mitosis, reduces scarring, and rescues function after myocardial infarction. *Proc Natl Acad Sci U S A* 2006;**103**:15546-15551.
132. Sdek P, Zhao P, Wang Y, Huang CJ, Ko CY, Butler PC*, et al.* Rb and p130 control cell cycle gene silencing to maintain the postmitotic phenotype in cardiac myocytes. *J Cell Biol* 2011;**194**:407-423.
133. Porrello ER, Mahmoud AI, Simpson E, Johnson BA, Grinsfelder D, Canseco D*, et al.* Regulation of neonatal and adult mammalian heart regeneration by the miR-15 family. *Proc Natl Acad Sci U S A* 2013;**110**:187-192.
134. Zhao L, Borikova AL, Ben-Yair R, Guner-Ataman B, MacRae CA, Lee RT*, et al.* Notch signaling regulates cardiomyocyte proliferation during zebrafish heart regeneration. *Proc Natl Acad Sci U S A* 2014;**111**:1403-1408.
135. Korf-Klingebiel M, Kempf T, Sauer T, Brinkmann E, Fischer P, Meyer GP*, et al.* Bone marrow cells are a rich source of growth factors and cytokines: implications for cell therapy trials after myocardial infarction. *Eur Heart J* 2008;**29**:2851-2858.
136. Burchfield JS, Iwasaki M, Koyanagi M, Urbich C, Rosenthal N, Zeiher AM*, et al.* Interleukin-10 from transplanted bone marrow mononuclear cells contributes to cardiac protection after myocardial infarction. *Circ Res* 2008;**103**:203-211.
137. Kinnaird T, Stabile E, Burnett MS, Shou M, Lee CW, Barr S*, et al.* Local delivery of marrow-derived stromal cells augments collateral perfusion through paracrine mechanisms. *Circulation* 2004;**109**:1543-1549.
138. Ohnishi S, Sumiyoshi H, Kitamura S, Nagaya N. Mesenchymal stem cells attenuate cardiac fibroblast proliferation and collagen synthesis through paracrine actions. *FEBS Lett* 2007;**581**:3961-3966.
139. Nagaya N, Fujii T, Iwase T, Ohgushi H, Itoh T, Uematsu M*, et al.* Intravenous administration of mesenchymal stem cells improves cardiac function in rats with acute myocardial infarction through angiogenesis and myogenesis. *Am J Physiol Heart Circ Physiol* 2004;**287**:H2670-2676.
140. Maxeiner H, Krehbiehl N, Muller A, Woitasky N, Akinturk H, Muller M*, et al.* New insights into paracrine mechanisms of human cardiac progenitor cells. *Eur J Heart Fail* 2010;**12**:730-737.
141. Stastna M, Chimenti I, Marban E, Van Eyk JE. Identification and functionality of proteomes secreted by rat cardiac stem cells and neonatal cardiomyocytes. *Proteomics* 2010;**10**:245-253.
142. Chimenti I, Smith RR, Li TS, Gerstenblith G, Messina E, Giacomello A*, et al.* Relative roles of direct regeneration versus paracrine effects of

human cardiosphere-derived cells transplanted into infarcted mice. *Circ Res* 2010;**106**:971-980.
143. Nakamura T, Mizuno S, Matsumoto K, Sawa Y, Matsuda H. Myocardial protection from ischemia/reperfusion injury by endogenous and exogenous HGF. *J Clin Invest* 2000;**106**:1511-1519.
144. Kawaguchi N, Smith AJ, Waring CD, Hasan MK, Miyamoto S, Matsuoka R*, et al.* c-kitpos GATA-4 high rat cardiac stem cells foster adult cardiomyocyte survival through IGF-1 paracrine signalling. *PLoS One* 2010;**5**:e14297.
145. Rota M, Padin-Iruegas ME, Misao Y, De Angelis A, Maestroni S, Ferreira-Martins J*, et al.* Local activation or implantation of cardiac progenitor cells rescues scarred infarcted myocardium improving cardiac function. *Circ Res* 2008;**103**:107-116.
146. Ellison GM, Torella D, Dellegrottaglie S, Perez-Martinez C, Perez de Prado A, Vicinanza C*, et al.* Endogenous cardiac stem cell activation by insulin-like growth factor-1/hepatocyte growth factor intracoronary injection fosters survival and regeneration of the infarcted pig heart. *J Am Coll Cardiol* 2011;**58**:977-986.
147. Rosenblatt-Velin N, Lepore MG, Cartoni C, Beermann F, Pedrazzini T. FGF-2 controls the differentiation of resident cardiac precursors into functional cardiomyocytes. *J Clin Invest* 2005;**115**:1724-1733.
148. Limana F, Germani A, Zacheo A, Kajstura J, Di Carlo A, Borsellino G*, et al.* Exogenous high-mobility group box 1 protein induces myocardial regeneration after infarction via enhanced cardiac C-kit+ cell proliferation and differentiation. *Circ Res* 2005;**97**:e73-83.
149. Kuhn B, del Monte F, Hajjar RJ, Chang YS, Lebeche D, Arab S*, et al.* Periostin induces proliferation of differentiated cardiomyocytes and promotes cardiac repair. *Nat Med* 2007;**13**:962-969.
150. Padin-Iruegas ME, Misao Y, Davis ME, Segers VF, Esposito G, Tokunou T*, et al.* Cardiac progenitor cells and biotinylated insulin-like growth factor-1 nanofibers improve endogenous and exogenous myocardial regeneration after infarction. *Circulation* 2009;**120**:876-887.
151. Palumbo R, Bianchi ME. High mobility group box 1 protein, a cue for stem cell recruitment. *Biochem Pharmacol* 2004;**68**:1165-1170.
152. Low TL, Hu SK, Goldstein AL. Complete amino acid sequence of bovine thymosin beta 4: a thymic hormone that induces terminal deoxynucleotidyl transferase activity in thymocyte populations. *Proc Natl Acad Sci U S A* 1981;**78**:1162-1166.
153. Goldstein AL, Slater FD, White A. Preparation, assay, and partial purification of a thymic lymphocytopoietic factor (thymosin). *Proc Natl Acad Sci U S A* 1966;**56**:1010-1017.
154. Hooper JA, McDaniel MC, Thurman GB, Cohen GH, Schulof RS, Goldstein AL. Purification and properties of bovine thymosin. *Ann N Y Acad Sci* 1975;**249**:125-144.
155. Erickson-Viitanen S, Ruggieri S, Natalini P, Horecker BL. Thymosin beta 10, a new analog of thymosin beta 4 in mammalian tissues. *Arch Biochem Biophys* 1983;**225**:407-413.
156. Banyard J, Hutchinson LM, Zetter BR. Thymosin beta-NB is the human isoform of rat thymosin beta15. *Ann N Y Acad Sci* 2007;**1112**:286-296.

157. Gomez-Marquez J, Dosil M, Segade F, Bustelo XR, Pichel JG, Dominguez F*, et al.* Thymosin-beta 4 gene. Preliminary characterization and expression in tissues, thymic cells, and lymphocytes. *J Immunol* 1989;**143**:2740-2744.
158. Hannappel E, Xu GJ, Morgan J, Hempstead J, Horecker BL. Thymosin beta 4: a ubiquitous peptide in rat and mouse tissues. *Proc Natl Acad Sci U S A* 1982;**79**:2172-2175.
159. Hannappel E, van Kampen M. Determination of thymosin beta 4 in human blood cells and serum. *J Chromatogr* 1987;**397**:279-285.
160. Safer D, Golla R, Nachmias VT. Isolation of a 5-kilodalton actin-sequestering peptide from human blood platelets. *Proc Natl Acad Sci U S A* 1990;**87**:2536-2540.
161. Safer D, Elzinga M, Nachmias VT. Thymosin beta 4 and Fx, an actin-sequestering peptide, are indistinguishable. *J Biol Chem* 1991;**266**:4029-4032.
162. Cassimeris L, Safer D, Nachmias VT, Zigmond SH. Thymosin beta 4 sequesters the majority of G-actin in resting human polymorphonuclear leukocytes. *J Cell Biol* 1992;**119**:1261-1270.
163. Weber A, Nachmias VT, Pennise CR, Pring M, Safer D. Interaction of thymosin beta 4 with muscle and platelet actin: implications for actin sequestration in resting platelets. *Biochemistry* 1992;**31**:6179-6185.
164. Van Troys M, Dewitte D, Goethals M, Carlier M, Vandekerckhove J, Ampe C. The actin binding site of thymosin beta 4 mapped by mutational analysis. *The EMBO journal* 1996;**15**:201-210.
165. Safer D, Sosnick T, Elzinga M. Thymosin beta 4 binds actin in an extended conformation and contacts both the barbed and pointed ends. *Biochemistry* 1997;**36**:5806-5816.
166. Domanski M, Hertzog M, Coutant J, Gutsche-Perelroizen I, Bontems F, Carlier M-F*, et al.* Coupling of folding and binding of thymosin beta4 upon interaction with monomeric actin monitored by nuclear magnetic resonance. *J Biol Chem* 2004;**279**:23637-23645.
167. Carlier M, Jean C, Rieger K, Lenfant M, Pantaloni D. Modulation of the interaction between G-actin and thymosin beta 4 by the ATP/ADP ratio: possible implication in the regulation of actin dynamics. *Proc Natl Acad Sci U S A* 1993;**90**:5034-5038.
168. Goldschmidt-Clermont P, Furman M, Wachsstock D, Safer D, Nachmias V, Pollard T. The control of actin nucleotide exchange by thymosin beta 4 and profilin. A potential regulatory mechanism for actin polymerization in cells. *Molecular biology of the cell* 1992;**3**:1015-1024.
169. Sanders MC, Goldstein AL, Wang YL. Thymosin beta 4 (Fx peptide) is a potent regulator of actin polymerization in living cells. *Proc Natl Acad Sci U S A* 1992;**89**:4678-4682.
170. Bock-Marquette I, Saxena A, White MD, Dimaio JM, Srivastava D. Thymosin beta4 activates integrin-linked kinase and promotes cardiac cell migration, survival and cardiac repair. *Nature* 2004;**432**:466-472.
171. Zhao Y, Qiu F, Xu S, Yu L, Fu G. Thymosin beta4 activates integrin-linked kinase and decreases endothelial progenitor cells apoptosis under serum deprivation. *J Cell Physiol* 2011;**226**:2798-2806.
172. Sopko N, Qin Y, Finan A, Dadabayev A, Chigurupati S, Qin J*, et al.* Significance of thymosin beta4 and implication of PINCH-1-ILK-alpha-

parvin (PIP) complex in human dilated cardiomyopathy. *PLoS One* 2011;**6**:e20184.
173. Tang MC, Chan LC, Yeh YC, Chen CY, Chou TY, Wang WS*, et al.* Thymosin beta 4 induces colon cancer cell migration and clinical metastasis via enhancing ILK/IQGAP1/Rac1 signal transduction pathway. *Cancer Lett* 2011;**308**:162-171.
174. Dobreva I, Fielding A, Foster LJ, Dedhar S. Mapping the integrin-linked kinase interactome using SILAC. *J Proteome Res* 2008;**7**:1740-1749.
175. Qiu FY, Song XX, Zheng H, Zhao YB, Fu GS. Thymosin beta4 induces endothelial progenitor cell migration via PI3K/Akt/eNOS signal transduction pathway. *J Cardiovasc Pharmacol* 2009;**53**:209-214.
176. Li J, Yu L, Zhao Y, Fu G, Zhou B. Thymosin beta4 reduces senescence of endothelial progenitor cells via the PI3K/Akt/eNOS signal transduction pathway. *Mol Med Rep* 2013;**7**:598-602.
177. Bednarek R, Boncela J, Smolarczyk K, Cierniewska-Cieslak A, Wyroba E, Cierniewski C. Ku80 as a novel receptor for thymosin beta4 that mediates its intracellular activity different from G-actin sequestering. *J Biol Chem* 2008;**283**:1534-1544.
178. Al-Nedawi KN, Czyz M, Bednarek R, Szemraj J, Swiatkowska M, Cierniewska-Cieslak A*, et al.* Thymosin beta 4 induces the synthesis of plasminogen activator inhibitor 1 in cultured endothelial cells and increases its extracellular expression. *Blood* 2004;**103**:1319-1324.
179. Santra M, Chopp M, Zhang ZG, Lu M, Santra S, Nalani A*, et al.* Thymosin beta 4 mediates oligodendrocyte differentiation by upregulating p38 MAPK. *Glia* 2012;**60**:1826-1838.
180. Oh SY, Song JH, Gil JE, Kim JH, Yeom YI, Moon EY. ERK activation by thymosin-beta-4 (TB4) overexpression induces paclitaxel-resistance. *Exp Cell Res* 2006;**312**:1651-1657.
181. Oh JM, Ryoo IJ, Yang Y, Kim HS, Yang KH, Moon EY. Hypoxia-inducible transcription factor (HIF)-1 alpha stabilization by actin-sequestering protein, thymosin beta-4 (TB4) in Hela cervical tumor cells. *Cancer Lett* 2008;**264**:29-35.
182. Ryu YK, Lee YS, Lee GH, Song KS, Kim YS, Moon EY. Regulation of glycogen synthase kinase-3 by thymosin beta-4 is associated with gastric cancer cell migration. *Int J Cancer* 2012;**131**:2067-2077.
183. Lv S, Cheng G, Zhou Y, Xu G. Thymosin beta4 induces angiogenesis through Notch signaling in endothelial cells. *Mol Cell Biochem* 2013;**381**:283-290.
184. Grant D, Rose W, Yaen C, Goldstein A, Martinez J, Kleinman H. Thymosin beta4 enhances endothelial cell differentiation and angiogenesis. *Angiogenesis* 1999;**3**:125-135.
185. Huff T, Rosorius O, Otto AM, Muller CS, Ballweber E, Hannappel E*, et al.* Nuclear localisation of the G-actin sequestering peptide thymosin beta4. *J Cell Sci* 2004;**117**:5333-5341.
186. Zoubek RE, Hannappel E. Subcellular distribution of thymosin beta4. *Ann N Y Acad Sci* 2007;**1112**:442-450.
187. Brieger A, Plotz G, Zeuzem S, Trojan J. Thymosin beta 4 expression and nuclear transport are regulated by hMLH1. *Biochem Biophys Res Commun* 2007;**364**:731-736.

188. McDonald D, Carrero G, Andrin C, de Vries G, Hendzel MJ. Nucleoplasmic beta-actin exists in a dynamic equilibrium between low-mobility polymeric species and rapidly diffusing populations. *J Cell Biol* 2006;**172**:541-552.
189. Weller FE, Mutchnick MG, Goldstein AL, Naylor PH. Enzyme immunoassay measurement of thymosin beta 4 in human serum. *J Biol Response Mod* 1988;**7**:91-96.
190. Frohm M, Gunne H, Bergman AC, Agerberth B, Bergman T, Boman A*, et al.* Biochemical and antibacterial analysis of human wound and blister fluid. *Eur J Biochem* 1996;**237**:86-92.
191. Huang WQ, Wang QR. Bone marrow endothelial cells secrete thymosin beta4 and AcSDKP. *Exp Hematol* 2001;**29**:12-18.
192. Gondo H, Kudo J, White JW, Barr C, Selvanayagam P, Saunders GF. Differential expression of the human thymosin-beta 4 gene in lymphocytes, macrophages, and granulocytes. *J Immunol* 1987;**139**:3840-3848.
193. Kinseth MA, Anjard C, Fuller D, Guizzunti G, Loomis WF, Malhotra V. The Golgi-associated protein GRASP is required for unconventional protein secretion during development. *Cell* 2007;**130**:524-534.
194. Freeman KW, Bowman BR, Zetter BR. Regenerative protein thymosin beta-4 is a novel regulator of purinergic signaling. *FASEB J* 2011;**25**:907-915.
195. Heintz D, Reichert A, Mihelic-Rapp M, Stoeva S, Voelter W, Faulstich H. The sulfoxide of thymosin beta 4 almost lacks the polymerization-inhibiting capacity for actin. *Eur J Biochem* 1994;**223**:345-350.
196. Young JD, Lawrence AJ, MacLean AG, Leung BP, McInnes IB, Canas B*, et al.* Thymosin beta 4 sulfoxide is an anti-inflammatory agent generated by monocytes in the presence of glucocorticoids. *Nat Med* 1999;**5**:1424-1427.
197. Grillon C, Rieger K, Bakala J, Schott D, Morgat JL, Hannappel E*, et al.* Involvement of thymosin beta 4 and endoproteinase Asp-N in the biosynthesis of the tetrapeptide AcSerAspLysPro a regulator of the hematopoietic system. *FEBS Lett* 1990;**274**:30-34.
198. Cavasin MA, Rhaleb NE, Yang XP, Carretero OA. Prolyl oligopeptidase is involved in release of the antifibrotic peptide Ac-SDKP. *Hypertension* 2004;**43**:1140-1145.
199. Myohanen TT, Tenorio-Laranga J, Jokinen B, Vazquez-Sanchez R, Moreno-Baylach MJ, Garcia-Horsman JA*, et al.* Prolyl oligopeptidase induces angiogenesis both in vitro and in vivo in a novel regulatory manner. *Br J Pharmacol* 2011;**163**:1666-1678.
200. Grant D, Kinsella J, Kibbey M, LaFlamme S, Burbelo P, Goldstein A*, et al.* Matrigel induces thymosin beta 4 gene in differentiating endothelial cells. *J Cell Sci* 1995;**108 (Pt 12)**:3685-3694.
201. Malinda KM, Goldstein AL, Kleinman HK. Thymosin beta 4 stimulates directional migration of human umbilical vein endothelial cells. *FASEB J* 1997;**11**:474-481.
202. Malinda KM, Sidhu GS, Mani H, Banaudha K, Maheshwari RK, Goldstein AL*, et al.* Thymosin beta4 accelerates wound healing. *J Invest Dermatol* 1999;**113**:364-368.

203. Sosne G, Chan CC, Thai K, Kennedy M, Szliter EA, Hazlett LD*, et al.* Thymosin beta 4 promotes corneal wound healing and modulates inflammatory mediators in vivo. *Exp Eye Res* 2001;**72**:605-608.
204. Kobayashi T, Okada F, Fujii N, Tomita N, Ito S, Tazawa H*, et al.* Thymosin-beta4 regulates motility and metastasis of malignant mouse fibrosarcoma cells. *Am J Pathol* 2002;**160**:869-882.
205. Fan Y, Gong Y, Ghosh P, Graham L, Fox P. Spatial coordination of actin polymerization and ILK-Akt2 activity during endothelial cell migration. *Developmental cell* 2009;**16**:661-674.
206. Cierniewski CS, Papiewska-Pajak I, Malinowski M, Sacewicz-Hofman I, Wiktorska M, Kryczka J*, et al.* Thymosin beta4 regulates migration of colon cancer cells by a pathway involving interaction with Ku80. *Ann N Y Acad Sci* 2010;**1194**:60-71.
207. Qiu P, Kurpakus-Wheater M, Sosne G. Matrix metalloproteinase activity is necessary for thymosin beta 4 promotion of epithelial cell migration. *J Cell Physiol* 2007;**212**:165-173.
208. Philp D, Huff T, Gho YS, Hannappel E, Kleinman HK. The actin binding site on thymosin beta4 promotes angiogenesis. *FASEB J* 2003;**17**:2103-2105.
209. Cha HJ, Jeong MJ, Kleinman HK. Role of thymosin beta4 in tumor metastasis and angiogenesis. *J Natl Cancer Inst* 2003;**95**:1674-1680.
210. Sosne G, Szliter E, Barrett R, Kernacki K, Kleinman H, Hazlett L. Thymosin beta 4 promotes corneal wound healing and decreases inflammation in vivo following alkali injury. *Exp Eye Res* 2002;**74**:293-299.
211. Badamchian M, Damavandy AA, Damavandy H, Wadhwa SD, Katz B, Goldstein AL. Identification and quantification of thymosin beta4 in human saliva and tears. *Ann N Y Acad Sci* 2007;**1112**:458-465.
212. Tang YQ, Yeaman MR, Selsted ME. Antimicrobial peptides from human platelets. *Infect Immun* 2002;**70**:6524-6533.
213. Sosne G, Christopherson P, Barrett R, Fridman R. Thymosin-beta4 modulates corneal matrix metalloproteinase levels and polymorphonuclear cell infiltration after alkali injury. *Invest Ophthalmol Vis Sci* 2005;**46**:2388-2395.
214. Sosne G, Qiu P, Christopherson PL, Wheater MK. Thymosin beta 4 suppression of corneal NFkappaB: a potential anti-inflammatory pathway. *Exp Eye Res* 2007;**84**:663-669.
215. Qiu P, Wheater MK, Qiu Y, Sosne G. Thymosin beta4 inhibits TNF-alpha-induced NF-kappaB activation, IL-8 expression, and the sensitizing effects by its partners PINCH-1 and ILK. *FASEB J* 2011;**25**:1815-1826.
216. Badamchian M, O. Fagarasan M, L. Danner R, F. Suffredini A, Damavandy H, Goldstein AL. Thymosin β4 reduces lethality and down-regulates inflammatory mediators in endotoxin-induced septic shock. *Int Immunopharmacol* 2003;**3**(8):1225-33.
217. Peng H, Carretero OA, Raij L, Yang F, Kapke A, Rhaleb NE. Antifibrotic effects of N-acetyl-seryl-aspartyl-Lysyl-proline on the heart and kidney in aldosterone-salt hypertensive rats. *Hypertension* 2001;**37**:794-800.
218. Shibuya K, Kanasaki K, Isono M, Sato H, Omata M, Sugimoto T*, et al.* N-acetyl-seryl-aspartyl-lysyl-proline prevents renal insufficiency and

mesangial matrix expansion in diabetic db/db mice. *Diabetes* 2005;**54**:838-845.
219. Cavasin MA, Liao TD, Yang XP, Yang JJ, Carretero OA. Decreased endogenous levels of Ac-SDKP promote organ fibrosis. *Hypertension* 2007;**50**:130-136.
220. Ehrlich HP, Hazard SW, 3rd. Thymosin beta4 enhances repair by organizing connective tissue and preventing the appearance of myofibroblasts. *Ann N Y Acad Sci* 2010;**1194**:118-124.
221. Barnaeva E, Nadezhda A, Hannappel E, Sjogren MH, Rojkind M. Thymosin beta4 upregulates the expression of hepatocyte growth factor and downregulates the expression of PDGF-beta receptor in human hepatic stellate cells. *Ann N Y Acad Sci* 2007;**1112**:154-160.
222. Reyes-Gordillo K, Shah R, Arellanes-Robledo J, Rojkind M, Lakshman MR. Protective effects of thymosin beta4 on carbon tetrachloride-induced acute hepatotoxicity in rats. *Ann N Y Acad Sci* 2012;**1269**:61-68.
223. Zuo Y, Chun B, Potthoff SA, Kazi N, Brolin TJ, Orhan D*, et al.* Thymosin beta4 and its degradation product, Ac-SDKP, are novel reparative factors in renal fibrosis. *Kidney Int* 2013;**84**:1166-1175.
224. Conte E, Genovese T, Gili E, Esposito E, Iemmolo M, Fruciano M*, et al.* Protective effects of thymosin beta4 in a mouse model of lung fibrosis. *Ann N Y Acad Sci* 2012;**1269**:69-73.
225. Conte E, Genovese T, Gili E, Esposito E, Iemmolo M, Fruciano M*, et al.* Thymosin beta4 protects C57BL/6 mice from bleomycin-induced damage in the lung. *Eur J Clin Invest* 2013;**43**:309-315.
226. Sosne G, Siddiqi A, Kurpakus-Wheater M. Thymosin-beta4 inhibits corneal epithelial cell apoptosis after ethanol exposure in vitro. *Invest Ophthalmol Vis Sci* 2004;**45**:1095-1100.
227. Sosne G, Albeiruti AR, Hollis B, Siddiqi A, Ellenberg D, Kurpakus-Wheater M. Thymosin beta4 inhibits benzalkonium chloride-mediated apoptosis in corneal and conjunctival epithelial cells in vitro. *Exp Eye Res* 2006;**83**:502-507.
228. Ho J, Chuang C-H, Ho C-Y, Shih Y-RV, Lee O, Su Y. Internalization is essential for the antiapoptotic effects of exogenous thymosin beta-4 on human corneal epithelial cells. *Invest Ophthalmol Vis Sci* 2007;**48**:27-33.
229. Yang H, Cui GB, Jiao XY, Wang J, Ju G, You SW. Thymosin-beta4 attenuates ethanol-induced neurotoxicity in cultured cerebral cortical astrocytes by inhibiting apoptosis. *Cell Mol Neurobiol* 2010;**30**:149-160.
230. Choi SY, Kim DK, Eun B, Kim K, Sun W, Kim H. Anti-apoptotic function of thymosin-beta in developing chick spinal motoneurons. *Biochem Biophys Res Commun* 2006;**346**:872-878.
231. Tapp H, Deepe R, Ingram JA, Yarmola EG, Bubb MR, Hanley EN, Jr.*, et al.* Exogenous thymosin beta4 prevents apoptosis in human intervertebral annulus cells in vitro. *Biotech Histochem* 2009;**84**:287-294.
232. Reti R, Kwon E, Qiu P, Wheater M, Sosne G. Thymosin beta4 is cytoprotective in human gingival fibroblasts. *Eur J Oral Sci* 2008;**116**:424-430.
233. Hsiao HL, Wang WS, Chen PM, Su Y. Overexpression of thymosin beta-4 renders SW480 colon carcinoma cells more resistant to apoptosis triggered by FasL and two topoisomerase II inhibitors via downregulating

Fas and upregulating Survivin expression, respectively. *Carcinogenesis* 2006;**27**:936-944.
234. Philp D, St-Surin S, Cha HJ, Moon HS, Kleinman HK, Elkin M. Thymosin beta 4 induces hair growth via stem cell migration and differentiation. *Ann N Y Acad Sci* 2007;**1112**:95-103.
235. Shelton EL, Poole SD, Reese J, Bader DM. Omental grafting: a cell-based therapy for blood vessel repair. *J Tissue Eng Regen Med* 2013;**7**:421-433.
236. Lee SI, Kim DS, Lee HJ, Cha HJ, Kim EC. The role of thymosin beta 4 on odontogenic differentiation in human dental pulp cells. *PLoS One* 2013;**8**:e61960.
237. Jeon BJ, Yang Y, Kyung Shim S, Yang HM, Cho D, Ik Bang S. Thymosin beta-4 promotes mesenchymal stem cell proliferation via an interleukin-8-dependent mechanism. *Exp Cell Res* 2013;**319**:2526-2534.
238. Clark EA, Golub TR, Lander ES, Hynes RO. Genomic analysis of metastasis reveals an essential role for RhoC. *Nature* 2000;**406**:532-535.
239. Wang WS, Chen PM, Hsiao HL, Wang HS, Liang WY, Su Y. Overexpression of the thymosin beta-4 gene is associated with increased invasion of SW480 colon carcinoma cells and the distant metastasis of human colorectal carcinoma. *Oncogene* 2004;**23**:6666-6671.
240. Huang CM, Ananthaswamy HN, Barnes S, Ma Y, Kawai M, Elmets CA. Mass spectrometric proteomics profiles of in vivo tumor secretomes: capillary ultrafiltration sampling of regressive tumor masses. *Proteomics* 2006;**6**:6107-6116.
241. Kang YJ, Jo JO, Ock MS, Chang HK, Lee SH, Ahn BK*, et al.* Thymosin beta4 was upregulated in recurred colorectal cancers. *J Clin Pathol* 2014;**67**:188-190.
242. Ruff D, Crockford D, Girardi G, Zhang Y. A randomized, placebo-controlled, single and multiple dose study of intravenous thymosin beta4 in healthy volunteers. *Ann N Y Acad Sci* 2010;**1194**:223-229.
243. Wang WS, Chen PM, Hsiao HL, Ju SY, Su Y. Overexpression of the thymosin beta-4 gene is associated with malignant progression of SW480 colon cancer cells. *Oncogene* 2003;**22**:3297-3306.
244. Huang HC, Hu CH, Tang MC, Wang WS, Chen PM, Su Y. Thymosin beta4 triggers an epithelial-mesenchymal transition in colorectal carcinoma by upregulating integrin-linked kinase. *Oncogene* 2007;**26**:2781-2790.
245. Wang ZY, Zeng FQ, Zhu ZH, Jiang GS, Lv L, Wan F*, et al.* Evaluation of thymosin beta4 in the regulation of epithelial-mesenchymal transformation in urothelial carcinoma. *Urol Oncol* 2012;**30**:167-176.
246. Caers J, Hose D, Kuipers I, Bos TJ, Van Valckenborgh E, Menu E*, et al.* Thymosin beta4 has tumor suppressive effects and its decreased expression results in poor prognosis and decreased survival in multiple myeloma. *Haematologica* 2010;**95**:163-167.
247. Tokura Y, Nakayama Y, Fukada S, Nara N, Yamamoto H, Matsuda R*, et al.* Muscle injury-induced thymosin beta4 acts as a chemoattractant for myoblasts. *J Biochem* 2011;**149**:43-48.
248. Xu B, Yang M, Li Z, Zhang Y, Jiang Z, Guan S*, et al.* Thymosin beta4 enhances the healing of medial collateral ligament injury in rat. *Regul Pept* 2013;**184**:1-5.

249. Matsuo K, Akasaki Y, Adachi K, Zhang M, Ishikawa A, Jimi E*, et al.* Promoting effects of thymosin beta4 on granulation tissue and new bone formation after tooth extraction in rats. *Oral Surg Oral Med Oral Pathol Oral Radiol* 2012;**114**:17-26.
250. Adachi K, Matsuo K, Akasaki Y, Kanao M, Maeda T, Ishikawa A*, et al.* Effects of thymosin beta4 on the bone formation of calvarial defects in rats. *J Prosthodont Res* 2013;**57**:162-168.
251. Guarnera G, DeRosa A, Camerini R. The effect of thymosin treatment of venous ulcers. *Ann N Y Acad Sci* 2010;**1194**:207-212.
252. Treadwell T, Kleinman HK, Crockford D, Hardy MA, Guarnera GT, Goldstein AL. The regenerative peptide thymosin beta4 accelerates the rate of dermal healing in preclinical animal models and in patients. *Ann N Y Acad Sci* 2012;**1270**:37-44.
253. Popoli P, Pepponi R, Martire A, Armida M, Pezzola A, Galluzzo M*, et al.* Neuroprotective effects of thymosin beta4 in experimental models of excitotoxicity. *Ann N Y Acad Sci* 2007;**1112**:219-224.
254. Zhang J, Zhang ZG, Morris D, Li Y, Roberts C, Elias SB*, et al.* Neurological functional recovery after thymosin beta4 treatment in mice with experimental auto encephalomyelitis. *Neuroscience* 2009;**164**:1887-1893.
255. Xiong Y, Zhang Y, Mahmood A, Meng Y, Zhang ZG, Morris DC*, et al.* Neuroprotective and neurorestorative effects of thymosin beta4 treatment initiated 6 hours after traumatic brain injury in rats. *J Neurosurg* 2012;**116**:1081-1092.
256. Xiong Y, Mahmood A, Meng Y, Zhang Y, Zhang ZG, Morris DC*, et al.* Neuroprotective and neurorestorative effects of thymosin beta4 treatment following experimental traumatic brain injury. *Ann N Y Acad Sci* 2012;**1270**:51-58.
257. Morris DC, Chopp M, Zhang L, Lu M, Zhang ZG. Thymosin beta4 improves functional neurological outcome in a rat model of embolic stroke. *Neuroscience* 2010;**169**:674-682.
258. Smart N, Risebro CA, Melville AA, Moses K, Schwartz RJ, Chien KR*, et al.* Thymosin beta4 induces adult epicardial progenitor mobilization and neovascularization. *Nature* 2007;**445**:177-182.
259. Banerjee I, Zhang J, Moore-Morris T, Lange S, Shen T, Dalton ND*, et al.* Thymosin beta 4 is dispensable for murine cardiac development and function. *Circ Res* 2012;**110**:456-464.
260. Smart N, Risebro CA, Clark JE, Ehler E, Miquerol L, Rossdeutsch A*, et al.* Thymosin beta4 facilitates epicardial neovascularization of the injured adult heart. *Ann N Y Acad Sci* 2010;**1194**:97-104.
261. Shrivastava S, Srivastava D, Olson EN, DiMaio JM, Bock-Marquette I. Thymosin beta4 and cardiac repair. *Ann N Y Acad Sci* 2010;**1194**:87-96.
262. Cai C-L, Martin J, Sun Y, Cui L, Wang L, Ouyang K*, et al.* A myocardial lineage derives from Tbx18 epicardial cells. *Nature* 2008;**454**:104-108.
263. Zhou B, Ma Q, Rajagopal S, Wu S, Domian I, Rivera-Feliciano J*, et al.* Epicardial progenitors contribute to the cardiomyocyte lineage in the developing heart. *Nature* 2008;**454**:109-113.
264. Smart N, Bollini S, Dube KN, Vieira JM, Zhou B, Davidson S*, et al.* De novo cardiomyocytes from within the activated adult heart after injury. *Nature* 2011;**474**:640-644.

265. Zhou B, Honor LB, Ma Q, Oh JH, Lin RZ, Melero-Martin JM*, et al.* Thymosin beta 4 treatment after myocardial infarction does not reprogram epicardial cells into cardiomyocytes. *J Mol Cell Cardiol* 2012;**52**:43-47.
266. Yang F, Yang XP, Liu YH, Xu J, Cingolani O, Rhaleb NE*, et al.* Ac-SDKP reverses inflammation and fibrosis in rats with heart failure after myocardial infarction. *Hypertension* 2004;**43**:229-236.
267. Kumar S, Gupta S. Thymosin beta 4 prevents oxidative stress by targeting antioxidant and anti-apoptotic genes in cardiac fibroblasts. *PLoS One* 2011;**6**:e26912.
268. Wei C, Kumar S, Kim IK, Gupta S. Thymosin beta 4 protects cardiomyocytes from oxidative stress by targeting anti-oxidative enzymes and anti-apoptotic genes. *PLoS One* 2012;**7**:e42586.
269. Srivastava D, Saxena A, Michael Dimaio J, Bock-Marquette I. Thymosin beta4 is cardioprotective after myocardial infarction. *Ann N Y Acad Sci* 2007;**1112**:161-170.
270. Kawamoto A, Gwon H, Iwaguro H, Yamaguchi J, Uchida S, Masuda H*, et al.* Therapeutic potential of ex vivo expanded endothelial progenitor cells for myocardial ischemia. *Circulation* 2001;**103**:634-637.
271. Kupatt C, Hinkel R, Lamparter M, von Brühl M-L, Pohl T, Horstkotte J*, et al.* Retroinfusion of embryonic endothelial progenitor cells attenuates ischemia-reperfusion injury in pigs: role of phosphatidylinositol 3-kinase/AKT kinase. *Circulation* 2005;**112**:22.
272. Kupatt C, Horstkotte J, Vlastos G, Pfosser A, Lebherz C, Semisch M*, et al.* Embryonic endothelial progenitor cells expressing a broad range of proangiogenic and remodeling factors enhance vascularization and tissue recovery in acute and chronic ischemia. *FASEB J* 2005;**19**:1576-1578.
273. Hinkel R, El-Aouni C, Olson T, Horstkotte J, Mayer S, Müller S*, et al.* Thymosin beta4 is an essential paracrine factor of embryonic endothelial progenitor cell-mediated cardioprotection. *Circulation* 2008;**117**:2232-2240.
274. Hinkel R, Bock-Marquette I, Hatzopoulos A, Hazopoulos A, Kupatt C. Thymosin beta4: a key factor for protective effects of eEPCs in acute and chronic ischemia. *Ann NY Acad Sci* 2010;**1194**:105-111.
275. Chang ZT, Hong L, Wang H, Lai HL, Li LF, Yin QL. Application of peripheral-blood-derived endothelial progenitor cell for treating ischemia-reperfusion injury and infarction: a preclinical study in rat models. *J Cardiothorac Surg* 2013;**8**:33.
276. Leonard DG, Ziff EB, Greene LA. Identification and characterization of mRNAs regulated by nerve growth factor in PC12 cells. *Mol Cell Biol* 1987;**7**:3156-3167.
277. Oh IS, So SS, Jahng KY, Kim HG. Hepatocyte growth factor upregulates thymosin beta4 in human umbilical vein endothelial cells. *Biochem Biophys Res Commun* 2002;**296**:401-405.
278. Yoshioka S, Takahashi Y, Okimura Y, Takahashi K, Iguchi G, Iida K*, et al.* Gene expression profile in the heart of spontaneous dwarf rat: in vivo effects of growth hormone. *Biochem Biophys Res Commun* 2006;**341**:88-93.

279. Lee HR, Yoon SY, Song SB, Park Y, Kim TS, Kim S*, et al.* Interleukin-18-mediated interferon-gamma secretion is regulated by thymosin beta 4 in human NK cells. *Immunobiology* 2011;**216**:1155-1162.
280. Atkinson MJ, Freeman MW, Kronenberg HM. Thymosin beta 4 is expressed in ROS 17/2.8 osteosarcoma cells in a regulated manner. *Mol Endocrinol* 1990;**4**:69-74.
281. Jain AK, Moore SM, Yamaguchi K, Eling TE, Baek SJ. Selective nonsteroidal anti-inflammatory drugs induce thymosin beta-4 and alter actin cytoskeletal organization in human colorectal cancer cells. *J Pharmacol Exp Ther* 2004;**311**:885-891.
282. Otto AM, Muller CS, Huff T, Hannappel E. Chemotherapeutic drugs change actin skeleton organization and the expression of beta-thymosins in human breast cancer cells. *J Cancer Res Clin Oncol* 2002;**128**:247-256.
283. Iguchi K, Usami Y, Hirano K, Hamatake M, Shibata M, Ishida R. Decreased thymosin beta4 in apoptosis induced by a variety of antitumor drugs. *Biochem Pharmacol* 1999;**57**:1105-1111.
284. Hannappel E. Thymosin beta4 and its posttranslational modifications. *Ann N Y Acad Sci* 2010;**1194**:27-35.
285. Iguchi K, Ito M, Usui S, Mizokami A, Namiki M, Hirano K. Downregulation of thymosin beta4 expression by androgen in prostate cancer LNCaP cells. *J Androl* 2008;**29**:207-212.
286. Schneikert J, Peterziel H, Defossez PA, Klocker H, de Launoit Y, Cato AC. Androgen receptor-Ets protein interaction is a novel mechanism for steroid hormone-mediated down-modulation of matrix metalloproteinase expression. *J Biol Chem* 1996;**271**:23907-23913.
287. Palvimo JJ, Reinikainen P, Ikonen T, Kallio PJ, Moilanen A, Janne OA. Mutual transcriptional interference between RelA and androgen receptor. *J Biol Chem* 1996;**271**:24151-24156.
288. Kim A, Son M, Kim KI, Yang Y, Song EY, Lee HG*, et al.* Elevation of intracellular cyclic AMP inhibits NF-kappaB-mediated thymosin beta4 expression in melanoma cells. *Exp Cell Res* 2009;**315**:3325-3335.
289. Smart N, Dube KN, Riley PR. Identification of Thymosin beta4 as an effector of Hand1-mediated vascular development. *Nat Commun* 2010;**1**:46.
290. Zhou Y, Li S, Huang Q, Xie L, Zhu X. Nanog suppresses cell migration by downregulating thymosin beta4 and Rnd3. *J Mol Cell Biol* 2013;**5**:239-249.
291. Gingras AC, Raught B, Sonenberg N. eIF4 initiation factors: effectors of mRNA recruitment to ribosomes and regulators of translation. *Annu Rev Biochem* 1999;**68**:913-963.
292. Muckenthaler M, Gray NK, Hentze MW. IRP-1 binding to ferritin mRNA prevents the recruitment of the small ribosomal subunit by the cap-binding complex eIF4F. *Mol Cell* 1998;**2**:383-388.
293. Paraskeva E, Gray NK, Schlager B, Wehr K, Hentze MW. Ribosomal pausing and scanning arrest as mechanisms of translational regulation from cap-distal iron-responsive elements. *Mol Cell Biol* 1999;**19**:807-816.
294. Stebbins-Boaz B, Cao Q, de Moor CH, Mendez R, Richter JD. Maskin is a CPEB-associated factor that transiently interacts with eIF-4E. *Mol Cell* 1999;**4**:1017-1027.

295. Groppo R, Richter JD. CPEB control of NF-kappaB nuclear localization and interleukin-6 production mediates cellular senescence. *Mol Cell Biol* 2011;**31**:2707-2714.
296. Nelson MR, Leidal AM, Smibert CA. Drosophila Cup is an eIF4E-binding protein that functions in Smaug-mediated translational repression. *EMBO J* 2004;**23**:150-159.
297. Baez MV, Boccaccio GL. Mammalian Smaug is a translational repressor that forms cytoplasmic foci similar to stress granules. *J Biol Chem* 2005;**280**:43131-43140.
298. Cao Q, Richter JD. Dissolution of the maskin-eIF4E complex by cytoplasmic polyadenylation and poly(A)-binding protein controls cyclin B1 mRNA translation and oocyte maturation. *EMBO J* 2002;**21**:3852-3862.
299. Hodgman R, Tay J, Mendez R, Richter JD. CPEB phosphorylation and cytoplasmic polyadenylation are catalyzed by the kinase IAK1/Eg2 in maturing mouse oocytes. *Development* 2001;**128**:2815-2822.
300. Lau NC, Lim LP, Weinstein EG, Bartel DP. An abundant class of tiny RNAs with probable regulatory roles in Caenorhabditis elegans. *Science* 2001;**294**:858-862.
301. Lee RC, Ambros V. An extensive class of small RNAs in Caenorhabditis elegans. *Science* 2001;**294**:862-864.
302. Lagos-Quintana M, Rauhut R, Lendeckel W, Tuschl T. Identification of novel genes coding for small expressed RNAs. *Science* 2001;**294**:853-858.
303. Lee Y, Jeon K, Lee JT, Kim S, Kim VN. MicroRNA maturation: stepwise processing and subcellular localization. *EMBO J* 2002;**21**:4663-4670.
304. Aravin AA, Lagos-Quintana M, Yalcin A, Zavolan M, Marks D, Snyder B*, et al.* The small RNA profile during Drosophila melanogaster development. *Dev Cell* 2003;**5**:337-350.
305. Lee Y, Ahn C, Han J, Choi H, Kim J, Yim J*, et al.* The nuclear RNase III Drosha initiates microRNA processing. *Nature* 2003;**425**:415-419.
306. Hutvagner G, McLachlan J, Pasquinelli AE, Balint E, Tuschl T, Zamore PD. A cellular function for the RNA-interference enzyme Dicer in the maturation of the let-7 small temporal RNA. *Science* 2001;**293**:834-838.
307. Noland CL, Doudna JA. Multiple sensors ensure guide strand selection in human RNAi pathways. *RNA* 2013.
308. Okamura K, Phillips MD, Tyler DM, Duan H, Chou YT, Lai EC. The regulatory activity of microRNA* species has substantial influence on microRNA and 3' UTR evolution. *Nat Struct Mol Biol* 2008;**15**:354-363.
309. Gregory RI, Chendrimada TP, Cooch N, Shiekhattar R. Human RISC couples microRNA biogenesis and posttranscriptional gene silencing. *Cell* 2005;**123**:631-640.
310. Robb GB, Rana TM. RNA helicase A interacts with RISC in human cells and functions in RISC loading. *Mol Cell* 2007;**26**:523-537.
311. Chendrimada TP, Gregory RI, Kumaraswamy E, Norman J, Cooch N, Nishikura K*, et al.* TRBP recruits the Dicer complex to Ago2 for microRNA processing and gene silencing. *Nature* 2005;**436**:740-744.
312. Meister G, Landthaler M, Patkaniowska A, Dorsett Y, Teng G, Tuschl T. Human Argonaute2 mediates RNA cleavage targeted by miRNAs and siRNAs. *Mol Cell* 2004;**15**:185-197.

313. Jeffrey SS. Cancer biomarker profiling with microRNAs. *Nat Biotechnol* 2008;**26**:400-401.
314. Lai EC. Micro RNAs are complementary to 3' UTR sequence motifs that mediate negative post-transcriptional regulation. *Nat Genet* 2002;**30**:363-364.
315. Orom UA, Nielsen FC, Lund AH. MicroRNA-10a binds the 5'UTR of ribosomal protein mRNAs and enhances their translation. *Mol Cell* 2008;**30**:460-471.
316. Zamore PD, Tuschl T, Sharp PA, Bartel DP. RNAi: double-stranded RNA directs the ATP-dependent cleavage of mRNA at 21 to 23 nucleotide intervals. *Cell* 2000;**101**:25-33.
317. Humphreys DT, Westman BJ, Martin DI, Preiss T. MicroRNAs control translation initiation by inhibiting eukaryotic initiation factor 4E/cap and poly(A) tail function. *Proc Natl Acad Sci U S A* 2005;**102**:16961-16966.
318. Kiriakidou M, Tan GS, Lamprinaki S, De Planell-Saguer M, Nelson PT, Mourelatos Z. An mRNA m7G cap binding-like motif within human Ago2 represses translation. *Cell* 2007;**129**:1141-1151.
319. Chendrimada TP, Finn KJ, Ji X, Baillat D, Gregory RI, Liebhaber SA*, et al.* MicroRNA silencing through RISC recruitment of eIF6. *Nature* 2007;**447**:823-828.
320. Petersen CP, Bordeleau ME, Pelletier J, Sharp PA. Short RNAs repress translation after initiation in mammalian cells. *Mol Cell* 2006;**21**:533-542.
321. Behm-Ansmant I, Rehwinkel J, Doerks T, Stark A, Bork P, Izaurralde E. mRNA degradation by miRNAs and GW182 requires both CCR4:NOT deadenylase and DCP1:DCP2 decapping complexes. *Genes Dev* 2006;**20**:1885-1898.
322. Wu L, Fan J, Belasco JG. MicroRNAs direct rapid deadenylation of mRNA. *Proc Natl Acad Sci U S A* 2006;**103**:4034-4039.
323. Lim LP, Lau NC, Garrett-Engele P, Grimson A, Schelter JM, Castle J*, et al.* Microarray analysis shows that some microRNAs downregulate large numbers of target mRNAs. *Nature* 2005;**433**:769-773.
324. Selbach M, Schwanhausser B, Thierfelder N, Fang Z, Khanin R, Rajewsky N. Widespread changes in protein synthesis induced by microRNAs. *Nature* 2008;**455**:58-63.
325. Guo H, Ingolia NT, Weissman JS, Bartel DP. Mammalian microRNAs predominantly act to decrease target mRNA levels. *Nature* 2010;**466**:835-840.
326. Lagos-Quintana M, Rauhut R, Yalcin A, Meyer J, Lendeckel W, Tuschl T. Identification of tissue-specific microRNAs from mouse. *Curr Biol* 2002;**12**:735-739.
327. Guo Z, Maki M, Ding R, Yang Y, Zhang B, Xiong L. Genome-wide survey of tissue-specific microRNA and transcription factor regulatory networks in 12 tissues. *Sci Rep* 2014;**4**:5150.
328. Sluijter JP, van Mil A, van Vliet P, Metz CH, Liu J, Doevendans PA*, et al.* MicroRNA-1 and -499 regulate differentiation and proliferation in human-derived cardiomyocyte progenitor cells. *Arterioscler Thromb Vasc Biol* 2010;**30**:859-868.
329. Hosoda T, Zheng H, Cabral-da-Silva M, Sanada F, Ide-Iwata N, Ogorek B*, et al.* Human cardiac stem cell differentiation is regulated by a mircrine mechanism. *Circulation* 2011;**123**:1287-1296.

330. Zhao Y, Samal E, Srivastava D. Serum response factor regulates a muscle-specific microRNA that targets Hand2 during cardiogenesis. *Nature* 2005;**436**:214-220.
331. Lee YS, Kim HK, Chung S, Kim KS, Dutta A. Depletion of human micro-RNA miR-125b reveals that it is critical for the proliferation of differentiated cells but not for the down-regulation of putative targets during differentiation. *J Biol Chem* 2005;**280**:16635-16641.
332. Hayashita Y, Osada H, Tatematsu Y, Yamada H, Yanagisawa K, Tomida S*, et al.* A polycistronic microRNA cluster, miR-17-92, is overexpressed in human lung cancers and enhances cell proliferation. *Cancer Res* 2005;**65**:9628-9632.
333. Chan JA, Krichevsky AM, Kosik KS. MicroRNA-21 is an antiapoptotic factor in human glioblastoma cells. *Cancer Res* 2005;**65**:6029-6033.
334. Cimmino A, Calin GA, Fabbri M, Iorio MV, Ferracin M, Shimizu M*, et al.* miR-15 and miR-16 induce apoptosis by targeting BCL2. *Proc Natl Acad Sci U S A* 2005;**102**:13944-13949.
335. Cannell IG, Kong YW, Johnston SJ, Chen ML, Collins HM, Dobbyn HC*, et al.* p38 MAPK/MK2-mediated induction of miR-34c following DNA damage prevents Myc-dependent DNA replication. *Proc Natl Acad Sci U S A* 2010;**107**:5375-5380.
336. Wei J, Shi Y, Zheng L, Zhou B, Inose H, Wang J*, et al.* miR-34s inhibit osteoblast proliferation and differentiation in the mouse by targeting SATB2. *J Cell Biol* 2012;**197**:509-521.
337. Poy MN, Eliasson L, Krutzfeldt J, Kuwajima S, Ma X, Macdonald PE*, et al.* A pancreatic islet-specific microRNA regulates insulin secretion. *Nature* 2004;**432**:226-230.
338. Goren Y, Kushnir M, Zafrir B, Tabak S, Lewis BS, Amir O. Serum levels of microRNAs in patients with heart failure. *Eur J Heart Fail* 2012;**14**:147-154.
339. Vogel B, Keller A, Frese KS, Leidinger P, Sedaghat-Hamedani F, Kayvanpour E*, et al.* Multivariate miRNA signatures as biomarkers for non-ischaemic systolic heart failure. *Eur Heart J* 2013;**34**:2812-2822.
340. Schobitz B, Netzker R, Hannappel E, Brand K. Rapid induction of thymosin beta 4 in concanavalin A-stimulated thymocytes by translational control. *J Biol Chem* 1990;**265**:15387-15391.
341. Enright AJ, John B, Gaul U, Tuschl T, Sander C, Marks DS. MicroRNA targets in Drosophila. *Genome Biol* 2003;**5**:R1.
342. John B, Enright AJ, Aravin A, Tuschl T, Sander C, Marks DS. Human MicroRNA targets. *PLoS Biol* 2004;**2**:e363.
343. Lewis BP, Burge CB, Bartel DP. Conserved seed pairing, often flanked by adenosines, indicates that thousands of human genes are microRNA targets. *Cell* 2005;**120**:15-20.
344. Maragkakis M, Reczko M, Simossis VA, Alexiou P, Papadopoulos GL, Dalamagas T*, et al.* DIANA-microT web server: elucidating microRNA functions through target prediction. *Nucleic Acids Res* 2009;**37**:W273-276.
345. Dweep H, Sticht C, Pandey P, Gretz N. miRWalk--database: prediction of possible miRNA binding sites by "walking" the genes of three genomes. *J Biomed Inform* 2011;**44**:839-847.

346. Betel D, Koppal A, Agius P, Sander C, Leslie C. Comprehensive modeling of microRNA targets predicts functional non-conserved and non-canonical sites. *Genome Biol* 2010;**11**:R90.
347. Jo JO, Kang YJ, Ock MS, Kleinman HK, Chang HK, Cha HJ. Thymosin beta4 expression in human tissues and in tumors using tissue microarrays. *Appl Immunohistochem Mol Morphol* 2011;**19**:160-167.
348. Franco D, Lamers WH, Moorman AF. Patterns of expression in the developing myocardium: towards a morphologically integrated transcriptional model. *Cardiovasc Res* 1998;**38**:25-53.
349. Tomanek RJ, Lotun K, Clark EB, Suvarna PR, Hu N. VEGF and bFGF stimulate myocardial vascularization in embryonic chick. *Am J Physiol* 1998;**274**:H1620-1626.
350. Andrews RG, Singer JW, Bernstein ID. Precursors of colony-forming cells in humans can be distinguished from colony-forming cells by expression of the CD33 and CD34 antigens and light scatter properties. *J Exp Med* 1989;**169**:1721-1731.
351. Strauss LC, Rowley SD, La Russa VF, Sharkis SJ, Stuart RK, Civin CI. Antigenic analysis of hematopoiesis. V. Characterization of My-10 antigen expression by normal lymphohematopoietic progenitor cells. *Exp Hematol* 1986;**14**:878-886.
352. Banerjee I, Fuseler JW, Price RL, Borg TK, Baudino TA. Determination of cell types and numbers during cardiac development in the neonatal and adult rat and mouse. *Am J Physiol Heart Circ Physiol* 2007;**293**:H1883-1891.
353. Mori L, Bellini A, Stacey MA, Schmidt M, Mattoli S. Fibrocytes contribute to the myofibroblast population in wounded skin and originate from the bone marrow. *Exp Cell Res* 2005;**304**:81-90.
354. Barth PJ, Westhoff CC. CD34+ fibrocytes: morphology, histogenesis and function. *Curr Stem Cell Res Ther* 2007;**2**:221-227.
355. Lei PP, Qu YQ, Shuai Q, Tao SM, Bao YX, Wang Y*, et al.* Fibrocytes are associated with the fibrosis of coronary heart disease. *Pathol Res Pract* 2013;**209**:36-43.
356. O'Connell RM, Taganov KD, Boldin MP, Cheng G, Baltimore D. MicroRNA-155 is induced during the macrophage inflammatory response. *Proc Natl Acad Sci U S A* 2007;**104**:1604-1609.
357. Martinez-Nunez RT, Louafi F, Sanchez-Elsner T. The interleukin 13 (IL-13) pathway in human macrophages is modulated by microRNA-155 via direct targeting of interleukin 13 receptor alpha1 (IL13Ralpha1). *J Biol Chem* 2011;**286**:1786-1794.
358. Louafi F, Martinez-Nunez RT, Sanchez-Elsner T. MicroRNA-155 targets SMAD2 and modulates the response of macrophages to transforming growth factor-{beta}. *J Biol Chem* 2010;**285**:41328-41336.
359. Fabbri M, Garzon R, Cimmino A, Liu Z, Zanesi N, Callegari E*, et al.* MicroRNA-29 family reverts aberrant methylation in lung cancer by targeting DNA methyltransferases 3A and 3B. *Proc Natl Acad Sci U S A* 2007;**104**:15805-15810.
360. Shah AP, Youngquist ST, McClung CD, Tzvetkova E, Hanif MA, Rosborough JP*, et al.* Markers of progenitor cell recruitment and differentiation rise early during ischemia and continue during

resuscitation in a porcine acute ischemia model. *J Interferon Cytokine Res* 2011;**31**:509-513.
361. Moon EY, Im YS, Ryu YK, Kang JH. Actin-sequestering protein, thymosin beta-4, is a novel hypoxia responsive regulator. *Clin Exp Metastasis* 2010;**27**:601-609.
362. Masuda N, Ohnishi T, Kawamoto S, Monden M, Okubo K. Analysis of chemical modification of RNA from formalin-fixed samples and optimization of molecular biology applications for such samples. *Nucleic Acids Res* 1999;**27**:4436-4443.
363. Cox ML, Schray CL, Luster CN, Stewart ZS, Korytko PJ, KN MK*, et al.* Assessment of fixatives, fixation, and tissue processing on morphology and RNA integrity. *Exp Mol Pathol* 2006;**80**:183-191.
364. Goldsworthy SM, Stockton PS, Trempus CS, Foley JF, Maronpot RR. Effects of fixation on RNA extraction and amplification from laser capture microdissected tissue. *Mol Carcinog* 1999;**25**:86-91.
365. Pan Y, Ouyang Z, Wong WH, Baker JC. A new FACS approach isolates hESC derived endoderm using transcription factors. *PLoS One* 2011;**6**:e17536.
366. Gnecchi M, He H, Noiseux N, Liang OD, Zhang L, Morello F*, et al.* Evidence supporting paracrine hypothesis for Akt-modified mesenchymal stem cell-mediated cardiac protection and functional improvement. *FASEB J* 2006;**20**:661-669.
367. Sethi P, Lukiw WJ. Micro-RNA abundance and stability in human brain: specific alterations in Alzheimer's disease temporal lobe neocortex. *Neurosci Lett* 2009;**459**:100-104.
368. Krol J, Busskamp V, Markiewicz I, Stadler MB, Ribi S, Richter J*, et al.* Characterizing light-regulated retinal microRNAs reveals rapid turnover as a common property of neuronal microRNAs. *Cell* 2010;**141**:618-631.
369. McCall MN, Kent OA, Yu J, Fox-Talbot K, Zaiman AL, Halushka MK. MicroRNA profiling of diverse endothelial cell types. *BMC Med Genomics* 2011;**4**:78.
370. Morin RD, O'Connor MD, Griffith M, Kuchenbauer F, Delaney A, Prabhu AL*, et al.* Application of massively parallel sequencing to microRNA profiling and discovery in human embryonic stem cells. *Genome Res* 2008;**18**:610-621.
371. Wyman SK, Knouf EC, Parkin RK, Fritz BR, Lin DW, Dennis LM*, et al.* Post-transcriptional generation of miRNA variants by multiple nucleotidyl transferases contributes to miRNA transcriptome complexity. *Genome Res* 2011;**21**:1450-1461.
372. Schamberger A, Orban TI. 3' IsomiR species and DNA contamination influence reliable quantification of microRNAs by stem-loop quantitative PCR. *PLoS One* 2014;**9**:e106315.
373. Griffiths-Jones S. The microRNA Registry. *Nucleic Acids Res* 2004;**32**:D109-111.
374. Griffiths-Jones S, Grocock RJ, van Dongen S, Bateman A, Enright AJ. miRBase: microRNA sequences, targets and gene nomenclature. *Nucleic Acids Res* 2006;**34**:D140-144.
375. Griffiths-Jones S, Saini HK, van Dongen S, Enright AJ. miRBase: tools for microRNA genomics. *Nucleic Acids Res* 2008;**36**:D154-158.

376. Kozomara A, Griffiths-Jones S. miRBase: integrating microRNA annotation and deep-sequencing data. *Nucleic Acids Res* 2011;**39**:D152-157.
377. Kozomara A, Griffiths-Jones S. miRBase: annotating high confidence microRNAs using deep sequencing data. *Nucleic Acids Res* 2014;**42**:D68-73.
378. Stark MS, Tyagi S, Nancarrow DJ, Boyle GM, Cook AL, Whiteman DC*, et al.* Characterization of the Melanoma miRNAome by Deep Sequencing. *PLoS One* 2010;**5**:e9685.
379. Witten D, Tibshirani R, Gu SG, Fire A, Lui WO. Ultra-high throughput sequencing-based small RNA discovery and discrete statistical biomarker analysis in a collection of cervical tumours and matched controls. *BMC Biol* 2010;**8**:58.
380. Meunier J, Lemoine F, Soumillon M, Liechti A, Weier M, Guschanski K*, et al.* Birth and expression evolution of mammalian microRNA genes. *Genome Res* 2013;**23**:34-45.
381. Kuchen S, Resch W, Yamane A, Kuo N, Li Z, Chakraborty T*, et al.* Regulation of microRNA expression and abundance during lymphopoiesis. *Immunity* 2010;**32**:828-839.
382. Streit S, Michalski CW, Erkan M, Kleeff J, Friess H. Northern blot analysis for detection and quantification of RNA in pancreatic cancer cells and tissues. *Nat Protoc* 2009;**4**:37-43.
383. Liu T, Shen D, Xing S, Chen J, Yu Z, Wang J*, et al.* Attenuation of exogenous angiotensin II stress-induced damage and apoptosis in human vascular endothelial cells via microRNA-155 expression. *Int J Mol Med* 2013;**31**:188-196.
384. Mayr C, Bartel DP. Widespread shortening of 3'UTRs by alternative cleavage and polyadenylation activates oncogenes in cancer cells. *Cell* 2009;**138**:673-684.
385. Rane S, He M, Sayed D, Vashistha H, Malhotra A, Sadoshima J*, et al.* Downregulation of miR-199a derepresses hypoxia-inducible factor-1alpha and Sirtuin 1 and recapitulates hypoxia preconditioning in cardiac myocytes. *Circ Res* 2009;**104**:879-886.
386. Tian Y, Zhang YZ, Chen W. MicroRNA-199a-3p and microRNA-34a regulate apoptosis in human osteosarcoma cells. *Biosci Rep* 2014;**34**.
387. Duan Z, Choy E, Harmon D, Liu X, Susa M, Mankin H*, et al.* MicroRNA-199a-3p is downregulated in human osteosarcoma and regulates cell proliferation and migration. *Mol Cancer Ther* 2011;**10**:1337-1345.
388. Wirsching HG, Krishnan S, Florea AM, Frei K, Krayenbuhl N, Hasenbach K*, et al.* Thymosin beta 4 gene silencing decreases stemness and invasiveness in glioblastoma. *Brain* 2014;**137**:433-448.
389. Welten SM, Bastiaansen AJ, de Jong R, de Vries MR, Peters EH, Boonstra M*, et al.* Inhibition of 14q32 MicroRNAs miR-329, miR-487b, miR-494 and miR-495 Increases Neovascularization and Blood Flow Recovery after Ischemia. *Circ Res* 2014.
390. Li Z, Cao Y, Jie Z, Liu Y, Li Y, Li J*, et al.* miR-495 and miR-551a inhibit the migration and invasion of human gastric cancer cells by directly interacting with PRL-3. *Cancer Lett* 2012;**323**:41-47.
391. Formosa A, Markert EK, Lena AM, Italiano D, Finazzi-Agro E, Levine AJ*, et al.* MicroRNAs, miR-154, miR-299-5p, miR-376a, miR-376c, miR-377,

miR-381, miR-487b, miR-485-3p, miR-495 and miR-654-3p, mapped to the 14q32.31 locus, regulate proliferation, apoptosis, migration and invasion in metastatic prostate cancer cells. *Oncogene* 2013.
392. Chu H, Chen X, Wang H, Du Y, Wang Y, Zang W*, et al.* MiR-495 regulates proliferation and migration in NSCLC by targeting MTA3. *Tumour Biol* 2014;**35**:3487-3494.
393. Poliseno L, Tuccoli A, Mariani L, Evangelista M, Citti L, Woods K*, et al.* MicroRNAs modulate the angiogenic properties of HUVECs. *Blood* 2006;**108**:3068-3071.
394. Chang TY, Huang TS, Wang HW, Chang SJ, Lo HH, Chiu YL*, et al.* miRNome traits analysis on endothelial lineage cells discloses biomarker potential circulating microRNAs which affect progenitor activities. *BMC Genomics* 2014;**15**:802.
395. Suarez Y, Fernandez-Hernando C, Pober JS, Sessa WC. Dicer dependent microRNAs regulate gene expression and functions in human endothelial cells. *Circ Res* 2007;**100**:1164-1173.
396. Bracken CP, Li X, Wright JA, Lawrence DM, Pillman KA, Salmanidis M*, et al.* Genome-wide identification of miR-200 targets reveals a regulatory network controlling cell invasion. *EMBO J* 2014;**33**:2040-2056.
397. Lu Y, Lu J, Li X, Zhu H, Fan X, Zhu S*, et al.* MiR-200a inhibits epithelial-mesenchymal transition of pancreatic cancer stem cell. *BMC Cancer* 2014;**14**:85.
398. Pichler M, Ress AL, Winter E, Stiegelbauer V, Karbiener M, Schwarzenbacher D*, et al.* MiR-200a regulates epithelial to mesenchymal transition-related gene expression and determines prognosis in colorectal cancer patients. *Br J Cancer* 2014;**110**:1614-1621.
399. Song YX, Yue ZY, Wang ZN, Xu YY, Luo Y, Xu HM*, et al.* MicroRNA-148b is frequently down-regulated in gastric cancer and acts as a tumor suppressor by inhibiting cell proliferation. *Mol Cancer* 2011;**10**:1.
400. Song Y, Xu Y, Wang Z, Chen Y, Yue Z, Gao P*, et al.* MicroRNA-148b suppresses cell growth by targeting cholecystokinin-2 receptor in colorectal cancer. *Int J Cancer* 2012;**131**:1042-1051.
401. Zhao G, Zhang JG, Liu Y, Qin Q, Wang B, Tian K*, et al.* miR-148b functions as a tumor suppressor in pancreatic cancer by targeting AMPKalpha1. *Mol Cancer Ther* 2013;**12**:83-93.
402. Liu GL, Liu X, Lv XB, Wang XP, Fang XS, Sang Y. miR-148b functions as a tumor suppressor in non-small cell lung cancer by targeting carcinoembryonic antigen (CEA). *Int J Clin Exp Med* 2014;**7**:1990-1999.
403. Guo J, Feng Z, Huang Z, Wang H, Lu W. MicroRNA-217 Functions as a Tumour Suppressor Gene and Correlates with Cell Resistance to Cisplatin in Lung Cancer. *Mol Cells* 2014.
404. Su J, Wang Q, Liu Y, Zhong M. miR-217 inhibits invasion of hepatocellular carcinoma cells through direct suppression of E2F3. *Mol Cell Biochem* 2014;**392**:289-296.
405. Zhao G, Deng S, Zhu S, Wang B, Li X, Liu Y*, et al.* Chronic pancreatitis and pancreatic cancer demonstrate active epithelial-mesenchymal transition profile, regulated by miR-217-SIRT1 pathway. *Cancer Lett* 2014.

406. Kumar MS, Erkeland SJ, Pester RE, Chen CY, Ebert MS, Sharp PA*, et al.* Suppression of non-small cell lung tumor development by the let-7 microRNA family. *Proc Natl Acad Sci U S A* 2008;**105**:3903-3908.
407. Dacic S, Kelly L, Shuai Y, Nikiforova MN. miRNA expression profiling of lung adenocarcinomas: correlation with mutational status. *Mod Pathol* 2010;**23**:1577-1582.
408. Cheung IY, Farazi TA, Ostrovnaya I, Xu H, Tran H, Mihailovic A*, et al.* Deep MicroRNA sequencing reveals downregulation of miR-29a in neuroblastoma central nervous system metastasis. *Genes Chromosomes Cancer* 2014;**53**:803-814.
409. Han HS, Son SM, Yun J, Jo YN, Lee OJ. MicroRNA-29a suppresses the growth, migration, and invasion of lung adenocarcinoma cells by targeting carcinoembryonic antigen-related cell adhesion molecule 6. *FEBS Lett* 2014.
410. van Solingen C, Seghers L, Bijkerk R, Duijs JM, Roeten MK, van Oeveren-Rietdijk AM*, et al.* Antagomir-mediated silencing of endothelial cell specific microRNA-126 impairs ischemia-induced angiogenesis. *J Cell Mol Med* 2009;**13**:1577-1585.
411. Fish JE, Santoro MM, Morton SU, Yu S, Yeh RF, Wythe JD*, et al.* miR-126 regulates angiogenic signaling and vascular integrity. *Dev Cell* 2008;**15**:272-284.
412. Bhaumik D, Scott GK, Schokrpur S, Patil CK, Campisi J, Benz CC. Expression of microRNA-146 suppresses NF-kappaB activity with reduction of metastatic potential in breast cancer cells. *Oncogene* 2008;**27**:5643-5647.
413. Perry MM, Moschos SA, Williams AE, Shepherd NJ, Larner-Svensson HM, Lindsay MA. Rapid changes in microRNA-146a expression negatively regulate the IL-1beta-induced inflammatory response in human lung alveolar epithelial cells. *J Immunol* 2008;**180**:5689-5698.
414. Wang X, Ha T, Liu L, Zou J, Zhang X, Kalbfleisch J*, et al.* Increased expression of microRNA-146a decreases myocardial ischaemia/reperfusion injury. *Cardiovasc Res* 2013;**97**:432-442.
415. Voellenkle C, Rooij J, Guffanti A, Brini E, Fasanaro P, Isaia E*, et al.* Deep-sequencing of endothelial cells exposed to hypoxia reveals the complexity of known and novel microRNAs. *RNA* 2012;**18**:472-484.
416. Ramachandran V, Chen X. Degradation of microRNAs by a family of exoribonucleases in Arabidopsis. *Science* 2008;**321**:1490-1492.
417. Chatterjee S, Grosshans H. Active turnover modulates mature microRNA activity in Caenorhabditis elegans. *Nature* 2009;**461**:546-549.
418. Das SK, Sokhi UK, Bhutia SK, Azab B, Su ZZ, Sarkar D*, et al.* Human polynucleotide phosphorylase selectively and preferentially degrades microRNA-221 in human melanoma cells. *Proc Natl Acad Sci U S A* 2010;**107**:11948-11953.
419. Memczak S, Jens M, Elefsinioti A, Torti F, Krueger J, Rybak A*, et al.* Circular RNAs are a large class of animal RNAs with regulatory potency. *Nature* 2013;**495**:333-338.
420. Hansen TB, Jensen TI, Clausen BH, Bramsen JB, Finsen B, Damgaard CK*, et al.* Natural RNA circles function as efficient microRNA sponges. *Nature* 2013;**495**:384-388.

421. Sosne G, Dunn S, Crockford D, Kim C, Dixon E. Thymosin Beta 4 Eye Drops Significantly Improve Signs and Symptoms of Severe Dry Eye in a Physician-Sponsored Phase 2 Clinical Trial. *Invest Ophthalmol Vis Sci* 2013;**54**:6033-.
422. Crockford D. Development of thymosin beta4 for treatment of patients with ischemic heart disease. *Ann N Y Acad Sci* 2007;**1112**:385-395.
423. RegeneRx - Pipeline / Clinical Trials: http://www.regenerx.com/wt/page/clinical_trials (accessed 27/09/14).
424. Chiu LL, Reis LA, Momen A, Radisic M. Controlled release of thymosin beta4 from injected collagen-chitosan hydrogels promotes angiogenesis and prevents tissue loss after myocardial infarction. *Regen Med* 2012;**7**:523-533.
425. Thatcher JE, Welch T, Eberhart RC, Schelly ZA, DiMaio JM. Thymosin beta4 sustained release from poly(lactide-co-glycolide) microspheres: synthesis and implications for treatment of myocardial ischemia. *Ann N Y Acad Sci* 2012;**1270**:112-119.
426. Chen S, Shimoda M, Chen J, Grayburn PA. Stimulation of adult resident cardiac progenitor cells by durable myocardial expression of thymosin beta 4 with ultrasound-targeted microbubble delivery. *Gene Ther* 2013;**20**:225-233.
427. Lennox KA, Behlke MA. Chemical modification and design of anti-miRNA oligonucleotides. *Gene Ther* 2011;**18**:1111-1120.
428. Wahlquist C, Jeong D, Rojas-Munoz A, Kho C, Lee A, Mitsuyama S*, et al.* Inhibition of miR-25 improves cardiac contractility in the failing heart. *Nature* 2014;**508**:531-535.
429. Bonauer A, Carmona G, Iwasaki M, Mione M, Koyanagi M, Fischer A*, et al.* MicroRNA-92a controls angiogenesis and functional recovery of ischemic tissues in mice. *Science* 2009;**324**:1710-1713.
430. Hinkel R, Penzkofer D, Zuhlke S, Fischer A, Husada W, Xu QF*, et al.* Inhibition of microRNA-92a protects against ischemia/reperfusion injury in a large-animal model. *Circulation* 2013;**128**:1066-1075.
431. Bellera N, Barba I, Rodriguez-Sinovas A, Ferret E, Asin MA, Gonzalez-Alujas MT*, et al.* Single intracoronary injection of encapsulated antagomir-92a promotes angiogenesis and prevents adverse infarct remodeling. *J Am Heart Assoc* 2014;**3**.
432. Lesnik JKA, T. J. Permanent knockdown of microRNAs using lentivectors. *BioTechniques* 2010;**48**:321-323.
433. Fan M, Chen W, Liu W, Du GQ, Jiang SL, Tian WC*, et al.* The effect of age on the efficacy of human mesenchymal stem cell transplantation after a myocardial infarction. *Rejuvenation Res* 2010;**13**:429-438.
434. Wen Z, Huang W, Feng Y, Cai W, Wang Y, Wang X*, et al.* MicroRNA-377 Regulates Mesenchymal Stem Cell-Induced Angiogenesis in Ischemic Hearts by Targeting VEGF. *PLoS One* 2014;**9**:e104666.
435. Ye L, Zhang P, Duval S, Su L, Xiong Q, Zhang J. Thymosin beta4 increases the potency of transplanted mesenchymal stem cells for myocardial repair. *Circulation* 2013;**128**:S32-41.
436. Yan B, Singla RD, Abdelli LS, Singal PK, Singla DK. Regulation of PTEN/Akt pathway enhances cardiomyogenesis and attenuates adverse left ventricular remodeling following thymosin beta4 Overexpressing

embryonic stem cell transplantation in the infarcted heart. *PLoS One* 2013;**8**:e75580.
437. Kumar A, Patel A, Duvalsaint L, Desai M, Marks ED. Thymosin beta4 coated nanofiber scaffolds for the repair of damaged cardiac tissue. *J Nanobiotechnology* 2014;**12**:10.
438. Agostini M, Knight RA. miR-34: from bench to bedside. *Oncotarget* 2014;**5**:872-881.